UNIVERSITY OF CALIFORNIA
SANTA CRUZ

# TROPICAL PACIFIC CLIMATE AND El NIÑO STRENGTH OVER THE PAST FIVE MILLION YEARS

A dissertation submitted in partial satisfaction
of the requirements for the degree of

DOCTOR OR PHILOSOPHY

in

EARTH SCIENCES

by

**Sarah M. White**

September 2019

The dissertation of Sarah M. White is approved:

_____
Professor Ana Christina Ravelo, chair

_____
Professor James C. Zachos

_____
Professor Andrew Moore

_____
Professor Patrick Y. Chuang

_____
Quentin Williams
Acting Vice Provost and Dean of Graduate Studies

Table of Contents

# List of Figures and Tables

**Abstract**

Tropical Pacific climate and El Niño strength over the past five million years
By Sarah White

The tropical Pacific has an outsized influence on global climate – it is the center of the El Niño-Southern Oscillation (ENSO), the dominant source of interannual climate variability, and the seat of the West Pacific Warm Pool (WPWP), a major source of energy to the atmosphere. The future evolution of the tropical Pacific is unclear; the WPWP's response to increased $pCO_2$ is not well constrained, and ENSO may either strengthen or weaken. To investigate ENSO's dependence on the mean climate, and on various positive and negative feedbacks, I collected paleo-ENSO data from time periods with different mean climate: the mid- and early Holocene, and the Pliocene. My data are based on Mg/Ca measurements of individual foraminifera from marine sediment cores from the central and eastern equatorial Pacific. By measuring many individuals in a sample, I reconstruct the distribution of temperatures. Differences in the warm "tail" of the distribution are attributable to changes in El Niño amplitude.

I found that El Niño amplitude was dampened (relative to the late Holocene) during the mid- and early Holocene and throughout the early Pliocene, whereas during the mid-Pliocene, El Niño amplitude varied on centennial and/or orbital timescales, in agreement with modeling studies. Though modeling studies agree on changes in past ENSO, they disagree on the mechanisms of change, and here the proxy data (on both ENSO and mean climate) provide key constraints for model

validation. The dampening mechanism best supported by proxy data, and which provides a unified explanation of our findings from all time periods, is that a deeper thermocline in the mid- and early Holocene and in the early Pliocene weakened the upwelling and thermocline feedbacks, thus weakening ENSO. This work highlights the importance of the thermocline, which should help predict ENSO's response to anthropogenic change.

To investigate the WPWP's response to varying $pCO_2$, I focus on the Pliocene, the most recent epoch in which $pCO_2$ was higher than preindustrial. Only two Pliocene temperature records exist from the heart of the WPWP, and they show different trends. The foraminiferal Mg/Ca-based SST record shows Pliocene WPWP temperatures similar to today, but the $TEX_{86}$ temperature proxy indicates a WPWP cooling trend since the Pliocene. The $TEX_{86}$ studies, which claim that Pliocene WPWP temperatures were warmer than today, echo the claims of modeling studies, which produce a warmer WPWP whenever $pCO_2$ is higher than preindustrial. Though much of the debate over Pliocene WPWP SSTs has focused on changes in seawater Mg/Ca, spatial variations in proxy agreement point to dissolution as a key factor. Dissolution, which imparts a cool bias to Mg/Ca temperatures, varies across ocean basins depending on $\Delta[CO_3^{2-}]$, the difference from the carbonate ion concentration needed for calcite saturation. By necessity, dissolution corrections use the modern value of $\Delta[CO_3^{2-}]$ for the entire record, so it is possible that Pliocene proxy discrepancies could stem from varying $\Delta[CO_3^{2-}]$ over time. To constrain the effect of

changing dissolution on the Mg/Ca SST record, I collected benthic foraminiferal B/Ca data (a proxy for $\Delta[CO_3^{2-}]$) from the WPWP spanning the past 5.5 Myr.

I found no long-term trend in $\Delta[CO_3^{2-}]$ over the past 5.5 Ma, implying no dissolution bias in the trend of the Mg/Ca record. After accounting for changes in seawater Mg/Ca, I estimate the temperature of the WPWP during the Pliocene to be ~1°C warmer than today. As such, the 2-2.5°C trend shown in $TEX_{86}$ records is not supported by the Mg/Ca data, and likely stems from a bias in the $TEX_{86}$ data toward subsurface temperatures.

**Acknowledgements**

I am very grateful for all the help and support from my family, including my husband Tristan Rocheleau. My lab group and other fellow grads at UCSC made my time in Santa Cruz happy and fulfilling, and were always there when times were tough. I am also very lucky to have had Christina Ravelo as my advisor. I look up to her not only as a great scientist but as a great person. My committee was helpful and encouraging, especially when I failed to win grants, and I'm thankful for their feedback.

The text of this dissertation includes a reprint of the following previously published material:

White, S.M., Ravelo, A.C., Polissar, P. (2018). Dampened El Niño in the early and mid-Holocene due to insolation-forced warming/deepening of the thermocline. *Geophysical Research Letters 45*. https://doi.org/10.1002/2017GL075433 .

The co-authors listed in this publication directed and supervised the research which forms the basis for the dissertation.

## Chapter 1: Introduction

This dissertation explores tropical Pacific mean climatic state and El Niño strength during warm periods of the past five million years (Myr), including the Holocene (modern to 11,700 years ago) and the Pliocene (2.58 to 5.33 million years ago, Ma). The El Niño-Southern Oscillation (ENSO) is the strongest mode of interannual variability in the modern climate. El Niño events are centered in the tropical Pacific, and affect precipitation and ecosystems throughout the Pacific basin. ENSO's response to climate forcing from greenhouse gases or changes in insolation is unclear; models disagree on whether ENSO will strengthen or weaken with anthropogenic climate change [e.g. *Chen et al.*, 2017; *Christensen et al.*, 2013; *Kim et al.*, 2014b]. Model studies also disagree on the reason for the disagreement [*Chen et al.*, 2017; *Ham and Kug*, 2016; *Kim et al.*, 2014a; *Rashid et al.*, 2016; *Zheng et al.*, 2016]. Paleo-proxy data on ENSO strength from warmer climates of the past are thus necessary to test the relationships between mean state and ENSO, and deduce the relative importance of various drivers and feedbacks in causing changes in ENSO. There are also gaps in our knowledge of tropical Pacific mean state, which must be filled in order to provide context for paleo-ENSO data and elucidate how the mean state itself responds to climatic forcing. Gathering proxy data to determine paleo-ENSO strength and constrain uncertainties in past mean state is thus a primary goal of this dissertation.

The Holocene provides an excellent test of the effect of changes in climate forcing on El Niño strength. During the mid- and the early Holocene, Earth's

perihelion occurred during northern hemisphere autumn and summer, respectively, instead of during northern hemisphere winter as it does today. Studies using an idealized model found that an imposed warming in the tropics, such as that from increased insolation, caused dampened ENSO [*Clement et al.*, 1996]. Dampened model ENSO appeared to be caused by "dynamical cooling" in the eastern equatorial Pacific, which increased the east-west temperature gradient across the Pacific basin and quelled incipient El Niño events [*Clement et al.*, 1996]. The model was most sensitive to warming in late summer/early fall, leading the authors to surmise that higher September insolation in the mid-Holocene caused dampened ENSO [*Clement et al.*, 1999]. However, the model used by Clement et al. was restricted to the tropics, so it inherently could not test extratropical mechanisms of ENSO change. Liu et al. [*Liu et al.*, 2000] used a different idealized model to show that changes in insolation could force changes in ENSO strength via the thermocline, whose waters originate mostly in the southern extratropics. In this model, higher June insolation caused dampened ENSO by dampening the upwelling feedback (a positive ocean-atmosphere feedback that helps generate ENSO). This scenario was verified in a fully coupled general circulation model with transient forcing over the past 21,000 years [*Liu et al.*, 2014]. The mechanisms proposed by Clement et al. and Liu et al. predict different timings of dampened ENSO during the Holocene: the Clement et al. mechanism calls for dampened ENSO during the mid- but not early Holocene, whereas the Liu et al. mechanism calls for dampened ENSO during both time periods.

Over the past 20 years, numerous researchers have gathered paleo-ENSO data, with emphasis on the mid-Holocene [*Chen et al.*, 2016; *Cobb et al.*, 2013; *Conroy et al.*, 2008; *Driscoll et al.*, 2014; *Duprey et al.*, 2012; *Koutavas and Joanides*, 2012; *McGregor and Gagan*, 2004; *McGregor et al.*, 2013; *Moy et al.*, 2002; *Rodbell et al.*, 1999; *Sadekov et al.*, 2013; *Thompson et al.*, 2017; *Tudhope et al.*, 2001; *Woodroffe*, 2003; *Zhang et al.*, 2014b]. Many records show dampened El Niño strength in the mid-Holocene, but studies disagree on ENSO strength in the early Holocene, such that the mechanism by which insolation influences ENSO is unclear. In 2013, a compilation of coral data was published that spanned the past 7,000 years and appeared to show no trend in ENSO strength at all, throwing the entire premise of insolation-forced changes in Holocene ENSO into question [*Cobb et al.*, 2013]. Gaps and limitations in existing Holocene ENSO data prevent better understanding of ENSO's response to climate forcing. Specifically, the paucity of data from the early Holocene makes it difficult to determine whether there is a trend in ENSO strength, and what its timing is. Also, many records of Holocene ENSO are based on precipitation proxies, and/or are sourced from the far eastern or western Pacific, so they do not directly record the sea-surface temperature (SST) anomalies in the equatorial band in the central and eastern Pacific that define El Niño events [*Trenberth*, 1997].

Chapter 2 of my dissertation fills these data gaps by collecting proxy data on paleo-SSTs from the central equatorial Pacific spanning the mid- and early Holocene. These data enable me to address the following questions: 1) Was there a trend in

Holocene ENSO strength that could be attributed to insolation forcing, and if so, 2) by what mechanism did insolation change ENSO?

The data for Chapter 2 are based on trace metal measurements of individual mixed-layer dwelling foraminifera. The ratio of magnesium to calcium in foraminiferal calcite is a proxy for calcification temperature; more magnesium substitutes into the calcite crystal lattice at higher temperatures [*Lea et al.*, 1999]. By measuring many individual foraminifera in a marine sediment sample, I was able to reconstruct the distribution of temperature in the mixed layer during the time interval reflected in each sample. To extract information about El Niño strength from the temperature distributions, I constructed quantile-quantile (QQ) plots comparing each downcore sample to the most recent sample. Differences in the warm "tail" of the downcore distribution are attributable to changes in El Niño amplitude. Simpler metrics for analyzing distributions, such as standard deviation, are also affected by seasonality and so cannot isolate changes in El Niño.

I found that El Niño amplitude was dampened in both the mid- and the early Holocene, implying forcing of ENSO strength by June insolation [*White et al.*, 2018]. This is consistent with modeling studies: Models with mid- and early Holocene boundary conditions unanimously show dampened ENSO due to changes in insolation. To determine which mechanism of change is best supported by proxy data, I undertook a compilation of previously published data on tropical Pacific mean state. The Liu et al. mechanism [*Liu et al.*, 2000; *Liu et al.*, 2014], which entails a weakening of the upwelling feedback due to insolation-forced warming of

thermocline source waters, is the mechanism best supported by existing proxy data [*White et al.*, 2018].

To further test the importance of the thermocline in determining El Niño strength, and to explore the effect of other changes in mean state, I turned to the Pliocene. During the Pliocene, global average temperatures were 1.8°C to 3.6°C warmer than preindustrial [*Haywood et al.*, 2013], and $pCO_2$ was higher than preindustrial and similar to current levels [*Bartoli et al.*, 2011; *Pagani et al.*, 2009; *Seki et al.*, 2010]. SSTs in the eastern equatorial Pacific (EEP) were much higher than today [*Dekens et al.*, 2007; *Lawrence et al.*, 2006; *Rousselle et al.*, 2013; *Zhang et al.*, 2014a], but the West Pacific Warm Pool (WPWP) appears to have had a similar temperature to today [*Wara et al.*, 2005] (though this interpretation has recently been called into question). Higher SSTs in the east and relatively unchanged SSTs in the west yielded a much lower zonal temperature gradient [e.g. *Fedorov et al.*, 2013]. The tropical Pacific thermocline was also much warmer and/or deeper in the early Pliocene than today [*Ford et al.*, 2012; *Ford et al.*, 2015b; *Seki et al.*, 2012; *Steph et al.*, 2010]. As such, the Pliocene affords an excellent test of the importance of the thermocline feedback.

Limited proxy data are available on ENSO during the Pliocene. Published studies [*Scroxton et al.*, 2011; *Watanabe et al.*, 2011] report the presence of interannual temperature variability but do not quantify its strength relative to modern, and the data are from the far eastern and western Pacific, which are not the regions in which ENSO anomalies are defined. Published data are also very sparse, and none are

from the early Pliocene, the time period during which the thermocline was deepest [*Ford et al.*, 2015b].

For Chapter 3 of my dissertation, I collected proxy data on paleo-SSTs from the eastern equatorial Pacific (ODP site 849) from eleven time periods during the Pliocene, with emphasis on the early Pliocene. I collected and analyzed data in the same manner as for Chapter 2. Small sample sizes motivated me to undertake a more extensive analysis of uncertainty than I did for Chapter 2. To this end, I developed the "false positive test," a tool that builds on the Monte Carlo-based confidence intervals used in Chapter 2 to estimate the probability that a sample appearing to show dampened El Niño in fact came from a temperature distribution with the same ENSO as present.

I found that El Niño amplitude was dampened, relative to the late Holocene, throughout the early Pliocene. During the mid-Pliocene, ENSO amplitude varied on orbital and/or centennial timescales, with some samples showing dampened El Niño and some appearing similar to the late Holocene. These findings are consistent with previously published ENSO data and with modeling studies. The observed trend in EL Niño strength mirrors the long-term shoaling of the thermocline and strengthening of stratification in the EEP, pointing to thermocline conditions and the upwelling feedback as an important control on ENSO strength.

For Chapter 4 of my dissertation, I collected data to constrain the temperature of the WPWP during the Pliocene, which has recently been the subject of debate. The WPWP is an important source of sensible and latent heat to the atmosphere. Small

changes in SST have a large effect on convection and energy transfer to the atmosphere [*Tian et al.*, 2001], and its sensitivity to increased $pCO_2$ is an important model validation target. It also provides important context for my paleo-ENSO work, because the temperature of the WPWP affects the east-west temperature gradient, which can influence ENSO strength [e.g. *Clement et al.*, 1996].

Only two Plio-Pleistocene temperature records exist from the heart of the WPWP (at ODP site 806), and they show different trends. The foraminiferal Mg/Ca-based SST record shows Pliocene WPWP temperatures similar to today [*Wara et al.*, 2005], but data based on the $TEX_{86}$ temperature proxy indicate a WPWP cooling trend since the Pliocene, differing markedly from the Mg/Ca record [*Zhang et al.*, 2014a]. The $TEX_{86}$ study, which claims that Pliocene WPWP temperatures were warmer than today, echoes the claims of modeling studies, which produce a warmer WPWP whenever $pCO_2$ is higher than preindustrial [e.g. *Christensen et al.*, 2013; *Haywood et al.*, 2013; *Hill et al.*, 2014].

Much of the debate over Pliocene WPWP SSTs and the disagreement between the Mg/Ca and $TEX_{86}$ proxy records has focused on changes in seawater Mg/Ca [*Evans et al.*, 2016; *Medina-Elizalde et al.*, 2008; *O'Brien et al.*, 2014; *Zhang et al.*, 2014a]. Although seawater chemistry changes may cause some bias in the foraminiferal Mg/Ca record at 806, it cannot explain spatial variations in proxy disagreement, which point to dissolution as a key factor. Dissolution has long been known to impart a cool bias to Mg/Ca temperatures [*Brown and Elderfield*, 1996; *de Villiers*, 2005; *Dekens et al.*, 2002; *Fehrenbacher et al.*, 2006; *Johnstone et al.*, 2011;

*Regenberg et al.*, 2014; *Regenberg et al.*, 2006; *Rosenthal and Lohmann*, 2002]. Dissolution varies across ocean basins depending on $\Delta[CO_3^{2-}]$, the difference between in-situ carbonate ion concentration at the seafloor and the concentration needed for calcite saturation. Foraminiferal Mg/Ca-based temperature records often employ a dissolution correction based on $\Delta[CO_3^{2-}]$ [*Dekens et al.*, 2002; *Regenberg et al.*, 2014], but by necessity, they use the modern value of $\Delta[CO_3^{2-}]$ for the entire record. Thus, it is possible that Pliocene proxy discrepancies could stem from varying $\Delta[CO_3^{2-}]$ over time. To constrain the effect of changing dissolution on the Mg/Ca SST record, I collected benthic foraminiferal B/Ca data, a proxy for $\Delta[CO_3^{2-}]$, spanning the past 5.5 Myr. I also collected new planktic foraminiferal Mg/Ca data from the same samples, so that the Mg/Ca data could be corrected for dissolution with contemporaneous (B/Ca-based) values of $\Delta[CO_3^{2-}]$.

I found no long-term trend in $\Delta[CO_3^{2-}]$ over the past 5.5 Ma, implying no dissolution bias in the trend of the Mg/Ca record. Changes in seawater Mg/Ca create a ~1.8°C cool bias in the Pliocene Mg/Ca data, though with large uncertainty. Overall, the WPWP was likely ~1.1°C warmer in the Pliocene than today. The 2-2.5°C trend shown in $TEX_{86}$ records is not supported by the Mg/Ca data, and likely stems from a bias in the $TEX_{86}$ data toward subsurface temperatures [*Dong et al.*, 2015; *Hertzberg et al.*; *Jia et al.*, 2012; *Liddy et al.*, 2016; *Richey and Tierney*, 2016; *Seki et al.*, 2012]. Simulations of mid-Pliocene climate showing a WPWP 1.5-2.0°C warmer than today [*Haywood et al.*, 2013] could be brought into agreement with my somewhat lower temperature estimate via changes in storm mixing or cloud albedo

[*Barreiro and Philander*, 2008; *Burls and Fedorov*, 2014; *Fedorov et al.*, 2010]. The east-west temperature gradient during the Pliocene was thus much lower than today, in keeping with the original claims of the Wara et al. [*Wara et al.*, 2005] study.

Overall, my dissertation seeks to elucidate connections between climate forcing, tropical Pacific mean climatic state, and El Niño strength. Chapters 2 and 3 show that thermocline conditions are important in determining El Niño strength, and can explain changes in El Niño during both the Holocene and the Pliocene despite differences in climate forcing and other aspects of the mean state. Chapter 4 found that the West Pacific Warm Pool was about 1°C warmer in the Pliocene than today, suggesting that models may be underestimating processes that drain heat away from the warm pool. In sum, these findings should help guide modeling efforts to predict the tropical Pacific's response to anthropogenic change.

## References


Barreiro, M., and S. G. Philander (2008), Response of the tropical Pacific to changes in extratropical clouds, Climate Dynamics, 31(6), 713-729, doi: 10.1007/s00382-007-0363-5.

Bartoli, G., B. Hönisch, and R. E. Zeebe (2011), Atmospheric CO2decline during the Pliocene intensification of Northern Hemisphere glaciations, Paleoceanography, 26(4), n/a-n/a, doi: 10.1029/2010pa002055.

Brown, S. J., and H. Elderfield (1996), Variations in Mg/Ca and Sr/Ca ratios of planktonic foraminifera caused by postdepositional dissolution: Evidence of shallow Mg-dependent dissolution, Paleoceanography, 11(5), 543-551, doi: 10.1029/96pa01491.

Burls, N. J., and A. V. Fedorov (2014), Simulating Pliocene warmth and a permanent El Niño-like state: The role of cloud albedo, Paleoceanography, 29(10), 893-910, doi: 10.1002/2014pa002644.

Chen, L., T. Li, Y. Yu, and S. K. Behera (2017), A possible explanation for the divergent projection of ENSO amplitude change under global warming, Climate Dynamics, 49, 3799-3811, doi: 10.1007/s00382-017-3544-x.

Chen, S., S. S. Hoffmann, D. C. Lund, K. M. Cobb, J. Emile-Geay, and J. F. Adkins (2016), A high-resolution speleothem record of western equatorial Pacific rainfall: Implications for Holocene ENSO evolution, Earth and Planetary Science Letters, 442, 61-71, doi: 10.1016/j.epsl.2016.02.050.

Christensen, J. H., et al. (2013), Climate Phenomena and their Relevance for Future Regional Climate Change, in Climate Change 2013: The Physical Science Basis. Contribution of Working Group I to the Fifth Assessment Report of the Intergovernmental Panel on Climate Change, edited by T. F. Stocker, D. Qin, G.-K. Plattner, M. Tignor, S. K. Allen, J. Boschung, A. Nauels, Y. Xia, V. Bex and P. M. Midgley, Cambridge University Press, Cambridge, United Kingdom and New York, NY, USA.

Clement, A. C., R. Seager, and M. A. Cane (1999), Orbital controls on the El Niño/Southern Oscillation and the tropical climate, Paleoceanography, 14(4), 441-456, doi: 10.1029/1999pa900013.

Clement, A. C., R. Seager, M. A. Cane, and S. E. Zebiak (1996), An Ocean Dynamical Thermostat, Journal of Climate, 9, 2190-2196.

Cobb, K. M., N. Westphal, H. R. Sayani, J. T. Watson, E. Di Lorenzo, H. Cheng, R. L. Edwards, and C. D. Charles (2013), Highly variable El Niño-Southern Oscillation throughout the Holocene, Science, 339(6115), 67-70, doi: 10.1126/science.1228246.

Conroy, J. L., J. T. Overpeck, J. E. Cole, T. M. Shanahan, and M. Steinitz-Kannan (2008), Holocene changes in eastern tropical Pacific climate inferred from a Galápagos lake sediment record, Quaternary Science Reviews, 27(11-12), 1166-1180, doi: 10.1016/j.quascirev.2008.02.015.

de Villiers, S. (2005), Foraminiferal shell-weight evidence for sedimentary calcite dissolution above the lysocline, Deep Sea Research Part I: Oceanographic Research Papers, 52(5), 671-680, doi: 10.1016/j.dsr.2004.11.014.

Dekens, P. S., A. C. Ravelo, and M. D. McCarthy (2007), Warm upwelling regions in the Pliocene warm period, Paleoceanography, 22(3), n/a-n/a, doi: 10.1029/2006pa001394.

Dekens, P. S., D. W. Lea, D. K. Pak, and H. J. Spero (2002), Core top calibration of Mg/Ca in tropical foraminifera: refining paleotemperature estimation, Geochemistry, Geophysics, Geosystems, 3(4).

Dong, L., L. Li, Q. Li, H. Wang, and C. L. Zhang (2015), Hydroclimate implications of thermocline variability in the southern South China Sea over the past 180,000yr, Quaternary Research, 83(2), 370-377, doi: 10.1016/j.yqres.2014.12.003.

Driscoll, R., M. Eliot, T. Russon, K. Welsh, Y. Yokoyama, and A. Tudhope (2014), ENSO reconstructions over the past 60 ka using giant clams (Tridacna sp.) from Papua New Guinea, Geophysical Research Letters, 41, 6819-6825, doi: 10.1002/.

Duprey, N., C. E. Lazareth, T. Corrège, F. Le Cornec, C. Maes, N. Pujol, M. Madeng-Yogo, S. Caquineau, C. Soares Derome, and G. Cabioch (2012), Early mid-

Holocene SST variability and surface-ocean water balance in the southwest Pacific, Paleoceanography, 27(4), PA4207, doi: 10.1029/2012pa002350.

Evans, D., C. Brierley, M. E. Raymo, J. Erez, and W. Müller (2016), Planktic foraminifera shell chemistry response to seawater chemistry: Pliocene–Pleistocene seawater Mg/Ca, temperature and sea level change, Earth and Planetary Science Letters, 438, 139-148, doi: 10.1016/j.epsl.2016.01.013.

Fedorov, A. V., C. M. Brierley, and K. Emanuel (2010), Tropical cyclones and permanent El Niño in the early Pliocene epoch, Nature, 463(7284), 1066-1070, doi: 10.1038/nature08831.

Fedorov, A. V., C. M. Brierley, K. T. Lawrence, Z. Liu, P. S. Dekens, and A. C. Ravelo (2013), Patterns and mechanisms of early Pliocene warmth, Nature, 496(7443), 43-49, doi: 10.1038/nature12003.

Fehrenbacher, J., P. A. Martin, and G. Eshel (2006), Glacial deep water carbonate chemistry inferred from foraminiferal Mg/Ca: A case study from the western tropical Atlantic, Geochemistry, Geophysics, Geosystems, 7(9), n/a-n/a, doi: 10.1029/2005gc001156.

Ford, H. L., A. C. Ravelo, and S. Hovan (2012), A deep Eastern Equatorial Pacific thermocline during the early Pliocene warm period, Earth and Planetary Science Letters, 355-356, 152-161, doi: 10.1016/j.epsl.2012.08.027.

Ford, H. L., A. C. Ravelo, P. S. Dekens, J. P. LaRiviere, and M. W. Wara (2015b), The evolution of the equatorial thermocline and the early Pliocene El Padre mean state, Geophys Res Lett, 42, 4878-4887, doi: 10.1002/.

Ham, Y.-G., and J.-S. Kug (2016), ENSO amplitude changes due to greenhouse warming in CMIP5: Role of mean tropical precipitation in the twentieth century, Geophysical Research Letters, 43, 433-430, doi: 10.1002/2015GL066864.

Haywood, A. M., et al. (2013), Large-scale features of Pliocene climate: results from the Pliocene Model Intercomparison Project, Climate of the Past, 9(1), 191-209, doi: 10.5194/cp-9-191-2013.

Hertzberg, J. E., M. W. Schmidt, T. S. Bianchi, R. W. Smith, M. R. Shields, and F. Marcantonio (2016), Comparison of eastern tropical Pacific TEX86 and Globigerinoides ruber Mg/Ca derived sea surface temperatures: Insights from the Holocene and Last Glacial Maximum, Earth and Planetary Science Letters, 434, 320-332, doi: 10.1016/j.epsl.2015.11.050.

Hill, D. J., et al. (2014), Evaluating the dominant components of warming in Pliocene climate simulations, Climate of the Past, 10(1), 79-90, doi: 10.5194/cp-10-79-2014.

Jia, G., J. Zhang, J. Chen, P. a. Peng, and C. L. Zhang (2012), Archaeal tetraether lipids record subsurface water temperature in the South China Sea, Organic Geochemistry, 50, 68-77, doi: 10.1016/j.orggeochem.2012.07.002.

Johnstone, H. J. H., J. Yu, H. Elderfield, and M. Schulz (2011), Improving temperature estimates derived from Mg/Ca of planktonic foraminifera using X-ray computed tomography–based dissolution index, XDX, Paleoceanography, 26(1), doi: 10.1029/2009pa001902.

Kim, S. T., W. Cai, F.-F. Jin, and J.-Y. Yu (2014a), ENSO stability in coupled climate models and its association with mean state, Climate Dynamics, 42(11-12), 3313-3321, doi: 10.1007/s00382-013-1833-6.

Kim, S. T., W. Cai, F.-F. Jin, A. Santoso, L. Wu, E. Guilyardi, and S.-I. An (2014b), Response of El Niño sea surface temperature variability to greenhouse warming, Nature Climate Change, 4(9), 786-790, doi: 10.1038/nclimate2326.

Koutavas, A., and S. Joanides (2012), El Niño-Southern Oscillation extrema in the Holocene and Last Glacial Maximum, Paleoceanography, 27(4), PA4208, doi: 10.1029/2012pa002378.

Lawrence, K. T., Z. Liu, and T. D. Herbert (2006), Evolution of the eastern tropical Pacific through Plio-Pleistocene glaciation, Science, 312(5770), 79-83, doi: 10.1126/science.1120395.

Lea, D. W., T. A. Mashiotta, and H. J. Spero (1999), Controls on magnesium and strontium uptake in planktonic foraminifera determined by live culturing, Geochimica et Cosmochimica Acta, 63(16), 2369-2379.

Liddy, H. M., S. J. Feakins, and J. E. Tierney (2016), Cooling and drying in northeast Africa across the Pliocene, Earth and Planetary Science Letters, 449, 430-438, doi: 10.1016/j.epsl.2016.05.005.

Liu, Z., J. Kutzbach, and L. Wu (2000), Modeling climate shift of El Niño variability in the Holocene, Geophysical Research Letters, 27(15), 2265-2268.

Liu, Z., Z. Lu, X. Wen, B. L. Otto-Bliesner, A. Timmermann, and K. M. Cobb (2014), Evolution and forcing mechanisms of El Niño over the past 21,000 years, Nature, 515(7528), 550-553, doi: 10.1038/nature13963.

McGregor, H. V., and M. K. Gagan (2004), Western Pacific coral δ18O records of anomalous Holocene variability in the El Niño–Southern Oscillation, Geophysical Research Letters, 31(11), doi: 10.1029/2004gl019972.

McGregor, H. V., M. J. Fischer, M. K. Gagan, D. Fink, S. J. Phipps, H. Wong, and C. D. Woodroffe (2013), A weak El Niño/Southern Oscillation with delayed seasonal growth around 4,300 years ago, Nature Geoscience, 6(11), 949-953, doi: 10.1038/ngeo1936.

Medina-Elizalde, M., D. W. Lea, and M. S. Fantle (2008), Implications of seawater Mg/Ca variability for Plio-Pleistocene tropical climate reconstruction, Earth and Planetary Science Letters, 269(3-4), 585-595, doi: 10.1016/j.epsl.2008.03.014.

Moy, C. M., G. O. Seltzer, D. T. Rodbell, and D. M. Anderson (2002), Variability of El Nino-Southern Oscillation activity at millennial timescales during the Holocene epoch, Nature, 420(6912), 162-165, doi: 10.1038/nature01163.

O'Brien, C. L., G. L. Foster, M. A. Martínez-Botí, R. Abell, J. W. B. Rae, and R. D. Pancost (2014), High sea surface temperatures in tropical warm pools during the Pliocene, Nature Geoscience, 7(8), 606-611, doi: 10.1038/ngeo2194.

Pagani, M., Z. Liu, J. LaRiviere, and A. C. Ravelo (2009), High Earth-system climate sensitivity determined from Pliocene carbon dioxide concentrations, Nature Geoscience, 3(1), 27-30, doi: 10.1038/ngeo724.

Rashid, H. A., A. C. Hirst, and S. J. Marsland (2016), An atmospheric mechanism for ENSO amplitude changes under an abrupt quadrupling of CO2 concentration in CMIP5 models, Geophysical Research Letters, 43, 1687-1694, doi: 10.1002/2015GL066768.

Regenberg, M., A. Regenberg, D. Garbe-Schönberg, and D. W. Lea (2014), Global dissolution effects on planktonic foraminiferal Mg/Ca ratios controlled by the calcite-saturation state of bottom waters, Paleoceanography, 29(3), 127-142, doi: 10.1002/2013pa002492.

Regenberg, M., D. Nürnberg, S. Steph, J. Groeneveld, D. Garbe-Schönberg, R. Tiedemann, and W.-C. Dullo (2006), Assessing the effect of dissolution on planktonic foraminiferal Mg/Ca ratios: Evidence from Caribbean core tops, Geochemistry, Geophysics, Geosystems, 7(7), n/a-n/a, doi: 10.1029/2005gc001019.

Richey, J. N., and J. E. Tierney (2016), GDGT and alkenone flux in the northern Gulf of Mexico: Implications for the TEX86and UK'37paleothermometers, Paleoceanography, 31(12), 1547-1561, doi: 10.1002/2016pa003032.

Rodbell, D. T., G. O. Seltzer, D. M. Anderson, M. B. Abbott, D. B. Enfield, and J. H. Newman (1999), An ~15,000 year record of El Nino-driven alluviation in southwestern Ecuador, Science, 283, 516-520.

Rosenthal, Y., and G. P. Lohmann (2002), Accurate estimation of sea surface temperatures using dissolution-corrected calibrations for Mg/Ca paleothermometry, Paleoceanography, 17(3), 16-11-16-16, doi: 10.1029/2001pa000749.

Rousselle, G., C. Beltran, M.-A. Sicre, I. Raffi, and M. De Rafélis (2013), Changes in sea-surface conditions in the Equatorial Pacific during the middle Miocene–Pliocene as inferred from coccolith geochemistry, Earth and Planetary Science Letters, 361, 412-421, doi: 10.1016/j.epsl.2012.11.003.

Sadekov, A. Y., R. Ganeshram, L. Pichevin, R. Berdin, E. McClymont, H. Elderfield, and A. W. Tudhope (2013), Palaeoclimate reconstructions reveal a strong link between El Niño-Southern Oscillation and Tropical Pacific mean state, Nat Commun, 4, 2692, doi: 10.1038/ncomms3692.

Scroxton, N., S. G. Bonham, R. E. M. Rickaby, S. H. F. Lawrence, M. Hermoso, and A. M. Haywood (2011), Persistent El Niño-Southern Oscillation variation during the Pliocene Epoch, Paleoceanography, 26(2), n/a-n/a, doi: 10.1029/2010pa002097.

Seki, O., G. L. Foster, D. N. Schmidt, A. Mackensen, K. Kawamura, and R. D. Pancost (2010), Alkenone and boron-based Pliocene pCO2 records, Earth and Planetary Science Letters, 292(1-2), 201-211, doi: 10.1016/j.epsl.2010.01.037.

Seki, O., D. N. Schmidt, S. Schouten, E. C. Hopmans, J. S. Sinninghe Damsté, and R. D. Pancost (2012), Paleoceanographic changes in the Eastern Equatorial Pacific over the last 10 Myr, Paleoceanography, 27(3), doi: 10.1029/2011pa002158.

Steph, S., R. Tiedemann, M. Prange, J. Groeneveld, M. Schulz, A. Timmermann, D. Nürnberg, C. Rühlemann, C. Saukel, and G. H. Haug (2010), Early Pliocene increase in thermohaline overturning: A precondition for the development of the modern equatorial Pacific cold tongue, Paleoceanography, 25(2), doi: 10.1029/2008pa001645.

Thompson, D. M., et al. (2017), Tropical Pacific climate variability over the last 6000 years as recorded in Bainbridge Crater Lake, Galápagos, Paleoceanography, doi: 10.1002/2017pa003089.

Tian, B., G. J. Zhang, and V. Ramanathan (2001), Het balance in the Pacific warm pool atmosphere during TOGA COARE and CEPEX, Journal of Climate, 14, 1881-1893.

Trenberth, K. E. (1997), The definition of El Nino, Bulletin of the American Meteorological Society, 78(12), 2771-2777.

Tudhope, A. W., C. P. Chilcott, M. T. McCulloch, E. R. Cook, J. Chappell, R. M. Ellam, D. W. Lea, J. M. Lough, and G. B. Shimmield (2001), Variability in the El Nino-Southern Oscillation through a glacial-interglacial cycle, Science, 291(5508), 1511-1517, doi: 10.1126/science.1057969.

Wara, M. W., A. C. Ravelo, and M. L. Delaney (2005), Permanent El Niño-like conditions during the Pliocene Warm Period, Science, 309, 758-761.

Watanabe, T., et al. (2011), Permanent El Niño during the Pliocene warm period not supported by coral evidence, Nature, 471(7337), 209-211, doi: 10.1038/nature09777.

White, S. M., A. C. Ravelo, and P. J. Polissar (2018), Dampened El Niño in the early and mid-Holocene due to insolation-forced warming/deepening of the thermocline, Geophysical Research Letters, 45, doi: 10.1002/2017GL075433.

Woodroffe, C. D. (2003), Mid-late Holocene El Niño variability in the equatorial Pacific from coral microatolls, Geophysical Research Letters, 30(7), doi: 10.1029/2002gl015868.

Zhang, Y. G., M. Pagani, and Z. Liu (2014a), A 12-million-year temperature history of the tropical Pacific Ocean, Science, 344(6179), 84-87, doi: 10.1126/science.1246172.

Zhang, Z., G. Leduc, and J. P. Sachs (2014b), El Niño evolution during the Holocene revealed by a biomarker rain gauge in the Galápagos Islands, Earth and Planetary Science Letters, 404, 420-434, doi: 10.1016/j.epsl.2014.07.013.

Zheng, X.-T., S.-P. Xie, L.-H. Lv, and Z.-Q. Zhou (2016), Intermodel uncertainty in ENSO amplitude change tied to Pacific Ocean warming pattern, Journal of Climate, 29, 7265-7279, doi: 10.1175/JCLI-D-16-0039.1.

## Chapter 2: Dampened El Niño in the early and mid-Holocene due to insolation-forced warming of the thermocline

**Sarah M. White[1], A. Christina Ravelo[2], Pratigya J. Polissar[3]**

[1] Department of Earth and Planetary Sciences, University of California, Santa Cruz, CA

[2] Department of Ocean Sciences, University of California, Santa Cruz, CA.

[3] Department of Biology and Paleoenvironment, Lamont Doherty Earth Observatory of Columbia University, NY.

Corresponding author: Sarah White (smwhite@ucsc.edu)

**Key Points:**

- Our new data show a reduced amplitude of El Niño events during the early and mid-Holocene.
- Overall, proxy data supports both a June insolation-forced trend in ENSO strength, and decadal-centennial variability in ENSO strength.
- The best-supported mechanism for insolation forcing of Holocene ENSO is a weaker upwelling feedback, due to a warmer/deeper thermocline.

**Abstract**

El Niño-Southern Oscillation (ENSO) dominates interannual climate variability, thus understanding its response to climate forcing is critical. ENSO's sensitivity to changing insolation is poorly understood, due to contrasting interpretations of Holocene proxy records. Some records show dampened ENSO during the early to mid-Holocene, consistent with insolation forcing of ENSO amplitude, but other records emphasize decadal-centennial fluctuations in ENSO strength, with no clear trend. To clarify Holocene ENSO behavior, we collected proxy data spanning the last ~12 kyr, and find relatively low El Niño amplitude during the early to mid-Holocene. Our data, together with published work, indicate both a long-term trend in ENSO strength due to June insolation forcing and high-amplitude decadal-centennial fluctuations; both behaviors are shown in models. The best-supported mechanism for insolation-driven dampening of ENSO is weakening of the upwelling feedback by insolation-forced warming of thermocline source waters. Elucidating the thermocline's role will help predict future ENSO change.

## 1 Introduction

El Niño-Southern Oscillation (ENSO) is a key source of interannual climate variability, with global impacts including drought, floods, coral bleaching, and decreased fisheries yield. It remains uncertain whether ENSO will strengthen or weaken in response to anthropogenic climate change [*Christensen et al.*, 2013], due in part to a lack of understanding of ENSO's sensitivity to external forcing and

tropical Pacific mean climate. This ambiguity stems from contrasting conclusions drawn from Holocene proxy reconstructions of ENSO. Many reconstructions, including those derived from individual foraminifera, precipitation-sensitive indices, and corals/mollusks, show early and mid-Holocene dampening of ENSO; that is, El Niño and La Niña events had a lower amplitude and/or were less frequent relative to the late Holocene [*Chen et al.*, 2016; *Conroy et al.*, 2008; *Driscoll et al.*, 2014; *Duprey et al.*, 2012; *Koutavas and Joanides*, 2012; *McGregor and Gagan*, 2004; *McGregor et al.*, 2013; *Moy et al.*, 2002; *Rodbell et al.*, 1999; *Sadekov et al.*, 2013; *Thompson et al.*, 2017; *Tudhope et al.*, 2001; *Woodroffe*, 2003; *Zhang et al.*, 2014b]. These reconstructions implicate external forcing of ENSO amplitude by insolation. However, recent compilations of many coral/mollusk records depict a Holocene ENSO history dominated by decadal-centennial fluctuations, similar to that of the last millennium [*Cobb et al.*, 2003], with no long-term trend in ENSO strength attributable to insolation forcing [*Cobb et al.*, 2013; *Emile-Geay et al.*, 2016]. In contrast to the divergent interpretations of proxy data, modeling studies are unanimous in finding that changing insolation dampened ENSO during the early and mid-Holocene [e.g. *An and Choi*, 2014; *Braconnot et al.*, 2012; *Bush*, 2007; *Chiang et al.*, 2009; *Clement et al.*, 2000; *Liu et al.*, 2014; *Otto-Bliesner et al.*, 2003; *Roberts et al.*, 2014], while also showing high-amplitude decadal-centennial variability in ENSO strength throughout the Holocene [*Liu et al.*, 2014] similar to coral/mollusk reconstructions [*Cobb et al.*, 2013; *Emile-Geay et al.*, 2016]. Although model studies agree that changes in insolation dampened ENSO during the early and mid-Holocene,

they disagree on the mechanism. To validate model results, it is first necessary to develop a consensus view on Holocene ENSO behavior. If the balance of proxy data show a long-term trend in ENSO strength consistent with insolation forcing, then the mechanism by which insolation dampened ENSO can be assessed.

To determine whether there was a long-term trend in Holocene ENSO strength, we reconstructed temperature variability from individual foraminifera from the central equatorial Pacific during the Younger Dryas (YD) and the Holocene, filling key data gaps. Our new findings, together with published studies, provide strong evidence for a long-term trend of dampened ENSO during the early to mid-Holocene, consistent with insolation forcing, superimposed on high-amplitude decadal-centennial fluctuations in ENSO strength. This interpretation reconciles apparently divergent reconstructions of Holocene ENSO, and is consistent with model results. To test model-derived mechanisms for insolation-driven dampening of ENSO, we synthesized proxy data on Holocene tropical Pacific mean climate. We find that a weakened upwelling feedback, stemming from insolation-driven warming/deepening of the equatorial Pacific thermocline, is the best-supported mechanism for early and mid-Holocene ENSO dampening.

## 2 Methods and approach

### *2.1 Study site*

We used marine sediment cores MGL1208-14MC and 12GC (0°S, 156°W, 3049 m depth) from the central equatorial Pacific, near the Line Islands (Figure S1), where the mixed layer is ~100 m deep and the thermocline is at ~150 m (Figure S2). Our site is ideal for studying ENSO; the seasonal cycle amplitude in the mixed layer is only ±0.4°C, whereas the average peak sea surface temperature (SST) anomaly during El Niño events is +2°C [*Carton and Giese*, 2008]. Therefore, ENSO dominates SST variability at our site, unlike locations further east [*Thirumalai et al.*, 2013] (Figure S1). The modern SST distribution, based on the past 50 years of data [the SODA v2.1.6 dataset, *Carton and Giese*, 2008], shows that the warmest temperatures occur exclusively during El Niño events; seasonal variations are confined to the middle of the distribution. Further advantages of the site are that it lies within the Niño3.4 region, where ENSO events are defined [*Trenberth*, 1997], and enables side-by-side comparison to Line Islands coral records [e.g. *Cobb et al.*, 2013].

### *2.2 Analytical approach*

To reconstruct El Niño amplitude, we acquired Mg/Ca-based temperatures from individual tests of *Globigerinoides trilobus*, a mixed layer-dwelling foraminifer. We also measured Mg/Ca of pooled tests of *G. trilobus* through the Holocene and late deglaciation, to elucidate average mixed-layer temperatures at the site. Foraminiferal Mg/Ca was converted to SST using the Anand et al. [2003] multispecies calibration

with the Regenberg et al. [2014] multispecies dissolution correction. Radiocarbon dates were generated for every interval with individual foraminiferal data. See supporting information (SI) for details.

Foraminifera capture ~1 month "snapshots" of their environment, so by measuring 70-90 individuals from each sample, we reconstructed a distribution of SST representing monthly variability during seven time periods. Bioturbation broadens the time interval represented in each sample to ~800 years, given a 5 cm bioturbation depth [*Trauth et al.*, 1997]. To compare the SST distribution in each downcore interval to that of the coretop, we use quantile-quantile plots, following the method of Ford et al. [2015a]. Quantile-quantile plots allow visual isolation and comparison of certain parts of the distribution, enabling separation of ENSO-related variability from seasonality, which is impossible with a simple metric such as standard deviation. A distribution with less extreme warm temperatures (that is, the warmest temperatures are not as far above the mean) indicates lower amplitude of El Niño events, relative to the coretop. To highlight differences in the warmest quantiles, downcore quantile data are normalized to the coretop distribution (Figure S3 and SI).

## 3 Results

### *3.1 Comparison of coretop G. trilobus temperatures to benchmark datasets*

Individual *G. trilobus*-derived temperatures from the coretop (dated to 4030 YBP) agree with the modern temperature distribution in the mixed layer at our site

[*Carton and Giese*, 2008] (Figures 1 and S4, SI). This agreement implies that any bias from vertical migration or seasonal preference of the foraminifera is small. Our coretop data are also similar to contemporaneous coral data from nearby Christmas Island [*Cobb et al.*, 2013] (Figure S5 and SI), enabling direct comparison of the datasets. To minimize systematic biases in *G. trilobus* temperatures due to bioturbation and other processes, we present all downcore data as deviations from the coretop rather than the modern SST distribution. Confidence intervals are estimated by resampling the empirical continuous distribution function of each sample using a Monte Carlo simulation (see SI for details).

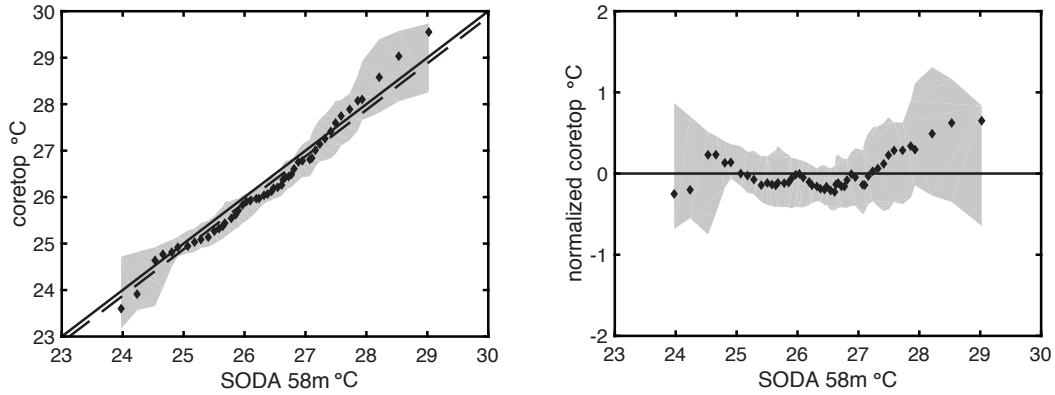


**Figure 1. *G. trilobus* as a recorder of modern temperature.**
Quantile-quantile (left) and normalized quantile-quantile (right) plots of modern monthly gridded temperatures in the middle of the mixed layer (58 m depth) near our site, (the SODA v2.1.6 dataset, *[Carton and Giese*, 2008]), plotted versus individual G. trilobus temperatures from the coretop. The coretop matches the modern temperature distribution within 90% confidence intervals (gray region).

*3.2 Sensitivity tests*

Sensitivity tests, performed by manipulating modern temperatures from the SODA dataset [*Carton and Giese*, 2008] and subsampling them, show that our

method can detect a decrease in El Niño amplitude as small as 20%, within 90% confidence intervals, and that even a 50% decrease in seasonal cycle amplitude doesn't affect the warmest quantiles. We also find that our observed trend in El Niño amplitude is unlikely to have arisen from random sampling of decadal-centennial variability in either ENSO strength [as described by *Wittenberg*, 2009] or in annual mean temperature [as described for the Line Islands region by *Cobb et al.*, 2003] in the absence of a true long-term trend (Figures S6-S8 and SI).

*3.3 Downcore temperature data*

There is a clear trend in our individual foraminiferal data: the late Holocene and YD intervals are similar to the coretop, whereas the five early and mid-Holocene intervals have less extreme warm temperatures, significant at the 90% confidence level, indicating reduced El Niño amplitude (Figure 2). These findings remain significant at the 80% confidence level after accounting for 0.4°C uncertainty in each data point, which stems from instrumental uncertainty, intratest variations, differential dissolution, and changes in salinity (Figure S9 and SI). Our findings remain similarly significant if we use the late Holocene sample as the baseline for comparison, instead of the coretop (Figure S10). Long-term average Mg/Ca-derived SST estimates at our site show similar trends to those from the East Equatorial Pacific (EEP), with slightly lower temperatures in the mid-Holocene relative to the early Holocene (Figure S11).

**Figure 2. Mixed layer temperature distributions from seven time intervals during the Holocene and YD at the Line Islands.**
Normalized quantile-quantile plots show the difference of each downcore quantile from the coretop quantile (y-axis) versus the coretop quantiles (x-axis). Patterned region highlights quantiles attributed solely to El Niño events, where points below the zero line indicate reduced amplitude of El Niño events. Gray shaded region indicates 90% confidence intervals.

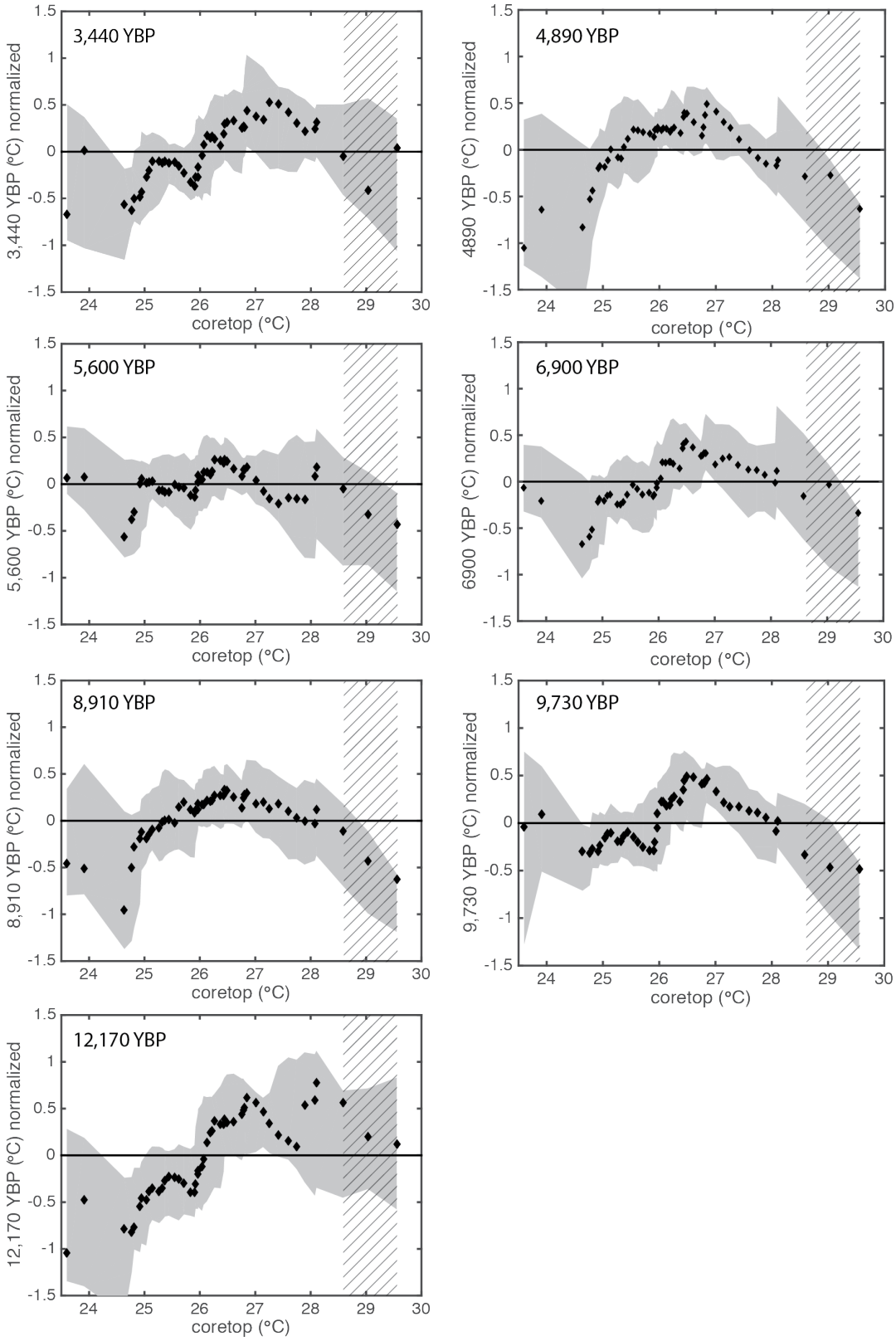
3,440 YBP
3,440 YBP (°C) normalized
4,890 YBP
4890 YBP (°C) normalized
5,600 YBP
5,600 YBP (°C) normalized
6,900 YBP
6900 YBP (°C) normalized
8,910 YBP
8,910 YBP (°C) normalized
9,730 YBP
9,730 YBP (°C) normalized
12,170 YBP
12,170 YBP (°C) normalized
coretop (°C)
1.5
1
0.5
0
-0.5
-1
-1.5
24
25
26
27
28
29
30

## 4 The Holocene history of ENSO

Our finding of reduced El Niño amplitude during the early and mid-Holocene, compared to the late Holocene and YD, is best evaluated in the context of previously published data and model studies, which are synthesized and presented in the following sections. Data (Table S3) from individual foraminifera, precipitation records, and corals/mollusks are consistent with models indicating both high-amplitude decadal-centennial fluctuations and a long-term trend in ENSO strength [*Liu et al.*, 2014], and therefore provide evidence of insolation forcing of ENSO.

### *4.1 Individual foraminiferal records*

Individual foraminiferal data in the EEP [*Koutavas and Joanides*, 2012] show strongly dampened ENSO in the mid-Holocene but more variability in ENSO strength during the early Holocene. This early Holocene variability was originally interpreted to indicate enhanced ENSO strength; however, it can also be explained by greater decadal-centennial variability in ENSO strength (section 4.3) superimposed on dampened ENSO on average, which agrees with similar data from a nearby site [*Sadekov et al.*, 2013]. Eastern tropical Pacific warm pool subsurface temperatures show slightly dampened variability in the early Holocene, albeit not statistically significant [*Leduc et al.*, 2009]. In any case, these subsurface data to not contradict our results since a deeper thermocline (section 5.1) can alter subsurface variability independently of changes in ENSO. In general, individual foraminiferal records are

consistent with dampened ENSO during the early to mid-Holocene, in agreement with our findings, and support insolation forcing of ENSO.

### *4.2 Precipitation-based records*

Records of El Niño-related precipitation all show dampened El Niño in the mid-Holocene [*Chen et al.*, 2016; *Conroy et al.*, 2008; *Moy et al.*, 2002; *Rodbell et al.*, 1999; *Thompson et al.*, 2017; *Zhang et al.*, 2014b]. Some show dampened El Niño through the entire early and mid-Holocene [*Moy et al.*, 2002; *Rodbell et al.*, 1999] or very dampened El Niño in the mid-Holocene and moderately dampened El Niño in the early Holocene [*Chen et al.*, 2016], but a few studies from a Galapagos lake indicate that El Niño was not dampened in the early Holocene [*Conroy et al.*, 2008; *Zhang et al.*, 2014b]. Overall, for the mid-Holocene, precipitation-based El Niño records agree with our results, but for the early Holocene, these records disagree among themselves and (in some cases) with our data, likely due to greater non-ENSO related precipitation variability in the early Holocene caused by meltwater forcing [*Bush*, 2007; *Liu et al.*, 2014] (section 4.4). As such, precipitation data do not contradict dampened ENSO during both the early and mid-Holocene.

### *4.3 Coral and mollusk records*

Several coral and mollusk records, which provide decades-long, monthly-resolved records of ENSO from discrete time intervals, show dampened ENSO in the

early and mid-Holocene [*Carre et al.*, 2014; *Driscoll et al.*, 2014; *Duprey et al.*, 2012; *McGregor and Gagan*, 2004; *McGregor et al.*, 2013; *Tudhope et al.*, 2001; *Woodroffe*, 2003]. However, compilations of many such records depict a more complex picture, with substantially dampened ENSO from ~3-5 ka, and dampened ENSO on average but more record-to-record variability in ENSO strength during the early Holocene, which was argued to be inconsistent with a long-term trend in ENSO strength [*Cobb et al.*, 2013; *Emile-Geay et al.*, 2016]. The record-to-record variability likely reflects decadal-centennial variations in ENSO strength, as shown in proxy data from the last millennium [*Cobb et al.*, 2013] and in unforced model runs [*Wittenberg*, 2009; *Wittenberg et al.*, 2014]. These unforced short-term fluctuations were likely present throughout the Holocene, and may have been of similar magnitude to a long-term trend in ENSO strength from insolation forcing [*Liu et al.*, 2014, shown in Figure 3d], making detection of a trend difficult [*Liu et al.*, 2014]. In addition, there may have been forced decadal-centennial fluctuations in ENSO strength during the early Holocene (section 4.4), further hampering detection of a trend. Overall, the coral data can be interpreted as showing dampened ENSO on average during the early to mid-Holocene relative to the late Holocene, consistent with insolation forcing, combined with superimposed decadal-centennial variability in ENSO strength. These two behaviors are not mutually exclusive; both are shown in models [*Liu et al.*, 2014].

*4.4 Decadal-centennial forcings of ENSO strength during the early Holocene*

Some of the observed decadal-centennial variability in early Holocene ENSO strength may have been forced by changing meltwater [*Braconnot et al.*, 2012; *Liu et al.*, 2014] or total solar irradiance [*Marchitto et al.*, 2010]. Models find that increased meltwater in the North Atlantic strengthens ENSO [*Braconnot et al.*, 2012; *Liu et al.*, 2014; *Timmermann et al.*, 2007]. At 10 ka, sea level was ~40 m lower than today [*Bard et al.*, 1996], so meltwater pulses in the early Holocene could have created decadal-centennial periods of strengthened ENSO superimposed on a long-term insolation-forced dampening of ENSO. Meltwater pulses would also disrupt teleconnections between precipitation-sensitive proxies in the eastern Pacific [*Conroy et al.*, 2008; *Zhang et al.*, 2014b] and Nino3.4 SST, creating an increase in precipitation variability unrelated to ENSO [*Liu et al.*, 2014]. Another potential source of decadal-centennial forcing is total solar irradiance, which varied more in the early Holocene than the mid- to late Holocene [*Marchitto et al.*, 2010]. Changing solar irradiance is theoretically capable of affecting ENSO via ocean dynamical cooling [*Emile-Geay et al.*, 2007], and is correlated with centennial-scale variations in early Holocene ENSO [*Marchitto et al.*, 2010]. Overall, the apparent increase in decadal-centennial variability in early Holocene ENSO strength shown in coral/mollusk records [*Cobb et al.*, 2013; *Emile-Geay et al.*, 2016] is likely an accurate representation of ENSO's behavior in response to a range of forcings. However, these short-term fluctuations cannot be taken as evidence for the lack of a long-term insolation-forced trend.

*4.5 Model results*

Model studies are unanimous in simulating dampened ENSO during the early and mid-Holocene [e.g. *An and Choi*, 2014; *Braconnot et al.*, 2012; *Bush*, 2007; *Chiang et al.*, 2009; *Clement et al.*, 2000; *Otto-Bliesner et al.*, 2003; *Pausata et al.*, 2017; *Roberts et al.*, 2014]. Model results from discrete time intervals are reported relative to preindustrial conditions, whereas our data are reported relative to the coretop (Figure 3). Despite the difference in baseline, our findings are consistent with model results because both fall on a Holocene-long trend in ENSO strength [Figure 3d, *Liu et al.*, 2014] in which both the early and mid-Holocene had dampened ENSO compared to our two youngest samples. The Liu et al. [2014] results also show high-amplitude decadal-centennial variations in ENSO strength. Overall, model results are consistent with Holocene proxy data in showing a long-term trend in ENSO strength due to insolation forcing, superimposed on short-term fluctuations in ENSO strength. Importantly, models show that these different scales of variability are not mutually exclusive.

**Figure 3. Reconstructions of ENSO in the context of model results, thermocline temperatures, and composite SST records from the WEP and EEP.** Wide shaded bars show sample intervals from this study, each spanning ~800 years; pink/blue indicate lower/similar amplitude El Niño events, respectively, to the coretop. Narrow bars show modeling results; dark pink/dark blue show reduced/similar ENSO to preindustrial, from modeling studies at 3.5 ka [*Otto-Bliesner et al.*, 2003], 6 ka [*An and Choi*, 2014; *Bush*, 2007; *Chiang et al.*, 2009; *Otto-Bliesner et al.*, 2003], 8.5 ka [*Otto-Bliesner et al.*, 2003; *Roberts et al.*, 2014], 9 ka [*Bush*, 2007], 9.5 ka [*Braconnot et al.*, 2012], and 11 ka [*Otto-Bliesner et al.*, 2003], respectively. a) September (dashed) and June (solid) insolation at the equator [*Berger*, 1978]. b) Subsurface temperatures from *P. obliquiloculata* Mg/Ca in the WEP (light blue [*Dang et al.*, 2012] and purple [*Xu et al.*, 2008]), and *N. dutertrei* Mg/Ca in the EEP (dark blue [*Sadekov et al.*, 2013]). c) Composite SST anomalies (with respect to average temperature 0-4 ka) from WEP Mg/Ca and coral Sr/Ca records (dark red), EEP Mg/Ca records (orange), and EEP alkenone records (olive green). Colored regions denote standard deviation of temperatures from all composited records. d) Transient model run forced with insolation, $CO_2$, meltwater, and ice sheets, showing standard deviation of SST in the Nino3.4 box bandpass filtered at 1.5-7 years [*Liu et al.*, 2014] (thin gray line), and 700 yr smoothed model data (thick gray line).

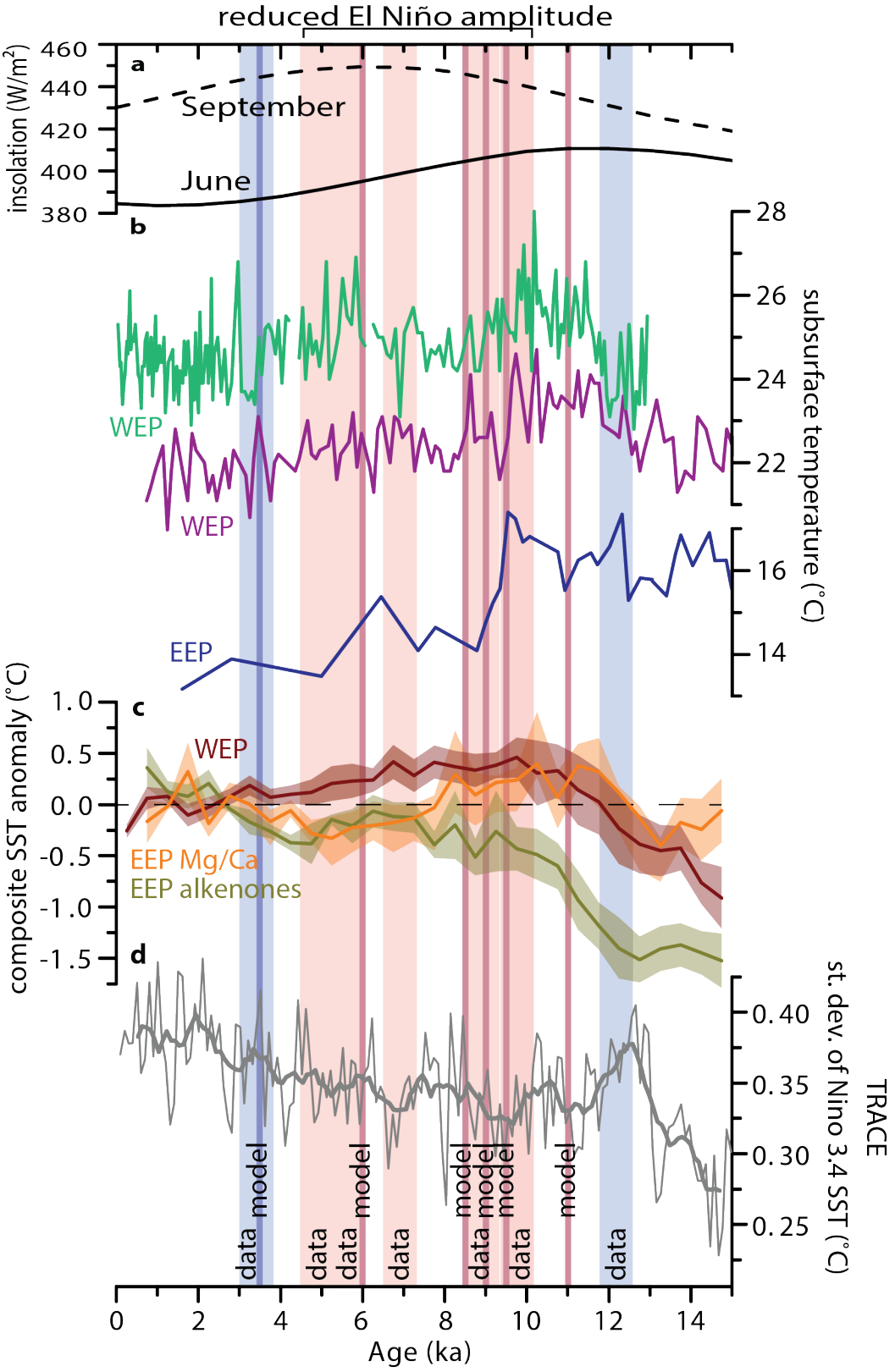
reduced El Niño amplitude
a
insolation (W/m²)
460
440
420
400
380
September
June
b
28
26
24
22
subsurface temperature (°C)
WEP
WEP
16
14
EEP
c
composite SST anomaly (°C)
1.0
0.5
0.0
-0.5
-1.0
-1.5
WEP
EEP Mg/Ca
EEP alkenones
d
0.40
0.35
0.30
0.25
st. dev. of Nino 3.4 SST (°C)
TRACE
data
model
data
data
model
data
model
model
data
model
data
0
2
4
6
8
10
12
14
Age (ka)

## 5 Mechanism of observed trend in Holocene ENSO strength

In general, Holocene proxy data show dampened ENSO in the early to mid-Holocene relative to the late Holocene, consistent with insolation forcing of ENSO. This interpretation agrees with numerous modeling and proxy studies [e.g. *An and Choi*, 2014; *Braconnot et al.*, 2012; *Bush*, 2007; *Chen et al.*, 2016; *Chiang et al.*, 2009; *Clement et al.*, 2000; *Koutavas and Joanides*, 2012; *Liu et al.*, 2014; *McGregor and Gagan*, 2004; *Otto-Bliesner et al.*, 2003; *Roberts et al.*, 2014; *Rodbell et al.*, 1999; *Tudhope et al.*, 2001]. Given data-model agreement, and armed with our new data compilation, we are now poised to address the question: by what mechanism did insolation dampen ENSO? We review three mechanisms, and test whether they are supported by proxy data of tropical Pacific surface and subsurface temperature. We also discuss the implications of June versus September insolation forcing.

### *5.1 Weaker upwelling feedback*

One proposed mechanism for Holocene ENSO dampening is weakening of the upwelling feedback, caused by mean warming of the thermocline due to insolation-forced warming of southern subtropical/midlatitude surface waters [*Liu et al.*, 2000; *Liu et al.*, 2014; *Roberts et al.*, 2014]. A warmer thermocline, with respect to SST, weakens stratification, decreasing the effect of upwelling on SST and weakening a key positive feedback that generates ENSO [*Liu et al.*, 2014]. Thermocline waters in the equatorial Pacific are sourced from surface waters in the subtropics [*Hanawa and Talley*, 2001] and midlatitudes, with successively deeper layers of the

thermocline/sub-thermocline sourced from successively higher latitudes [*Toggweiler et al.*, 1991]. Importantly, about three times more water is transported into the equatorial thermocline from the south than from the north [*Johnson and McPhaden*, 1999] because northern waters are blocked by the ITCZ [*Johnson and McPhaden*, 1999; *Lu and McCreary*, 1995]. These southern subtropical/midlatitude surface waters, centered on 120°W and ~20°S-40°S, subduct during austral winter when the mixed layer deepens [*Hanawa and Talley*, 2001; *Johnson and McPhaden*, 1999; *O'Connor et al.*, 2002; *Toggweiler et al.*, 1991; *Wong and Johnson*, 2003]. Therefore, the equatorial thermocline temperature is sensitive to SSTs in the subtropical/midlatitude South Pacific during austral winter, and would thus respond to changing June insolation [*Liu et al.*, 2014].

Another thermocline-based mechanism for dampened early and mid-Holocene ENSO is that changes in insolation weakened the trades in late winter/early spring, allowing westerly wind anomalies to generate downwelling Kelvin waves [*Karamperidou et al.*, 2015]. These waves reached the EEP by late summer/early fall and depressed the thermocline, weakening the upwelling feedback and dampening ENSO [*Karamperidou et al.*, 2015]. Because modeled trade wind strength is tied to the subtropical highs [*Karamperidou et al.*, 2015], this mechanism, as with the thermocline warming mechanism [*Liu et al.*, 2014], is likely driven by changes in June insolation.

To test whether the weaker upwelling feedback mechanism is supported by proxy data, we examined tropical Pacific thermocline records. Subsurface

temperatures in the EEP and West Equatorial Pacific (WEP) show a warmer/deeper thermocline in the early Holocene and cooling toward present [*Dang et al.*, 2012; *Sadekov et al.*, 2013; *Xu et al.*, 2008] (Figure 3b), with weaker EEP stratification in the early and mid-Holocene [data from *Sadekov et al.*, 2013]. Subsurface temperatures on the Peru margin were also warmer in the early Holocene [*Bova et al.*, 2015; *Kalansky et al.*, 2015], consistent with evidence for a warmer early and mid-Holocene thermocline in the open ocean. The Karamperidou et al. [2015] mechanism predicts a deeper thermocline only in late summer/early fall, not in the annual average, but this likely aligns with seasonal bias in the proxy record, which emphasizes the upwelling season [*Thunell et al.*, 1983]. No proxy records exist from the thermocline source region, but the nearest record (from the Peru margin at 30°S) shows peak SSTs in the early Holocene that cooled toward present [*Kaiser et al.*, 2008], agreeing with equatorial thermocline records. Climate models also show warmer SSTs in the thermocline source region during austral winter/spring in the early and mid-Holocene, and show this warm anomaly subducting into the equatorial thermocline [*Liu et al.*, 2014], mirroring modern observations [*Wong and Johnson*, 2003]. Overall, the idea that early and mid-Holocene ENSO dampening resulted from a weaker upwelling feedback due to a warmer/deeper thermocline is well supported.

### *5.2 Decreased air-sea coupling*

Another proposed mechanism for early to mid-Holocene ENSO dampening is that insolation forcing caused cooler SSTs basin-wide, reducing air-sea coupling such

that a given SST anomaly produced a smaller atmospheric anomaly, stabilizing ENSO [e.g. *An and Choi*, 2014]. To assess whether cooler SSTs existed basin-wide in the early and mid-Holocene, we created composite SST anomaly records for the WEP and EEP (Figure 3), using published Mg/Ca and alkenone records (see Figures S11-S12, Table S4, and SI for details). In both the EEP and WEP, our Mg/Ca-based SST anomaly records show warmer SST in the early Holocene, contrary to predictions of cooler SST. However, as shown by [*Gill et al.*, 2016], alkenone records diverge from Mg/Ca records in showing cooler early Holocene SST (Figures 3 and S11). While alkenone records support cooler early and mid-Holocene SST, the majority of reconstructions are based on Mg/Ca data and do not show cooler SSTs; as such, there is not clear support for the decreased air-sea coupling hypothesis [e.g. *An and Choi*, 2014].

### *5.3 Stronger Walker Circulation*

An alternative explanation for Holocene ENSO dampening is that Walker Circulation was stronger, either because higher summer/fall insolation created a larger east-west SST difference [*Clement et al.*, 2000; *Koutavas and Joanides*, 2012; *Otto-Bliesner et al.*, 2003; *Sadekov et al.*, 2013] or because the Asian monsoon and trade winds were stronger [e.g. *Braconnot et al.*, 2012; *Bush*, 2007]. Evidence for a larger east-west SST difference in the early to mid-Holocene is unclear because Mg/Ca and alkenone records disagree in the EEP (Figure 3c). Comparing Mg/Ca data from the WEP and the EEP yields similar east-west SST differences in the early and

late Holocene, implying that enhanced Walker Circulation cannot explain dampened ENSO in the early Holocene. On the other hand, EEP alkenone data yield a higher east-west SST gradient during the early and mid-Holocene, supporting the Walker Circulation hypothesis. However, given the seasonality of alkenone production in the EEP [*Leduc et al.*, 2010; *Timmermann et al.*, 2014], the alkenone-SST estimates likely reflect winter conditions, which would not be expected to dampen ENSO [*Clement et al.*, 2000]. For clarification, we turn to thermocline tilt, a better indicator of Walker Circulation strength than east-west SST difference [*DiNezio et al.*, 2011]. Warmer early and mid-Holocene temperatures in both the EEP and WEP thermocline [*Dang et al.*, 2012; *Sadekov et al.*, 2013; *Xu et al.*, 2008] suggest basin-wide warming and/or deepening of the thermocline, and do not support a steeper thermocline tilt and strengthened Walker Circulation.

Our conclusion that the stronger Walker Circulation mechanism is not well supported differs from other studies, which argue that changing east-west SST difference does explain variations in ENSO strength [*Koutavas and Joanides*, 2012; *Sadekov et al.*, 2013]. However, Koutavas and Joanides [2012] rely on ENSO being dampened in the mid- but not early Holocene, contrary to our results, and Sadekov et al. [2013] combine temperature records from the EEP and the eastern tropical Pacific warm pool, which does not represent the EEP or Walker Circulation. Overall, considering our new early Holocene ENSO data and SST synthesis, the stronger Walker Circulation mechanism is not well supported.

*5.4 June versus September insolation forcing*

Because September insolation is always higher than June insolation at the equator, it was originally proposed as the driver of long-term changes in ENSO [*Clement et al.*, 2000]. Mechanisms that operate entirely within the tropics, including the decreased air-sea coupling and stronger Walker Circulation mechanisms, would thus be expected to produce changes in ENSO that follow September insolation timing. However, our finding of dampened ENSO during both the early and mid-Holocene implicates June, not September, insolation as the driver (Figure 3a). June insolation forcing implies an extratropical mechanism of ENSO dampening, supporting the weaker upwelling feedback hypothesis (including changes stemming from mean annual warming or seasonal deepening).

## 6 El Niño during the Younger Dryas

Our data from 12,170 YPB, during the YD, show similar El Niño amplitude as the late Holocene. Bioturbation, age uncertainty, and possible changes in sedimentation rate may mean that our sample contains some non-YD specimens; higher resolution data are needed to confirm our observations. However, our findings are in rough agreement with model results and individual foraminiferal records [*Liu et al.*, 2014; *Sadekov et al.*, 2013], which show slightly stronger ENSO. Similar or strengthened ENSO during the YD cannot be attributed to insolation; instead, it is likely linked to meltwater forcing. Models find that meltwater input to the North Atlantic amplifies ENSO via a southward shift of the intertropical convergence zone

(ITCZ), which weakens the EEP seasonal cycle and thereby strengthens ENSO via frequency entrainment [*Braconnot et al.*, 2012; *Liu et al.*, 2014; *Timmermann et al.*, 2007]. Data showing a southward shift in the ITCZ over the EEP during the YD [e.g. *Benway et al.*, 2006] support this mechanism.

## 7 Conclusions

Our new Holocene ENSO data and synthesis supports the idea that changing June insolation dampened ENSO during the early and mid-Holocene. This forced evolution of ENSO was likely accompanied by large decadal-centennial variability in ENSO strength, as suggested previously. However, this variability does not preclude a long-term trend, as has been previously argued. The best supported mechanism for early and mid-Holocene ENSO dampening is a weakening of the upwelling feedback, due to insolation-forced mean warming or seasonal deepening of the thermocline. Mechanisms that invoke decreased air-sea coupling and stronger Walker circulation are not well supported by the data. Currently, the effect of stratification and upwelling relative to Walker Circulation is a source of disparity among predictions of ENSO under anthropogenic climate change [*DiNezio et al.*, 2012]. Given the importance of the upwelling feedback in the Holocene evolution of ENSO, improving its representation in models should be a key target for improving predictions of ENSO behavior.

**Acknowledgments, Samples, and Data**

We thank Jean Lynch-Stieglitz and the rest of the MGL1208 shipboard party, Rob Franks for analytical assistance, and Tom Guilderson for radiocarbon analysis. Funding was provided by NSF grants OCE-1405178 and 1204254, and student grants from the Geological Society of America/ExxonMobil and Friends of Long Marine Lab. Our data are deposited at the National Oceanic and Atmospheric Administration National Climatic Data Center. We thank two anonymous reviewers, whose thoughtful comments brought to light some interesting points, and two previous reviewers, whose feedback on an earlier version of this manuscript improved it greatly.

**Supporting Information for Dampened El Niño in the early and mid-Holocene due to insolation-forced warming of the thermocline**

## Text S1. Analytical Methods

*S1.1 Individual foraminiferal analyses*

To reconstruct temperature variability, we measured individual *Globigerinoides trilobus* (i.e. *Globigerinoides sacculifer* without sac-like final chamber), which inhabits the mixed layer in the equatorial Pacific [*Faul et al.*, 2000; *Watkins et al.*, 1996]. Individual *G. trilobus* were analyzed for Mg/Ca by laser ablation-inductively coupled plasma-mass spectrometry (LA-ICP-MS) following the protocol of [*Sadekov et al.*, 2009]. To avoid ontogenetic effects [*Elderfield et al.*, 2002], we used a narrow size fraction (350-425 μm). Sample preparation was similar to that described in previous studies [*Eggins et al.*, 2003; *Sadekov et al.*, 2009; *Vetter et al.*, 2013], and included sonicating each specimen in deionized water for two minutes and rinsing with methanol. The final chamber of the foraminiferal shell was then removed from the rest of the shell with a microspatula and mounted onto carbon tape for analysis.

Trace element analyses were performed with a laser ablation system (Photon Machines Analyte.193 with HelEx sample cell) coupled to a Thermo ElementXS inductively coupled plasma-mass spectrometer, using methods similar to [*Ford et al.*, 2015a], which were based on those of [*Eggins et al.*, 2003]. Specimens were analyzed from inner to outer shell surface, and data acquisition lasted on average 40-60 s. Four 50 μm spots were ablated from each specimen and analyzed for selected isotopes

($^{11}$B, $^{24}$Mg, $^{25}$Mg, $^{27}$Al, $^{43}$Ca, $^{44}$Ca, $^{55}$Mn, $^{66}$Zn, $^{88}$Sr). Elemental ratios from the four ablated spots were averaged to get one representative value. Average intra-test standard deviation for Mg/Ca is 0.09 mmol/mol; specimens with a standard deviation >0.20 mmol/mol were not included in data. $^{27}$Al and $^{55}$Mn were used as indicators of clay and oxide contamination, and parts of the data traces that had peaks in these isotopes were removed before computing mean elemental ratios, as was the Mg peak associated with the inner surface of the shell. As such, our data should include very little influence from contamination.

NIST glass standard 610 was analyzed repeatedly throughout each analytical run, and was used to compute a time-varying, isotope-specific calibration which corrects for any slight drift in elemental intensities which occurs over the course of an analytical run. The NIST glass was analyzed at 4 Hz and 2.77 J/cm$^2$ laser fluence, with a mean value and 1σ standard deviation for Mg/Ca of 8.75 ± 0.06 mmol/mol (n = 333 over 26 analytical days). Carbonate standards and samples were analyzed at 4 Hz and 1.01 J/cm$^2$ laser fluence. Carbonate standard mean value and 1σ standard deviation for JCt-1, MACS-3, and JCp-1 for Mg/Ca was 1.20 ± 0.19 mmol/mol (n=404), 7.75 ± 0.44 mmol/mol (n=455), and 4.15 ±0.44 mmol/mol (n=108), respectively.

*S1.2 Pooled foraminiferal analyses*

Pooled samples of 50 G. trilobus specimens were analyzed to generate a record of average temperature through the Holocene and late deglaciation at the site. Samples (without sac-like final chamber, 350-425 μm size fraction) were gently

crushed, homogenized, and partitioned into aliquots prior to cleaning. Cleaning was performed according to the protocol of Martin and Lea [2002], which includes reductive and oxidative cleaning steps, a weak acid leach, and a final rinse in acid-cleaned vials. Mg/Ca analyses are performed on a PerkinElmer Optima 8300 inductively coupled plasma optical emission spectrometer (ICP-OES). Long-term Mg/Ca reproducibility (1σ) for an in-house liquid consistency standard (FLCS2, mean Mg/Ca=3.30) is 0.03 mmol/mol.

**Text S2. Mg/Ca temperature calculations**

To calculate temperature from foraminiferal calcite, we apply a multispecies dissolution correction to the measured Mg/Ca value [*Regenberg et al.*, 2014], using a modern value of $\Delta[CO_3^{2-}]$ = 2 μmol/kg calculated with CO2calc software [*Robbins et al.*, 2010], derived from temperature, salinity, and carbon system data collected on the CLIVAR P16 line at 0°N, 151°W [*Feely et al.*, 2008]. We then apply a sediment trap-based multispecies temperature calibration [*Anand et al.*, 2003], Mg/Ca = 0.38±0.02*exp(0.090±0.003*T), where T is temperature. Sixty-eight to ninety specimens were analyzed from each time interval; the number of specimens and average calculated temperature for each interval are shown in Table S1.

**Text S3. Radiocarbon age determination and age model**

Radiocarbon dates were generated for every sediment interval for which we collected single foraminiferal data, including the coretop and five downcore intervals (spaced every 5 cm) in core 14MC, and 24-25 cm and 28-29 cm depth in core 12GC. Radiocarbon ages were obtained from G. ruber, a mixed layer-dwelling species with

very similar depth habitat to the species used for individual foraminiferal analyses (G. trilobus). Samples were sonicated in DI water and rinsed with methanol, then prepared and analyzed at Lawrence Livermore National Laboratory's Center for Accelerator Mass Spectrometry, following standard methodology in the graphite preparation lab. Radiocarbon ages were converted to calendar ages using the MARINE13 calibration [Reimer et al., 2013] within the CALIB7.1 radiocarbon calibration program [Stuiver and Reimer, 1993] (version 5.0), with a ΔR of 10 ±15 years, based on data from nearby Christmas Island at 1.8°N, 157°W [Zaunbrecher et al., 2010]. We note that the true uncertainty in reservoir age may be higher, in light of modern coral studies from the tropical Pacific showing spatial and temporal variability in Δ14C due to fluctuations in upwelling and circulation [Druffel and Griffin, 1993; Zaunbrecher et al., 2010]. Median calibrated ages, 1σ, and 2σ ranges are given in Table S2.

The coretop was dated to 4030 cal YPB; downcore intervals were dated to 3,440, 4,890, 5,600, 6,900, 8,910, 9,730, and 12,170 cal YBP. The apparent age reversal in the top five centimeters is consistent with findings from other cores near the Line Islands [Lynch-Stieglitz et al., 2015], and is likely due to incomplete homogenization by bioturbation combined with coretop dissolution, which has been noted in this region [Berelson et al., 1997], and a generally increasing abundance of G. ruber downcore (Figure S13).

For the purpose of plotting bulk G. trilobus Mg/Ca-derived temperatures in Figure S11, ages were linearly interpolated between radiocarbon tie points, and

samples in the uppermost 5 cm of core 14MC (in which the radiocarbon data show an age reversal) are plotted as unconnected points, to connote uncertainty in the ages.

**Text S4. Statistical approach to reconstructing ENSO**

To visualize the data and facilitate comparison between different time intervals, we constructed normalized quantile-quantile (Q-Q) plots of the data (Figures 2 and S3). To calculate quantile values, an empirical continuous distribution function (ECDF) was constructed from each dataset, and the value of that function was interpolated at 2% intervals. To compare two datasets, the quantiles from each dataset are plotted against each other, forming a Q-Q plot (Figure S3c). If the two distributions are exactly the same, all the x-y pairs will fall on the 1:1 line; deviations from the 1:1 line show differences between the two distributions. Changes in slope indicate differences in the distribution (including standard deviation, kurtosis, or skewness). A change in average temperature with no change in the shape of the distribution will plot as a line parallel to, but offset from, the 1:1 line. A major benefit of QQ plots is that both axes have the same units as the original datasets (temperature). To emphasize differences between the two distributions apart from changes in the mean temperature, we present data in normalized Q-Q plots, in which we effectively move the 1:1 line to go through the average value of the comparison dataset, and then plot deviations from the new 1:1 line (Figure S3d).

In the mixed layer at our site, modern temperatures in the top three quantiles (>92$^{nd}$ percentile) occurred exclusively during El Niño events [*Carton and Giese*, 2008]. We thus interpret data in these top three quantiles to be representative of El

Niño events, such that a relative decrease in the temperatures of these quantiles would indicate a reduction in the amplitude of El Niño events. This would appear on a normalized Q-Q plot as the warmest three quantiles plotting below the zero line. Temperatures from moderate El Niño events are found in the 40$^{th}$ through 92$^{nd}$ quantiles, along with temperatures from "normal" months; as such, variations in these quantiles cannot definitively be attributed to changes in ENSO, so our interpretations of ENSO are based only on the very warmest quantiles. Because La Niña events are not as different from "normal" seasonality as El Niño events, our data are not very sensitive to La Niña, so any change or lack of change in the cool tail of the distribution cannot definitively be attributed to changes in La Niña.

90% confidence intervals (gray region in Figures 2 and S3-S10) are estimated for every quantile in every downcore interval (y-values on normalized Q-Q plots), using a Monte Carlo simulation similar to that employed by Ford et al. [2015a]. Confidence intervals are calculated as follows: the 70-90 temperatures from the downcore interval are used to make an empirical continuous distribution function (ECDF). Monte Carlo datasets are generated by sampling at random points along the ECDF, such that 10,000 new datasets are created, each containing the same number of points as the measured distribution being resampled. Quantile values are calculated for each Monte Carlo dataset, and are sorted such that all 10,000 values for the coldest quantile are ordered from coldest to warmest, and so on for all 50 quantiles. The 500$^{th}$ and 9500$^{th}$ values for each quantile (top and bottom 5%) are then selected as representing the bounds of the 90% confidence interval.

We note that in individual foraminiferal datasets, bioturbation does not "smooth" variance, except by broadening the timeframe over which temperatures are sampled. This broadening may act to include more decadal-centennial variability in ENSO strength and/or average temperature in the sampled timeframe, effects which we explore in the sensitivity tests described below.

**Text S5. Coretop *G. trilobus* data**

*S5.1 Comparison of coretop G. trilobus temperatures to modern temperatures*

Our coretop *G. trilobus* temperature distribution agrees well (within 90% confidence intervals) with temperature distributions throughout the mixed layer in terms of the average temperature, standard deviation, and shape of the distribution, when compared to SODA data at fixed depths (5 m, 25 m, and 58 m, [*Carton and Giese*, 2008]). The coretop has a somewhat higher standard deviation than the modern temperatures, as expected given that the coretop spans a much longer period of time. The best match of our data to modern temperatures occurs at 58 m, which is consistent with regional estimates of *G. trilobus* calcification depth [*Faul et al.*, 2000]; for this reason, we frame our results in terms of temperature variability at 58 m. However, because the modern temperature distribution at 58 m is very similar to that at 5 m, our results could just as reasonably be interpreted as reflecting SST. See Figure S4 for coretop-SODA data comparisons.

We note that any concerns regarding migrating depth of calcification in *G. trilobus* [e.g. *Rosenthal et al.*, 2000] or seasonality in foraminiferal production are allayed by the good agreement of our data to year-round temperatures at a single

depth. In addition, our strategy of comparing all downcore data to the coretop distribution should account for any vertical movement of *G. trilobus* or seasonality of production, provided these biases were similar during both time periods.

### *S5.2 Comparison of coretop G. trilobus temperatures to contemporaneous coral $\delta^{18}O$*

In an effort to test coretop *G. trilobus* temperatures against contemporaneous (4030 YBP) SST variability, and to test individual foraminifera against corals as recorders of SST variability, we compared our coretop *G. trilobus* Mg/Ca temperatures to two coral $\delta^{18}O$ records with monthly resolution from Christmas Island at 2°N, dated to 3433 to 3476 YBP and spanning 49 and 69 years, respectively [*Cobb et al.*, 2013]. For the purpose of comparison, we transformed the $\delta^{18}O$ data into temperature, using the $\delta^{18}O$-temperature sensitivity of -0.18‰ per °C reported for Christmas Island corals of the same species by [*Evans et al.*, 1998], and forcing the average temperature to equal that of today. Our assignment of an average temperature to the coral data does not impact the coretop/coral comparison because all data are normalized.

We find that the foraminiferal coretop temperature distribution is similar to the temperature distribution recorded by contemporaneous corals, within 90% confidence intervals (Figure S5, top row). To test whether the slightly greater variability observed in the foraminiferal distribution is due to the difference in location (foraminiferal data come from 0°N, 156°W, whereas coral data come from 2°N, 157°W), we compared unaltered SODA data from the two locations (Figure S5,

bottom row). The equatorial site has somewhat more variable temperatures than the Christmas Island site, which likely explains most of the slight difference between the foraminiferal and coral-derived temperatures.

**Text S6. Sensitivity tests**

To test our ability to detect various prescribed changes in ENSO, seasonality, and decadal-centennial variability in ENSO strength or annual mean temperature, we performed sensitivity tests by duplicating SODA data (which spans 50 years) to create a 800-year-long synthetic temperature record (to match the length of time represented in our sediment samples). We then altered ENSO, seasonality, or decadal-centennial variability in ENSO strength or annual mean temperature, and performed a Monte Carlo simulation of 10,000 subsamples of 70 data points to determine median results and 90% confidence intervals. The results are presented as normalized quantile-quantile plots in Figures S6-S8; details of each sensitivity test are given in figure captions.

Large decreases in ENSO are easily detected, and even a decrease of as little as 20% in the amplitude of El Niño anomalies can be detected using our method, within the 90% confidence interval (Figure S6). A 50% decrease in the amplitude of the seasonal cycle does not affect the warmest quantiles, and yields no significant change in any part of the distribution (Figure S6e), boosting confidence in the attribution of changes in the very warmest quantiles to changes in El Niño. Because La Niña anomalies are smaller than El Niño anomalies, we can only detect large (50%) reductions in the amplitude of La Niña anomalies with 90% confidence (Figure

S6f). For this reason, we focus our discussion on changes in El Niño amplitude through the Holocene.

We simulated decadal-centennial variability in ENSO strength by increasing or decreasing the amplitude of ENSO anomalies in some 50-year blocks of SODA data but not others, and then subsampling the entire synthetic timeseries (800 years for these tests). When subsampling a hypothetical 800 year timeseries with 50-year periods of increased and decreased ENSO but no net change, we found that most subsamples would show no significant change, but some extreme subsamples (near the edges of the 90% confidence interval) would show a spurious increase or decrease (Figure S7). Even with moderate or extreme net decreases in ENSO, as long as there remain some extreme high temperatures in the timeseries, some subsamplings will capture these extremes and show no apparent net change in ENSO (Figure S7). However, the probability of getting a spurious trend is extremely low. If there was no real trend in ENSO through the Holocene, such that the probability of finding increased, decreased, or similar ENSO as the coretop was the same (1/3) for every time interval, then the probability of getting our result of "same, decreased, decreased, decreased, decreased, same" is $(1/3)^7 = 0.05\%$.

To test whether our method might mistake decadal-centennial variability in annual mean temperature for changes in ENSO, we altered the annual mean temperature in some 50-year blocks of SODA data but not others, and then subsampled the entire 800-year synthetic timeseries. Coral data from Palmyra (northern Line Islands, 6°N) show that annual average temperature varied by ±0.3°C

on decadal-centennial timescales during the past millennium [*Cobb et al.*, 2003], so we tested the effect of ±0.3°C, ±0.5°C, and ±1°C changes in annual mean temperature. We find that small changes in annual mean temperature within a sample interval (±0.3°C and ±0.5°C) have a very small effect on the subsampled data (Figure S8). Only the ±1°C trial produced results that might be mistaken for changes in ENSO, but this is a much larger change in annual mean temperature (on decadal-centennial timescales) than expected for our site.

## Text S7. Accounting for additional uncertainty in individual foraminiferal Mg/Ca temperatures

*S7.1 Instrumental uncertainty and intra-test variability*

The instrumental uncertainty of the LA-ICP-MS Mg/Ca measurements, taken from the 1σ error on measurements of the NIST 610 standard, is ~1%. This corresponds to 0.11°C for a foraminiferal Mg/Ca value of 5.0 mmol/mol using the [*Anand et al.*, 2003] temperature calibration. There is also some variability in Mg/Ca among the 4 spots measured on each foraminiferal test chamber. The average standard deviation among spots was 0.09 mmol/mol, and tests with a standard deviation among spots >0.2 mmol/mol were not included in our data analyses. A standard deviation of 0.2 mmol/mol yields a standard error on the calculated mean value for each foraminiferal test of 0.1 mmol/mol. Using this as a conservative reflection of measurement uncertainty on individual foraminifera, we calculate a 1σ uncertainty of 0.225°C for a foraminiferal Mg/Ca value of 5.0 mmol/mol. This error includes the instrumental uncertainty, which is inherent in each measurement.

Note that the Anand et al [2003] Mg/Ca temperature calibration used here specifies a 1σ uncertainty of 1.2°C due to scatter in the original calibration data, which adds to the error in our absolute reported temperatures. However, given the good agreement of our coretop data with both the modern SST distribution and contemporaneous coral data, it appears that this uncertainty does not add further random, uncorrelated variance to our data and thus does not change the relative comparison between downcore data and the coretop. Also, we are explicitly accounting for measurement uncertainty and salinity effects, which are included in the calibration uncertainty. As such, this absolute error introduced in the temperature conversion does not affect our overall interpretation of changes in El Niño amplitude because we compare centered distributions that are unaffected by the absolute temperature.

*S7.2 The effect of salinity on G. trilobus Mg/Ca*

Several studies have found a small effect of salinity on foraminiferal Mg/Ca [e.g. *Hönisch et al.*, 2013; *Khider et al.*, 2015]. However, variations in salinity at our study site are subtle enough that they have only a small impact on our calculated temperatures. The past 50 years of reanalysis data near our site shows that monthly salinity values have a standard deviation of only 0.15 psu, including ENSO variability [*Carton and Giese*, 2008]. Salinity changes related to El Niño events are inconsistent; some events have higher salinity, some have lower, and the anomaly often changes sign over the course of the event [*Carton and Giese*, 2008]. The salinity anomaly during the peak El Niño SST anomaly is similarly inconsistent between events

[*Carton and Giese*, 2008]. Overall, the average salinity during both El Niño and La Niña events is 0.02 psu lower than average [*Carton and Giese*, 2008].

For these reasons, salinity variations at the site act to create a small amount of random noise in the foraminiferal Mg/Ca data, instead of biasing the representation of El Niño events specifically. Using the *G. sacculifer* Mg/Ca sensitivity of 4.7% per psu reported by [*Hönisch et al.*, 2013], the noise added by salinity variations at the site equates to ±0.07°C (1σ).

*S7.3 The effect of variations in sediment pore water chemistry on individual foraminiferal Mg/Ca temperatures*

Dissolution has long been known to create a cold bias in foraminiferal Mg/Ca-derived temperatures [*Brown and Elderfield*, 1996; *de Villiers*, 2005; *Dekens et al.*, 2002; *Fehrenbacher et al.*, 2006; *Johnstone et al.*, 2011; *Regenberg et al.*, 2014; *Regenberg et al.*, 2006; *Rosenthal and Lohmann*, 2002]. For this reason, we apply a dissolution correction to all our foraminiferal temperatures, based on the deviation of carbonate ion concentration at the seafloor near our site from that required for calcite saturation, Δ[CO32-]. This correction is based on modern measurements of carbonate system parameters, and thus does not account for possible variations in Δ[CO32-] over time. However, temporal changes in Δ[CO32-] do not affect our interpretation because we normalize all our data, so any bias in average temperature imposed by a change in Δ[CO32-] is removed in our analysis.

It is still possible, however, that slight differences in pore water chemistry at the centimeter scale could create differential dissolution among individual

foraminifera in a sample. Porewater data from the central equatorial Pacific [Jahnke et al., 1982] on ∑DIC and alkalinity variations within the upper centimeters of sediment show changes in ∑DIC and alkalinity of up to 100 μmol/kg. These differences correspond to changes in [CO32-] (and thus Δ[CO32-]) of 2.5 μmol/kg, as calculated in the CO2calc software [Robbins et al., 2010]. Using ±2.5 μmol/kg as a (likely upper-end) estimate of differences in Δ[CO32-] within a sediment sample, we calculate a resultant difference in temperature of ±0.3°C, as applied to a foraminiferal sample with measured Mg/Ca of 4.0 mmol/mol.

*S7.4 Modeled effect of overall uncertainty in individual foraminiferal Mg/Ca temperatures*

When all sources of uncertainty (measurement uncertainty, changes in salinity, changes in Δ[CO32-]) are added in quadrature, the total 1σ uncertainty is 0.4°C.

To explore the effect of this uncertainty on our data analysis, we performed Monte Carlo simulations to add 0.4°C of random noise to each downcore data point. In detail, we created vectors of random Gaussian-distributed "noise" with a mean of 0°C and a standard deviation of 0.4°C, then added noise to each data point before constructing the empirical continuous distribution function (ECDF) of the dataset. We did this 300 times with different noise vectors to yield 300 noisy ECDFs. We then resampled each ECDF 300 times at 70 random points (or 84 points, etc., depending on the number of points in the original dataset) along the distribution to create 300 synthetic datasets from each of the 300 noisy ECDFs, yielding 9,000 Monte Carlo

realizations. Quantile values were calculated from each dataset, and for each quantile, were ordered from coldest to warmest. The 450th and 8550th values were chosen to bound the 90% confidence intervals, and the 1125th and the 7875th values were chosen to bound the 80% confidence intervals. Results are presented in Figure S9. Our findings of reduced El Niño amplitude during the early and mid-Holocene remain significant at the 80% level.

**Text S8. Composite SST records for the WEP and the EEP**

To better assess temperature trends in the WEP and the EEP, we created composite SST anomaly records for both regions from 0-15 ka. In the WEP, we used planktic foraminiferal Mg/Ca records and one coral Sr/Ca record. We did not include records from the South China Sea or the Indian Ocean, because these regions are not representative of the west Pacific warm pool, the most relevant region for ENSO. We also did not include alkenone records near their 28.5°C saturation point [*Conte et al.*, 2006]. One alkenone record, from core MD06-3075 [*Fraser et al.*, 2014], is nearly co-located with a Mg/Ca record from core MD98-2181 [*Stott et al.*, 2007], and shows the opposite trend, with warming from early to late Holocene. This alkenone record was not included in our composite anomaly record because its trend is opposite to the Mg/Ca records, but it is included in Figure S11 for reference.

For the EEP, we constructed separate records for planktic foraminiferal Mg/Ca and alkenone data, because Mg/Ca and alkenones likely record different seasons in that region [*Leduc et al.*, 2010; *Timmermann et al.*, 2014]. Mg/Ca records included those based on *G. ruber* and *G. sacculifer* (both surface-dwelling). We did

not include records from the eastern tropical Pacific warm pool or the Peru Margin in our compilation, because these regions are not representative of the EEP. Figure S11 shows all original data from each site, along with our pooled *G. trilobus* Mg/Ca based temperature record (not included in the WEP or EEP compilations). Figure S12 shows site locations, and Table S4 lists original references for all temperature records that comprise our composite anomaly record.

To create the anomaly records, we first normalized all the data in each record to its own average temperature during the past four thousand years. We then reduced each record to 500-year resolution by averaging data points within 500-year bins. If no data existed within a given 500-year bin, the value for that bin was left blank. To create composite SST anomaly records, we averaged all binned values from each region or proxy. As such, data from all sites is weighted equally. In Figure 3, the composite anomaly records are presented with a 1σ confidence interval (shown as shaded color regions), calculated from the standard deviation of temperatures in each 500-year bin.

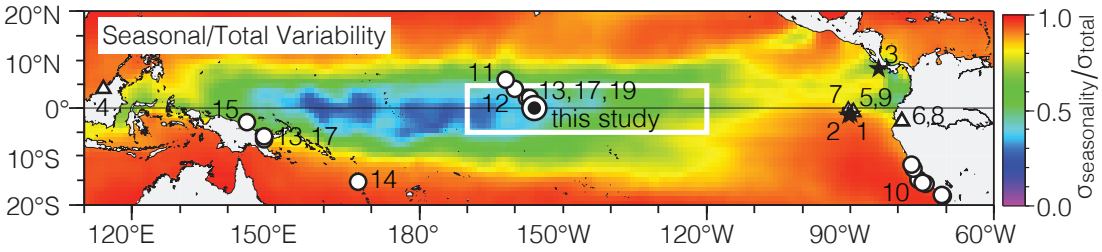


**Figure S1. Site locations.**

Location of cores used in this study and published ENSO records, numbered as they appear in the text: individual foraminiferal records (stars), precipitation records (triangles), coral/mollusk records (circles). Background map shows the proportion of SST variability from seasonality, calculated from the standard deviation of monthly SSTs from the HadISST1 dataset [*Rayner*, 2003]. Cool colors indicate dominance of interannual and longer timescale variability. White lines delineate the Niño3.4 box.

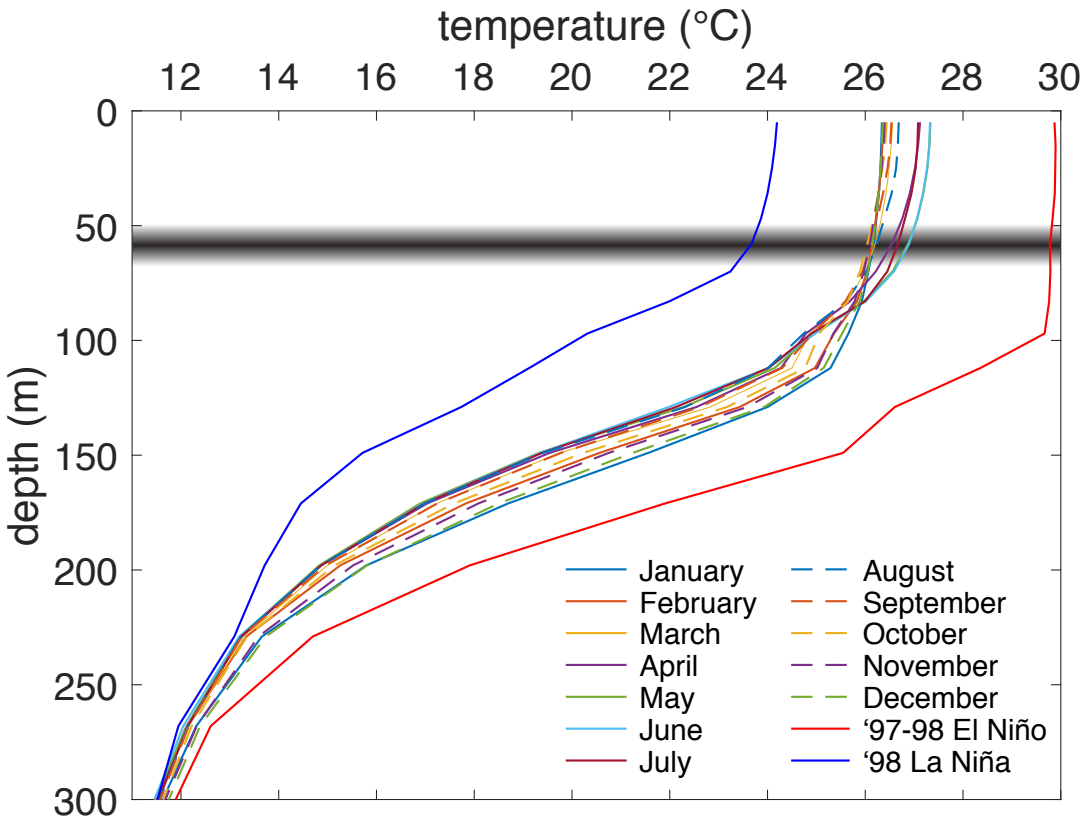


**Figure S2. Temperature-depth profiles.**
Temperature-depth profiles near the study site, showing averaged data from "normal" (non-El Niño/La Niña) months, plus peak anomalies during the 1997-1998 El Niño and the 1998-1999 La Niña events. The El Niño/La Niña profiles are somewhat diachronous, since anomalies in the subsurface lead those at the surface by a few months. The mixed layer is ~100 m deep, and the thermocline (centered on the 20°C isotherm) is ~150 m deep. The depth habitat of *G. trilobus* at the study site (shaded bar) is within the mixed layer. Data from [*Carton and Giese*, 2008].

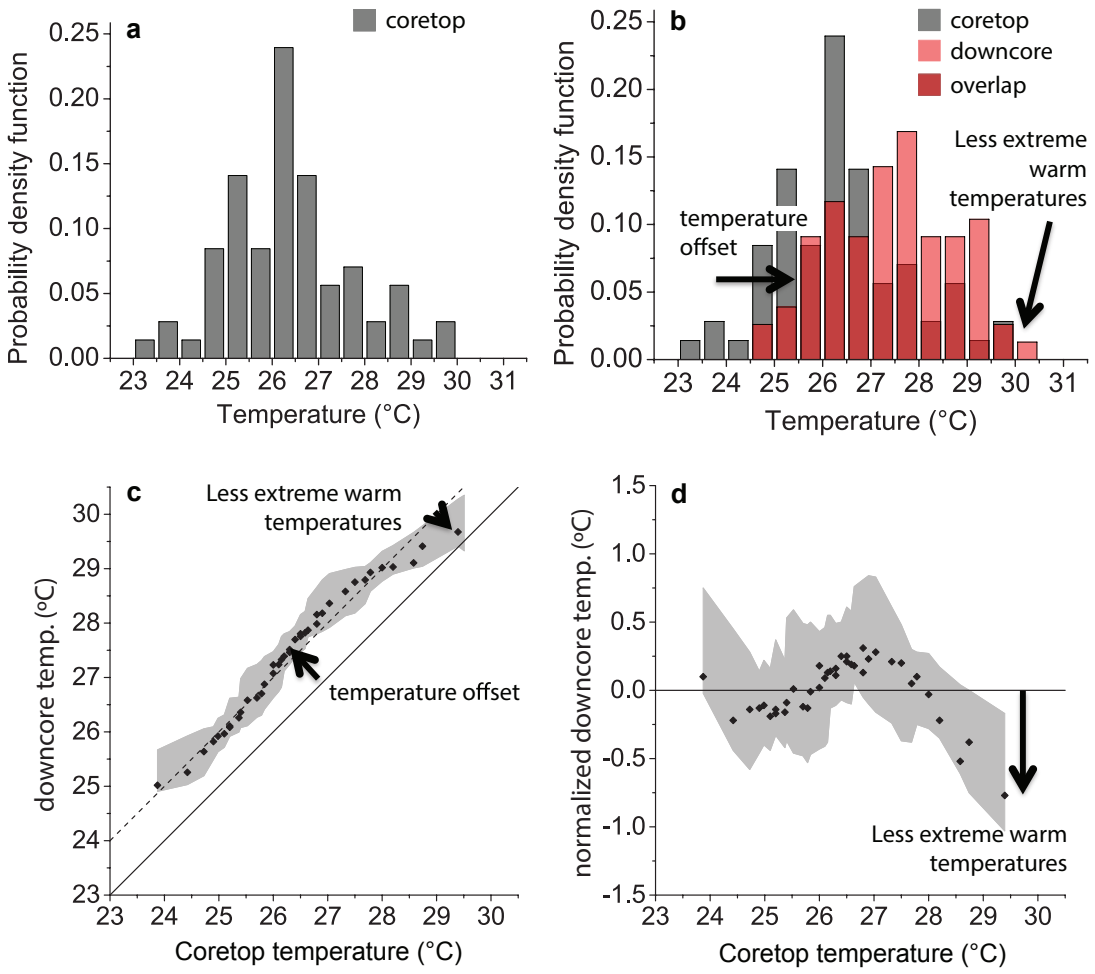


**Figure S3. Interpretation of data using normalized quantile-quantile plots.** The distribution of Mg/Ca-based *G. trilobus* temperatures from the coretop can be plotted in a histogram (a) and compared to a downcore distribution of *G. trilobus* temperatures (b). Note that in this example, the downcore distribution is warmer than the coretop overall, but has relatively less extreme warm temperatures. These features can be seen in a quantile-quantile plot of the data (c). To emphasize differences in the distributions separate from changes in average temperature, we normalize the quantile data to the dashed line in (c), yielding the normalized quantile-quantile plot in (d). Gray region shows 90% confidence intervals, estimated by Monte Carlo simulations.

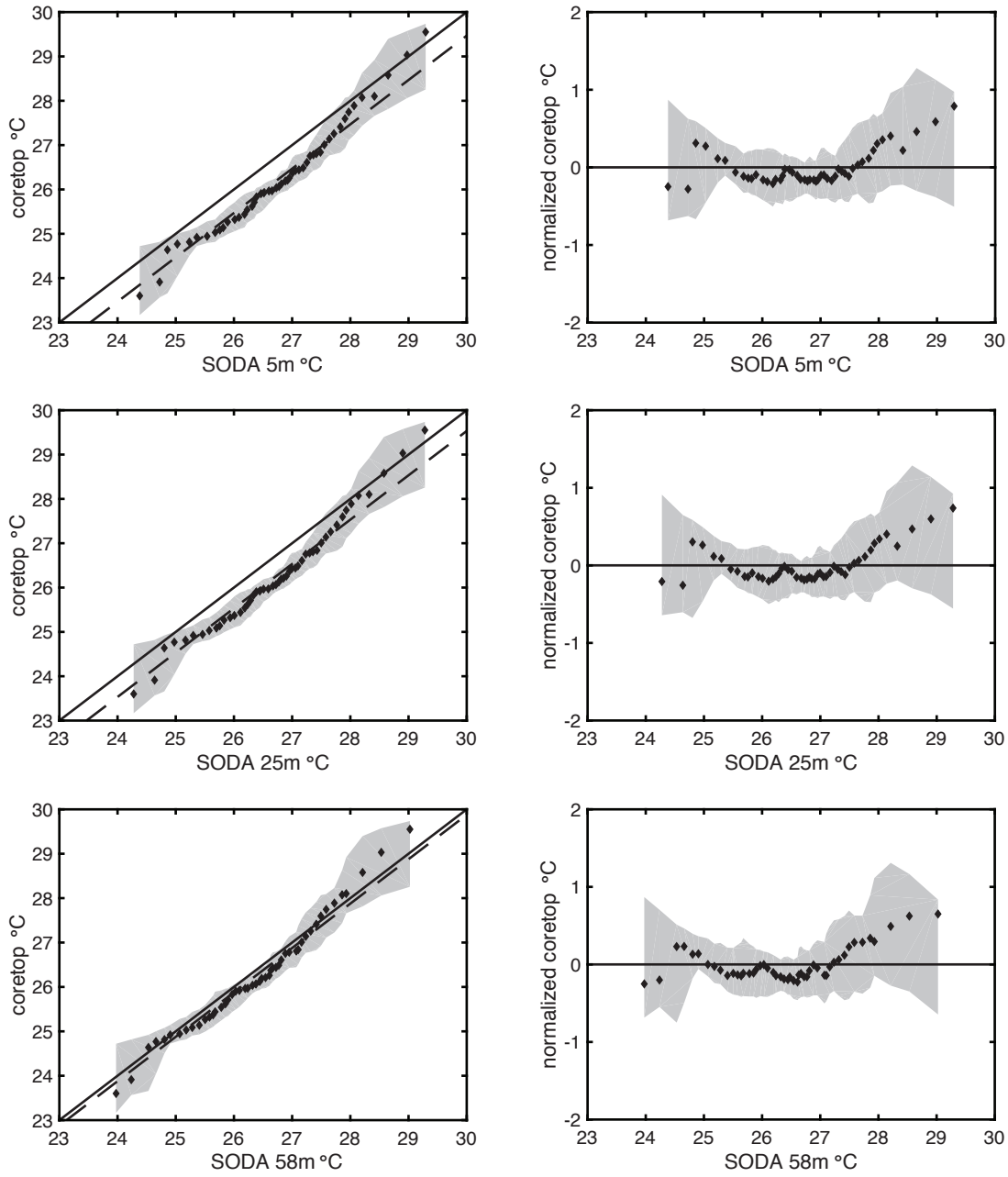


**Figure S4. Mixed-layer temperatures and *G. trilobus* data.**
Quantile-quantile (left) and normalized quantile-quantile (right) plots of modern monthly gridded temperatures near our site at 5 m, 25 m, and 58 m depth from the SODA v2.1.6 dataset [Carton and Giese, 2008] plotted versus individual *G. trilobus* temperatures from the coretop. Bottom row duplicates Figure 1 in the main text. The best match of coretop to modern temperatures occurs at 58 m, but the match is similarly good (within 90% confidence intervals, gray region) at all depths, after accounting for small differences in average temperature.

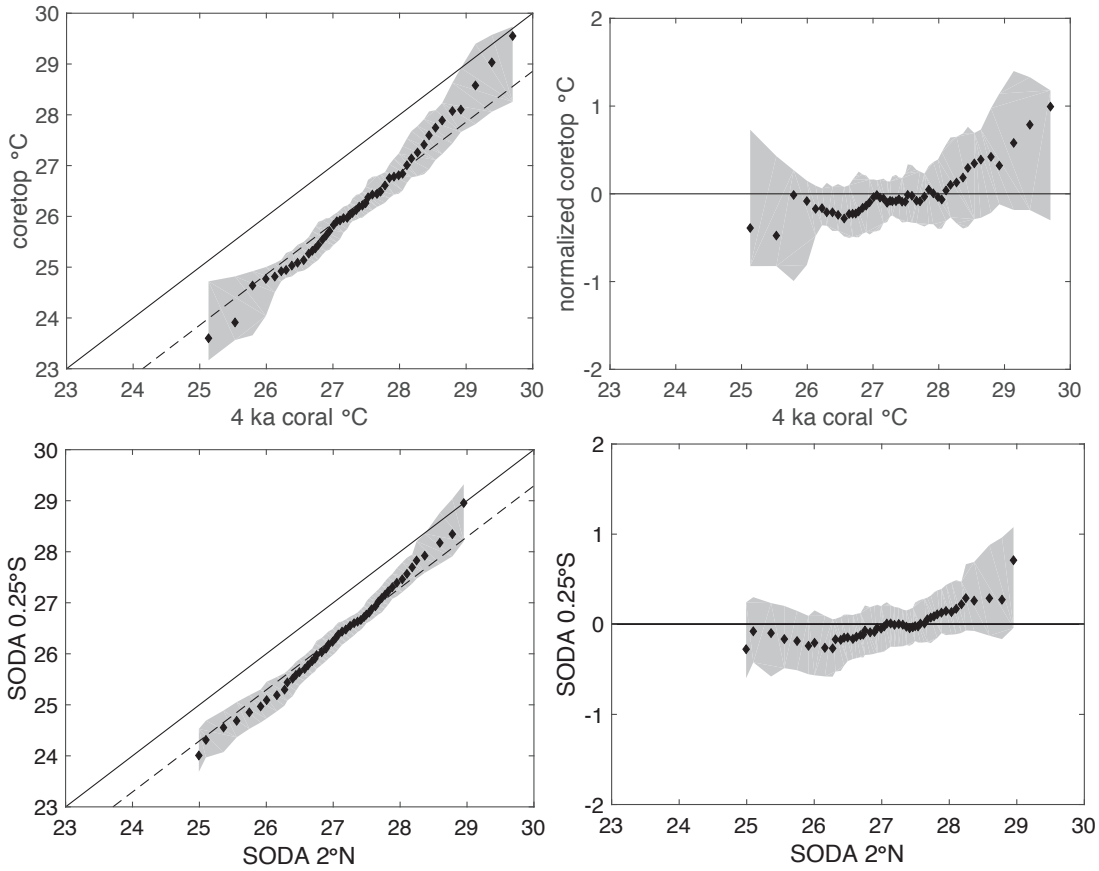


**Figure S5. *G. trilobus*-coral comparison.**

(Top row) Comparison of coretop *G. trilobus* –based temperatures to nearby contemporaneous coral $\delta^{18}O$-based temperatures. Coral $\delta^{18}O$ data is from Christmas Island at 2°N, 157°W from two specimens dated to 3946±18 YBP and 4080±16 YBP and spanning 49 and 69 years, respectively [*Cobb et al.*, 2013]. (Bottom row) Comparison of modern temperature distributions [*Carton and Giese*, 2008] at our study site (0°N, 156°W) and at Christmas Island. The top row shows that foraminiferal temperatures are slightly more variable than those recorded by the corals, though not significantly, and much of the difference can be explained by the difference in location, as shown in the bottom row.

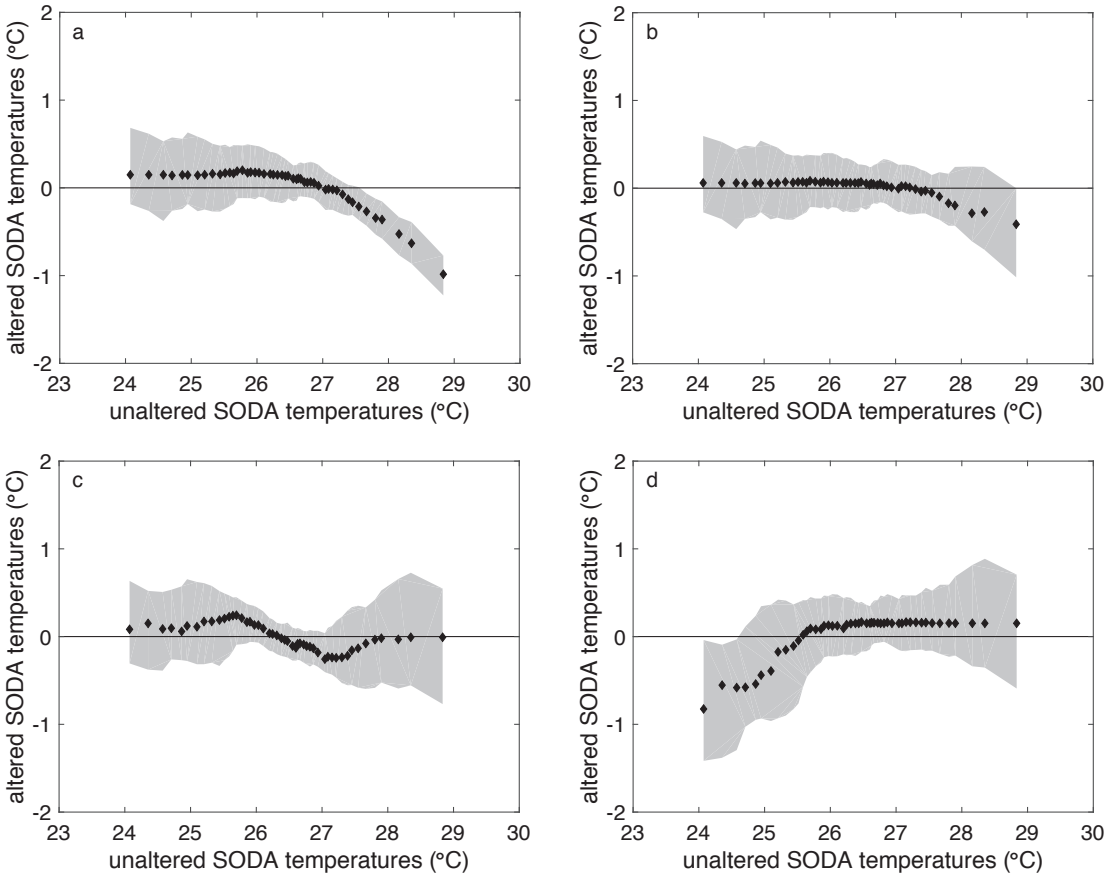


**Figure S6. Sensitivity tests: ENSO and seasonality.**
Sensitivity performed on SODA data near our site from 58 m water depth [*Carton and Giese*, 2008], plotted as normalized quantile-quantile plots. Gray region shows 90% confidence intervals. a-b) 50% and 20% (respectively) reduction in the amplitude of the temperature anomaly during each El Niño month, with respect to the average seasonal cycle; c) 50% decrease in the amplitude of the seasonal cycle, calculated by taking each non-El Niño or La Niña month and adding half the difference between that temperature and the annual mean; d) 50% reduction in the amplitude of monthly La Niña temperature anomalies, with respect to the average seasonal cycle.

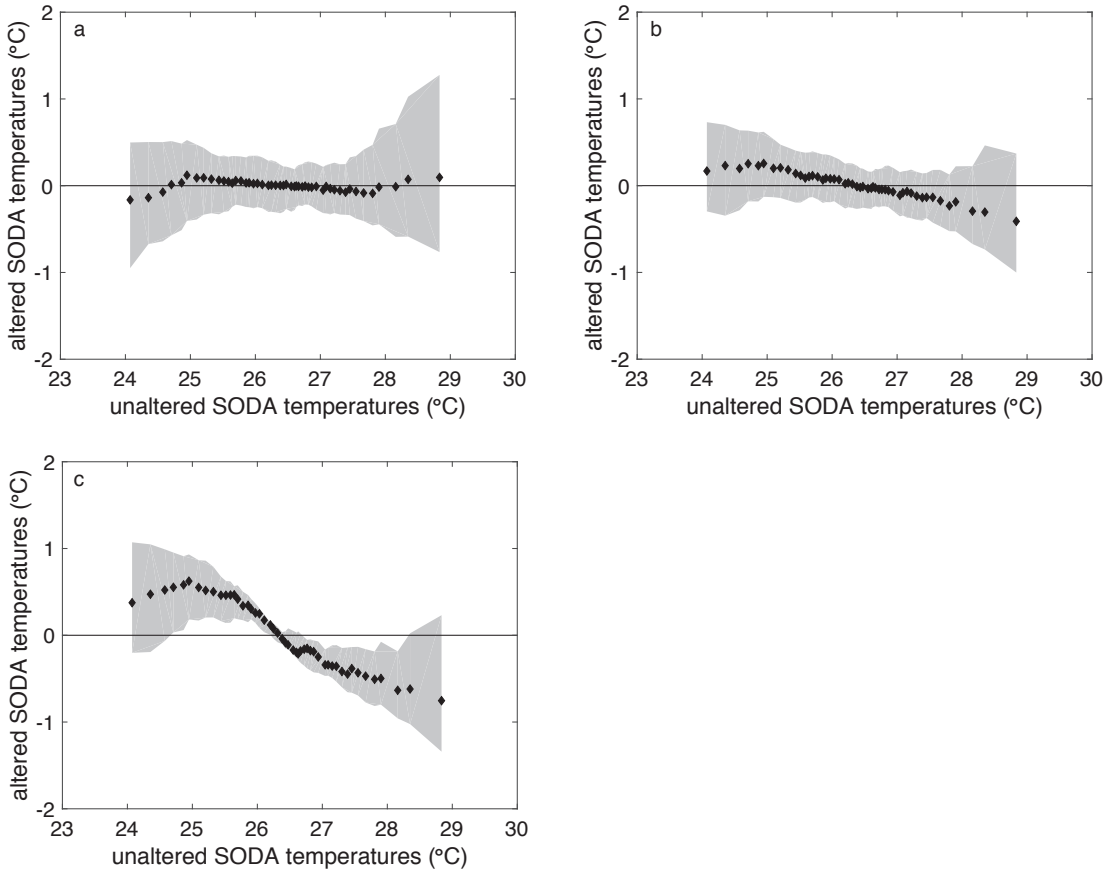


**Figure S7. Sensitivity tests: decadal variability.**

Sensitivity tests performed on SODA data near our site from 58 m water depth [*Carton and Giese*, 2008], plotted as normalized quantile-quantile plots. Gray region shows 90% confidence intervals. a-c) decadal variability (performed on an 800-year synthetic record) – a) shows greater variability but no net change, with three 50-yr periods of +50% ENSO, three 50-yr periods of +25% ENSO, three 50-yr periods of -50% ENSO, three 50-yr periods of -25% ENSO, and four unaltered 50-yr periods, with respect to the average seasonal cycle; b) shows a net reduction in ENSO, with one 50-yr period of no ENSO, three 50-yr periods of -50% ENSO, three 50-yr periods of -25% ENSO, and nine unaltered 50-yr periods, with respect to the average seasonal cycle; c) shows a very strong net reduction in ENSO, with ten 50-yr periods of no ENSO and six unaltered 50-yr periods, with respect to the seasonal cycle.

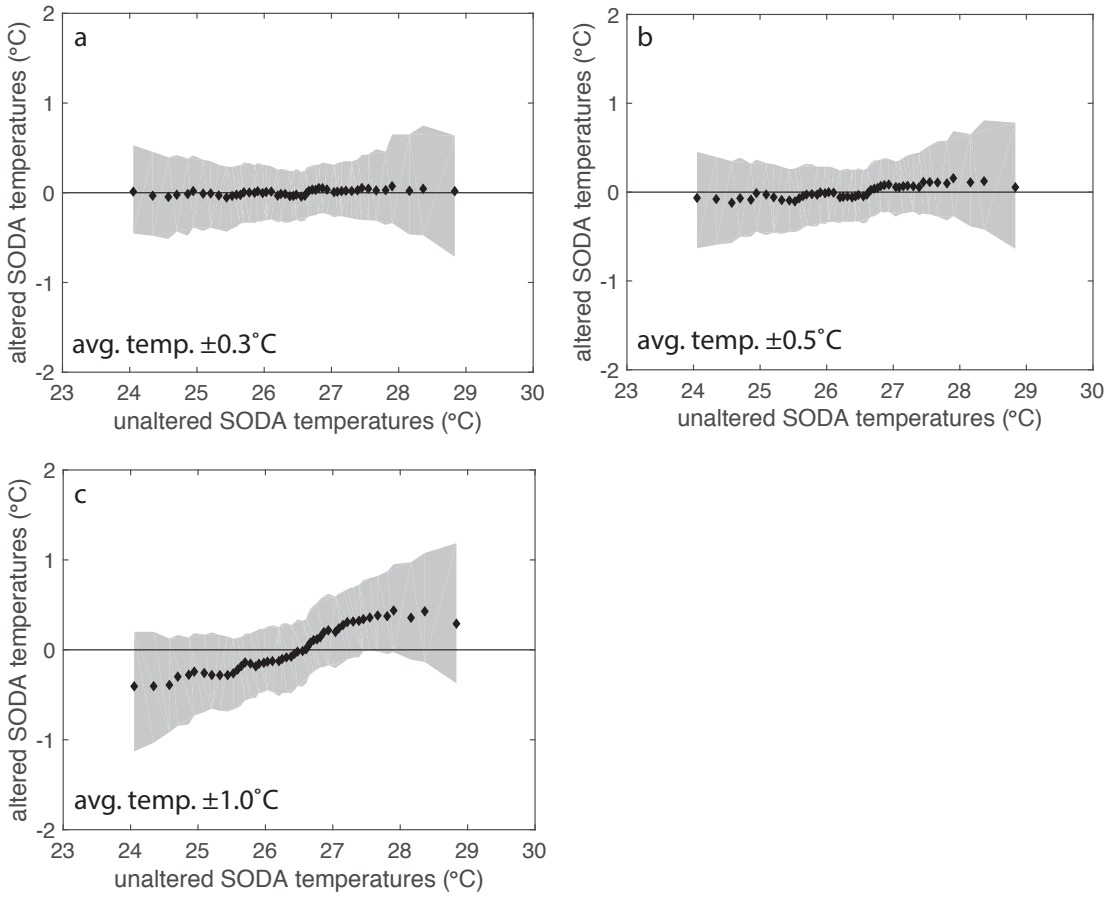


**Figure S8. Sensitivity tests: centennial variability in mean temperature.** Sensitivity tests demonstrating the effect of centennial-scale variations in annual mean temperature with no change in ENSO, plotted as normalized quantile-quantile plots (gray region shows 90% confidence intervals). 800-year synthetic records (based on SODA data) were altered such that 300 years had x added to every temperature, 300 years had x subtracted from every temperature, and 200 years were unaltered, where x varied from 0.3°C (a) to 0.5°C (b) to 1.0°C (c). Coral data from the Line Islands indicates that decadal-centennial variability in annual mean temperature was only ±0.3°C during the past millennium [*Cobb et al.*, 2003], so the ±1°C case is an extreme example included only for illustrative purposes.

**Figure S9. Effect of uncertainty.**

All *G. trilobus* individual foraminiferal Mg/Ca-based temperatures as in Figure 2, but with ±0.4°C random noise added to each data point before performing the Monte Carlo simulation to estimate confidence intervals. Gray shaded region shows 90% confidence intervals; thin lines show 80% confidence intervals. Our finding of reduced El Niño amplitude during the mid and early Holocene compared to the late Holocene and YD remains valid at the 80% confidence level.

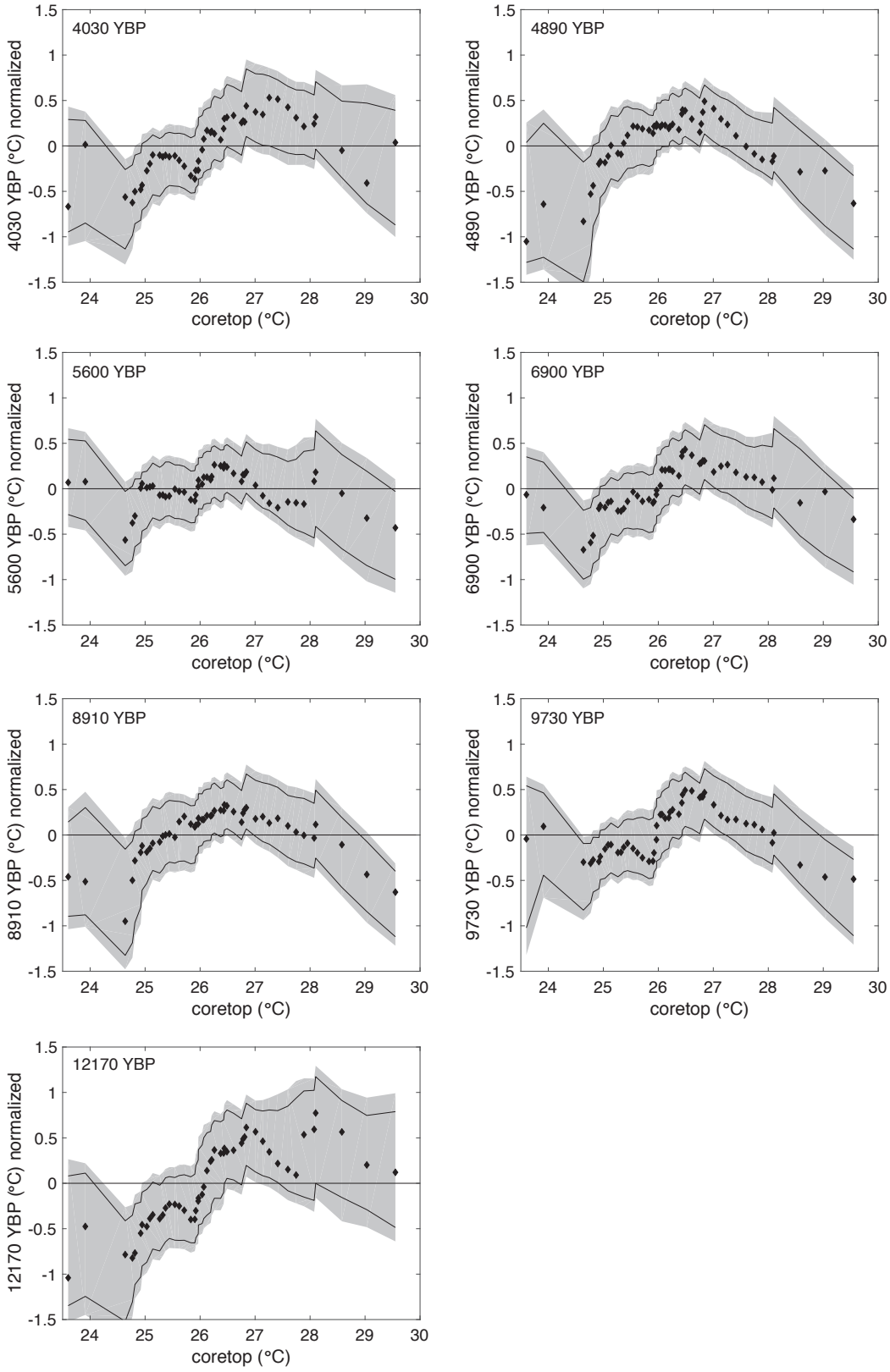
4030 YBP
4030 YBP (°C) normalized
4890 YBP
4890 YBP (°C) normalized
5600 YBP
5600 YBP (°C) normalized
6900 YBP
6900 YBP (°C) normalized
8910 YBP
8910 YBP (°C) normalized
9730 YBP
9730 YBP (°C) normalized
12170 YBP
12170 YBP (°C) normalized
coretop (°C)
1.5
1
0.5
0
-0.5
-1
-1.5
24
25
26
27
28
29
30

**Figure S10. Effect of different baseline dataset.**
All *G. trilobus* individual foraminiferal Mg/Ca-based temperatures as in Figure 2, but using the late Holocene sample (3,440 YBP) as the baseline for comparison instead of the coretop. Gray shaded region shows 90% confidence intervals. Our findings of reduced El Niño amplitude during the mid and early Holocene compared to the coretop and YD remains valid at the 90% confidence level.

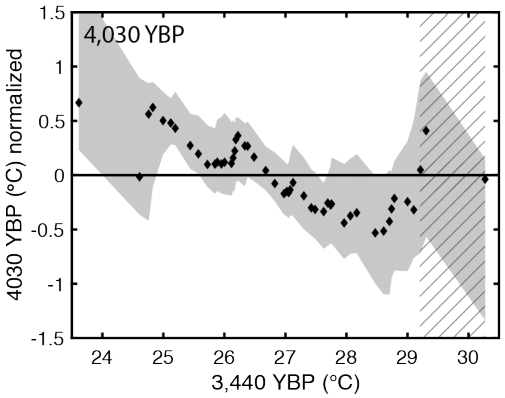
4,030 YBP
4030 YBP (°C) normalized
3,440 YBP (°C)

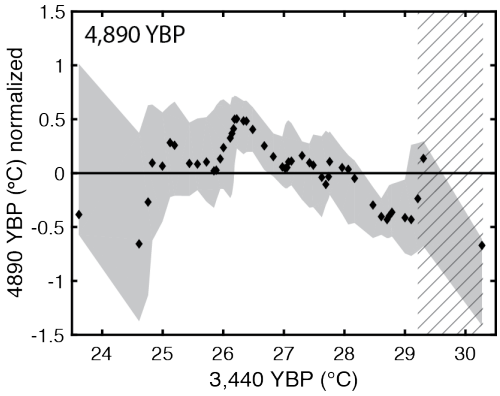
4,890 YBP
4890 YBP (°C) normalized
3,440 YBP (°C)

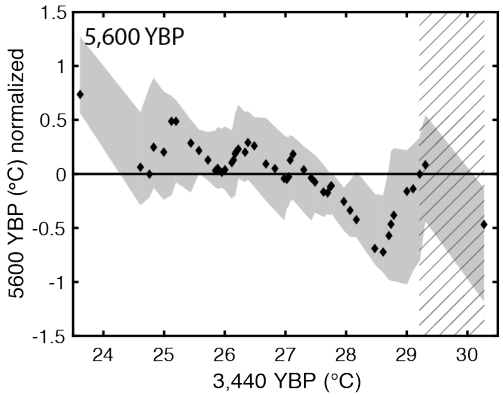
5,600 YBP
5600 YBP (°C) normalized
3,440 YBP (°C)

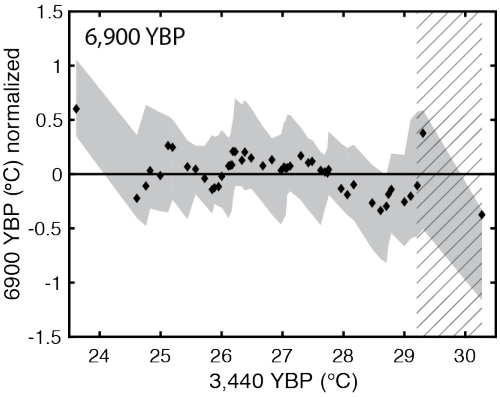
6,900 YBP
6900 YBP (°C) normalized
3,440 YBP (°C)

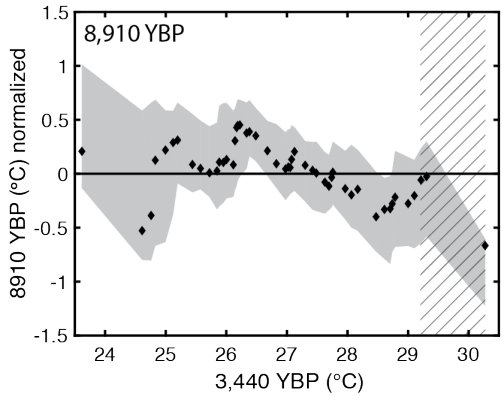
8,910 YBP
8910 YBP (°C) normalized
3,440 YBP (°C)

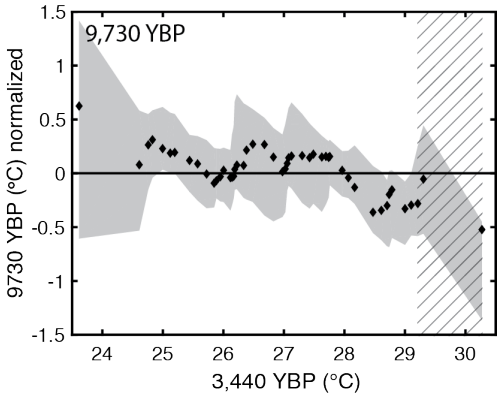
9,730 YBP
9730 YBP (°C) normalized
3,440 YBP (°C)

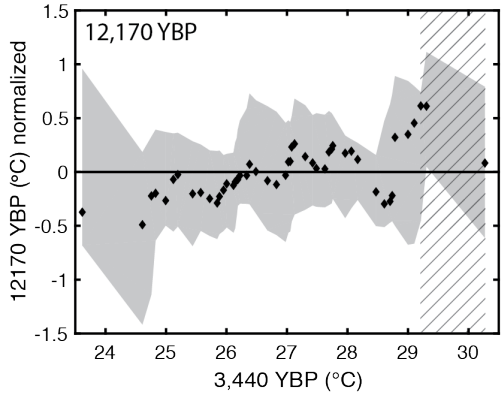
12,170 YBP
12170 YBP (°C) normalized
3,440 YBP (°C)

**Figure S11. Raw data used to make SST composites.**
Raw SST records used to make composite WEP and EEP SST anomaly records, plus pooled *G. trilobus* SST record from cores 14MC and 12GC in the central equatorial Pacific (CEP; our study site). Data from the coretop to 8910 YBP is from 14MC; data from 8510 to 13390 YBP is from 12GC. All WEP records are based on planktic foraminiferal Mg/Ca, except for the Muschu/Koil Is. record (short dashed line), which is based on Sr/Ca of *Porites* coral. The alkenone record from MD06-3075 [*Fraser et al.*, 2014] is not included in the composite WEP anomaly record, because it has a very different trend. All Mg/Ca records from the WEP and the EEP are based on *G. ruber* except those marked by dashed lines, which are based on *G. trilobus.* The coral Sr/Ca record was reported in the original publication as temperature anomalies with respect to modern conditions; for plotting purposes, we added the reported anomalies to the modern mean annual SST at the site. Due to the apparent age reversal near the top of core 14MC, we plot data from the first 5 cm without connecting lines, to denote uncertainty in relative ages. See Supplementary Table 4 for references.

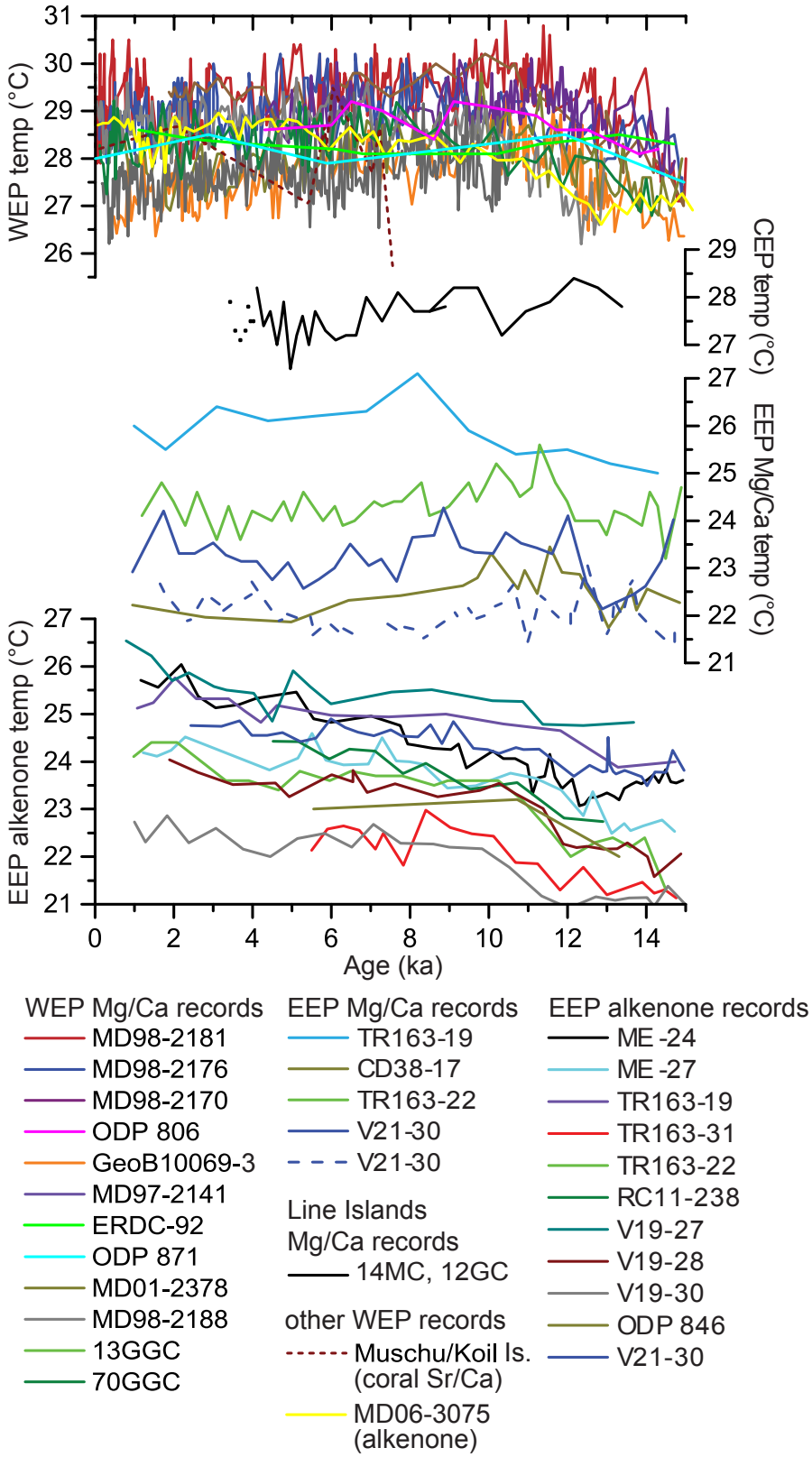
WEP temp (°C)
CEP temp (°C)
EEP Mg/Ca temp (°C)
EEP alkenone temp (°C)
Age (ka)
WEP Mg/Ca records
MD98-2181
MD98-2176
MD98-2170
ODP 806
GeoB10069-3
MD97-2141
ERDC-92
ODP 871
MD01-2378
MD98-2188
13GGC
70GGC
EEP Mg/Ca records
TR163-19
CD38-17
TR163-22
V21-30
V21-30
Line Islands Mg/Ca records
14MC, 12GC
other WEP records
Muschu/Koil Is. (coral Sr/Ca)
MD06-3075 (alkenone)
EEP alkenone records
ME -24
ME -27
TR163-19
TR163-31
TR163-22
RC11-238
V19-27
V19-28
V19-30
ODP 846
V21-30

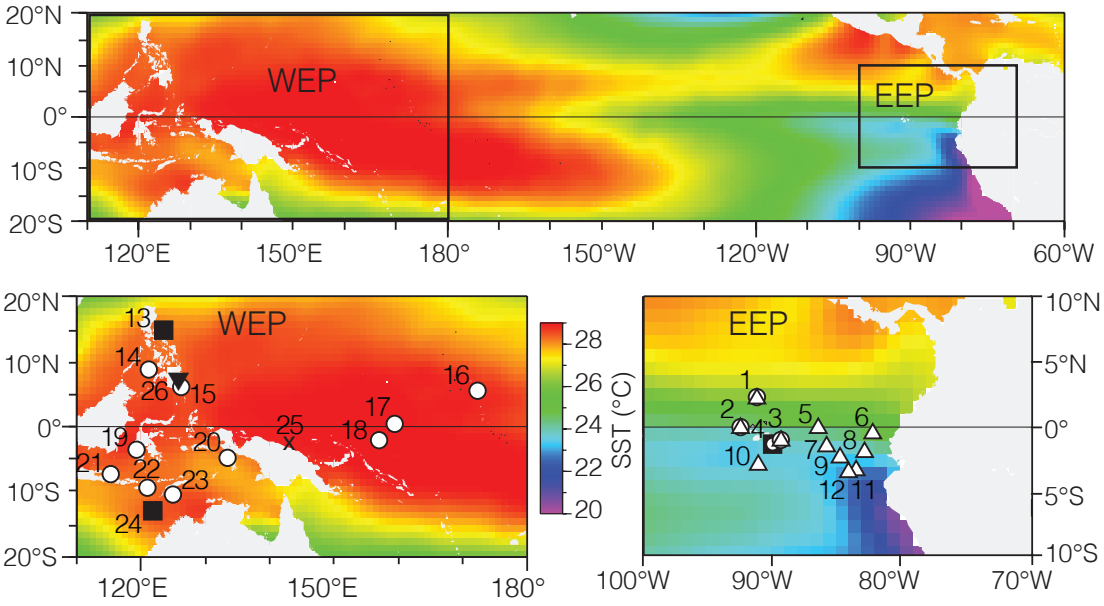


**Figure S12. Site locations for SST composites.**
Locations of subsurface records plotted in Figure 3 (black squares), and of planktic foraminiferal Mg/Ca (circles), coral Sr/Ca (cross) and alkenone (triangles) records used to make composite SST records for the WEP and the EEP. Background map shows mean annual sea surface temperatures from the HadISST1 dataset [*Rayner*, 2003]. List of sites is in Supplementary Table 4.

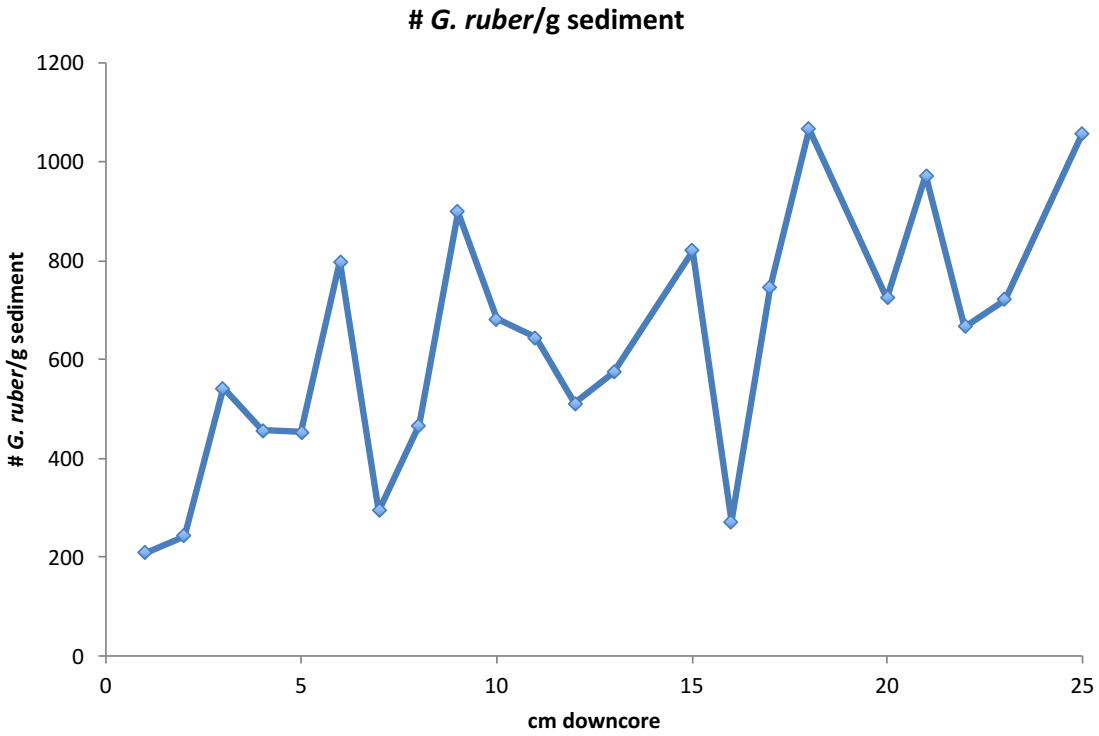


**Figure S13. Downcore *G. ruber* abundance.**
Abundance of *G. ruber*, the species used to measure radiocarbon ages of samples, in core 14MC. The number of *G. ruber* was counted in sample splits consisting of >300 specimens of the >250 μm size fraction. Counts were converted to # *G. ruber* per gram of sediment by dividing by the dry weight of the bulk (unwashed, un-sieved) sample. The general downcore increase in *G. ruber* abundance may contribute to the apparent age reversal in the top few centimeters of the core.

**Table S1. Sample information.**

Average calculated temperature and number of specimens in each sediment interval (with ages in calibrated years before present, "cal YBP"), compared to the average temperature at 58 m (in the middle of the mixed layer) near our site [*Carton and Giese*, 2008].

| | average (°C) | 1σ | # specimens |
|---|---|---|---|
| SODA 58m | 26.38 | 1.18 | n/a |
| coretop | 26.3 | 1.39 | 68 |
| 3440 cal YBP | 26.9 | 1.59 | 78 |
| 4890 cal YBP | 27.0 | 1.47 | 90 |
| 5600 cal YBP | 26.9 | 1.35 | 77 |
| 6900 cal YBP | 26.8 | 1.46 | 84 |
| 8910 cal YBP | 26.7 | 1.45 | 78 |
| 9730 cal YBP | 27.2 | 1.45 | 89 |
| 12170 cal YBP | 27.0 | 1.79 | 70 |

**Table S2. Radiocarbon data for each single foraminiferal interval.**
Cal YBP is calibrated years before 1950, using the CALIB7.1 radiocarbon calibration program [*Stuiver and Reimer*, 1993] (version 5.0). Median probability ages have been rounded to the nearest 10 years.

| core | depth (cm) | D14C | 14C age | 14C age error | ΔR | ΔR error | cal YBP (median probability) | 1σ age range | 2σ age range | CAMS # |
|---|---|---|---|---|---|---|---|---|---|---|
| 14MC | 0.0-0.5 | -394.7 | 4,030 | 40 | 10 | 15 | 4,030 | 3,962-4,098 | 3,891-4,167 | 166284 |
| 14MC | 4.5-5.0 | -357.9 | 3,560 | 30 | 10 | 15 | 3,440 | 3,381-3,476 | 3,354-3,539 | 166177 |
| 14MC | 9.5-10.0 | -441.7 | 4,680 | 30 | 10 | 15 | 4,890 | 4,838-4,930 | 4,814-4,992 | 166285 |
| 14MC | 14-15 | -479.4 | 5,245 | 35 | 10 | 15 | 5,600 | 5,565-5,638 | 5,505-5,691 | 166286 |
| 14MC | 19-20 | -550.5 | 6,425 | 30 | 10 | 15 | 6,900 | 6,843-6,946 | 6,785-6,993 | 166178 |
| 14MC | 24-25 | -646.2 | 8,345 | 35 | 10 | 15 | 8,910 | 8,856-8,986 | 8,753-9,010 | 166287 |
| 12GC | 24-25 | -675.8 | 9,050 | 30 | 10 | 15 | 9,730 | 9,649-9,807 | 9,584-9,878 | 166176 |
| 12GC | 28-29 | -737.8 | 10,750 | 35 | 10 | 15 | 12,170 | 12,042-12,264 | 11,993-12,415 | 166175 |

## Table S3. List of ENSO studies discussed in the text, denoted on Figure S1.

Single foraminiferal studies

| Map # | Reference | Site | Lat/Long | Proxy | Proxy detail |
|---|---|---|---|---|---|
| 1 | Koutavas and Joanides 2012 | V21-30 | 1.22°S, 89.68°W | $\delta^{18}O$ | *G. ruber* (sea surface) |
| 2 | Sadekov et al 2013 | CD38-17 | 1.6°S, 90.43°W | Mg/Ca (2 specimens per sample) | *N. dutertrei* (thermocline) |
| 3 | Leduc et al. 2009 | MD02-2529 | 8.21°N, 84.12°W | $\delta^{18}O$ | *N. dutertrei* (thermocline) |

Precipitation records

| Map # | Reference | Site | Lat/Long | Proxy |
|---|---|---|---|---|
| 4 | Chen et al., 2016 | BA03 | 4°N, 114°E | speleothem $\delta^{18}O$ |
| 5 | Conroy et al., 2008 | El Junco Lake | 0.8°S, 89.3°W | % sand in sediment |
| 6 | Moy et al., 2002 | Laguna Pallcacocha | 2.77°S, 79.23°W | clastic laminae in sediments |
| 7 | Riedinger et al, 2002 | Bainbridge Lake | 0.5°S, 90.5° | siliciclastic laminae |
| 8 | Rodbell et al., 1999 | Laguna Pallcacocha | 2.77°S, 79.23°W | clastic laminae in sediments |
| 9 | Zhang et al., 2014 | El Junco Lake | 0.8°S, 89.3°W | concentration and δD of algal lipids |

Coral/mollusk

| Map # | Reference | Site | Lat/Long | Proxy | Proxy detail |
|---|---|---|---|---|---|
| 10 | Carre et al., 2014 | coastal Peru | 11°S-18°S | bivalve $\delta^{18}O$ | *M. donacium,* from several coastal sites |
| 11 | Cobb et al., 2003 | Palmyra Island | 6°N, 162°W | $\delta^{18}O$ | *Porites* sp. |
| 12 | Cobb et al., 2013 | Kiritimati, Fanning Islands | 2°N, 157°W; 4°N, 160°W | $\delta^{18}O$ | *Porites* sp. |
| 13 | Driscoll et al. 2014 | Huon Peninsula | 6.5°S, 147.5°E | $\delta^{18}O$ | *Tridacna* sp. |
| 14 | Duprey et al 2012 | Espiritu Santo Island | 15.35°S, 167.18°E | $\delta^{18}O$ | *Tridacna* maximus, *Porites* sp. |
| 15 | McGregor and Gagan 2004 | Koil, Muschu Islands | 3°S, 144°E | $\delta^{18}O$ | *Porites* sp. |
| 16 | McGregor et al. 2013 | Kiritimati Island | 1.74°N, 157.21°E | $\delta^{18}O$ | *Porites* sp. |
| 17 | Tudhope et al., 2001 | Huon Peninsula | 6°S, 147.°5E | $\delta^{18}O$ | *Porites* sp. |
| 18 | Woodroffe et al., 2003 | Kiritimati Island | 2°N, 157.5°W | $\delta^{18}O$ | *Porites* sp. microatolls |

**Table S4. List of references used to make composite SST records, and thermocline temperature records.**

Site locations are shown in Figure S12. Note that the Fraser et al. [2014] record was not included in the WEP composite record, because it has a very different trend.

EEP SST

| Map # | Reference | Site | Lat/Long | Proxy | Proxy detail |
|---|---|---|---|---|---|
| 1 | Dubois et al 2009, Lea et al 2000 | TR163-19 | 2.25°N, 90.95°W | Mg/Ca, alkenones | *G. ruber* |
| 2 | Dubois et al 2009, Lea et al 2006 | TR163-22 | 0.05°N, 92.38°W | Mg/Ca, alkenones | *G. ruber* |
| 3 | Koutavas and Sachs 2008, Koutavas & Joanides 2012 | V21-30 | 1.22°S, 89.68°W | Mg/Ca, alkenones | *G. ruber, G. sacculifer* |
| 4 | Sadekov et al 2013 | CD38-17 | 1.6°S, 90.43°W | Mg/Ca, alkenones | *G. ruber* |
| 5 | Dubois et al 2009 | ME-24JC | 0.02°S, 86.45°W | alkenones | |
| 6 | Koutavas and Sachs 2008 | V19-27 | 0.47°S, 82.07°W | alkenones | |
| 7 | Koutavas and Sachs 2008 | RC11-238 | 1.52°S, 85.82°W | alkenones | |
| 8 | Dubois et al 2009 | ME-27JC | 1.85°S, 82.78°W | alkenones | |
| 9 | Koutavas and Sachs 2008 | V19-28 | 2.37°S, 84.65°W | alkenones | |
| 10 | Lawrence et al 2006 | ODP 846 | 3°S, 91°W | alkenones | |
| 11 | Koutavas and Sachs 2008 | V19-30 | 3.38°S, 83.52°W | alkenones | |
| 12 | Dubois et al 2009 | TR163-31 | 3.62°S, 83.97°W | alkenones | |

WEP SST

| Map # | Reference | Site | Lat/Long | Proxy | Proxy detail |
|---|---|---|---|---|---|
| 13 | Dang et al 2012 | MD98-2188 | 14.82°N, 123.49°E | Mg/Ca | *G. ruber* |
| 14 | Rosenthal et al 2003 | MD97-2141 | 8.78°N, 121.28°E | Mg/Ca | *G. ruber* |
| 15 | Stott et al 2007 | MD98-2181 | 6.45°N, 125.83°E | Mg/Ca | *G. ruber* |
| 16 | Dyez and Ravelo 2012 | ODP 871 | 5.55°N, 172.35°E | Mg/Ca | *G. ruber* |
| 17 | Lea et al 2000 | ODP 806 | 0.32°N, 159.36°E | Mg/Ca | *G. ruber* |
| 18 | Palmer and Pearson 2003 | ERDC-92 | 2.23°S, 157°E | Mg/Ca | *G. sacculifer* |
| 19 | Linsley et al 2010 | 70GGC | 3.57°S, 119.38°E | Mg/Ca | *G. ruber* |
| 20 | Stott et al 2007 | MD98-2176 | 5°S, 133.43°E | Mg/Ca | *G. ruber* |
| 21 | Linsley et al 2010 | 13GGC | 7.4°S, 115.2°E | Mg/Ca | *G. ruber* |
| 22 | Gibbons et al 2014 | GeoB10069-3 | 9.6°S, 120.92°E | Mg/Ca | *G. ruber* |
| 23 | Stott et al 2007 | MD98-2170 | 10.5°S, 125°E | Mg/Ca | *G. ruber* |
| 24 | Xu et al 2008 | MD01-2378 | 13.08°S, 121.78°E | Mg/Ca | *G. ruber* |
| 25 | Abram et al 2009 | Koil, Muschu Islands | 3°S, 144°E | coral Sr/Ca | *Porites* sp. |
| 26 | Fraser et al 2014 | MD06-3075 | 6.5°N, 125.83°E | alkenones | |

thermocline

| Map # | Reference | Site | Lat/Long | Proxy | Proxy detail |
|---|---|---|---|---|---|
| 13 | Dang et al 2012 | MD98-2188 | 14.82°N, 123.49°E | Mg/Ca | *P. obliquiloculata* |
| 24 | Xu et al 2008 | MD01-2378 | 13.08°S, 121.78°E | Mg/Ca | *P. obliquiloculata* |
| 4 | Sadekov et al 2013 | CD38-17 | 1.6°S, 90.43°W | Mg/Ca | *N. dutertrei* |

## References

An, S.-I., and J. Choi (2014), Mid-Holocene tropical Pacific climate state, annual cycle, and ENSO in PMIP2 and PMIP3, Climate Dynamics, 43(3-4), 957-970, doi: 10.1007/s00382-013-1880-z.

Anand, P., H. Elderfield, and M. H. Conte (2003), Calibration of Mg/Ca thermometry in planktonic foraminifera from a sediment trap time series, Paleoceanography, 18(2), doi: 10.1029/2002pa000846.

Bard, E., B. Hamelin, M. Arnold, L. Montaggioni, G. Cabioch, G. Faure, and F. Rougerie (1996), Deglacial sea-level record from Tahiti corals and the timing of global meltwater discharge, Nature, 382, 241-244.

Benway, H. M., A. C. Mix, B. A. Haley, and G. P. Klinkhammer (2006), Eastern Pacific Warm Pool paleosalinity and climate variability: 0-30 kyr, Paleoceanography, 21(3), PA3008, doi: 10.1029/2005pa001208.

Berelson, W. M., et al. (1997), Biogenic budgets of particle rain, benthic remineralization and sediment accumulation in the equatorial Pacific, Deep Sea Research Part II: Topical Studies in Oceanography, 44(9-10), 2251-2282.

Berger, A. L. (1978), Long-term variations of caloric insolation resulting from the Earth's orbital elements, Quaternary Research, 9, 139-167.

Bova, S. C., T. Herbert, Y. Rosenthal, J. Kalansky, M. Altabet, C. Chazen, A. Mojarro, and J. Zech (2015), Links between eastern equatorial Pacific stratification and atmospheric CO2 rise during the last deglaciation, Paleoceanography, 30(11), 1407-1424, doi: 10.1002/2015pa002816.

Braconnot, P., Y. Luan, S. Brewer, and W. Zheng (2012), Impact of Earth’s orbit and freshwater fluxes on Holocene climate mean seasonal cycle and ENSO characteristics, Climate Dynamics, 38(5-6), 1081-1092, doi: 10.1007/s00382-011-1029-x.

Brown, S. J., and H. Elderfield (1996), Variations in Mg/Ca and Sr/Ca ratios of planktonic foraminifera caused by postdepositional dissolution: Evidence of shallow Mg-dependent dissolution, Paleoceanography, 11(5), 543-551, doi: 10.1029/96pa01491.

Bush, A. B. G. (2007), Extratropical Influences on the El Niño–Southern Oscillation through the Late Quaternary, Journal of Climate, 20(5), 788-800, doi: 10.1175/jcli4048.1.

Carre, M., J. P. Sachs, S. Purca, A. J. Schauer, P. Braconnot, R. A. Falcon, M. Julien, and D. Lavallee (2014), Holocene history of ENSO variance and asymmetry in the eastern tropical Pacific, Science, 345(6200), 1045-1048, doi: 10.1126/science.1228246.

Carton, J. A., and B. S. Giese (2008), A Reanalysis of Ocean Climate Using Simple Ocean Data Assimilation (SODA), Monthly Weather Review, 136(8), 2999-3017, doi: 10.1175/2007mwr1978.1.

Chen, S., S. S. Hoffmann, D. C. Lund, K. M. Cobb, J. Emile-Geay, and J. F. Adkins (2016), A high-resolution speleothem record of western equatorial Pacific rainfall: Implications for Holocene ENSO evolution, Earth and Planetary Science Letters, 442, 61-71, doi: 10.1016/j.epsl.2016.02.050.

Chiang, J. C. H., Y. Fang, and P. Chang (2009), Pacific Climate Change and ENSO Activity in the Mid-Holocene, Journal of Climate, 22(4), 923-939, doi: 10.1175/2008jcli2644.1.

Christensen, J. H., et al. (2013), Climate Phenomena and their Relevance for Future Regional Climate Change, in Climate Change 2013: The Physical Science Basis. Contribution of Working Group I to the Fifth Assessment Report of the Intergovernmental Panel on Climate Change, edited by T. F. Stocker, D. Qin, G.-K. Plattner, M. Tignor, S. K. Allen, J. Boschung, A. Nauels, Y. Xia, V. Bex and P. M. Midgley, Cambridge University Press, Cambridge, United Kingdom and New York, NY, USA.

Clement, A. C., R. Seager, and M. A. Cane (2000), Suppression of El Niño during the Mid-Holocene by changes in the Earth's orbit, Paleoceanography, 15(6), 731-737, doi: 10.1029/1999pa000466.

Cobb, K. M., C. D. Charles, H. Cheng, and R. L. Edwards (2003), El Niño-Southern Oscillation and tropical Pacific climate during the last millennium, Nature, 424, 271-276.

Cobb, K. M., N. Westphal, H. R. Sayani, J. T. Watson, E. Di Lorenzo, H. Cheng, R. L. Edwards, and C. D. Charles (2013), Highly variable El Niño-Southern Oscillation throughout the Holocene, Science, 339(6115), 67-70, doi: 10.1126/science.1228246.

Conroy, J. L., J. T. Overpeck, J. E. Cole, T. M. Shanahan, and M. Steinitz-Kannan (2008), Holocene changes in eastern tropical Pacific climate inferred from a Galápagos lake sediment record, Quaternary Science Reviews, 27(11-12), 1166-1180, doi: 10.1016/j.quascirev.2008.02.015.

Conte, M. H., M.-A. Sicre, C. Rühlemann, J. C. Weber, S. Schulte, D. Schulz-Bull, and T. Blanz (2006), Global temperature calibration of the alkenone unsaturation index (Uk′37) in surface waters and comparison with surface sediments, Geochemistry, Geophysics, Geosystems, 7(2), Q02005, doi: 10.1029/2005gc001054.

Dang, H., Z. Jian, F. Bassinot, P. Qiao, and X. Cheng (2012), Decoupled Holocene variability in surface and thermocline water temperatures of the Indo-Pacific Warm Pool, Geophysical Research Letters, 39(1), L01701, doi: 10.1029/2011gl050154.

de Villiers, S. (2005), Foraminiferal shell-weight evidence for sedimentary calcite dissolution above the lysocline, Deep Sea Research Part I: Oceanographic Research Papers, 52(5), 671-680, doi: 10.1016/j.dsr.2004.11.014.

Dekens, P. S., D. W. Lea, D. K. Pak, and H. J. Spero (2002), Core top calibration of Mg/Ca in tropical foraminifera: refining paleotemperature estimation, Geochemistry, Geophysics, Geosystems, 3(4).

DiNezio, P. N., B. P. Kirtman, A. C. Clement, S.-K. Lee, G. A. Vecchi, and A. Wittenberg (2012), Mean Climate Controls on the Simulated Response of ENSO to Increasing Greenhouse Gases, Journal of Climate, 25(21), 7399-7420, doi: 10.1175/jcli-d-11-00494.1.

DiNezio, P. N., A. Clement, G. A. Vecchi, B. Soden, A. J. Broccoli, B. L. Otto-Bliesner, and P. Braconnot (2011), The response of the Walker circulation to Last Glacial Maximum forcing: Implications for detection in proxies, Paleoceanography, 26(3), PA3217, doi: 10.1029/2010pa002083.

Driscoll, R., M. Eliot, T. Russon, K. Welsh, Y. Yokoyama, and A. Tudhope (2014), ENSO reconstructions over the past 60 ka using giant clams (Tridacna sp.) from Papua New Guinea, Geophysical Research Letters, 41, 6819-6825, doi: 10.1002/.

Druffel, E. R. M., and S. Griffin (1993), Large variations of surface ocean radiocarbon: Evidence of circulation changes in the southwestern Pacific, Journal of Geophysical Research, 98(C11), 20249, doi: 10.1029/93jc02113.

Duprey, N., C. E. Lazareth, T. Corrège, F. Le Cornec, C. Maes, N. Pujol, M. Madeng-Yogo, S. Caquineau, C. Soares Derome, and G. Cabioch (2012), Early mid-Holocene SST variability and surface-ocean water balance in the southwest Pacific, Paleoceanography, 27(4), PA4207, doi: 10.1029/2012pa002350.

Eggins, S., P. De Deckker, and J. Marshall (2003), Mg/Ca variation in planktonic foraminifera tests: implications for reconstructing palaeo-seawater temperature and habitat migration, Earth and Planetary Science Letters, 212(3-4), 291-306, doi: 10.1016/s0012-821x(03)00283-8.

Elderfield, H., M. Vautravers, and M. Cooper (2002), The relationship between shell size and Mg/Ca,Sr/Ca, d18O, and d13C of species of planktonic foraminifera, Geochemistry, Geophysics, Geosystems, 3(8).

Emile-Geay, J., M. Cane, R. Seager, A. Kaplan, and P. Almasi (2007), El Niño as a mediator of the solar influence on climate, Paleoceanography, 22(3), PA3210, doi: 10.1029/2006pa001304.

Emile-Geay, J., et al. (2016), Links between tropical Pacific seasonal, interannual and orbital variability during the Holocene, Nature Geoscience, doi: 10.1038/ngeo2608.

Evans, M. N., R. G. Fairbanks, and J. L. Rubenstone (1998), The thermal oceanographic signal of El Nino reconstructed from a Kiritimati Island coral, Journal of Geophysical Research, 104, 13409-13421.

Faul, K. L., A. C. Ravelo, and M. L. Delaney (2000), Reconstructions of upwelling, productivity, and photic zone depth in the eastern equatorial Pacific Ocean

using planktonic foraminiferal stable isotopes and abundances, Journal of Foraminiferal Research, 30(2), 110-125.

Feely, R. A., et al. (2008), CLIVAR CO2 Sections P16S_2005 (6 January - 19 February 2005) and P16N_2006 (13 February - 30 March, 2006). Ed. A. Kozyr, in *Carbon Dioxide, Hydrographic, and Chemical Data Obtained During the R/Vs Roger Revelle and Thomas G. Thompson Repeat Hydrography Cruises in the Pacific Ocean*, edited by O. R. N. L. Carbon Dioxide Information Analysis Center, U.S. Department of Energy, Oak Ridge, Tennessee.

Fehrenbacher, J., P. A. Martin, and G. Eshel (2006), Glacial deep water carbonate chemistry inferred from foraminiferal Mg/Ca: A case study from the western tropical Atlantic, Geochemistry, Geophysics, Geosystems, 7(9), n/a-n/a, doi: 10.1029/2005gc001156.

Ford, H. L., A. C. Ravelo, and P. J. Polissar (2015a), Reduced El Niño-Southern Oscillation during the Last Glacial Maximum, Science, 347(6219), 255-258.

Fraser, N., W. Kuhnt, A. Holbourn, T. Bolliet, N. Andersen, T. Blanz, and L. Beaufort (2014), Precipitation variability within the West Pacific Warm Pool over the past 120ka: Evidence from the Davao Gulf, southern Philippines, Paleoceanography, 29, 1094-1110, doi: doi:10.1002/ 2013PA002599.

Gill, E. C., B. Rajagopalan, P. Molnar, and T. M. Marchitto (2016), Reduced-dimension reconstruction of the equatorial Pacific SST and zonal wind fields over the past 10,000 years using Mg/Ca and alkenone records, Paleoceanography, doi: 10.1002/2016pa002948.

Hanawa, K., and L. D. Talley (2001), Mode Waters, International Geophysics Series, 77, 373-386.

Hönisch, B., K. A. Allen, D. W. Lea, H. J. Spero, S. M. Eggins, J. Arbuszewski, P. deMenocal, Y. Rosenthal, A. D. Russell, and H. Elderfield (2013), The influence of salinity on Mg/Ca in planktic foraminifers – Evidence from cultures, core-top sediments and complementary δ18O, Geochimica et Cosmochimica Acta, 121, 196-213, doi: 10.1016/j.gca.2013.07.028.

Jahnke, R., D. Heggie, S. Emerson, and V. Grundmanis (1982), Pore waters of the central Pacific Ocean: nutrient results, Earth and Planetary Science Letters, 61, 233-256.

Johnson, G. C., and M. J. McPhaden (1999), Interior pycnocline flow from the subtropical to the equatorial Pacific Ocean, Journal of Physical Oceanography, 29, 3073-3089.

Johnstone, H. J. H., J. Yu, H. Elderfield, and M. Schulz (2011), Improving temperature estimates derived from Mg/Ca of planktonic foraminifera using X-ray computed tomography–based dissolution index, XDX, Paleoceanography, 26(1), doi: 10.1029/2009pa001902.

Kaiser, J., E. Schefuss, F. Lamy, M. Mohtadi, and D. Hebbeln (2008), Glacial to Holocene changes in sea surface temperature and coastal vegetation in north central Chile: high versus low latitude forcing, Quaternary Science Reviews, 27, 2064-2075.

Kalansky, J., Y. Rosenthal, T. Herbert, S. Bova, and M. Altabet (2015), Southern Ocean contributions to the Eastern Equatorial Pacific heat content during the Holocene, Earth and Planetary Science Letters, 424, 158-167, doi: 10.1016/j.epsl.2015.05.013.

Karamperidou, C., P. N. Di Nezio, A. Timmermann, F.-F. Jin, and K. M. Cobb (2015), The response of ENSO flavors to mid-Holocene climate: Implications for proxy interpretation, Paleoceanography, 30(5), 527-547, doi: 10.1002/2014pa002742.

Khider, D., G. Huerta, C. Jackson, L. D. Stott, and J. Emile-Geay (2015), A Bayesian, multivariate calibration forGlobigerinoides ruberMg/Ca, Geochemistry, Geophysics, Geosystems, 16(9), 2916-2932, doi: 10.1002/2015gc005844.

Koutavas, A., and S. Joanides (2012), El Niño-Southern Oscillation extrema in the Holocene and Last Glacial Maximum, Paleoceanography, 27(4), PA4208, doi: 10.1029/2012pa002378.

Leduc, G., L. Vidal, O. Cartapanis, and E. Bard (2009), Modes of eastern equatorial Pacific thermocline variability: Implications for ENSO dynamics over the last

glacial period, Paleoceanography, 24(3), PA3202, doi: 10.1029/2008pa001701.

Leduc, G., R. Schneider, J. H. Kim, and G. Lohmann (2010), Holocene and Eemian sea surface temperature trends as revealed by alkenone and Mg/Ca paleothermometry, Quaternary Science Reviews, 29(7-8), 989-1004, doi: 10.1016/j.quascirev.2010.01.004.

Liu, Z., J. Kutzbach, and L. Wu (2000), Modeling climate shift of El Niño variability in the Holocene, Geophysical Research Letters, 27(15), 2265-2268.

Liu, Z., Z. Lu, X. Wen, B. L. Otto-Bliesner, A. Timmermann, and K. M. Cobb (2014), Evolution and forcing mechanisms of El Niño over the past 21,000 years, Nature, 515(7528), 550-553, doi: 10.1038/nature13963.

Lu, P., and J. P. McCreary (1995), Influence of the ITCZ on the flow of thermocline water from the subtropical to the equatorial Pacific Ocean, Journal of Physical Oceanography, 25, 3076-3088.

Lynch-Stieglitz, J., et al. (2015), Glacial-interglacial changes in central tropical Pacific surface seawater property gradients, Paleoceanography, 30(5), 423-438, doi: 10.1002/2014pa002746.

Marchitto, T. M., R. Muscheler, J. D. Ortiz, J. D. Carriquiry, and A. van Geen (2010), Dynamical response of the tropical Pacific Ocean to solar forcing during the early Holocene, Science, 330(6009), 1378-1381, doi: 10.1126/science.1194887.

McGregor, H. V., and M. K. Gagan (2004), Western Pacific coral δ18O records of anomalous Holocene variability in the El Niño–Southern Oscillation, Geophysical Research Letters, 31(11), doi: 10.1029/2004gl019972.

McGregor, H. V., M. J. Fischer, M. K. Gagan, D. Fink, S. J. Phipps, H. Wong, and C. D. Woodroffe (2013), A weak El Niño/Southern Oscillation with delayed seasonal growth around 4,300 years ago, Nature Geoscience, 6(11), 949-953, doi: 10.1038/ngeo1936.

Moy, C. M., G. O. Seltzer, D. T. Rodbell, and D. M. Anderson (2002), Variability of El Nino-Southern Oscillation activity at millennial timescales during the Holocene epoch, Nature, 420(6912), 162-165, doi: 10.1038/nature01163.

O'Connor, B. M., R. A. Fine, K. A. Maillet, and D. B. Olson (2002), Formation rates of subtropical underwater in the Pacific Ocean, Deep Sea Research Part I: Oceanographic Research Papers, 49, 1571-1590.

Otto-Bliesner, B. L., E. C. Brady, S.-I. Shin, Z. Liu, and C. Shields (2003), Modeling El Niño and its tropical teleconnections during the last glacial-interglacial cycle, Geophysical Research Letters, 30(23), doi: 10.1029/2003gl018553.

Pausata, F. S. R., Q. Zhang, F. Muschitiello, Z. Lu, L. Chafik, E. M. Niedermeyer, J. C. Stager, K. M. Cobb, and Z. Liu (2017), Greening of the Sahara suppressed ENSO activity during the mid-Holocene, Nat Commun, 8, 16020, doi: 10.1038/ncomms16020.

Rayner, N. A. (2003), Global analyses of sea surface temperature, sea ice, and night marine air temperature since the late nineteenth century, Journal of Geophysical Research, 108(D14), doi: 10.1029/2002jd002670.

Regenberg, M., A. Regenberg, D. Garbe-Schönberg, and D. W. Lea (2014), Global dissolution effects on planktonic foraminiferal Mg/Ca ratios controlled by the calcite-saturation state of bottom waters, Paleoceanography, 29(3), 127-142, doi: 10.1002/2013pa002492.

Regenberg, M., D. Nürnberg, S. Steph, J. Groeneveld, D. Garbe-Schönberg, R. Tiedemann, and W.-C. Dullo (2006), Assessing the effect of dissolution on planktonic foraminiferal Mg/Ca ratios: Evidence from Caribbean core tops, Geochemistry, Geophysics, Geosystems, 7(7), n/a-n/a, doi: 10.1029/2005gc001019.

Reimer, P. J., et al. (2013), IntCal13 and Marine13 radiocarbon age calibration curves 0–50,000 years cal BP, Radiocarbon, 55(4), 1869-1887.

Robbins, L. L., M. E. Hansen, J. A. Kleypas, and S. C. Meylan (2010), CO2calc—A user-friendly seawater carbon calculator for Windows, Max OS X, and iOS

(iPhone), in *U.S. Geological Survey Open-File Report 2010–1280, 17 p.*, edited.

Roberts, W. H. G., D. S. Battisti, and A. W. Tudhope (2014), ENSO in the Mid-Holocene according to CSM and HadCM3, Journal of Climate, 27(3), 1223-1242, doi: 10.1175/jcli-d-13-00251.1.

Rodbell, D. T., G. O. Seltzer, D. M. Anderson, M. B. Abbott, D. B. Enfield, and J. H. Newman (1999), An ~15,000 year record of El Nino-driven alluviation in southwestern Ecuador, Science, 283, 516-520.

Rosenthal, Y., and G. P. Lohmann (2002), Accurate estimation of sea surface temperatures using dissolution-corrected calibrations for Mg/Ca paleothermometry, Paleoceanography, 17(3), 16-11-16-16, doi: 10.1029/2001pa000749.

Rosenthal, Y., G. P. Lohmann, K. C. Lohmann, and R. M. Sherrell (2000), Incorporation and preservation of Mg inGlobigerinoides sacculifer:implications for reconstructing the temperature and18O/16O of seawater, Paleoceanography, 15(1), 135-145, doi: 10.1029/1999pa000415.

Sadekov, A. Y., S. M. Eggins, P. De Deckker, U. Ninnemann, W. Kuhnt, and F. Bassinot (2009), Surface and subsurface seawater temperature reconstruction using Mg/Ca microanalysis of planktonic foraminifera Globigerinoides ruber, Globigerinoides sacculifer, and Pulleniatina obliquiloculata, Paleoceanography, 24(3), doi: 10.1029/2008pa001664.

Sadekov, A. Y., R. Ganeshram, L. Pichevin, R. Berdin, E. McClymont, H. Elderfield, and A. W. Tudhope (2013), Palaeoclimate reconstructions reveal a strong link between El Niño-Southern Oscillation and Tropical Pacific mean state, Nat Commun, 4, 2692, doi: 10.1038/ncomms3692.

Stott, L., A. Timmermann, and R. Thunell (2007), Southern hemisphere and deep-sea warming led deglacial atmospheric CO2 rise and tropical warming, Science, 318(5849), 435-438.

Stuiver, M., and P. J. Reimer (1993), Extended 14C data base and revised Calib3.0 14C age calibration program, Radiocarbon, 35(1), 215-230.

Thirumalai, K., J. W. Partin, C. S. Jackson, and T. M. Quinn (2013), Statistical constraints on El Niño Southern Oscillation reconstructions using individual foraminifera: A sensitivity analysis, Paleoceanography, 28(3), 401-412, doi: 10.1002/palo.20037.

Thompson, D. M., et al. (2017), Tropical Pacific climate variability over the last 6000 years as recorded in Bainbridge Crater Lake, Galápagos, Paleoceanography, doi: 10.1002/2017pa003089.

Thunell, R. C., W. B. Curry, and S. Honjo (1983), Seasonal variation in the flux of planktonic foraminifera: time series sediment trap results from the Panama Basin, Earth and Planetary Science Letters, 64, 44-55.

Timmermann, A., J. Sachs, and O. E. Timm (2014), Assessing divergent SST behavior during the last 21 ka derived from alkenones andG. ruber-Mg/Ca in the equatorial Pacific, Paleoceanography, 29(6), 680-696, doi: 10.1002/2013pa002598.

Timmermann, A., et al. (2007), The Influence of a Weakening of the Atlantic Meridional Overturning Circulation on ENSO, Journal of Climate, 20(19), 4899-4919, doi: 10.1175/jcli4283.1.

Toggweiler, J. R., K. Dixon, and W. S. Broecker (1991), The Peru upwelling and the ventilation of the South Pacific thermocline, Journal of Geophysical Research, 96(C11), 20,467-420,497, doi: 0.1029/91JC02063.

Trauth, M. H., M. Sarnthein, and M. Arnold (1997), Bioturbational mixing depth and carbon flux at the seafloor, Paleoceanography, 12(3), 517-526.

Trenberth, K. E. (1997), The definition of El Nino, Bulletin of the American Meteorological Society, 78(12), 2771-2777.

Tudhope, A. W., C. P. Chilcott, M. T. McCulloch, E. R. Cook, J. Chappell, R. M. Ellam, D. W. Lea, J. M. Lough, and G. B. Shimmield (2001), Variability in the El Nino-Southern Oscillation through a glacial-interglacial cycle, Science, 291(5508), 1511-1517, doi: 10.1126/science.1057969.

Vetter, L., H. J. Spero, A. D. Russell, and J. S. Fehrenbacher (2013), LA-ICP-MS depth profiling perspective on cleaning protocols for elemental analyses in planktic foraminifers, Geochemistry, Geophysics, Geosystems, 14(8), 2916-2931, doi: 10.1002/ggge.20163.

Watkins, J. M., A. C. Mix, and J. Wilson (1996), Living planktic foraminifera: tracers of circulation and productivity regimes in the central equatorial Pacific, Deep Sea Research Part II: Topical Studies in Oceanography, 43(4-6), 1257-1282.

Wittenberg, A. T. (2009), Are historical records sufficient to constrain ENSO simulations?, Geophysical Research Letters, 36(12), doi: 10.1029/2009gl038710.

Wittenberg, A. T., A. Rosati, T. L. Delworth, G. A. Vecchi, and F. Zeng (2014), ENSO Modulation: Is It Decadally Predictable?, Journal of Climate, 27(7), 2667-2681, doi: 10.1175/jcli-d-13-00577.1.

Wong, A. P. S., and G. C. Johnson (2003), South Pacific Eastern Subtropical Mode Water, Journal of Physical Oceanography, 33, 1493-1509.

Woodroffe, C. D. (2003), Mid-late Holocene El Niño variability in the equatorial Pacific from coral microatolls, Geophysical Research Letters, 30(7), doi: 10.1029/2002gl015868.

Xu, J., A. Holbourn, W. Kuhnt, Z. Jian, and H. Kawamura (2008), Changes in the thermocline structure of the Indonesian outflow during Terminations I and II, Earth and Planetary Science Letters, 273(1-2), 152-162, doi: 10.1016/j.epsl.2008.06.029.

Zaunbrecher, L. K., K. M. Cobb, J. W. Beck, C. D. Charles, E. R. M. Druffel, R. G. Fairbanks, S. Griffin, and H. R. Sayani (2010), Coral records of central tropical Pacific radiocarbon variability during the last millennium, Paleoceanography, 25(4), doi: 10.1029/2009pa001788.

Zhang, Z., G. Leduc, and J. P. Sachs (2014b), El Niño evolution during the Holocene revealed by a biomarker rain gauge in the Galápagos Islands, Earth and Planetary Science Letters, 404, 420-434, doi: 10.1016/j.epsl.2014.07.013.

# Chapter 3: Dampened El Niño in the early Pliocene warm period

Sarah M. White[1]*, A. Christina Ravelo[2]

[1] Department of Earth and Planetary Sciences, University of California, Santa Cruz, CA.

[2] Department of Ocean Sciences, University of California, Santa Cruz, CA.

* Corresponding author: Sarah White (smwhite@ucsc.edu)

## Abstract

El Niño-Southern Oscillation (ENSO) is the strongest mode of interannual climate variability, and its predicted response to anthropogenic climate change remains unclear. Determining ENSO's sensitivity to climatic mean state and the strength of positive and negative feedbacks, notably the thermocline feedback, will help constrain its future behavior. To this end, we collected ENSO proxy data from the early and mid-Pliocene, a time period during which the tropical Pacific thermocline was much deeper than today. We found that El Niño events had a reduced amplitude throughout the early Pliocene, compared to the late Holocene. By the mid-Pliocene, El Niño amplitude was sometimes reduced and sometimes similar to the late Holocene. This trend in Pliocene ENSO amplitude mirrors the long-term shoaling of the thermocline from the early to the mid-Pliocene, and thus supports an important role for the strength of the thermocline feedback in dictating ENSO strength.

## 1 Introduction

El Niño events, marked by anomalously warm sea-surface temperatures (SSTs) in the eastern and central equatorial Pacific, cause drought, floods, and ecosystem shifts over the circum-Pacific region, and occur every three to seven years as part of the El Niño-Southern Oscillation (ENSO). ENSO is the strongest mode of interannual climate variability, and its predicted response to anthropogenic climate change remains unclear. The disparity among predictions stems from a lack of understanding of ENSO's sensitivity to mean climate and various positive and negative feedbacks, including the thermocline feedback. Different models have a stronger or weaker thermocline feedback in historical model runs [*Kim et al.*, 2014a], and also exhibit differing changes in the strength of the thermocline feedback under future warming [*Chen et al.*, 2017]. Paleo-proxy data from the Holocene and Last Glacial Maximum indicate that tropical Pacific thermocline depth, a major control on the strength of the thermocline feedback, seems to dictate ENSO strength [*Ford et al.*, 2015a; *White et al.*, 2018]. However, different models place differing emphasis on the thermocline feedback [*Kim et al.*, 2014a].

The Pliocene is an excellent test case of the importance of thermocline depth, because the tropical Pacific thermocline was much deeper than today in the early Pliocene, and shoaled toward present [*Ford et al.*, 2012; *Ford et al.*, 2015b; *Seki et al.*, 2012; *Steph et al.*, 2010]. Modeling efforts have focused on the mid-Pliocene PRISM interval (Pliocene Research, Interpretation and Synoptic Mapping, targeting 3.264-3.025 Ma), including the PlioMIP model intercomparison. However, because

the thermocline was not much deeper during the PRISM interval than today [*Ford et al.*, 2012; *Haywood et al.*, 2013], it does not provide the best test of the effect of a deep thermocline on ENSO. Other studies tested the effect of various factors at play during the early Pliocene, including an open Central American Seaway (CAS), a deeper/wider Indonesian seaway, higher $pCO_2$, weaker tropical Pacific zonal winds and SST gradients, altered Andean orography, and a deeper thermocline [*Brierley and Fedorov*, 2016; *Feng and Poulsen*, 2014; *Jochum et al.*, 2009; *Manucharyan and Fedorov*, 2014; *Song et al.*, 2017; *von der Heydt et al.*, 2011]. Studies report different effects on ENSO; for example, an open CAS may have strengthened [*Song et al.*, 2017] or dampened [*von der Heydt et al.*, 2011] ENSO depending on the model and the imposed boundary conditions (i.e. sill depth of the CAS [*Brierley and Fedorov*, 2016]). Centennial-scale variability in ENSO adds further difficulty, necessitating longer model runs and larger proxy datasets to achieve confidence in interpreting results, [e.g. *Tindall et al.*, 2016]). Although there is limited ENSO data from the mid-Pliocene [*Scroxton et al.*, 2011; *Watanabe et al.*, 2011], none is from the early Pliocene.

New data from the early Pliocene are thus needed to test the importance of thermocline depth in dictating ENSO strength. To this end, we collected individual foraminiferal temperature data from the eastern equatorial Pacific (EEP). We analyzed samples every half million years from 5 Ma to the PRISM interval, plus multiple samples at high resolution in the PRISM interval and at 4.5 Ma, to evaluate

long-term trends in ENSO strength and verify the presence/absence of orbital-scale variations.

This study focuses on ODP site 849 in the EEP, located within the Niño3 region (Fig. 1). The site is well-suited for studying ENSO; the seasonal range of SST is ±1.5°C, whereas the average peak El Niño anomaly is +2.8°C, and the very warmest temperatures occur exclusively during El Niño months, as shown in a reanalysis dataset (the Simple Ocean Data Assimilation, "SODA" [*Carton and Giese*, 2008]). We are thus able to distinguish changes in seasonality versus ENSO, as described below.

## 2 Materials and Methods

### *2.1 Analytical Methods*

We collected trace metal data from individual tests of the foraminifer *Globigerinoides sacculifer* without sac-like final chamber, recently renamed *Trilobatus trilobus* [*Spezzaferri et al.*, 2015]; here we retain the name *G. sacculifer* for consistency with White et al. [2018]. Individual *G. sacculifer* were picked from the 250-350 μm size fraction to avoid ontogenetic effects. Specimens were sonicated for 30 s and rinsed in methanol, then part of the last (f0) chamber was separated from the test with a microspatula and mounted on carbon tape for analysis.

Mg/Ca data were acquired following the method of White et al. [*White et al.*, 2018] on an average of 48 specimens per sample. See Table S1 for sample names and number of specimens from each. Analysis was performed by laser ablation-

inductively coupled plasma-mass spectrometry (LA-ICP-MS) at the University of California, Santa Cruz using a Photon Machines Analyte.193 with HelEx sample cell coupled to a Thermo ElementXS. Samples were ablated at 4 Hz and 0.70/cm$^2$ laser fluence; the NIST 610 glass standard was ablated at 4 Hz and 1.62 J/cm$^2$ laser fluence. Samples and standards were analyzed for $^{11}$B, $^{24}$Mg, $^{25}$Mg, $^{27}$Al, $^{43}$Ca, $^{44}$Ca, $^{55}$Mn, $^{66}$Zn, and $^{88}$Sr. Measured elemental intensities were converted to molar ratios by calibration to the NIST 610 glass standard. The NIST 610 was analyzed at the beginning and end of each instrument run, and every six specimens, in order to correct for any instrumental drift. Average measured values of Mg/Ca in the NIST 610 were 8.745 mmol/mol ±1.5%. Average measured values of Mg/Ca in the NIST 612 (used as an independent check on precision) were 1.09 mmol/mol ±3.4%.

Test fragments were ablated from the inner to the outer surface, and sample acquisition lasted ~60 s. Three or four 50μm spots were ablated per fragment, depending on size, and elemental ratios from all spots were averaged to get a representative value for each specimen. The average standard deviation of Mg/Ca among spots was 0.084 mmol/mol; specimens with a standard deviation >0.25 mmol/mol were not included in final data. $^{27}$Al and $^{55}$Mn were used as contaminant indicators, and parts of the elemental profiles with high $^{27}$Al and $^{55}$Mn were excised before computing profile mean values, as was the peak in Mg associated with the inner surface of each shell.

*2.2 Temperature calibration and age estimates*

We converted foraminiferal Mg/Ca ratios to temperature using a *G. sacculifer*-specific calibration with depth-based dissolution correction [*Dekens et al.*, 2002]. Sample ages are from the age model of Mix et al. [1995], which is based on benthic foraminiferal $\delta^{18}O$ data from our site. Samples dated to 3.071 Ma, 3.082 Ma, and 3.087 Ma are from Hole 849C, whereas all other samples are from Hole 849D. As such, there is some uncertainty (plus or minus a few thousand years) in the ages of these samples relative to all others, which is denoted by asterisks next to sample ages in Fig. 2. The amount of time represented in each sample varies from ~1250-1600 years in the early Pliocene to ~2900 years in the mid-Pliocene, based on the sedimentation rate and an estimated bioturbation depth of 8 cm [*Trauth et al.*, 1997]. We note that in an individual foraminiferal dataset, bioturbation does not reduce variance, but rather broadens the timeframe over which temperatures are sampled.

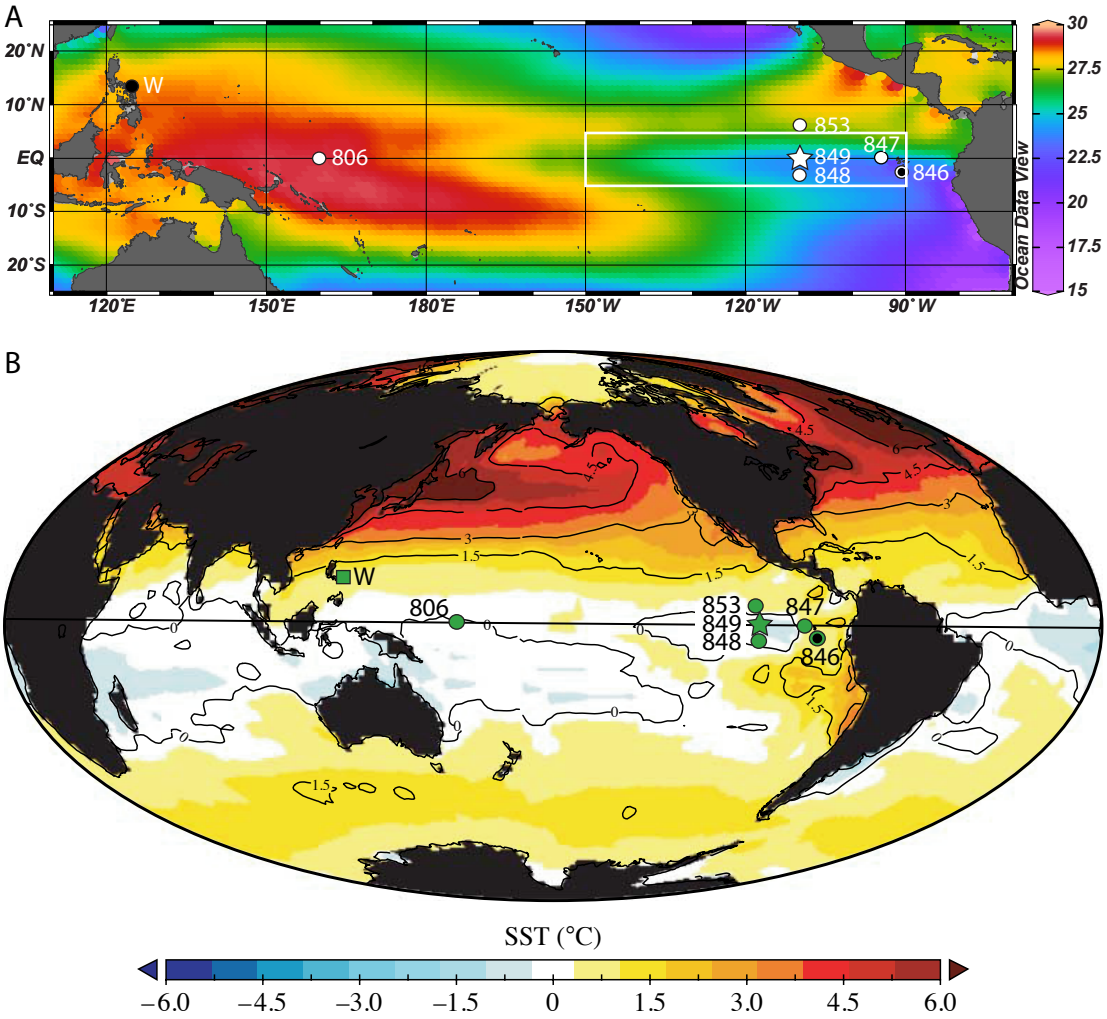


**Figure. 1. Sites referenced in this study.**

(A) ODP site 849 (0°N, 110°W, 3839 m water depth), the site of our Pliocene El Niño record (star), the sites of other published Pliocene ENSO reconstructions (black circles; "W" denotes coral record of Watanabe et al. [2011]), and the locations of Plio-Pleistocene temperature records shown in Fig. 4 (white circles), superimposed on a map of modern SST [*Locarnini et al.*, 2013]. Site 846 has both a Pliocene ENSO record and a Plio-Pleistocene temperature record. White box delineates Niño3 region. (B) Anomaly map showing PRISM3 proxy-based SST reconstruction (3.3-3.0 Ma) minus modern SST [*Dowsett and Robinson*, 2009], with site locations from this study.

## 3 Results

To reconstruct ENSO at Site 849, we collected foraminiferal Mg/Ca ratios (a proxy for seawater temperature) from individual tests of the mixed-layer dwelling *Globigerinoides sacculifer* (without sac-like final chamber) (see Materials and Methods). Because *G. sacculifer* lives for about one month, acquiring data from many individuals provides a reconstruction of the monthly distribution of temperatures over time. To diagnose changes in Pliocene ENSO, we use quantile-quantile (QQ) plots, a method that compares distributions enabling visual separation of ENSO from seasonality. Pliocene samples are normalized to the late Holocene sample to minimize bias from bioturbation and other sedimentary or foraminiferal processes and remove changes in mean temperature (see supplementary text and Fig. S1). To identify changes in ENSO, we examine the very warmest quantiles, representative of El Niño events. A significant decrease in the temperature of the uppermost quantiles, relative to the mean, indicates a decrease in the amplitude of El Niño events compared to the late Holocene, referred to as "dampened El Niño."

### *3.1 G. sacculifer as recorders of mixed layer temperatures*

Individual *G. sacculifer* temperatures at Site 849 from the late Holocene (2800 years before present [*Ford et al.*, 2015a]) provide an excellent match to the temperature distribution in the mixed layer and uppermost thermocline (Fig. 2 and S2), consistent with previous work constraining the calcification depth of *G. sacculifer* in the eastern equatorial Pacific [*Faul et al.*, 2000]. Because *G. sacculifer*

captures the entire temperature distribution, it appears to have little to no seasonal bias. The warmest 20% of *G. sacculifer* data matches temperatures from 15 m depth (well within the mixed layer), as shown by how close the points are to the 1:1 line. Because the cooler parts of the *G. sacculifer* temperature distribution come from deeper in the water column, we base our interpretations of changes in ENSO exclusively on the warmest 20% of the data, thus focusing on mixed layer temperature variability. This means that we interpret changes in El Niño amplitude, and not La Niña.

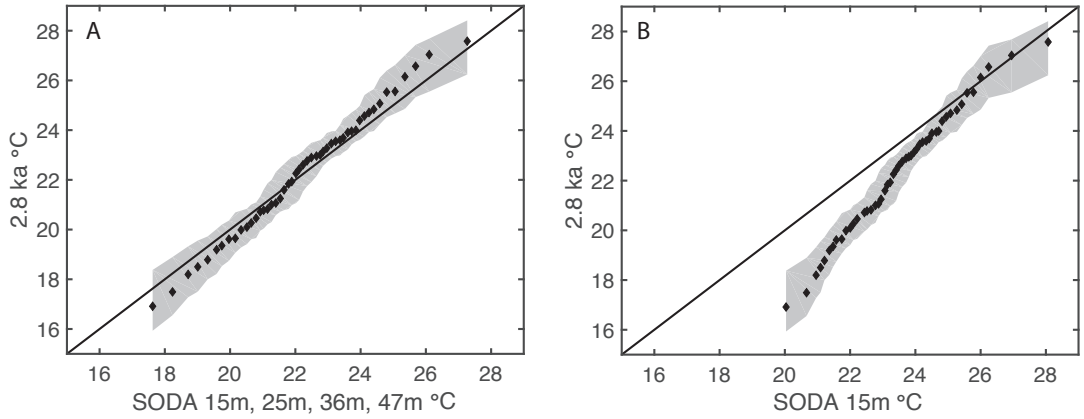


**Figure 2. *G. sacculifer* as recorder of modern temperatures.**
(A) QQ plot of modern monthly temperatures near our site [*Carton and Giese*, 2008] composited from 15 m, 25 m, 36 m, and 47 m depth versus individual *G. sacculifer* temperatures from the coretop, with 95% confidence intervals (gray region). Black line shows 1:1 line. Confidence intervals are estimated by bootstrapping the empirical continuous distribution function of each Pliocene sample using Monte Carlo methods. (B) Same as A, but with modern monthly temperatures from 15 m depth only.

To examine how changes in ENSO and seasonality at Site 849 appear in our foraminiferal data, we performed sensitivity tests. Our data can capture a decrease in El Niño amplitude of as little as 20%, and even a 50% decrease in seasonality does not affect the warmest quantiles (Figs. S3-S4). Tectonic drift in site position has a

negligible effect on the temperature distribution (Fig. S5). Centennial-millennial shifts in mean temperature (likely between ±0.3°C and ±0.5°C at ODP 849 [*Cobb et al.*, 2003; *Conroy et al.*, 2010; *Rustic et al.*, 2015]) would have little effect on our results because they have far lower amplitude than the seasonal cycle or ENSO [*White et al.*, 2018].

### *3.2 Pliocene single foraminiferal temperature data*

For all our early Pliocene samples (5.038 Ma to 3.481 Ma), the uppermost quantiles are significantly below the zero line on a normalized QQ plot, indicating dampened El Niño relative to the late Holocene sample (Fig. 3). For the mid-Pliocene samples (3.071 Ma to 3.088 Ma), some show dampened El Niño, while others show similar El Niño amplitude to the late Holocene within 95% confidence intervals.

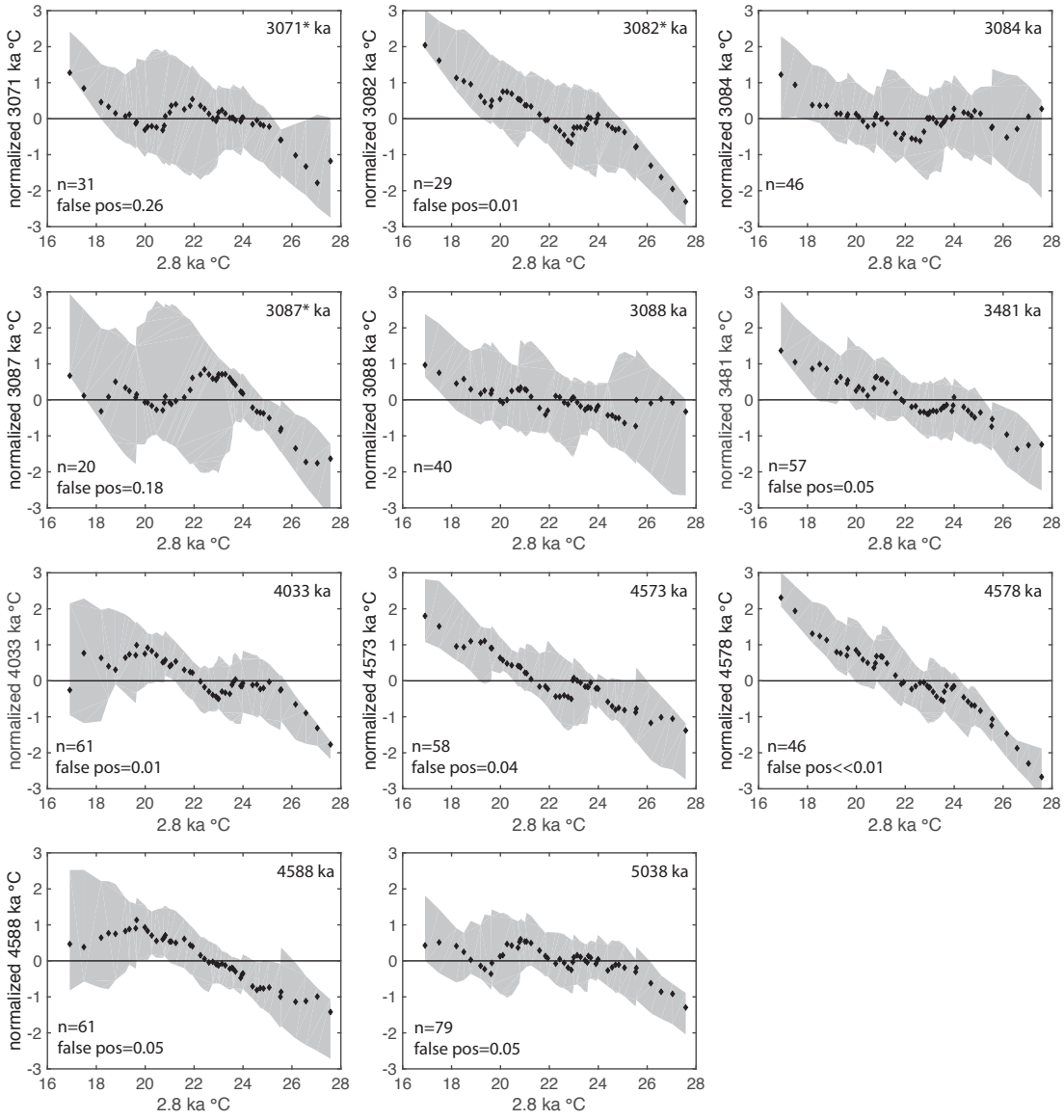


**Figure 3. *G. sacculifer*-derived temperature distributions from the mid- and early Pliocene at Site 849.**

Plots compare the late Holocene temperature distribution (x axis, all plots) to Pliocene distributions that have been normalized to remove any difference in mean temperature between the two datasets (y axis, all plots). Asterisks denote uncertainty (plus or minus a few thousand years) in these ages relative to all others, since these samples are from a different hole (849C vs. 849D). Gray shading indicates 95% confidence intervals. The number of specimens and the probability of that specific result being a "false positive" is indicated for each sample that shows dampened El Niño.

We tested the robustness of our results by estimating the probability of getting a subsample in which the uppermost quantiles are further below the zero line on a normalized QQ plot than our samples, when in fact there is no change in El Niño (i.e. a "false positive;" Figs. 3, S6, and supplementary materials). For seven out of the nine samples showing dampened El Niño, the false positive rate is ≤5%. The other samples, aged 3.071 Ma and 3.087 Ma, have much higher false positive rates, but are still more likely than not to reflect dampened El Niño. Overall, the false positive tests support the idea that El Niño was generally dampened in the early Pliocene, and by the mid-Pliocene (~3.1 Ma), El Niño was sometimes dampened and sometimes similar to the late Holocene.

To test the potential effect of changes in sample mean temperature caused by shifts in thermocline depth, we constructed QQ plots normalized to the portion of the foraminiferal distribution lying entirely within the mixed layer (the warmest 50%), rather than the mean of the entire sample distribution (Fig. S7 and supplementary materials). We also tested the effect of changes in Mg/Ca of seawater over the Plio-Pleistocene, by re-calculating all foraminiferal temperatures using the Evans et al. [*Evans et al.*, 2016] calibration (Fig. S8 and supplementary materials). Additionally, we incorporated a 0.51°C 1σ uncertainty in each data point (Fig. S9 and supplementary materials). In all cases, our interpretations remain the same for all samples (albeit with higher false positive rates) except the 3.071 Ma sample, which shows El Niño similar to the late Holocene.

Our data indicate that El Niño was dampened throughout the early Pliocene. By the mid-Pliocene, El Niño was sometimes weaker and sometimes stronger (similar to the late Holocene), appearing to vary on orbital timescales, though we cannot distinguish between different sources of variability. Dampened seasonality alone cannot explain our data; only dampened ENSO, or a dampening of both ENSO and seasonality, can explain our data (Figs. S3-S4). An alternative conceptual framework to illustrate our findings is that, in the Pliocene, Site 849 was more like the modern central equatorial Pacific, where both ENSO and seasonality are weaker than at Site 849.

*3.3 Comparison to existing Pliocene proxy data and simulations*

The record of Scroxton et al. is based on individual mixed-layer and thermocline-dwelling foraminiferal $\delta^{18}O$ data from ODP site 846, and includes samples from 3.076 Ma, 3.156 Ma, 3.328 Ma, and 3.727 Ma [*Scroxton et al.*, 2011]. The authors concluded that ENSO was persistent throughout the Pliocene, but did not quantify whether it was stronger or weaker than today. We re-analyzed their *G. ruber* data[2011] using normalized QQ plots. Data from 3.076 and 3.328 Ma show similar El Niño to the late Holocene and data from 3.156 Ma and 3.727 Ma show dampened El Niño (Fig. S10), in agreement with our findings. Watanabe et al. presented two 35-year-long coral $\delta^{18}O$ records from the Philippines from 3.5-3.8 Ma, and concluded that ENSO was present but did not quantify its strength relative to today [*Watanabe et*

*al.*, 2011]. Their data are thus consistent with ours, in that we observe dampened but not necessarily absent Pliocene ENSO.

Modeling studies of Pliocene climate include 1) efforts through PlioMIP to fully re-create mid-Pliocene climate during the PRISM interval using a full suite of boundary conditions including 405 ppm $pCO_2$ and 25 m higher sea level [*Dowsett et al.*, 2010]; and 2) sensitivity tests isolating the effect on tropical Pacific mean state and ENSO of an open CAS, deeper/wider Indonesian gateway, higher $pCO_2$, weaker zonal winds and SST gradients, altered Andean orography, and a deeper thermocline; these studies are reviewed in the Discussion. Eight out of nine models in the PlioMIP simulated dampened ENSO [*Brierley*, 2015], in broad agreement with our mid-Pliocene results, which show dampened ENSO in three out of five samples. PlioMIP models were forced with fixed modern orbital parameters, whereas our data reflect varying orbital parameters over ~20 kyr, which may explain why we observed more sample-to-sample variation in El Niño strength. Interestingly, Brierley [2015] found that neither zonal temperature gradient nor the seasonal cycle nor the elevation of the Andes Mountains explained the results from all models – indicating that the dampening mechanism was model-dependent. However, he did not explore the effect of thermocline depth.

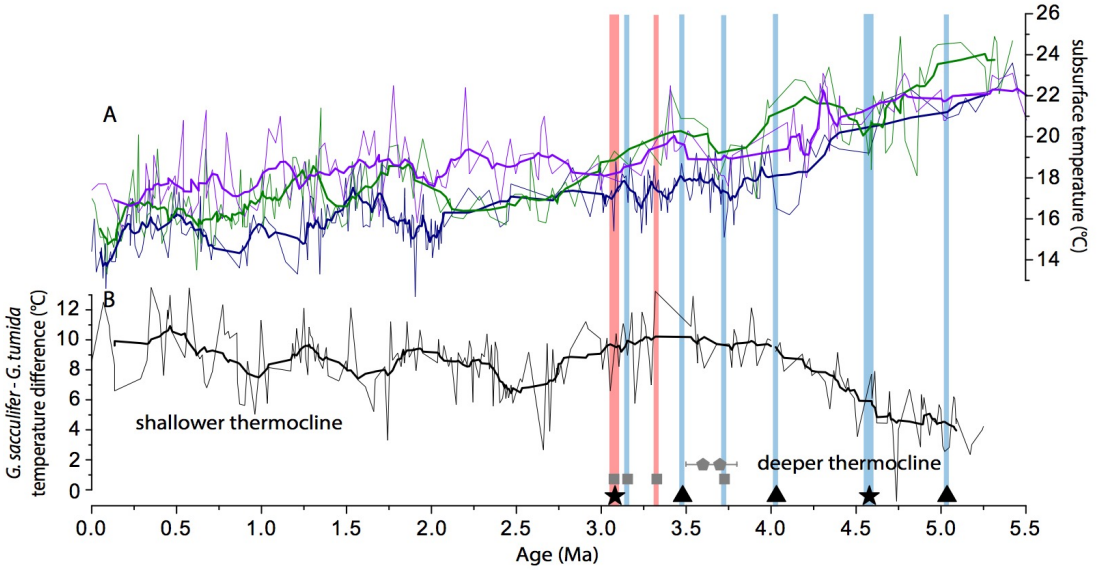


**Figure 4. Plio-Pleistocene tropical Pacific subsurface temperatures and paleo-El Niño.**

(A) Subsurface temperature records from *G. tumida* Mg/Ca at Sites 853, 849, and 848 in the EEP [*Ford et al.*, 2012] (purple, navy blue, and green, respectively). (B) Surface-subsurface temperature gradient record from Site 847 in the EEP, based on δ18O difference between *G. sacculifer* and *G. tumida* [*Wara et al.*, 2005]. Symbols at the bottom indicate ENSO proxy data: Black stars and triangles (this study) denote multiple closely-spaced samples and single samples, respectively; gray squares denote data from Scroxton et al. [2011]; gray pentagons denote approximate ages of data from Watanabe et al. [2011] (published ages are 3.5-3.8 Ma). Vertical bars indicate El Niño findings, with thin bars denoting single samples and thick bars denoting multiple closely-spaced samples. Blue bars indicate dampened El Niño, red bars indicate similar El Niño as the late Holocene (or varying dampened/similar El Niño, in the case of our multiple ~3.1 Ma samples). The Watanabe et al. [2011] study found that ENSO was present but did not quantify its strength, so no vertical bars are placed on these data.

## 4 Discussion

Our Pliocene data, along with previously published data, support the hypothesis that mean thermocline depth regulates ENSO strength. The mechanism by which a deeper thermocline dampens ENSO is best understood within the framework of feedbacks. The thermocline takes part in two positive feedbacks that help generate

ENSO in the modern ocean: the upwelling feedback and the thermocline feedback. An anomalous decrease (increase) in upwelling, or an anomalous deepening (shoaling) of the thermocline in the EEP via a decrease (increase) in east-west thermocline tilt, in both cases causes warmer (cooler) SSTs in the EEP, lowering (raising) the zonal temperature gradient and weakening (strengthening) zonal winds, thus causing a further decrease (increase) in upwelling or deepening (shoaling) of the EEP thermocline. Both feedbacks depend on a shallow mean thermocline depth in the EEP. If the mean thermocline depth is deep, then anomalies in upwelling or thermocline tilt have little impact on SSTs, which greatly weakens the overall strength of the feedbacks – and weak positive feedbacks cause dampened ENSO.

Long-term records across the tropical Pacific show a warmer subsurface in the early Pliocene, which cooled dramatically by the mid-Pliocene and continued cooling gradually toward present [*Ford et al.*, 2012; *Ford et al.*, 2015b; *Seki et al.*, 2012; *Steph et al.*, 2010] (Fig. 4). The vertical temperature gradient, indicative of thermocline depth, was also much lower than today at 4.5-5 Ma [*Ford et al.*, 2015b; *Wara et al.*, 2005]. As such, a deeper thermocline can explain dampened El Niño in the early Pliocene, as shown in our four samples from 4.5-5 Ma. By the mid-Pliocene, the thermocline is inferred to have become shallow enough to interact with EEP SSTs [*Lawrence et al.*, 2006], which can explain periods of relatively stronger and weaker El Niño in our five samples 3.07-3.09 Ma. The relatively strong vertical temperature gradient of the mid-Pliocene EEP appears to have been established by ~4 Ma, and so does not seem to explain our observation of dampened El Nino at 4.033 Ma and 3.481

Ma. This may be an artifact of the sparseness of our data during this time – perhaps we are missing periods of relatively stronger El Niño, similar to the mid-Pliocene. Data on vertical temperature gradients in the EEP are also limited; only ODP 847 has both surface and subsurface records. Overall, long-term changes in thermocline conditions can explain the trend in our data, from dampened El Niño in the earliest Pliocene to variable El Niño in the mid-Pliocene.

The thermocline depth hypothesis has a broad base of support in the modeling literature. Liu et al.[2014] and Karamperidou et al.[2015] proposed it to explain dampened ENSO during the early and mid-Holocene, using global climate models. Sensitivity studies that altered the model physics to deepen the tropical Pacific thermocline [*Manucharyan and Fedorov*, 2014] also found that a deeper thermocline dampens ENSO by weakening the thermocline feedback. Von der Heydt et al. [2011] found that weaker zonal winds weaken ENSO via the wind's effect on thermocline tilt and the strength of the thermocline feedback. It is possible that the mechanism for dampened ENSO in the early Pliocene relied on SSTs and/or winds, independent of or in addition to changes in the thermocline. SST, winds, and thermocline depth are tightly linked in the tropical Pacific, and it is not possible to disentangle them in the current study. However, studies of ENSO during the Holocene and Last Glacial Maximum were able to distinguish these effects, and concluded that thermocline depth is a more important control on ENSO than SSTs or winds [*Ford et al.*, 2015a; *White et al.*, 2018].

Changes in oceanic gateways and Andean topography likely also had an impact on ENSO, but different studies found opposing effects. A deeper/wider Indonesian seaway may have dampened [*Jochum et al.*, 2009] or slightly strengthened ENSO [*Brierley and Fedorov*, 2016]. An open CAS may have weakened [*von der Heydt et al.*, 2011] or strengthened [*Song et al.*, 2017] ENSO, or strengthened ENSO but reduced the El Niño/La Niña asymmetry such that El Niño events had a lower amplitude [*Brierley and Fedorov*, 2016]. Lowering the Andes may strengthen ENSO [*Feng and Poulsen*, 2014], but the full PRISM boundary conditions, which include lower Andes, produce weaker ENSO in the same model [*Brierley*, 2015]. A clear source of disparity between studies is the exact boundary conditions imposed; for example, a CAS sill depth of 1200 m [*Song et al.*, 2017] versus 150 m [*Brierley and Fedorov*, 2016]. Overall, it is difficult to use our data to validate model sensitivity studies, since the timing and magnitude of gateway changes is poorly constrained by geologic data. The question also remains: by what mechanism would a change in seaways or Andean topography affect ENSO? Most proposed mechanisms act via SSTs and/or the thermocline. Our goal is to determine whether a deeper thermocline in the early Pliocene dampened ENSO, so we focus on how seaways and topography affected the tropical thermocline. Indeed, an open CAS has been shown to deepen the thermocline [*Brierley and Fedorov*, 2016; *Steph et al.*, 2010; *Zhang et al.*, 2012], with deeper sill depths causing a greater deepening of the thermocline [*Brierley and Fedorov*, 2016]. As such, in proposing that long-term

changes in the thermocline regulated ENSO during the Pliocene, we suggest that if the seaways acted on ENSO, they acted via the thermocline.

What caused the orbital-scale changes in mid-Pliocene El Niño strength? A likely explanation is orbital-scale variations in thermocline depth, such that both long-term and short-term changes in El Niño strength were accomplished through the same mechanism. In the early Pliocene, the mean thermocline was likely so deep that orbital-forced changes in depth were unable to affect the surface, rendering them incapable of affecting ENSO. By the mid-Pliocene, the mean thermocline is inferred to have shoaled enough that orbital-forced changes in depth affected EEP SSTs, enabling periods of stronger and weaker ENSO. Although records of tropical Pacific subsurface temperature [*Ford et al.*, 2012; *Ford et al.*, 2015b] are not of sufficient resolution to validate or invalidate this hypothesis for the Pliocene, it has been shown to explain dampened El Niño in the mid- and early Holocene [*White et al.*, 2018]. Until more records of orbital-scale changes in thermocline depth are available, our data are unable to distinguish between a thermocline mechanism and an SST-only mechanism. While observed changes in mid-Pliocene El Niño may occur over orbital timescales, it is also possible that they occur over centennial timescales, e.g. [*Tindall et al.*, 2016].

Overall, the observed changes in El Niño can be explained by long-term changes in tropical Pacific thermocline depth: a deep thermocline in the early Pliocene dampened El Niño, whereas the mid-Pliocene thermocline had shoaled enough that the ocean-atmosphere system became sensitized to orbital forcing,

enabling periods of stronger and weaker El Niño. The mechanism behind orbitally-paced changes in mid-Pliocene El Niño is less well constrained, but orbital forcing of thermocline depth is a reasonable candidate. The demonstrated importance of thermocline depth and the thermocline feedback in regulating ENSO strength should be considered in projections of ENSO's response to anthropogenic climate change.

**Acknowledgments**

We thank Rob Franks for analytical assistance and Esther Brady for enlightening conversations about Pliocene ENSO. We also thank Chris Brierley and two anonymous reviewers for very helpful feedback on an earlier version of the manuscript. Funding was provided by NSF grants OCE-1405178 and OCE-1204254. Our data are deposited at the National Oceanic and Atmospheric Administration National Climatic Data Center. The authors declare that they have no competing interests. Author contributions: A.C.R. conceived the study, procured funding, and provided guidance and feedback on data collection, writing, and editing. S.M.W. collected and analyzed the data and wrote the paper.

## Supplementary Materials for Dampened El Niño in the early Pliocene warm period

### Text S1. Potential influence of manganese-bearing phases

Many Pliocene specimens had a Mn peak near the inner surface, slightly deeper in the test wall than the Mg peak. As such, peaks in Mn did not coincide with peaks in Mg, but nonetheless, we removed both from data traces before calculating mean values. Overall, the mean value of Mn/Ca in our Pliocene specimens was 1.09 mmol/mol, compared to 0.10 mmol/mol in our late Holocene specimens. Mn/Ca values were highest in the mid-Pliocene samples (1.87 mmol/mol on average), and declined downcore, falling to 0.30 mmol/mol in our earliest Pliocene sample. Our results are similar to those of Wara et al. [2005], who found Mn/Ca values of 1.45 ±0.31 mmol/mol for Pliocene samples from ODP site 847 (~1650 km further east along the equator). In every sample except one, Mn/Ca and Mg/Ca showed little to no correlation, with R2 values ranging from 0.01 to 0.1. In the 3.084 Ma sample, the R2 value was 0.36. The lack of correlation between Mn/Ca and Mg/Ca in all but one sample gives us confidence that our results are not biased by contamination from manganese-bearing phases – and our overall interpretation of Pliocene El Niño does not hinge on the one sample that does show a slight correlation.

### Text S2. Statistical analysis, construction of confidence intervals, and interpretation of changes in ENSO

We use quantile-quantile (QQ) plots to compare foraminiferal Mg/Ca-based temperature distributions, instead of simple metrics such as standard deviation or

range. Standard deviation assumes a normal temperature distribution, but the asymmetry of ENSO (with stronger El Niños than La Niñas) creates non-normal temperature distributions in the modern eastern and central equatorial Pacific. Thus, changes in the distribution may not be accurately captured by standard deviation. In addition, standard deviation cannot distinguish changes in seasonality from changes in ENSO. Range is problematic because it is so susceptible to outliers (or lack thereof) and error from undersampling; thus it is the most difficult parameter to constrain [*Thirumalai et al.*, 2013]. QQ plots allow visual comparison and separation of specific parts of distributions. This fits our purposes because only the warm "tail" of the temperature distribution is representative of El Niño events and is outside the range of seasonal extremes. For this study, when comparing two temperature distributions, we remove the difference in mean temperature to create normalized QQ plots.

Fig. S1 demonstrates how QQ plots enable comparison of two distributions. To create the QQ plots, we construct an empirical continuous distribution function (ECDF) from each dataset, and interpolate and evaluate it at 2% intervals to calculate quantile values. To compare the two datasets, the quantiles from each dataset are plotted against each other, forming the QQ plot. Because both axes have the same temperature units as the original datasets, comparison is made easy. Points falling on the 1:1 line indicate equivalency in the compared distributions, while deviations from the 1:1 line mark differences between the distributions, with changes in slope indicating statistical differences including standard deviation, kurtosis, or skewness.

A constant shift in average temperature between the distributions will plot as a line parallel to, but offset from, the 1:1 line. To focus on deviations in the shapes of the distributions, we present data in normalized QQ plots, in which we shift the 1:1 line by the difference in mean temperature between the two datasets (dotted line in Fig. S1c), and only plot deviations from the adjusted 1:1 line, which becomes the zero line (Fig. S1d).

Monte Carlo simulations similar to those employed by Ford et al. [2015a] allow estimation of 95% confidence intervals for each quantile in every downcore interval (y-values on normalized QQ plots). These confidence intervals are calculated using the ECDF of the downcore interval. 10,000 Monte Carlo datasets are generated through a bootstrapping approach in which we sample this ECDF at random points, each dataset containing the same number of points as the original measured distribution. Quantile values are calculated for each Monte Carlo dataset, and sorted such that all 10,000 values for the coldest quantile are ordered from coldest to warmest, and so on for all 50 quantiles. The bounds of the 95% confidence interval are then determined by the $250^{th}$ and $9750^{th}$ value.

At the site studied in this paper, modern temperatures in the warmest quantiles in the mixed layer occurred exclusively during El Niño events [*Carton and Giese*, 2008]. Data in these top quantiles are thus expected to be representative of El Niño events, such that a relative decrease in the temperatures of these quantiles would indicate a decrease in the amplitude of El Niño events. A normalized QQ plot would show this as the warmest quantiles plotting below the zero line. Moderate El Niño

events and “normal” seasonal extremes, by contrast, only change temperatures in the middle and moderately warm quantiles, and as such our interpretations of ENSO are based only on the very warmest quantiles. La Niña events are not as different from “normal” seasonality as El Niño events, so small changes or lack of change in the cold end of the distribution cannot definitively be attributed to changes in La Niña.

**Text S3. Effect of tectonic drift in site position**

We tested the effect of long-term tectonic drift in site position from 1.25°S, 106.25°W five million years ago [*Mayer et al.*, 1992] to 0°N, 110°W today, by comparing the modern temperature distribution at 15 m depth [*Carton and Giese*, 2008] to the modern temperature distribution at the paleo-location (Fig. S5). The change in location has a negligible effect on the temperature distribution.

**Text S4. “False positive” tests**

We performed “false positive” tests to quantify the probability of getting a subsample that shows more extremely dampened El Niño amplitude than our samples (a “positive” result), when in fact there is no change in ENSO (making the positive result “false”). These tests reflect the effects of both sample size and uncertainty in sample mean. “More extremely dampened El Niño amplitude” is defined as equally great or greater of a decrease, compared to our samples, in the average value of the top four quantiles’ upper 95% confidence intervals relative to the zero line on the normalized QQ plot (AVGTOP4). The top four quantiles were chosen because they form the part of the temperature distribution that comes exclusively from El Niño

events, as shown in the SODA data [*Carton and Giese*, 2008]. These concepts are illustrated in Fig. S7.

For each of our samples, we first calculated the AVGTOP4. This number formed the basis of comparison for all our tests. Then we constructed the tests, as such: we chose a random subsample of unaltered SODA data composited from 15 m, 25 m, 36 m, and 47 m depth (to span *G. sacculifer*'s entire depth habitat) near site 849[*Carton and Giese*, 2008] to use as the baseline dataset (on the x axis), which functions as the late Holocene sample in our foraminiferal data analysis. We then chose another random subsample of unaltered SODA data to use as the comparison dataset (on the y axis), functioning as the downcore sample in our foraminiferal data analysis. For the y axis subsample, we generated 95% confidence intervals by bootstrapping its ECDF 500 times, as described in Text S2 above. We generated a normalized QQ plot of the data, and tested whether the AVGTOP4 was less than or equal to the AVGTOP4 of our sample. If so, this pairing of subsamples was considered to be a "false positive" result, in that the data meet the criteria we use to diagnose a reduction in El Niño amplitude, despite being drawn from parent populations with unaltered (not reduced) ENSO. We repeated this test 10,000 times, with different subsamples on the x and y axes each time, to generate an estimate of the overall probability of false positive results. We varied y axis subsample sizes to exactly match those of our samples (i.e. 20 to 79). X axis subsample size was fixed at 84, to match the size of the late Holocene sample we compared all our downcore data to. Results of these tests are shown in Fig. 3.

**Text S5. Construction of QQ plots normalized to mixed layer portion of distribution only**

To explore the potential effect of changes in foraminiferal sample mean due to shifts in thermocline depth, we normalized all downcore datasets to the difference in mean temperature of the warmest 50% of the dataset, rather than the mean of the entire foraminiferal temperature distribution. This is equivalent to making the dashed line in Fig. S1c, which becomes the horizontal black "zero line" on Fig. S1d, be shifted off the 1:1 line by the difference in mean between the warmest 50% of the two datasets, rather than the difference in mean between the two entire datasets. The idea behind this test is to restrict our analysis to the portion of the distribution that lies solely within the mixed layer. Examination of the late Holocene distribution relative to SODA [*Carton and Giese*, 2008] data at different depths shows that the warmest 50% of the distribution corresponds to depths of 25 m and shallower, which is within the mixed layer (Fig. S2).

The results of this test are shown in Fig. S7. All our interpretations of dampened El Niño or similar-to-late Holocene El Niño remain the same as in the original analysis (though with higher false positive rates) except for the sample at 3.071 Ma, which in this analysis appears similar to the late Holocene within 95% confidence intervals. The different interpretation for this sample does not change our overall interpretation of dampened El Niño throughout the early Pliocene and variable El Niño (sometimes dampened, sometimes similar to the late Holocene) in the mid-Pliocene.

**Text S6. Test of effect of changes in Mg/Ca of seawater**

The Mg/Ca of seawater may have changed over the past 5 Myr, given the 1 million-year residence time of Ca in the ocean [*Broecker and Peng*, 1982]. The Mg/Ca ratio of foraminiferal calcite appears to depend somewhat on the Mg/Ca ratio of seawater which affects the slope of the $Mg/Ca_{calcite}$-temperature relationship [*Evans et al.*, 2016]. In Figure S8, we present normalized QQ plots of all foraminiferal temperatures re-calculated using the Evans et al. calibration and Mg/Ca seawater values from the Evans et al. [*Evans et al.*, 2016] reconstruction, plus a 10.3% ruber-sacculifer adjustment and dissolution correction based on the Dekens et al. [*Dekens et al.*, 2002] depth-based correction, as described in Evans et al. [*Evans et al.*, 2016]. We do not employ the Evans et al. [*Evans et al.*, 2016] calibration in the main paper because it gives temperatures that are unrealistically cold across the tropical Pacific. At our site, it yields an average late Holocene temperature 1.6°C colder than the Dekens et al. [*Dekens et al.*, 2002] depth-based calibration, implying a depth habitat not consistent with plankton tow or coretop data from the eastern and central Pacific [*Faul et al.*, 2000; *Watkins et al.*, 1996]. However, when applied to downcore data and normalized to the late Holocene sample (also re-calculated using the Evans et al. calibration and modern Mg/Ca of seawater), the results are very similar to our original analysis, with only slightly higher false positive rates. The only sample that is interpreted differently is the 3.071 Ma sample, which appears similar to late Holocene El Niño within 95% confidence intervals.

**Text S7. Quantifying additional uncertainty in Mg/Ca-based individual foraminiferal temperature estimates**

*S7.1 Instrumental uncertainty and intra-test variability*

The instrumental uncertainty of our LA-ICP-MS Mg/Ca measurements, based on the 1σ standard deviation of our NIST 612 measurements, is 3.4%. There is also some variability among the 3-4 spots measured on each chamber. The average standard deviation among spots was 0.084 mmol/mol, with a maximum accepted value of 0.25 mmol/mol, which is 8.3% for a foraminifer with an average Mg/Ca value of 3.0 mmol/mol (typical of warmer specimens). Foraminifera above the 0.25 mmol/mol cutoff were excluded from plots and further analysis. As a pessimistic estimate of our uncertainty, we take a standard deviation of 0.25 mmol/mol among 3 spots, which yields a standard error on the calculation of mean Mg/Ca of 0.14 mmol/mol. For an average Mg/Ca value of 3.0 mmol/mol, a 0.14 mmol/mol uncertainty corresponds to 0.51°C. This value includes the instrumental uncertainty, which is inherent in each measurement.

*S7.2 The effect of salinity on the Mg/Ca of G. sacculifer*

Salinity has been shown to have a small effect on foraminiferal Mg/Ca, with higher salinity corresponding to higher Mg/Ca [e.g. *Hönisch et al.*, 2013; *Khider et al.*, 2015]. Monthly salinity values from the SODA dataset near our site[*Carton and Giese*, 2008] have a standard deviation over the past 50 years of 0.19 psu. El Niño months, on average, are 0.09 psu fresher than normal months, and the 1982/1983 and 1997/1998 extreme El Niño events had average salinities 0.16 psu fresher than

normal months. Using the Hönisch et al.[2013] *G. sacculifer* salinity sensitivity of 4.7% Mg/Ca per psu, an extreme El Niño event would bias our measured Mg/Ca by 0.08°C. This bias is present in both the late Holocene data and in all Pliocene data, so by comparing downcore data to our late Holocene sample instead of to modern measured temperatures, the effect of salinity is accounted for. In addition, the salinity bias is quite small compared to our other uncertainties. For these reasons, we do not include it in our total uncertainty estimate.

*S7.3 The effect of dissolution on individual foraminiferal temperatures*

It is well known that dissolution at the seafloor yields a cold bias in foraminiferal Mg/Ca values. To correct for this bias, we employ the Dekens et al. [2002] temperature calibration for G. sacculifer, which includes a dissolution correction based on core depth. It is possible that dissolution at ODP 849 could have been greater or lesser in the Pliocene than today due to changes in deep ocean circulation and ventilation, which would impart a cold or warm bias in mean measured Mg/Ca. However, it has been shown that changes in dissolution do not change the shape or characteristics of individual foraminiferal Mg/Ca-based temperature distributions [*Rongstad et al.*, 2017]. Rongstad et al. [*Rongstad et al.*, 2017] note there may be an exception in cases of extreme dissolution, but we do not observe extreme dissolution in our samples; foraminiferal shell wall thickness (based on laser ablation breakthrough time) was on par with well-preserved Holocene specimens, and we were able to find at least 25 G. sacculifer in each sample in this study. Because our interpretations of ENSO are based only on changes in the

temperature distribution, and not on changes in mean temperature, we are confident that any differences in dissolution at our site do not add to the uncertainty in individual data points.

We note that the stated uncertainty in the Dekens et al. [2002] temperature calibration of 1.4°C does not create additional uncertainty added to every individual data point. The scatter in the Dekens et al. [2002] calibration data likely stems from unaccounted-for differences in salinity among sites, instrumental error, error among replicates, and uncertainty in the value of the mean annual sea-surface temperature to which the data were calibrated. Here we explicitly quantify and account for salinity, instrumental error, and error among ablated spots – so adding the calibration uncertainty would be double-counting these effects.

*S7.4 Modeled effect of total uncertainty in individual foraminiferal Mg/Ca-based temperatures*

Based on the above analysis, the total 1σ uncertainty in our individual Mg/Ca temperatures is 0.51°C. We examined the effect of this uncertainty on our data analysis by adding noise to every downcore data point and re-calculating confidence intervals; results are shown in Fig. S7 and details are described below. To each downcore data point, we added a random number from a set of normally distributed random numbers with a mean of 0 and a standard deviation of 0.51, to create "noisy" data. We did this 100 times with different sets of random numbers, then constructed ECDFs (as described in Text S2) from all 100 noisy datasets. From each ECDF, we then created 100 bootstrapped datasets (each with the same number of points as the

original sample) by re-sampling the ECDF. In so doing, we created 10,000 (100 x 100) noisy Monte Carlo datasets from the original data. Quantiles were calculated from dataset, and for each quantile, were sorted from coldest to warmest. Confidence intervals were selected from the ordered quantile values; the $250^{th}$ and $9750^{th}$ values formed the 95% confidence intervals.

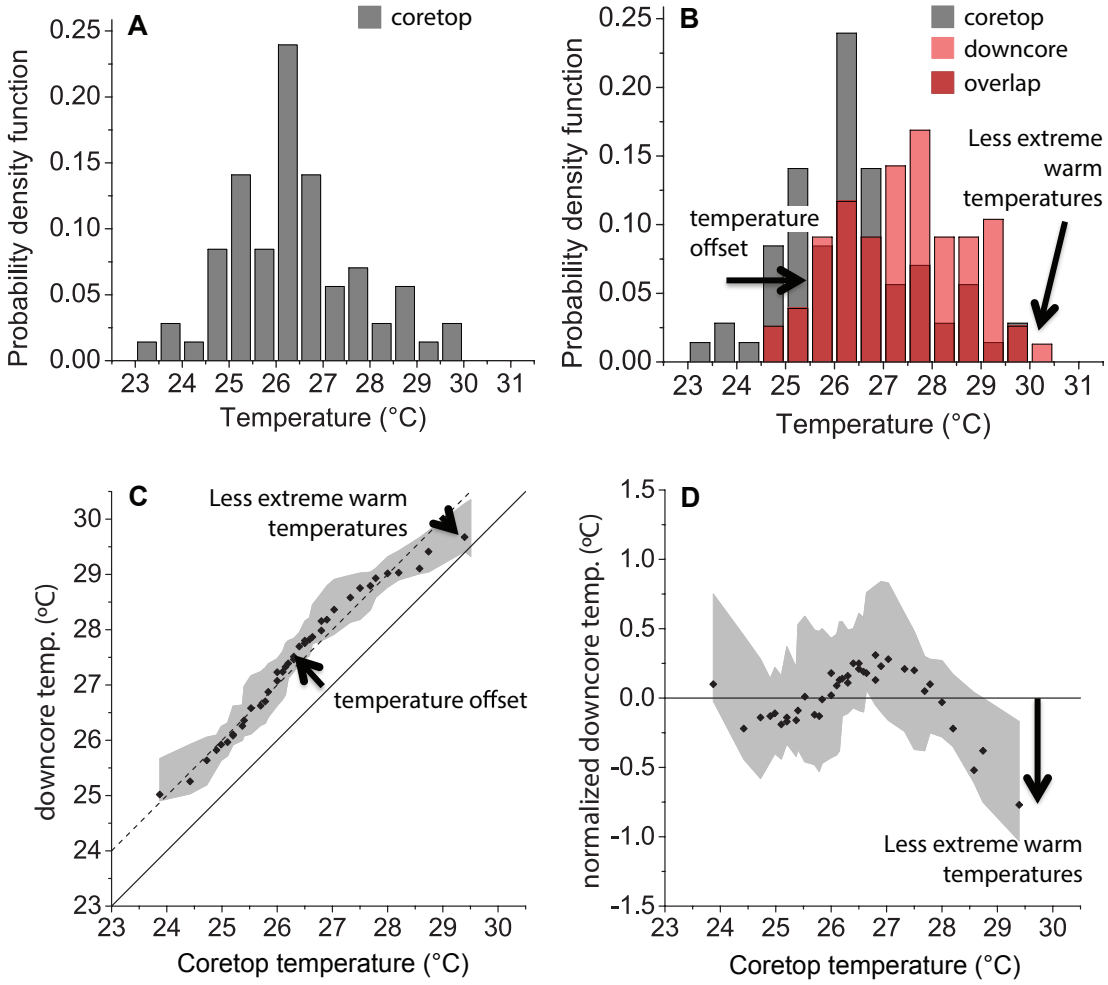


**Figure S1. Demonstration of data analysis.**

(A) An example temperature distribution, derived from individual *G. sacculifer* Mg/Ca temperatures from a coretop. (B) Another *G. sacculifer*-derived temperature distribution, from a downcore sample. The downcore distribution is warmer than the coretop distribution, but the very warmest temperatures are less extreme relative to the mean. (C) The same data plotted as a quantile-quantile plot. The offset in mean temperature between the two distributions appears as an upward shift of all the points off the 1:1 line (solid black line). The dotted line indicates the expected value of each quantile, if the two distributions are exactly the same except for the difference in mean. Note that the warmest quantiles fall below the dotted line. The gray envelope indicates 95% confidence intervals, estimated by bootstrapping an empirical continuous distribution function of the downcore data 10,000 times in a Monte Carlo simulation. (D) Normalized quantile-quantile plot. All quantiles are plotted as deviations from the dotted line in C, which becomes the zero line in D. In this example, the downcore distribution is interpreted as having a lower amplitude of El

Niño events than the coretop distribution, because the very warmest quantiles are significantly below the zero line. From [*White et al.*, 2018].

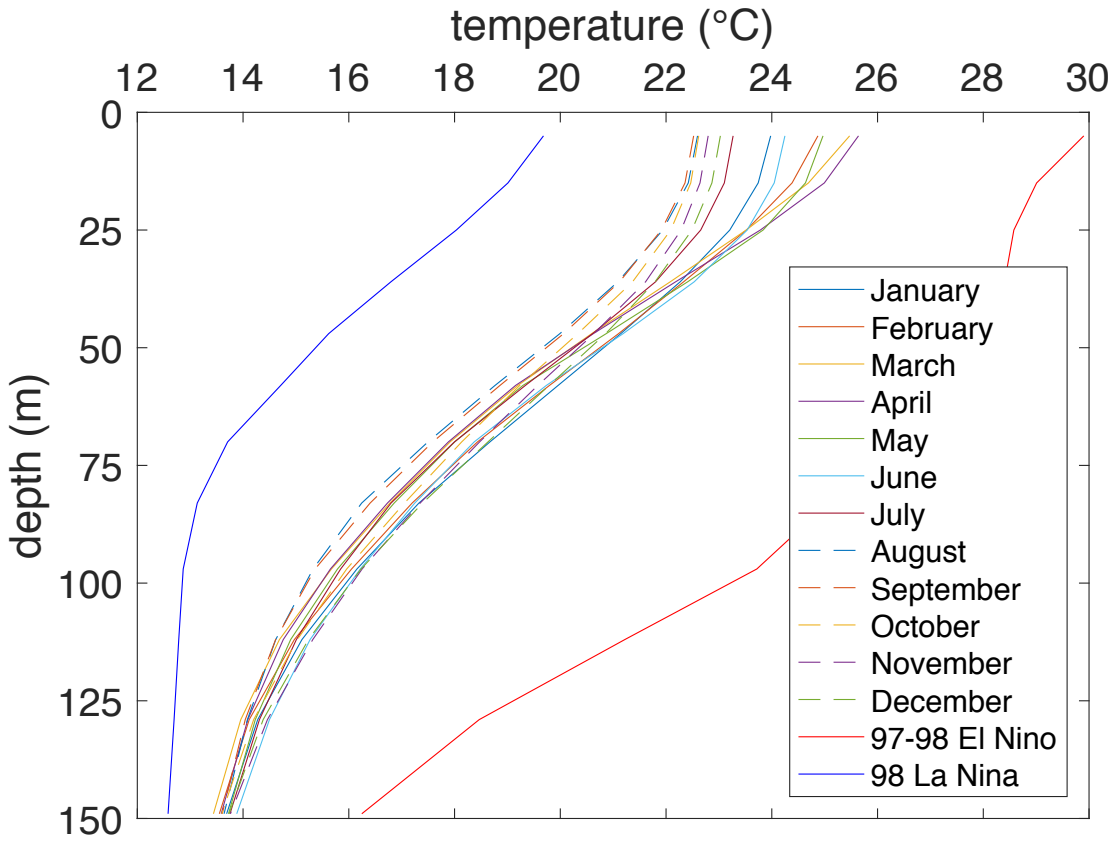


**Figure S2. Modern upper water column temperatures at Site 849.** Temperatures are from the SODA dataset [*Carton and Giese*, 2008], and profiles show monthly mean temperatures. The profiles for the 97-98 El Niño and 98-99 La Niña are diachronous; they were compiled from the peak anomalies during the event, which did not occur simultaneously at all depths.

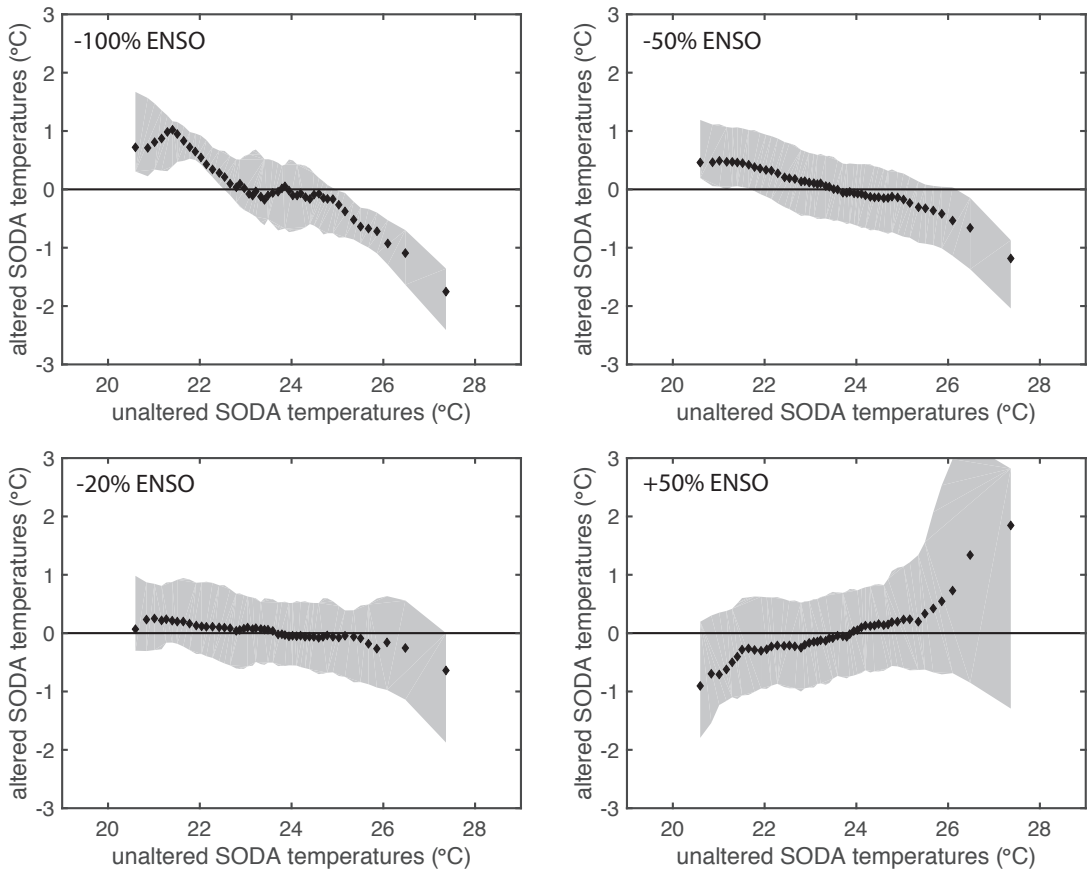


**Figure S3. Sensitivity tests showing the effect of changes in ENSO.**
Tests were performed on SODA data near our site from 15 m depth[*Carton and Giese*, 2008], and show the effect of changes in ENSO for a sample size of 48 specimens (our average sample size). Gray shading shows 95% confidence intervals. Plots show changes in the amplitude of the temperature anomaly during El Niño and La Niña months with respect to the average seasonal cycle.

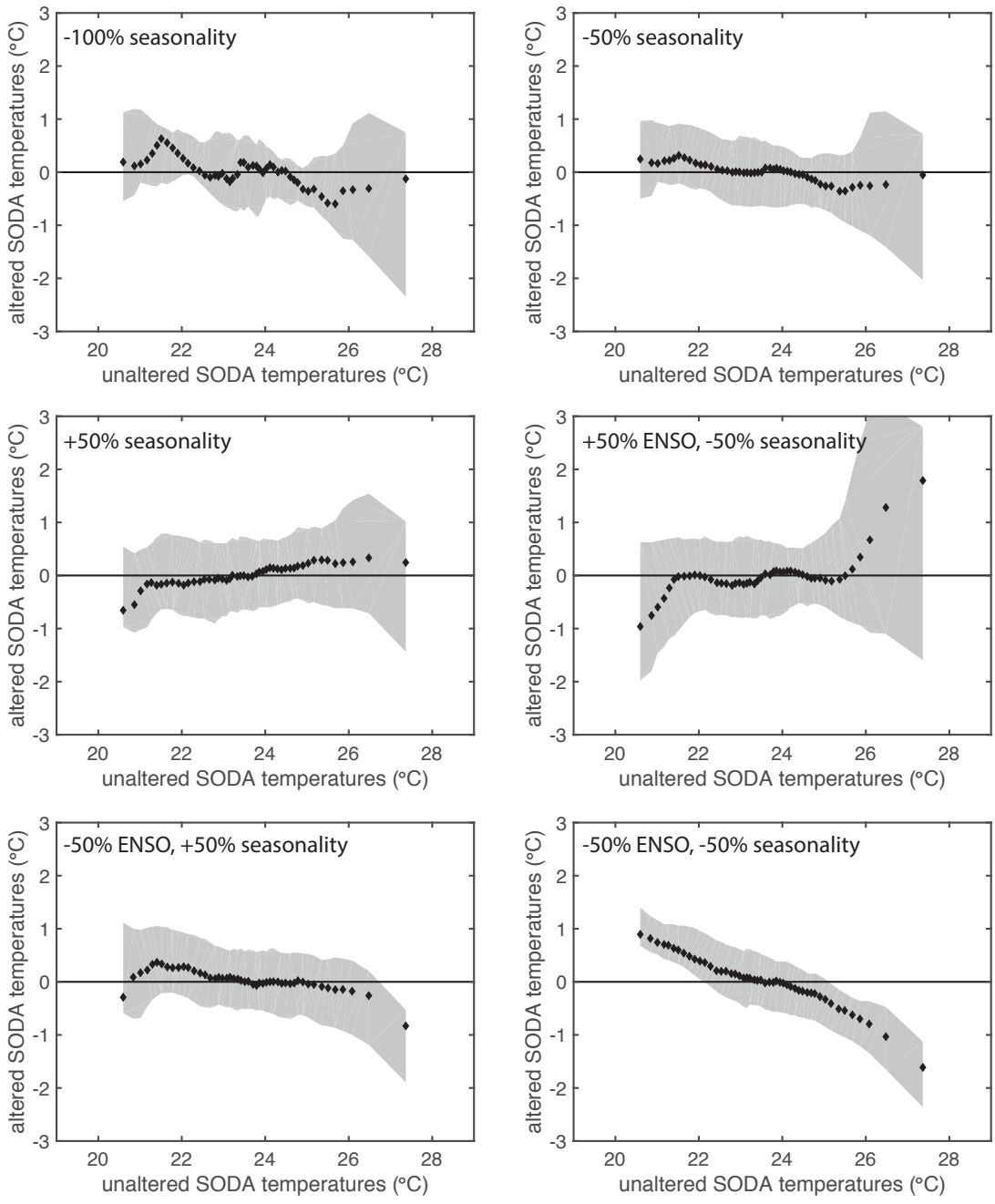


**Figure S4. Sensitivity tests showing the effect of changes in seasonality, and seasonality plus ENSO.**

Tests used SODA data near our site from 15 m depth [*Carton and Giese*, 2008], for a sample size of 48 specimens (our average sample size). Gray shading shows 95% confidence intervals. Changes in the amplitude of the seasonal cycle were calculated by taking each non-ENSO month and increasing or decreasing its anomaly with respect to the annual mean temperature.

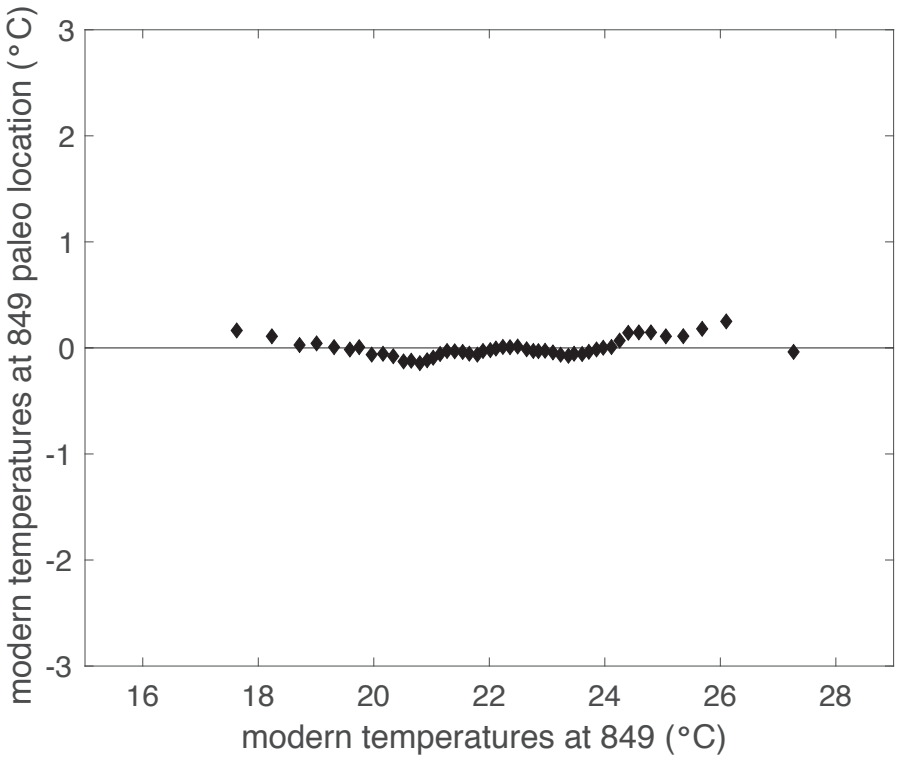


**Figure S5. The effect of changes in paleo-position of Site 849.**
Normalized QQ plot showing a test of the effect of the long-term shift in paleo-position of site 849. At 5 Ma, the site was at 1.25°S, 106.25°W [*Mayer et al.*, 1992]; currently, it is at 0°N, 110°W. SODA temperatures at 15 m water depth [*Carton and Giese*, 2008] from the current site location are on the x axis; SODA temperatures from 15 m water depth at the paleo-location are on the y-axis. The points all fall very close to the zero line, demonstrating that the two locations have very similar temperature distributions. Thus, the change in paleo-location does not introduce any bias in our results.

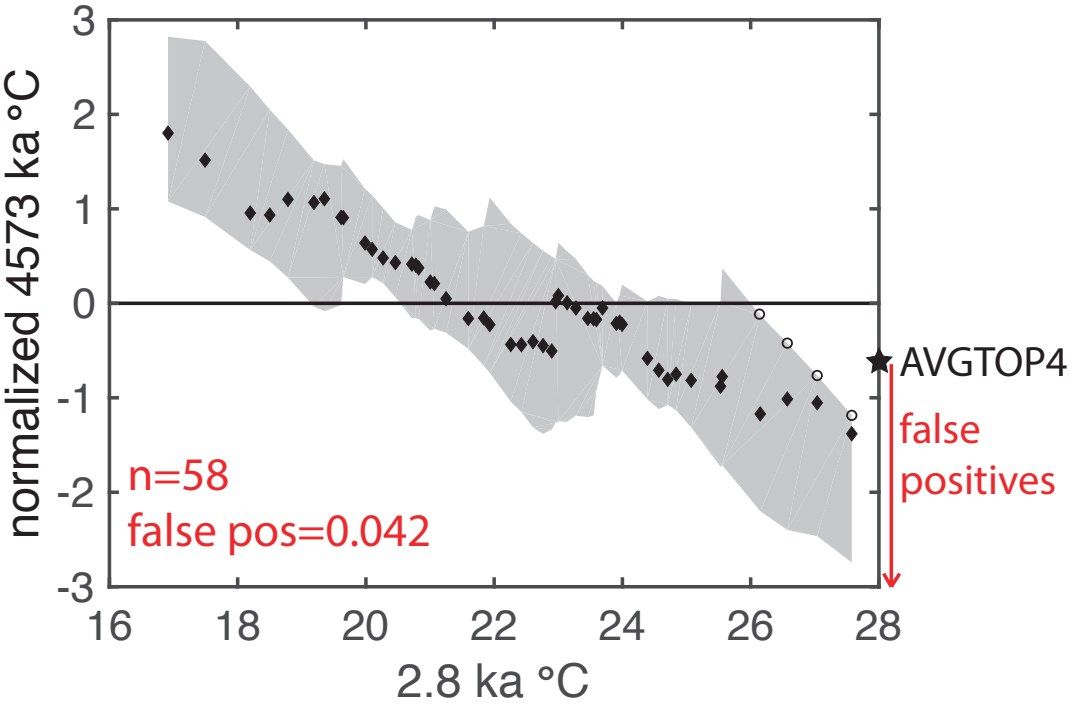


**Figure S6. Demonstration of "false positive" tests.**
The metric used to determine significance in the false positive tests is the AVGTOP4, the average value of the upper 95% confidence intervals of the top four quantiles. If an x-y pair of Monte Carlo datasets (y sample size=58 in this case) are drawn from a parent population with unchanged ENSO and yields an AVGTOP4 less than the AVGTOP4 of our sample, that x-y pair of datasets is considered a "false positive" for dampened El Niño. The false positive probability was calculated after performing this test 10,000 times. The figure above shows the upper 95% confidence intervals of the top 4 quantiles (black circles) and the AVGTOP4 of the sample (star). Details of how the false positive probabilities were calculated are provided in Text S4.

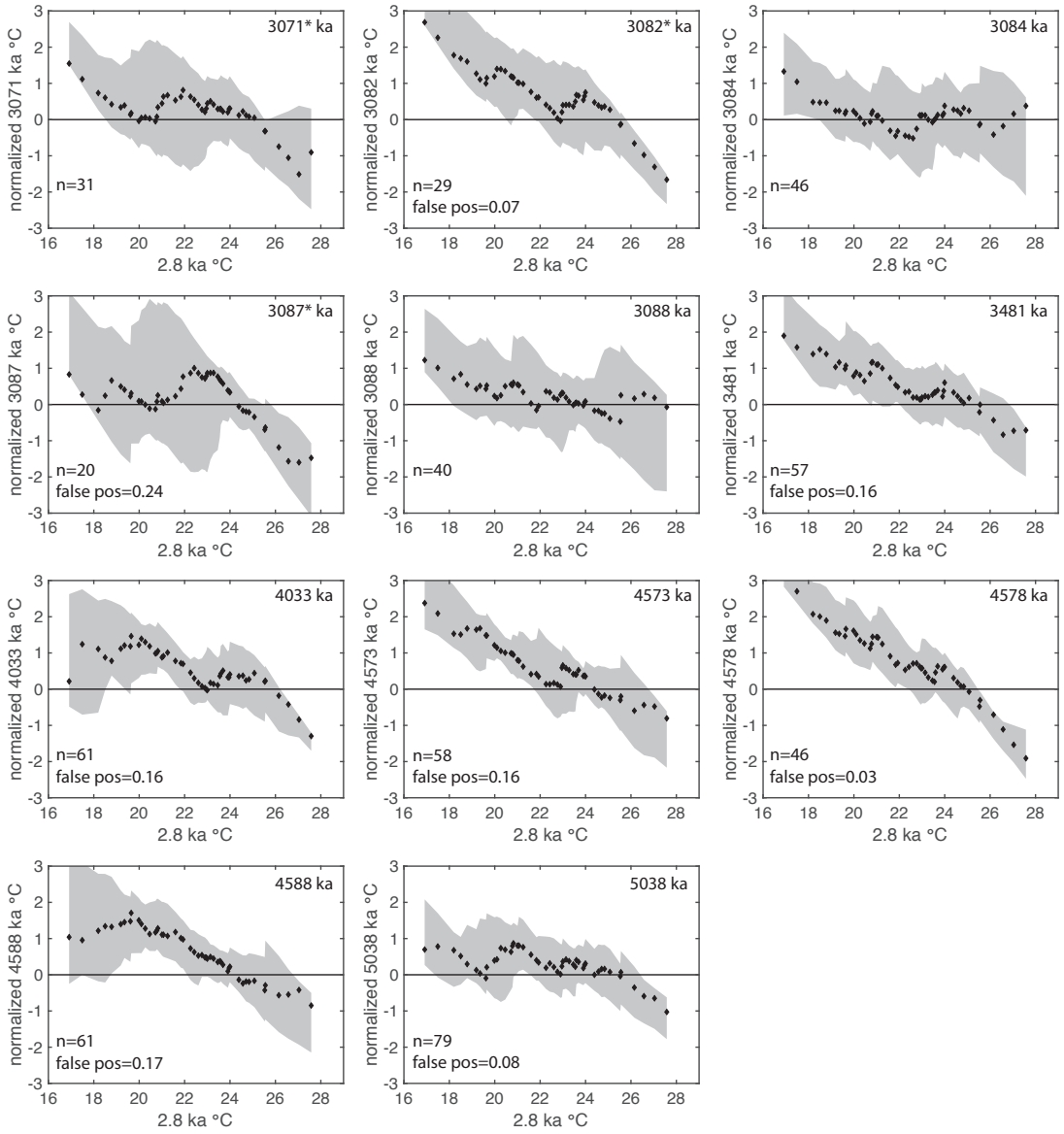


**Figure S7. QQ plots normalized to warmest 50% of the distribution.** To focus our analysis on the portion of the distribution lying solely in the mixed layer, we normalized downcore data to the difference in mean between the warmest 50% of the late Holocene vs. downcore datasets, rather than the difference in the entire sample distribution. For every sample, our interpretation of dampened El Niño or similar-to-late Holocene El Niño remains the same as in the original analysis, albeit with a higher false positive rate, except the 3.071 Ma sample, which now shows similar-to-late Holocene El Niño.

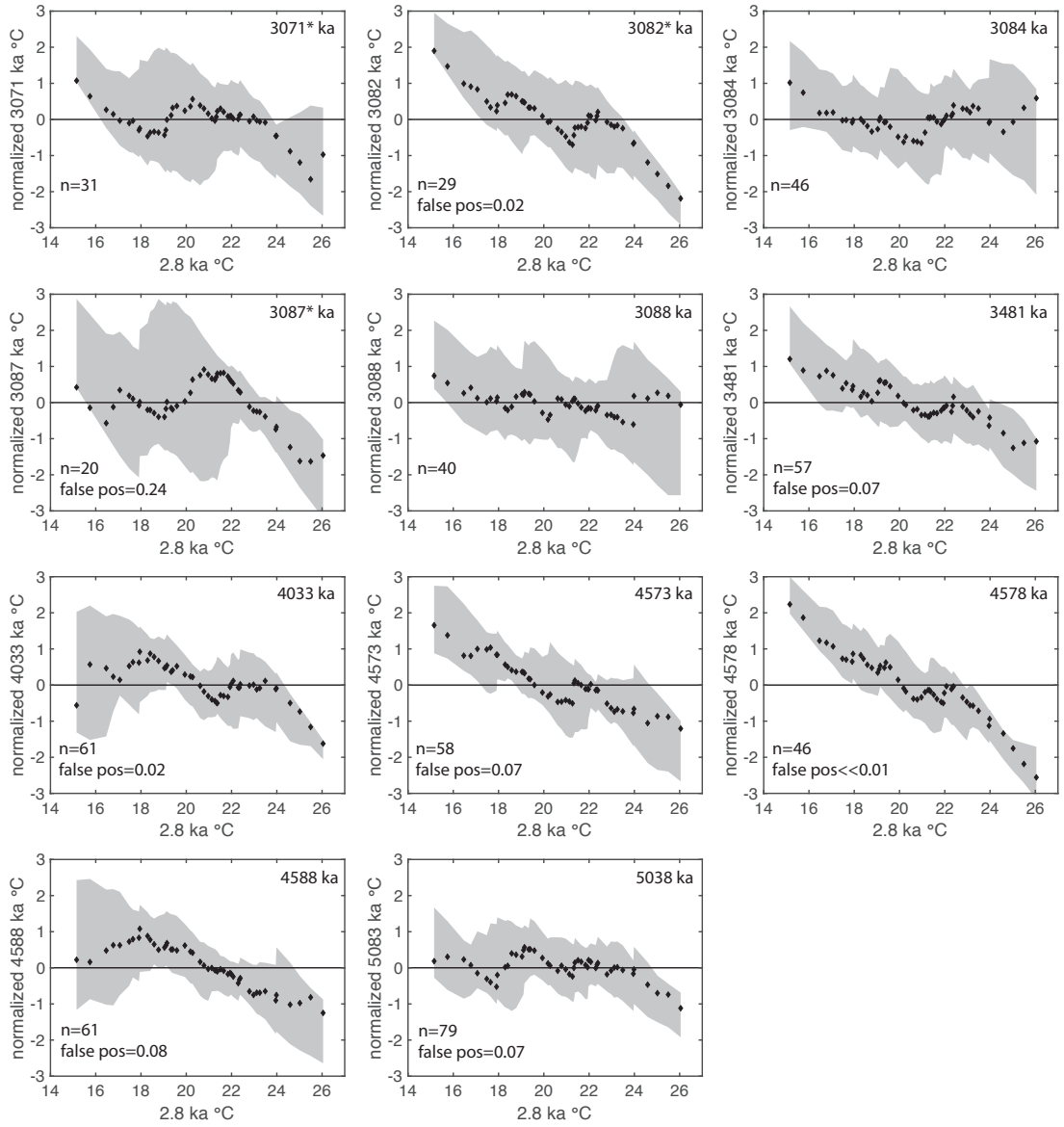


Figure S8. The effect of changes in Mg/Ca of seawater.
All foraminiferal temperatures are calculated with the Evans et al.[*Evans et al.*, 2016] calibration and Dekens et al. [*Dekens et al.*, 2002] depth-based dissolution correction. For every sample except that at 3.071 Ma, our interpretation of dampened or similar-to-late Holocene remains the same as when using the Dekens et al. [*Dekens et al.*, 2002] calibration alone, which does not account for changes in Mg/Ca of seawater. The 3.071 Ma sample now shows similar-to-late Holocene El Niño amplitude, within 95% confidence intervals.

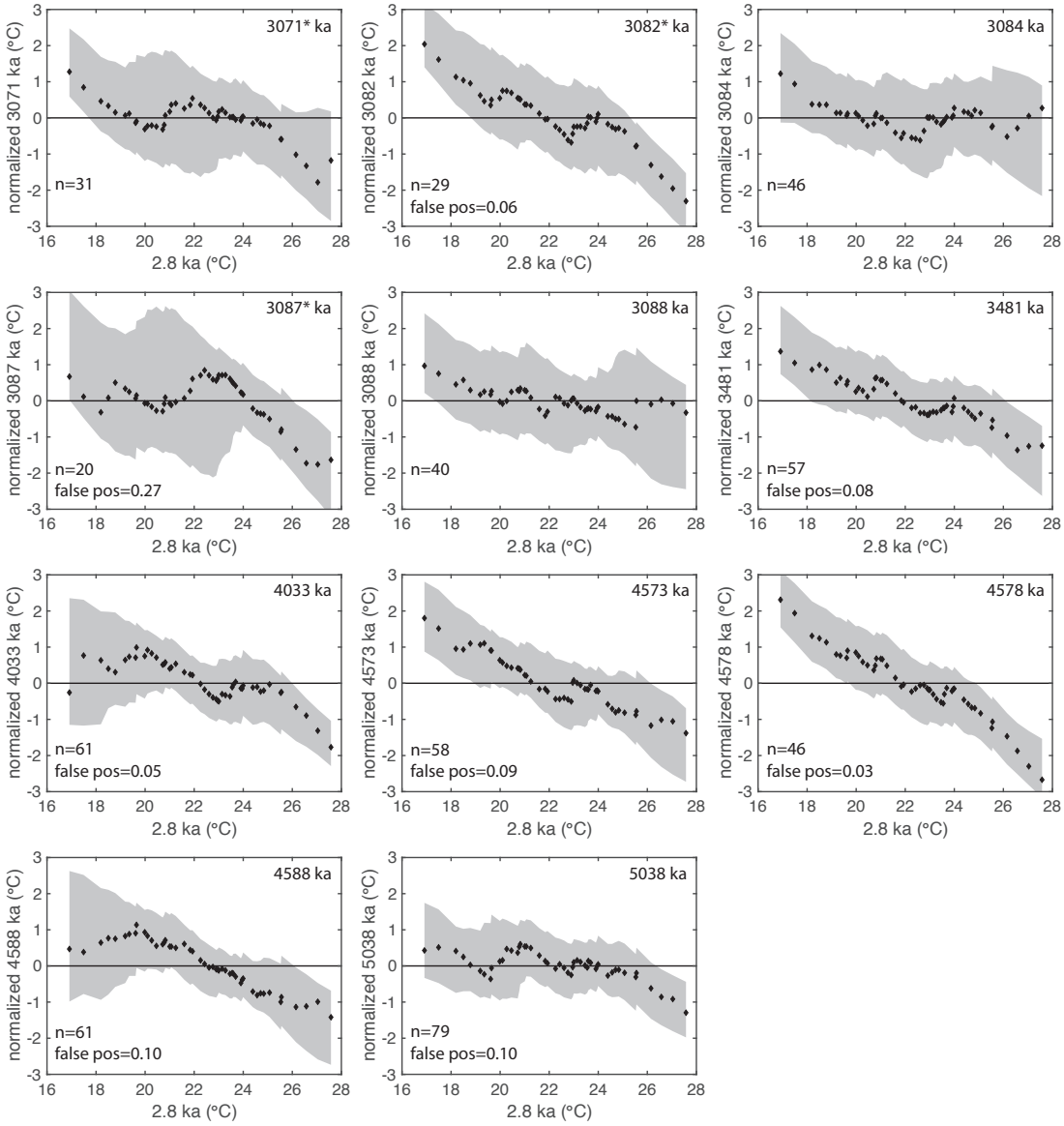


**Figure S9. Effect of additional uncertainty on single foraminiferal temperature data.**

All Pliocene single foraminiferal temperature data are as in Fig. 3, but with ±0.51°C 1σ random noise added to every data point, to illustrate the effect of additional uncertainties on our data. Gray shaded region shows 95% confidence intervals.

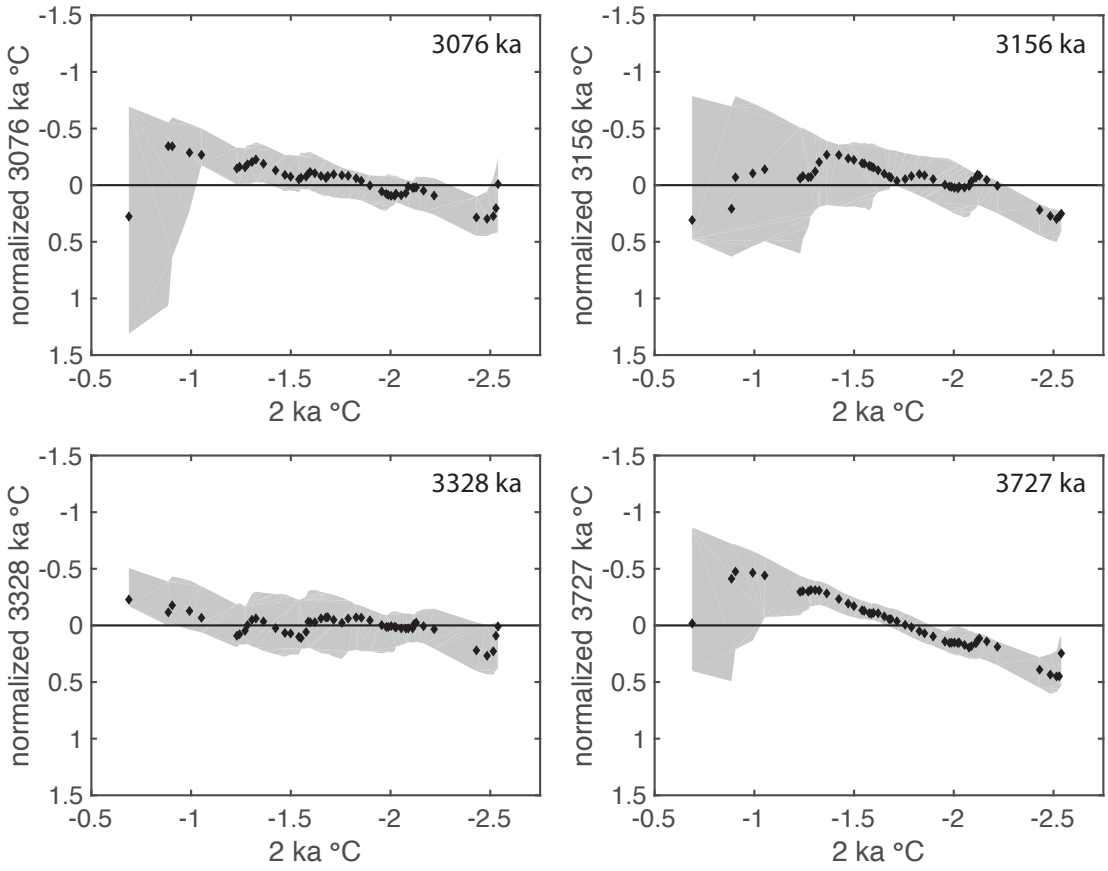


**Figure S10. Scroxton et al. [2011] data re-analyzed with QQ plots.** Normalized QQ plots of Pliocene single *G. ruber* $\delta^{18}O$ from Site 846 in the EEP [*Scroxton et al.*, 2011], plotted against late Holocene single *G. ruber* $\delta^{18}O$ data from a nearby site [*Koutavas and Joanides*, 2012], with 95% confidence intervals. When analyzed with QQ plots, the Scroxton et al. [2011] data show dampened El Niño at 3.156 Ma and 3.727 Ma, in agreement with our findings.

| Sample name | | | | | | | | | |
|---|---|---|---|---|---|---|---|---|---|
| Site | Hole | Core | Type | Section | Top (cm) | Bottom (cm) | # specimens | Age (Ma) | ΔT from late Holocene |
| 849 | A | 1 | H | 1 | 6 | 8 | 84 | 0.0028 | |
| 849 | C | 8 | H | 4 | 140 | 142 | 31 | 3.071 | -0.1 |
| 849 | C | 8 | H | 5 | 18 | 20 | 29 | 3.082 | 0.2 |
| 849 | D | 8 | H | 3 | 94 | 98 | 46 | 3.084 | -0.2 |
| 849 | C | 8 | H | 5 | 33 | 35 | 20 | 3.087 | -0.8 |
| 849 | D | 8 | H | 3 | 102 | 105 | 40 | 3.088 | 0.1 |
| 849 | D | 9 | H | 3 | 72 | 74 | 57 | 3.481 | 0.9 |
| 849 | D | 10 | H | 6 | 58 | 60 | 61 | 4.033 | -0.2 |
| 849 | D | 12 | X | 5 | 30 | 32 | 58 | 4.573 | 1.5 |
| 849 | D | 12 | X | 5 | 62 | 64 | 46 | 4.578 | 1.4 |
| 849 | D | 12 | X | 5 | 126 | 128 | 61 | 4.588 | 1.8 |
| 849 | D | 15 | X | 1 | 58 | 60 | 79 | 5.038 | 1.8 |

**Table S1. Samples used in this study.**
Age of late Holocene sample is from [*Ford et al.*, 2015a].

## References

Barreiro, M., and S. G. Philander (2008), Response of the tropical Pacific to changes in extratropical clouds, Climate Dynamics, 31(6), 713-729, doi: 10.1007/s00382-007-0363-5.

Barreiro, M., G. Philander, R. Pacanowski, and A. V. Fedorov (2005), Simulations of warm tropical conditions with application to middle Pliocene atmospheres, Climate Dynamics, 26(4), 349-365, doi: 10.1007/s00382-005-0086-4.

Bartoli, G., B. Hönisch, and R. E. Zeebe (2011), Atmospheric CO2decline during the Pliocene intensification of Northern Hemisphere glaciations, Paleoceanography, 26(4), n/a-n/a, doi: 10.1029/2010pa002055.

Berger, W. H., M.-C. Bonneau, and F. L. Parker (1982), Foraminifera on the deep-sea floor: lysocline and dissolution rate, Oceanologica Acta 5(2), 249-258.

Berger, W. H., R. M. Leckie, T. R. Janecek, R. Stax, and T. Takayama (1993), Carbonate sedimentation on Ontong Java Plateau: highlights and open questions, in Proceedings of the Ocean Drilling Program, Scientific Results, edited by W. H. Berger, L. W. Kroenke and L. A. Mayer, pp. 711-744, Ocean Drilling Program, College Station, TX.

Bijma, J., B. Hönisch, and R. E. Zeebe (2002), Impact of the ocean carbonate chemistry on living foraminiferal shell weight: Comment on "Carbonate ion concentration in glacial-age deep waters of the Caribbean Sea" by W. S. Broecker and E. Clark, Geochemistry, Geophysics, Geosystems, 3(11), 1-7, doi: 10.1029/2002gc000388.

Boyle, E. A. (1983), Manganese carbonate overgrowths on foraminifera tests, Geochimica et Cosmochimica Acta, 47, 1815-1819.

Brierley, C. M. (2015), Interannual climate variability seen in the Pliocene Model Intercomparison Project, Climate of the Past, 11(3), 605-618, doi: 10.5194/cp-11-605-2015.

Brierley, C. M., and A. V. Fedorov (2016), Comparing the impacts of Miocene–Pliocene changes in inter-ocean gateways on climate: Central American

Seaway, Bering Strait, and Indonesia, Earth and Planetary Science Letters, 444, 116-130, doi: 10.1016/j.epsl.2016.03.010.

Broecker, W. S., and T.-H. Peng (1982), Tracers in the Sea, Lamont-Doherty Geological Observatory, Columbia University, Palisades, New York.

Broecker, W. S., and E. Clark (1999), CaCO3size distribution: A paleocarbonate ion proxy?, Paleoceanography, 14(5), 596-604, doi: 10.1029/1999pa900016.

Brown, R. E., L. D. Anderson, E. Thomas, and J. C. Zachos (2011), A core-top calibration of B/Ca in the benthic foraminifers Nuttallides umbonifera and Oridorsalis umbonatus: A proxy for Cenozoic bottom water carbonate saturation, Earth and Planetary Science Letters, 310(3-4), 360-368, doi: 10.1016/j.epsl.2011.08.023.

Brown, S. J., and H. Elderfield (1996), Variations in Mg/Ca and Sr/Ca ratios of planktonic foraminifera caused by postdepositional dissolution: Evidence of shallow Mg-dependent dissolution, Paleoceanography, 11(5), 543-551, doi: 10.1029/96pa01491.

Burls, N. J., and A. V. Fedorov (2014), Simulating Pliocene warmth and a permanent El Niño-like state: The role of cloud albedo, Paleoceanography, 29(10), 893-910, doi: 10.1002/2014pa002644.

Burls, N. J., A. V. Fedorov, D. M. Sigman, S. L. Jaccard, R. Tiedemann, and G. H. Haug (2017), Active Pacific meridional overturning circulation (PMOC) during the warm Pliocene, Science Advances, 3.

Carton, J. A., and B. S. Giese (2008), A Reanalysis of Ocean Climate Using Simple Ocean Data Assimilation (SODA), Monthly Weather Review, 136(8), 2999-3017, doi: 10.1175/2007mwr1978.1.

Chen, L., T. Li, Y. Yu, and S. K. Behera (2017), A possible explanation for the divergent projection of ENSO amplitude change under global warming, Climate Dynamics, 49, 3799-3811, doi: 10.1007/s00382-017-3544-x.

Christensen, J. H., et al. (2013), Climate Phenomena and their Relevance for Future Regional Climate Change, in Climate Change 2013: The Physical Science Basis. Contribution of Working Group I to the Fifth Assessment Report of the Intergovernmental Panel on Climate Change, edited by T. F. Stocker, D. Qin, G.-K. Plattner, M. Tignor, S. K. Allen, J. Boschung, A. Nauels, Y. Xia, V. Bex and P. M. Midgley, Cambridge University Press, Cambridge, United Kingdom and New York, NY, USA.

Cobb, K. M., C. D. Charles, H. Cheng, and R. L. Edwards (2003), El Niño-Southern Oscillation and tropical Pacific climate during the last millennium, Nature, 424, 271-276.

Coggon, R. M., D. A. H. Teagle, C. E. Smith-Duque, J. C. Alt, and M. J. Cooper (2010), Reconstructing past seawater Mg/Ca and Sr/Ca from mid-ocean ridge flank calcium carbonate veins, Science, 327, 1114-1117.

Conroy, J. L., J. T. Overpeck, and J. E. Cole (2010), El Niño/Southern Oscillation and changes in the zonal gradient of tropical Pacific sea surfacetemperature over the last 1.2 ka, PAGES news, 18(1), 32-34.

Conte, M. H., M.-A. Sicre, C. Rühlemann, J. C. Weber, S. Schulte, D. Schulz-Bull, and T. Blanz (2006), Global temperature calibration of the alkenone unsaturation index (Uk′37) in surface waters and comparison with surface sediments, Geochemistry, Geophysics, Geosystems, 7(2), Q02005, doi: 10.1029/2005gc001054.

de Villiers, S. (2005), Foraminiferal shell-weight evidence for sedimentary calcite dissolution above the lysocline, Deep Sea Research Part I: Oceanographic Research Papers, 52(5), 671-680, doi: 10.1016/j.dsr.2004.11.014.

Dekens, P. S., A. C. Ravelo, and M. D. McCarthy (2007), Warm upwelling regions in the Pliocene warm period, Paleoceanography, 22(3), n/a-n/a, doi: 10.1029/2006pa001394.

Dekens, P. S., A. C. Ravelo, and E. M. Griffith (2016), Moderate changes in Mg/Ca of seawater through the last 5 Ma, paper presented at International Conference on Paleoceanography, Utrecht, Netherlands.

Dekens, P. S., D. W. Lea, D. K. Pak, and H. J. Spero (2002), Core top calibration of Mg/Ca in tropical foraminifera: refining paleotemperature estimation, Geochemistry, Geophysics, Geosystems, 3(4).

Dekens, P. S., A. C. Ravelo, M. D. McCarthy, and C. A. Edwards (2008), A 5 million year comparison of Mg/Ca and alkenone paleothermometers, Geochemistry, Geophysics, Geosystems, 9(10), n/a-n/a, doi: 10.1029/2007gc001931.

Dong, L., L. Li, Q. Li, H. Wang, and C. L. Zhang (2015), Hydroclimate implications of thermocline variability in the southern South China Sea over the past 180,000yr, Quaternary Research, 83(2), 370-377, doi: 10.1016/j.yqres.2014.12.003.

Dowsett, H. J., and M. M. Robinson (2009), Mid-Pliocene equatorial Pacific sea surface temperature reconstruction: a multi-proxy perspective, Philos Trans A Math Phys Eng Sci, 367(1886), 109-125, doi: 10.1098/rsta.2008.0206.

Dowsett, H. J., M. Robinson, A. M. Haywood, U. Salzmann, D. Hill, L. E. Sohl, M. Chandler, M. Williams, K. Foley, and D. K. Stoll (2010), The PRISM3D paleoenvironmental reconstruction, Stratigraphy, 7(2-3), 123-139.

Dyez, K. A., and A. C. Ravelo (2012), Late Pleistocene tropical Pacific temperature sensitivity to radiative greenhouse gas forcing, Geology, 41(1), 23-26, doi: 10.1130/g33425.1.

Evans, D., C. Brierley, M. E. Raymo, J. Erez, and W. Müller (2016), Planktic foraminifera shell chemistry response to seawater chemistry: Pliocene–Pleistocene seawater Mg/Ca, temperature and sea level change, Earth and Planetary Science Letters, 438, 139-148, doi: 10.1016/j.epsl.2016.01.013.

Farrell, J. W., and W. L. Prell (1991), Pacific CaCO3 preservation and d18O since 4 Ma: paleoceanographic and paleoclimatic implications, Paleoceanography, 6(4), 485-498.

Faul, K. L., A. C. Ravelo, and M. L. Delaney (2000), Reconstructions of upwelling, productivity, and photic zone depth in the eastern equatorial Pacific Ocean using planktonic foraminiferal stable isotopes and abundances, Journal of Foraminiferal Research, 30(2), 110-125.

Fedorov, A. V., C. M. Brierley, and K. Emanuel (2010), Tropical cyclones and permanent El Niño in the early Pliocene epoch, Nature, 463(7284), 1066-1070, doi: 10.1038/nature08831.

Fedorov, A. V., N. J. Burls, K. T. Lawrence, and L. C. Peterson (2015), Tightly linked zonal and meridional sea surface temperature gradients over the past five million years, Nature Geoscience, 8(12), 975-980, doi: 10.1038/ngeo2577.

Fedorov, A. V., C. M. Brierley, K. T. Lawrence, Z. Liu, P. S. Dekens, and A. C. Ravelo (2013), Patterns and mechanisms of early Pliocene warmth, Nature, 496(7443), 43-49, doi: 10.1038/nature12003.

Feng, R., and C. J. Poulsen (2014), Andean elevation control on tropical Pacific climate and ENSO, Paleoceanography, 29(8), 795-809, doi: 10.1002/2014pa002640.

Ford, H. L., and A. C. Ravelo (2019), Estimates of Pliocene Tropical Pacific Temperature Sensitivity to Radiative Greenhouse Gas Forcing, Paleoceanography and Paleoclimatology, doi: 10.1029/2018pa003461.

Ford, H. L., A. C. Ravelo, and S. Hovan (2012), A deep Eastern Equatorial Pacific thermocline during the early Pliocene warm period, Earth and Planetary Science Letters, 355-356, 152-161, doi: 10.1016/j.epsl.2012.08.027.

Ford, H. L., A. C. Ravelo, and P. J. Polissar (2015a), Reduced El Niño-Southern Oscillation during the Last Glacial Maximum, Science, 347(6219), 255-258.

Ford, H. L., A. C. Ravelo, P. S. Dekens, J. P. LaRiviere, and M. W. Wara (2015b), The evolution of the equatorial thermocline and the early Pliocene El Padre mean state, Geophys Res Lett, 42, 4878-4887, doi: 10.1002/.

Gray, W. R., and D. Evans (2019), Nonthermal Influences on Mg/Ca in Planktonic Foraminifera: A Review of Culture Studies and Application to the Last Glacial Maximum, Paleoceanography and Paleoclimatology, 34(3), 306-315, doi: 10.1029/2018pa003517.

Haynes, L., B. Honisch, K. A. Dyez, K. Holland, Y. Rosenthal, C. R. Fish, A. V. Subhas, and J. W. B. Rae (2017), Calibration of the B/Ca proxy in the planktic foraminifer Orbulina universa to Paleocene seawater conditions, Paleoceanography, 32, doi: 10.1002/.

Haywood, A. M., P. J. Valdes, and V. L. Peck (2007), A permanent El Niño-like state during the Pliocene?, Paleoceanography, 22(1), n/a-n/a, doi: 10.1029/2006pa001323.

Haywood, A. M., et al. (2013), Large-scale features of Pliocene climate: results from the Pliocene Model Intercomparison Project, Climate of the Past, 9(1), 191-209, doi: 10.5194/cp-9-191-2013.

Hemming, N. G., and G. N. Hanson (1992), Boron isotopic composition and concentration in modern marine carbonates, Geochimica et Cosmochimica Acta, 56, 537-543.

Hertzberg, J. E., M. W. Schmidt, T. S. Bianchi, R. W. Smith, M. R. Shields, and F. Marcantonio (2016), Comparison of eastern tropical Pacific TEX86 and Globigerinoides ruber Mg/Ca derived sea surface temperatures: Insights from the Holocene and Last Glacial Maximum, Earth and Planetary Science Letters, 434, 320-332, doi: 10.1016/j.epsl.2015.11.050.

Hill, D. J., et al. (2014), Evaluating the dominant components of warming in Pliocene climate simulations, Climate of the Past, 10(1), 79-90, doi: 10.5194/cp-10-79-2014.

Hönisch, B., K. A. Allen, D. W. Lea, H. J. Spero, S. M. Eggins, J. Arbuszewski, P. deMenocal, Y. Rosenthal, A. D. Russell, and H. Elderfield (2013), The influence of salinity on Mg/Ca in planktic foraminifers – Evidence from cultures, core-top sediments and complementary δ18O, Geochimica et Cosmochimica Acta, 121, 196-213, doi: 10.1016/j.gca.2013.07.028.

Horita, J., H. Zimmermann, and H. D. Holland (2002), Chemical evolution of seawater during the Phanerozoic: implications from the record of marine evaporites, Geochimica et Cosmochimica Acta, 66(21), 3733-3756.

Jia, G., J. Zhang, J. Chen, P. a. Peng, and C. L. Zhang (2012), Archaeal tetraether lipids record subsurface water temperature in the South China Sea, Organic Geochemistry, 50, 68-77, doi: 10.1016/j.orggeochem.2012.07.002.

Jochum, M., B. Fox-Kemper, P. H. Molnar, and C. Shields (2009), Differences in the Indonesian seaway in a coupled climate model and their relevance to Pliocene climate and El Niño, Paleoceanography, 24(1), n/a-n/a, doi: 10.1029/2008pa001678.

Karamperidou, C., P. N. Di Nezio, A. Timmermann, F.-F. Jin, and K. M. Cobb (2015), The response of ENSO flavors to mid-Holocene climate: Implications for proxy interpretation, Paleoceanography, 30(5), 527-547, doi: 10.1002/2014pa002742.

Karas, C., D. Nürnberg, A. K. Gupta, R. Tiedemann, K. Mohan, and T. Bickert (2009), Mid-Pliocene climate change amplified by a switch in Indonesian subsurface throughflow, Nature Geoscience, 2(6), 434-438, doi: 10.1038/ngeo520.

Kerr, J., R. Rickaby, J. Yu, H. Elderfield, and A. Y. Sadekov (2017), The effect of ocean alkalinity and carbon transfer on deep-sea carbonate ion concentration during the past five glacial cycles, Earth and Planetary Science Letters, 471, 42-53, doi: 10.1016/j.epsl.2017.04.042.

Khider, D., G. Huerta, C. Jackson, L. D. Stott, and J. Emile-Geay (2015), A Bayesian, multivariate calibration forGlobigerinoides ruberMg/Ca, Geochemistry, Geophysics, Geosystems, 16(9), 2916-2932, doi: 10.1002/2015gc005844.

Kim, S. T., W. Cai, F.-F. Jin, and J.-Y. Yu (2014a), ENSO stability in coupled climate models and its association with mean state, Climate Dynamics, 42(11-12), 3313-3321, doi: 10.1007/s00382-013-1833-6.

Koutavas, A., and S. Joanides (2012), El Niño-Southern Oscillation extrema in the Holocene and Last Glacial Maximum, Paleoceanography, 27(4), PA4208, doi: 10.1029/2012pa002378.

Lawrence, K. T., Z. Liu, and T. D. Herbert (2006), Evolution of the eastern tropical Pacific through Plio-Pleistocene glaciation, Science, 312(5770), 79-83, doi: 10.1126/science.1120395.

Lea, D. W., D. K. Pak, and H. J. Spero (2000), Climate impact of late Quaternary equatorial Pacific sea surface temperature variations, Science, 289, 1719-1724.

Lemarchand, D., J. Gaillardet, E. Lewin, and C. J. Allegre (2002), Boron isotope systematics in large rivers: implications for the marine boron budget and paleo-pH reconstruction over the Cenozoic, Chemical Geology, 190, 123-140.

Liddy, H. M., S. J. Feakins, and J. E. Tierney (2016), Cooling and drying in northeast Africa across the Pliocene, Earth and Planetary Science Letters, 449, 430-438, doi: 10.1016/j.epsl.2016.05.005.

Lisiecki, L. E., and M. E. Raymo (2005), A Pliocene-Pleistocene stack of 57 globally distributed benthic δ18O records, Paleoceanography, 20(1), n/a-n/a, doi: 10.1029/2004pa001071.

Liu, Z., Z. Lu, X. Wen, B. L. Otto-Bliesner, A. Timmermann, and K. M. Cobb (2014), Evolution and forcing mechanisms of El Niño over the past 21,000 years, Nature, 515(7528), 550-553, doi: 10.1038/nature13963.

Locarnini, R. A., et al. (2013), World Ocean Atlas 2013, Volume 1: Temperature, edited by S. Levitus, p. 40, NOAA Atlas NESDIS 73, U.S. Government Printing Office, Washington, D.C.

Lowenstein, T. K., M. N. Timofeeff, S. T. Brennan, L. A. Hardie, and R. V. Demicco (2001), Oscillations in Phanerozoic Seawater Chemistry: Evidence from Fluid Inclusions, Science, 294, 1086-1088.

Lyle, M. (2003), Neogene carbonate burial in the Pacific Ocean, Paleoceanography, 18(3), doi: 10.1029/2002pa000777.

Ma, X., J. Tian, W. Ma, K. Li, and J. Yu (2018), Changes of deep Pacific overturning circulation and carbonate chemistry during middle Miocene East Antarctic ice

sheet expansion, Earth and Planetary Science Letters, 484, 253-263, doi: 10.1016/j.epsl.2017.12.002.

Manucharyan, G. E., and A. V. Fedorov (2014), Robust ENSO across a Wide Range of Climates, Journal of Climate, 27(15), 5836-5850, doi: 10.1175/jcli-d-13-00759.1.

Martin, P. A., and D. W. Lea (2002), A simple evaluation of cleaning procedures on fossil benthic foraminiferal Mg/Ca, Geochemistry, Geophysics, Geosystems, 3(10), 1-8, doi: 10.1029/2001gc000280.

Martinez-Garcia, A., A. Rosell-Mele, E. L. McClymont, R. Gersonde, and G. H. Haug (2010), Subpolar link to the emergence of the modern equatorial Pacific cold tongue, Science, 328, 1550-1553.

Mayer, L. A., N. Pisias, and T. Janecek (1992), ODP Leg 138 introduction, in Proceedings of the Ocean DRilling Program, Initial Reports, edited, Ocean Drilling Program, College Station, TX.

Medina-Elizalde, M., D. W. Lea, and M. S. Fantle (2008), Implications of seawater Mg/Ca variability for Plio-Pleistocene tropical climate reconstruction, Earth and Planetary Science Letters, 269(3-4), 585-595, doi: 10.1016/j.epsl.2008.03.014.

Mix, A. C., N. G. Pisias, W. Rugh, J. Wilson, A. Morey, and T. K. Hagelberg (1995), Benthic foraminifer stable isotope record from site 849 (0-5 Ma): Local and global climate changes, in Proceedings of the Ocean Drilling Program, Scientific Results, edited by N. G. Pisias, L. A. Mayer, T. R. Janecek, A. Palmer-Julson and T. H. van Andel, Ocean Drilling Program, College Station TX.

Molnar, P., and M. A. Cane (2002), El Niño's tropical climate and teleconnections as a blueprint for pre-Ice Age climates, Paleoceanography, 17(2).

O'Brien, C. L., G. L. Foster, M. A. Martínez-Botí, R. Abell, J. W. B. Rae, and R. D. Pancost (2014), High sea surface temperatures in tropical warm pools during the Pliocene, Nature Geoscience, 7(8), 606-611, doi: 10.1038/ngeo2194.

Pagani, M., Z. Liu, J. LaRiviere, and A. C. Ravelo (2009), High Earth-system climate sensitivity determined from Pliocene carbon dioxide concentrations, Nature Geoscience, 3(1), 27-30, doi: 10.1038/ngeo724.

Rae, J. W. B., G. L. Foster, D. N. Schmidt, and T. Elliott (2011), Boron isotopes and B/Ca in benthic foraminifera: Proxies for the deep ocean carbonate system, Earth and Planetary Science Letters, 302(3-4), 403-413, doi: 10.1016/j.epsl.2010.12.034.

Raitzsch, M., E. C. Hathorne, H. Kuhnert, J. Groeneveld, and T. Bickert (2011), Modern and late Pleistocene B/Ca ratios of the benthic foraminifer Planulina wuellerstorfi determined with laser ablation ICP-MS, Geology, 39(11), 1039-1042, doi: 10.1130/g32009.1.

Rausch, S., F. Böhm, W. Bach, A. Klügel, and A. Eisenhauer (2013), Calcium carbonate veins in ocean crust record a threefold increase of seawater Mg/Ca in the past 30 million years, Earth and Planetary Science Letters, 362, 215-224, doi: 10.1016/j.epsl.2012.12.005.

Ravelo, A. C., P. S. Dekens, and M. McCarthy (2006), Evidence for El Niño–like conditions during the Pliocene, GSA Today, 16(3), 4, doi: 10.1130/1052-5173(2006)016<4:efenlc>2.0.co;2.

Ravelo, A. C., K. T. Lawrence, A. V. Fedorov, and H. L. Ford (2014), Comment on "A 12-million-year temperature history of the tropical Pacific Ocean", Science, 346(6216).

Regenberg, M., A. Regenberg, D. Garbe-Schönberg, and D. W. Lea (2014), Global dissolution effects on planktonic foraminiferal Mg/Ca ratios controlled by the calcite-saturation state of bottom waters, Paleoceanography, 29(3), 127-142, doi: 10.1002/2013pa002492.

Richey, J. N., and J. E. Tierney (2016), GDGT and alkenone flux in the northern Gulf of Mexico: Implications for the TEX86and UK'37paleothermometers, Paleoceanography, 31(12), 1547-1561, doi: 10.1002/2016pa003032.

Rohling, E. J., M. Medina-Elizalde, J. G. Shepherd, M. Siddall, and J. D. Stanford (2012), Sea Surface and High-Latitude Temperature Sensitivity to Radiative

Forcing of Climate over Several Glacial Cycles, Journal of Climate, 25(5), 1635-1656, doi: 10.1175/2011jcli4078.1.

Rongstad, B. L., T. M. Marchitto, and J. C. Herguera (2017), Understanding the Effects of Dissolution on the Mg/Ca Paleothermometer in Planktic Foraminifera: Evidence From a Novel Individual Foraminifera Method, Paleoceanography, 32(12), 1386-1402, doi: 10.1002/2017pa003179.

Rosenbloom, N. A., B. L. Otto-Bliesner, E. C. Brady, and P. J. Lawrence (2013), Simulating the mid-Pliocene Warm Period with the CCSM4 model, Geoscientific Model Development, 6(2), 549-561, doi: 10.5194/gmd-6-549-2013.

Rosenthal, Y., and G. P. Lohmann (2002), Accurate estimation of sea surface temperatures using dissolution-corrected calibrations for Mg/Ca paleothermometry, Paleoceanography, 17(3), 16-11-16-16, doi: 10.1029/2001pa000749.

Rousselle, G., C. Beltran, M.-A. Sicre, I. Raffi, and M. De Rafélis (2013), Changes in sea-surface conditions in the Equatorial Pacific during the middle Miocene–Pliocene as inferred from coccolith geochemistry, Earth and Planetary Science Letters, 361, 412-421, doi: 10.1016/j.epsl.2012.11.003.

Rustic, G. T., A. Koutavas, T. M. Marchitto, and B. K. Linsley (2015), Dynamical excitation of the tropical Pacific Ocean and ENSO variability by Little Ice Age cooling, Science, 350(6267), 1537-1541, doi: 10.1126/science.aac9937.

Sadekov, A. Y., S. M. Eggins, and P. De Deckker (2005), Characterization of Mg/Ca distributions in planktonic foraminifera species by electron microprobe mapping, Geochemistry, Geophysics, Geosystems, 6(12), n/a-n/a, doi: 10.1029/2005gc000973.

Sadekov, A. Y., R. Ganeshram, L. Pichevin, R. Berdin, E. McClymont, H. Elderfield, and A. W. Tudhope (2013), Palaeoclimate reconstructions reveal a strong link between El Niño-Southern Oscillation and Tropical Pacific mean state, Nat Commun, 4, 2692, doi: 10.1038/ncomms3692.

Scroxton, N., S. G. Bonham, R. E. M. Rickaby, S. H. F. Lawrence, M. Hermoso, and A. M. Haywood (2011), Persistent El Niño-Southern Oscillation variation during the Pliocene Epoch, Paleoceanography, 26(2), n/a-n/a, doi: 10.1029/2010pa002097.

Seki, O., G. L. Foster, D. N. Schmidt, A. Mackensen, K. Kawamura, and R. D. Pancost (2010), Alkenone and boron-based Pliocene pCO2 records, Earth and Planetary Science Letters, 292(1-2), 201-211, doi: 10.1016/j.epsl.2010.01.037.

Seki, O., D. N. Schmidt, S. Schouten, E. C. Hopmans, J. S. Sinninghe Damsté, and R. D. Pancost (2012), Paleoceanographic changes in the Eastern Equatorial Pacific over the last 10 Myr, Paleoceanography, 27(3), doi: 10.1029/2011pa002158.

Shukla, S. P., M. A. Chandler, J. Jonas, L. E. Sohl, K. Mankoff, and H. Dowsett (2009), Impact of a permanent El Niño (El Padre) and Indian Ocean Dipole in warm Pliocene climates, Paleoceanography, 24(2), n/a-n/a, doi: 10.1029/2008pa001682.

Song, Z., M. Latif, W. Park, U. Krebs-Kanzow, and B. Schneider (2017), Influence of seaway changes during the Pliocene on tropical Pacific climate in the Kiel climate model: mean state, annual cycle, ENSO, and their interactions, Climate Dynamics, 48(11-12), 3725-3740, doi: 10.1007/s00382-016-3298-x.

Spezzaferri, S., M. Kucera, P. N. Pearson, B. S. Wade, S. Rappo, C. R. Poole, R. Morard, and C. Stalder (2015), Fossil and genetic evidence for the polyphyletic nature of the planktonic foraminifera "Globigerinoides", and description of the new genus Trilobatus, PLoS One, 10(5), e0128108, doi: 10.1371/journal.pone.0128108.

Steph, S., R. Tiedemann, M. Prange, J. Groeneveld, M. Schulz, A. Timmermann, D. Nürnberg, C. Rühlemann, C. Saukel, and G. H. Haug (2010), Early Pliocene increase in thermohaline overturning: A precondition for the development of the modern equatorial Pacific cold tongue, Paleoceanography, 25(2), doi: 10.1029/2008pa001645.

Thirumalai, K., J. W. Partin, C. S. Jackson, and T. M. Quinn (2013), Statistical constraints on El Niño Southern Oscillation reconstructions using individual

foraminifera: A sensitivity analysis, Paleoceanography, 28(3), 401-412, doi: 10.1002/palo.20037.

Tian, B., G. J. Zhang, and V. Ramanathan (2001), Het balance in the Pacific warm pool atmosphere during TOGA COARE and CEPEX, Journal of Climate, 14, 1881-1893.

Tierney, J. E., and M. P. Tingley (2018), BAYSPLINE: A New Calibration for the Alkenone Paleothermometer, Paleoceanography and Paleoclimatology, 33(3), 281-301, doi: 10.1002/2017pa003201.

Tindall, J. C., A. M. Haywood, and F. W. Howell (2016), Accounting for centennial-scale variability when detecting changes in ENSO: A study of the Pliocene, Paleoceanography, doi: 10.1002/2016pa002951.

Trauth, M. H., M. Sarnthein, and M. Arnold (1997), Bioturbational mixing depth and carbon flux at the seafloor, Paleoceanography, 12(3), 517-526.

von der Heydt, A. S., A. Nnafie, and H. A. Dijkstra (2011), Cold tongue/Warm pool and ENSO dynamics in the Pliocene, Climate of the Past, 7(3), 903-915, doi: 10.5194/cp-7-903-2011.

Wara, M. W., A. C. Ravelo, and M. L. Delaney (2005), Permanent El Niño-like conditions during the Pliocene Warm Period, Science, 309, 758-761.

Watanabe, T., et al. (2011), Permanent El Niño during the Pliocene warm period not supported by coral evidence, Nature, 471(7337), 209-211, doi: 10.1038/nature09777.

Watkins, J. M., A. C. Mix, and J. Wilson (1996), Living planktic foraminifera: tracers of circulation and productivity regimes in the central equatorial Pacific, Deep Sea Research Part II: Topical Studies in Oceanography, 43(4-6), 1257-1282.

White, S. M., A. C. Ravelo, and P. J. Polissar (2018), Dampened El Niño in the early and mid-Holocene due to insolation-forced warming/deepening of the thermocline, Geophysical Research Letters, 45, doi: 10.1002/2017GL075433.

Yu, J., and H. Elderfield (2007), Benthic foraminiferal B/Ca ratios reflect deep water carbonate saturation state, Earth and Planetary Science Letters, 258(1-2), 73-86, doi: 10.1016/j.epsl.2007.03.025.

Yu, J., G. L. Foster, H. Elderfield, W. S. Broecker, and E. Clark (2010a), An evaluation of benthic foraminiferal B/Ca and δ11B for deep ocean carbonate ion and pH reconstructions, Earth and Planetary Science Letters, 293(1-2), 114-120, doi: 10.1016/j.epsl.2010.02.029.

Yu, J., W. S. Broecker, H. Elderfield, Z. Jin, J. McManus, and F. Zhang (2010b), Loss of Carbon from the deep sea since the last glacial maximum, Science, 330, 1084-1087.

Yu, J., R. F. Anderson, Z. Jin, J. W. B. Rae, B. N. Opdyke, and S. M. Eggins (2013), Responses of the deep ocean carbonate system to carbon reorganization during the Last Glacial–interglacial cycle, Quaternary Science Reviews, 76, 39-52, doi: 10.1016/j.quascirev.2013.06.020.

Zhang, X., et al. (2012), Changes in equatorial Pacific thermocline depth in response to Panamanian seaway closure: Insights from a multi-model study, Earth and Planetary Science Letters, 317-318, 76-84, doi: 10.1016/j.epsl.2011.11.028.

Zhang, Y. G., M. Pagani, and Z. Liu (2014a), A 12-million-year temperature history of the tropical Pacific Ocean, Science, 344(6179), 84-87, doi: 10.1126/science.1246172.

## Chapter 4: The temperature of the West Pacific Warm Pool in the Pliocene


### Abstract

The West Pacific Warm Pool (WPWP) is a major source of energy to the atmosphere, so constraining its response to increased $pCO_2$ is an important model validation target. The Pliocene is an excellent test case because it is the most recent epoch in which $pCO_2$ was higher than preindustrial. Only two Pliocene temperature records exist from the heart of the WPWP (at ODP site 806), and they show different trends. The foraminiferal Mg/Ca-based SST record shows Pliocene WPWP temperatures similar to today [*Wara et al.*, 2005], but the $TEX_{86}$ temperature proxy indicates a WPWP cooling trend since the Pliocene, differing markedly from Mg/Ca-temperature records [*Zhang et al.*, 2014a]. The $TEX_{86}$ studies, which claim that Pliocene WPWP temperatures were warmer than today, echo the claims of modeling studies, which produce a warmer WPWP whenever $pCO_2$ is higher than preindustrial.

Though much of the debate over Pliocene WPWP SSTs has focused on changes in seawater Mg/Ca, spatial variations in proxy agreement point to dissolution as a key factor. Dissolution, which imparts a cool bias to Mg/Ca temperatures, varies across ocean basins depending on $\Delta[CO_3^{2-}]$, the difference from the carbonate ion concentration needed for calcite saturation. By necessity, dissolution corrections use the modern value of $\Delta[CO_3^{2-}]$ for the entire record, so it is possible that Pliocene proxy discrepancies could stem from varying $\Delta[CO_3^{2-}]$ over time. To constrain the effect of changing dissolution on the Mg/Ca SST record, we collected benthic

foraminiferal B/Ca data (a proxy for $\Delta[CO_3^{2-}]$) from the WPWP spanning the past 5 Myr.

We find no long-term trend in $\Delta[CO_3^{2-}]$ over the past 5 Ma, implying no dissolution bias in the trend of the Mg/Ca record. Changes in seawater Mg/Ca create a ~1.8°C cool bias in the Pliocene Mg/Ca data, based on the [*Evans et al.*, 2016] seawater reconstruction and temperature calibration. After accounting for this bias, we find that the Pliocene WPWP was ~+1.1°C warmer than during the Holocene, ranging from +0.5°C to +1.9°C when uncertainties are included. As such, the 2-2.5°C trend shown in $TEX_{86}$ records is not supported by the Mg/Ca data, and likely stems from a bias in the $TEX_{86}$ data toward subsurface temperatures. Even after accounting for nonthermal effects on the Mg/Ca data, reconstructed temperatures still show a much lower zonal temperature gradient in the Pliocene tropical Pacific than today.

## 1 Introduction

### *1.1 Importance of the West Pacific Warm Pool*

The West Pacific Warm Pool (WPWP) is a significant source of latent and sensible heat to the atmosphere, and it drives the Walker Circulation, directs movements of the Intertropical Convergence Zone, and modulates the Hadley circulation [*Tian et al.*, 2001]. Small changes in the sea-surface temperature (SST) of the WPWP thus have substantial impacts on the atmosphere and global climate. Determining the SST of the WPWP during past epochs with different pCO2 provides a constraint on Earth system sensitivity, which is the net effect of short and long-term

climate processes including greenhouse gas forcing, ice-albedo feedbacks, and aerosols. Because ice-albedo feedbacks have little effect in the tropics [*Rohling et al.*, 2012], the temperature of the WPWP sets a lower bound on Earth system sensitivity. The Pliocene (2.6-5.3 Ma) was the most recent epoch in which pCO2 was higher than preindustrial levels and similar to current levels [*Bartoli et al.*, 2011; *Pagani et al.*, 2009; *Seki et al.*, 2010]. As such, determining the temperature of the WPWP during the Pliocene has become an important goal in the scientific community.

The state of the Pliocene tropical Pacific is the subject of heated debate, which hinges on the accuracy of a Mg/Ca-derived SST record from planktic foraminifera at ODP site 806 in the WPWP (Figures 1 and 2) [*Wara et al.*, 2005]. This record does not show a long-term cooling SST trend since 5.3 Ma. In contrast, a TEX86-derived temperature record from the same site suggests cooling in the WPWP since 5 Ma [*Zhang et al.*, 2014a]. These two findings yield different climate sensitivities. They also have different implications for the zonal (east-west) SST gradient, which is thought to be important for atmospheric circulation and ENSO [*Fedorov et al.*, 2015]. In the eastern equatorial Pacific, records from ODP 846, 847, 850, and U1338 using the Mg/Ca, UK'37, and TEX86 proxies all show much warmer SSTs in the Pliocene [*Dekens et al.*, 2007; *Lawrence et al.*, 2006; *Rousselle et al.*, 2013; *Seki et al.*, 2012; *Zhang et al.*, 2014a] (Figures 1 and 2). If the Pliocene WPWP had a similar temperature to today, the zonal gradient was much lower, resulting in a "permanent El Niño-like state" (or "El Padre", to clarify that it refers to mean climate, not El Niño

behavior [*Ravelo et al.*, 2014]). If, instead, the WPWP was warmer in the Pliocene, the zonal gradient would have been similar to today.

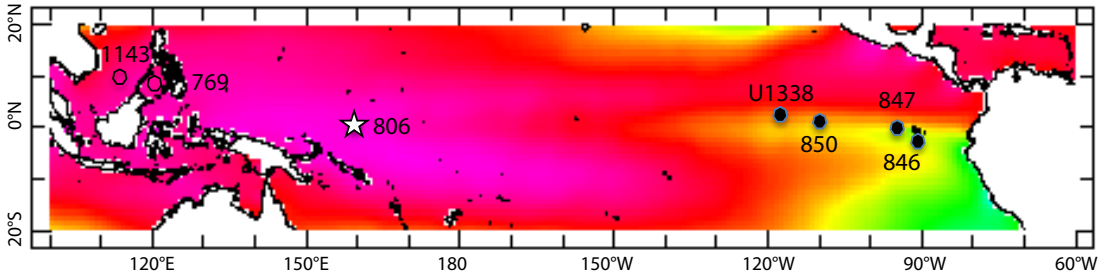


**Figure 1. Tropical Pacific annual average SSTs and sites referenced in this study.**
Pink is 29℃, green is 23.5℃. New data are from ODP site 806 (0°N, 160°E, 2520 m depth; marked by star). Filled black circles show eastern equatorial Pacific sites with Plio-Pleistocene temperature records (Figure 2). Empty circles show sites that monitor lateral expansion of the WPWP but not conditions at its heart. Adapted from [*Ravelo et al.*, 2014].

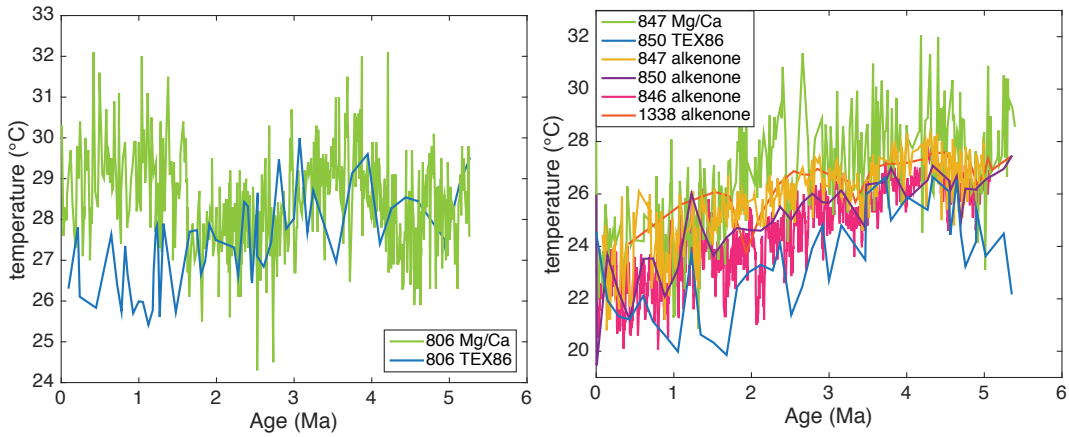


**Figure 2. Temperature records from the western and eastern Pacific.**
Plio-Pleistocene temperature records from site 806 in the WPWP (left) and sites 846, 847, 850, and U1338 in the eastern equatorial Pacific (right). Mg/Ca-derived records from [*Wara et al.*, 2005]; TEX86 -derived records from [*Zhang et al.*, 2014a]; alkenone-derived records from [*Dekens et al.*, 2007; *Lawrence et al.*, 2006; *Rousselle et al.*, 2013; *Zhang et al.*, 2014a]. Mg/Ca-derived records are not adjusted for changes in Mg/Ca of seawater.

The debate over the temperature of the WPWP in the Pliocene can be summarized as two main perspectives. On one hand, a similar-to-today WPWP does

not match expectations of tropical SST response to radiative forcing [*Hill et al.*, 2014]. The Pliocene Model Intercomparison Project (PlioMIP) yields WPWP SSTs 1.5-2˚C warmer than preindustrial and little change in zonal SST gradient [*Haywood et al.*, 2013]. This is supported by simulated anthropogenic tropical warming [*Christensen et al.*, 2013]. Also, over Pleistocene glacial-interglacial cycles, WPWP SST responds linearly to radiative forcing [*Dyez and Ravelo*, 2012; *Lea et al.*, 2000] with lower zonal SST gradient in cold climates and vice versa [*Ford et al.*, 2015a; *Koutavas and Joanides*, 2012; *Sadekov et al.*, 2013] (though this result is site-specific; see [*Lea et al.*, 2000]). In addition, $TEX_{86}$, used as an SST proxy, suggests cooling in the eastern equatorial Pacific, WPWP, and South China Sea since 5 Ma, attributed to decreasing $pCO_2$ [*O'Brien et al.*, 2014; *Zhang et al.*, 2014a]. Thus, it is expected that SST was uniformly warmer, resulting in a zonal SST gradient similar or slightly higher in the Pliocene when $pCO_2$ was higher, counter to the finding of a similar-to-today WPWP.

On the other hand, the balance of tropical Pacific data support an El Padre state [*Dowsett and Robinson*, 2009; *Ravelo et al.*, 2006; *Ravelo et al.*, 2014], and a cooler-than-expected WPWP could be explained by altered cloud albedo or enhanced ocean mixing [*Burls and Fedorov*, 2014; *Fedorov et al.*, 2010; *Fedorov et al.*, 2013]. The thermocline was also warmer/deeper in the Pliocene [*Ford et al.*, 2012; *Ford et al.*, 2015b], consistent with modeled processes impacting the zonal SST gradient [*Barreiro et al.*, 2005]. Teleconnections with the "El Padre" state also explain Pliocene continental climate [*Barreiro et al.*, 2005; *Molnar and Cane*, 2002; *Shukla*

*et al.*, 2009]. Overall, if the WPWP was indeed no warmer than today, many models may not accurately depict tropical Pacific climate components under global warming.

The finding of no Plio-Pleistocene trend in WPWP SSTs despite changes in global climate [*Wara et al.*, 2005] depends on Mg/Ca data from a single site, ODP 806. There are published records from ODP 1143 and 769 in the South China Sea [*O'Brien et al.*, 2014; *Zhang et al.*, 2014a], but these monitor expansion and contraction of the WPWP [*Ravelo et al.*, 2014], rather than the warmest area of the WPWP, so examining SSTs at 806 is still necessary to capture conditions at the heart of the WPWP. $U^{K'}_{37}$ is fully saturated above 28.5°C [*Conte et al.*, 2006], so it cannot provide reliable SSTs in the WPWP, leaving Mg/Ca and $TEX_{86}$ as the only viable temperature proxies. $TEX_{86}$ shows a cooling trend since 5 Ma that differs markedly from Mg/Ca records at the same west Pacific sites (Figure 2) [*O'Brien et al.*, 2014; *Zhang et al.*, 2014a]. However, $TEX_{86}$ is biased toward subsurface temperatures in tropical regions including the South China Sea [*Dong et al.*, 2015; *Hertzberg et al.*, 2016; *Jia et al.*, 2012; *Liddy et al.*, 2016; *Richey and Tierney*, 2016; *Seki et al.*, 2012], which could create a false trend (if interpreted as SST) as the thermocline cooled and shoaled since 5 Ma [*Ravelo et al.*, 2014]. Because of the possible biases in the $TEX_{86}$ proxy, quantifying the WPWP SSTs relies heavily on robust interpretations of Pliocene Mg/Ca data, including assessment of the non-temperature controls on foraminiferal Mg/Ca, which is the focus of this study.

## 2 Background

### *2.1 Controls on planktic foraminiferal Mg/Ca*

The dominant control on planktic foraminiferal Mg/Ca ratios is calcification temperature. Secondary controls include 1) salinity, 2) surface water pH, 3) the Mg/Ca ratio of seawater, and 4) partial dissolution of calcite at the seafloor and in the sediment. Intratest variations and diagenetic calcite overgrowths and infillings can also affect Mg/Ca. These secondary controls are discussed here, with a focus on the planktic foraminifer *T. trilobus* (i.e. *G. sacculifer* without sac-like final chamber; [*Spezzaferri et al.*, 2015]), the species used in this study and by [*Wara et al.*, 2005].

The effect of salinity on *T. trilobus* Mg/Ca is 5.4±1.0% [*Gray and Evans*, 2019], consistent with an earlier estimate of 4.7±1.2% per salinity unit [Hönisch et al., 2013]. Estimates of the salinity of the Pliocene WPWP are model dependent. Models forced with mid-Pliocene boundary conditions simulate a 0.1 to 0.2 psu fresher WPWP [*Haywood et al.*, 2007; *Rosenbloom et al.*, 2013]. However, a model with altered cloud albedo, designed to reproduce the lower meridional and zonal SST gradients shown in proxy data, simulates a 0.5 psu saltier Pliocene WPWP [*Burls et al.*, 2017]. As such, salinity changes in the Pliocene create a bias in the Mg/Ca temperature record that is small but of uncertain sign, ranging from -0.1°C to +0.3°C using the Gray and Evans [*Gray and Evans*, 2019] formulation.

*T. trilobus* Mg/Ca was recently found to not have a significant relationship with the pH of calcification waters, in contrast with earlier studies [*Gray and Evans*, 2019], so we do not calculate an effect of pH on our data. Intratest variations in

Mg/Ca [*Dueñas-Bohórquez et al*., 2011; *Sadekov et al.*, 2005] are likely partly responsible for the ~1°C error in all Mg/Ca temperature calibrations, but calibration error likely creates noise or inaccuracies in absolute temperature, rather than a false trend in a downcore dataset. Diagenetic calcite overgrowths have been shown to have a minimal impact on foraminiferal Mg/Ca (far less than on foraminiferal δ18O), and can be identified by their effect on foraminiferal Sr/Ca [Kozdon et al., 2013; Sexton et al., 2006]. We observe a weak correlation of Sr/Ca to Mg/Ca in our planktic Mg/Ca data (R2 = 0.15), so we do not expect diagenesis to have a strong effect on our data.

Much of the debate over the veracity of the Mg/Ca-derived SST record at 806 has revolved around the Mg/Ca ratio of seawater ($Mg/Ca_{sw}$) [*Evans et al.*, 2016; *Medina-Elizalde et al.*, 2008; *O'Brien et al.*, 2014; *Zhang et al.*, 2014a]. $Mg/Ca_{sw}$ may have changed since 5 Ma, given the 1 Myr residence time of Ca in seawater (Mg residence time is 13 Myr [*Broecker and Peng*, 1982]). Foraminiferal Mg/Ca is likely affected by $Mg/Ca_{sw}$ [e.g. *Evans et al.*, 2016]. Changes in $Mg/Ca_{sw}$ would affect all temperature records equally, but adjusting Pliocene Mg/Ca SSTs upward [*Medina-Elizalde et al.*, 2008; *O'Brien et al.*, 2014; *Zhang et al.*, 2014a] or altering the Mg/Ca-SST relationship [*Evans et al.*, 2016] has different effects in different areas; for example, it worsens the agreement between Mg/Ca and $U^{K'}_{37}/TEX_{86}$ in the eastern equatorial Pacific, where the un-adjusted records agree very well (Figure 2). For this reason, changes in $Mg/Ca_{sw}$ alone cannot improve proxy agreement generally, indicating that some spatially varying factor must be at play. For this study, we focus on the potential effect of dissolution, which varies regionally. The effect of potential

changes in $Mg/Ca_{sw}$ on the 806 record is discussed further in the section titled "The effect of changes in $Mg/Ca_{sw}$" below.

The fact that there is spatial variability in the differences between temperatures derived from Mg/Ca and those derived from $TEX_{86}$ suggests that dissolution could be affecting foraminiferal Mg/Ca. Dissolution varies regionally in response to ocean circulation and carbonate/organic matter supply. It has long been known to impart a cool bias to foraminiferal Mg/Ca, even above the calcite saturation horizon (the lysocline) [*Brown and Elderfield*, 1996; *de Villiers*, 2005; *Dekens et al.*, 2002; *Regenberg et al.*, 2014; *Rosenthal and Lohmann*, 2002]. Mg/Ca SST records usually apply a dissolution correction based on core depth or on $\Delta[CO_3^{2-}]$, the difference between the carbonate ion concentration ($[CO_3^{2-}]$) required for calcite saturation at the seafloor (a function of depth) and the in-situ $[CO_3^{2-}]$ [e.g. *Dekens et al.*, 2002; *Regenberg et al.*, 2014]. $\Delta[CO_3^{2-}]$ equals zero at the lysocline, which lies several hundred meters above the calcite compensation depth (CCD), the depth at which all calcite has been dissolved. Site 806 is 1000 m above the lysocline, but dissolution can still occur in CO2-rich microenvironments [*Berger et al.*]. The dissolution correction is large: the 34 μmol/kg glacial-Holocene shift in $\Delta[CO_3^{2-}]$ observed in the North Atlantic [*Yu et al.*, 2010b] is equivalent to a 2°C bias, using the [*Dekens et al.*, 2002] formulation. Standard practice is to apply dissolution corrections using the modern $\Delta[CO_3^{2-}]$ value for the entire downcore record, creating the possibility that long-term Mg/Ca-SST records are biased by temporal changes in $\Delta[CO_3^{2-}]$.

*2.2 Potential Plio-Pleistocene changes in dissolution at site 806*

Inferences about paleo-dissolution at site 806 may be drawn from multiple lines of evidence, but they have conflicting implications. The first line of evidence is planktic foraminiferal shell weight; lower weight implies greater dissolution [*Rosenthal and Lohmann*, 2002]. Shell weight data at 806 [*Wara et al.*, 2005] bear little relation to Mg/Ca temperature, implying little influence of dissolution on Mg/Ca SST. However, shell weight data are inconclusive because initial weight can vary independently of dissolution [*Bijma et al.*, 2002]. The second line of evidence is a compilation of $\%CaCO_3$ records from the central tropical Pacific, which shows that the CCD and lysocline were shallower in the Pliocene than in the late Pleistocene [*Farrell and Prell*, 1991; *Palike et al.*, 2012]. This implies greater dissolution (and thus a potential cold bias on Mg/Ca temperatures) during the Pliocene. The third line of evidence is the $\%CaCO_3$ record at 806 itself, which shows higher $\%CaCO_3$ in the early Pliocene than the late Pleistocene [*Kroenke et al.*, 1991; *Mayer et al.*, 1992], in apparent conflict with a shallower CCD. But, higher carbonate productivity could increase $\%CaCO_3$ independent of changes in the lysocline, and could inhibit foraminiferal dissolution. In addition, the [*Farrell and Prell*, 1991] study is from the central tropical Pacific, and may not be representative of western tropical site 806. Overall, based on previously published data, it is unclear whether dissolution at 806 was greater or lesser in the Pliocene than today. This uncertainty necessitates the collection of data on $\Delta[CO_3^{2-}]$ specifically at site 806 to determine changes in dissolution.

*2.3 The B/Ca proxy for Δ[$CO_3^{2-}$]*

Benthic foraminiferal B/Ca is a proxy for Δ[$CO_3^{2-}$], and captures shifts in Δ[$CO_3^{2-}$] even far above the lysocline [*Yu and Elderfield,* 2007]. Downcore benthic B/Ca data show shifts in Δ[$CO_3^{2-}$] consistent with glacial circulation changes [*Raitzsch et al.*, 2011; *Yu and Elderfield*, 2007; *Yu et al.*, 2010a]. Benthic B/Ca is preferable to other proxies, such as the $\delta^{11}B$ proxy, because it quantifies Δ[$CO_3^{2-}$] (not pH or related parameters) and does not require large sample size. Coretop B/Ca data from the WPWP yield Δ[$CO_3^{2-}$] values similar to modern [*Yu and Elderfield,* 2007].

It is possible that the B/Ca of benthic foraminifera has been affected by changes in [B] or [Ca] in seawater over the past 5 Myr. Culture data show that seawater [Ca] does not affect planktic foraminiferal B/Ca [*Haynes et al.*, 2017], so it is unlikely to affect our data. In contrast, [B] does affect planktic foraminiferal B/Ca [*Haynes et al.*, 2017], and the [B] of seawater was slightly higher at 5 Ma than it is today (~4.6 ppm rather than 4.5 ppm) [*Lemarchand et al.*, 2002]. The relationship between [$B(OH)_4^-$] (the species of B that is incorporated into foraminiferal calcite; [*Hemming and Hanson*, 1992]) and planktic foraminiferal B/Ca is: B/Ca = 1.38 * [$B(OH)_4^-$] – 23 [*Haynes et al.*, 2017]. Assuming that [$B(OH)_4^-$] was higher by the same proportion that [B] was, this 0.1 ppm change in [B] would have biased Pliocene foraminiferal B/Ca upward by ~3 μmol/mol. The impact of this change in B/Ca on Δ[$CO_3^{2-}$], using the [*Yu et al.*, 2013] relationship, is ~2.7 μmol/kg. However, this estimate is very speculative because it is based on a [$B(OH)_4^-$] to B/Ca relationship calibrated in planktic foraminifera. In this study, we use benthic foraminifera, which

likely have a different relationship to seawater chemistry than planktic foraminifera because they are much longer lived (~1 year versus ~1 month), so they likely have different vital controls on calcification. Alternatively, if we assume that benthic foraminiferal B/Ca changed in exact proportion to the change in seawater [B], this would create a bias in in benthic foraminiferal B/Ca of ~4.5 μmol/mol, resulting in a $\Delta[CO_3^{2-}]$ offset of ~4 μmol/kg. Again, this estimate is very speculative.

## 3 Approach

### *3.1 Reconstruction and application of downcore changes in dissolution*

For this study, we collected benthic foraminiferal B/Ca data from ODP site 806 over the same timeframe as the [*Wara et al.*, 2005] study, to ascertain whether dissolution at that site changed over time and biased the Mg/Ca temperature record. Samples were analyzed at slightly lower resolution (~50 kyr) than the original dataset, to focus on long-term trends rather than short-term variability. We also collected new *T. trilobus* Mg/Ca data from the same samples. We then reconstructed $\Delta[CO_3^{2-}]$ downcore, using the B/Ca- $\Delta[CO_3^{2-}]$ calibration of [*Yu et al.*, 2013]. To attain a temperature reconstruction that more accurately accounts for changes in dissolution, we use the B/Ca-derived values for $\Delta[CO_3^{2-}]$ to correct the Mg/Ca data for dissolution, which is included in the [*Dekens et al.*, 2002] Mg/Ca temperature calibration. In this way, each Mg/Ca data point is corrected with the contemporaneous value of $\Delta[CO_3^{2-}]$ rather than the modern value, as has been common practice. We employ the [*Dekens et al.*, 2002] temperature calibration with built-in $\Delta[CO_3^{2-}]$-based

dissolution correction because it yields the best agreement of coretop Mg/Ca to modern measured SST.

*3.2 Demonstration of approach*

We tested the accuracy of our approach (calculating SSTs with the Dekens et al. [2002] equation using B/Ca-derived values for $\Delta[CO_3^{2-}]$) by applying it to coretop data from the WPWP [*Dekens et al.*, 2002; *Yu and Elderfield*, 2007, this study]. Because coretop data in the WPWP were used to calibrate the *C. wuellerstorfi* B/Ca-$\Delta[CO_3^{2-}]$ proxy, our approach works well in that region; coretop B/Ca data yield values of $\Delta[CO_3^{2-}]$ similar to those estimated from GLODAP data [*Yu and Elderfield*, 2007]. When the $\Delta[CO_3^{2-}]$ values derived from coretop B/Ca are plugged into the $\Delta[CO_3^{2-}]$-based Mg/Ca SST calibration of Dekens et al. [2002], estimated SSTs match observed SST well (Figure 3). With no dissolution correction, the Mg/Ca-derived SSTs show a clear cooling trend for $\Delta[CO_3^{2-}]$ values below 15 μmol/kg; the dissolution correction removes this trend. Coretops located in water with $\Delta[CO_3^{2-}]$ values above 15 μmol/kg yield accurate SSTs without a dissolution correction. Thus, 15 μmol/kg is our cutoff for applying a dissolution correction, and we do not apply a dissolution correction to any downcore Mg/Ca data from samples with a B/Ca-derived value of $\Delta[CO_3^{2-}]$ greater than or equal to 15 μmol/kg.

Since the benthic B/Ca-$\Delta[CO_3^{2-}]$ equation [*Yu and Elderfield*, 2007; *Yu et al.*, 2013] and the planktic Mg/Ca-SST equation [*Dekens et al.*, 2002] were both calibrated with coretop data from the West Pacific Warm Pool, it is reassuring that combining the two calibrations produces accurate SST estimates. Although this

demonstration does not provide a completely independent check of our approach, it provides some confidence that correcting one proxy record with another in the tropical Pacific can improve Mg/Ca-based SST estimates.

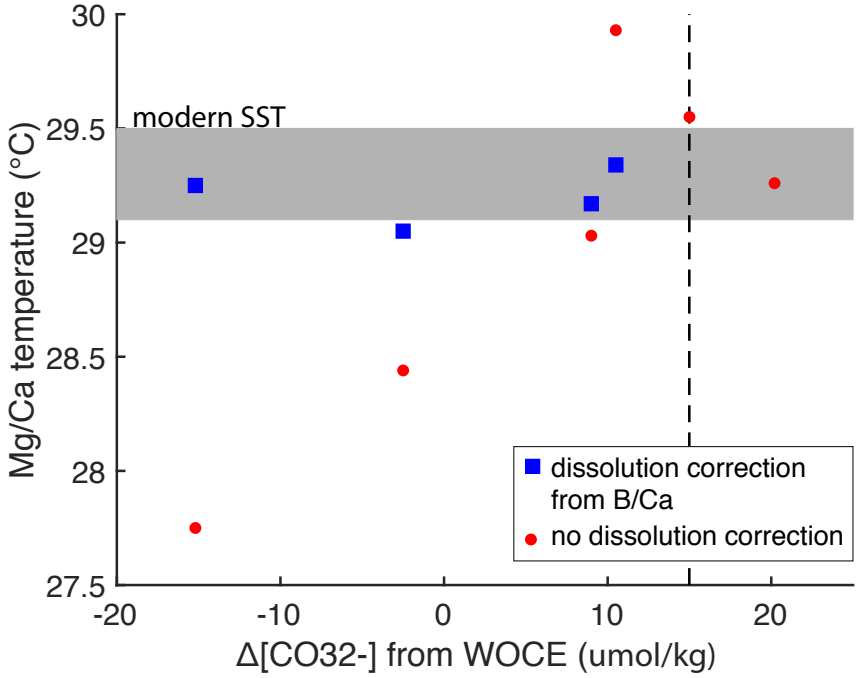


**Figure 3. Use of B/Ca data to apply a dissolution correction to Mg/Ca-based temperature estimates.**
Mg/Ca data [*Dekens et al.*, 2002, this study] from coretops with differing $\Delta[CO_3^{2-}]$ (calculated from WOCE data) but similar modern SST (gray bar) were converted to temperature using the [*Dekens et al.*, 2002] calibration but with no dissolution correction (red circles). Benthic foraminiferal B/Ca data from the same coretops [*Yu and Elderfield*, 2007, this study] were then used to estimate $\Delta[CO_3^{2-}]$ using the [*Yu et al.*, 2013] calibration, and that value of $\Delta[CO_3^{2-}]$ was plugged into the [*Dekens et al.*, 2002] calibration to correct for dissolution (blue squares). Note that the two data points with $\Delta[CO_3^{2-}]$ greater than or equal to 15 µmol/kg were not corrected for dissolution because the uncorrected temperatures match modern SST well.

## 4 Methods

### *4.1 Site and age model*

All samples were taken from ODP site 806 Hole C. The age model at site 806 has been updated [i.e. *Karas et al.*, 2009] since publication of the Wara et al. [*Wara et al.*, 2005] data, using benthic $\delta^{18}O$ from site 806 Hole B spanning 0-4 Ma. For this study, we applied the Karas et al. [2009] age model to the original Wara et al. [*Wara et al.*, 2005] data, and also transferred it to our samples from Hole C. For samples older than 4 Ma, we estimated ages by linearly interpolating between three biostratigraphic datums (details in Table S1).

### *4.1 Analytical methods*

#### 4.1.1 B/Ca analysis of benthic foraminifera

Sample size for B/Ca analysis ranged from 4 to 19 specimens, with an average sample size of 12, and was limited by the number of specimens present in each sediment interval. In general, Pliocene samples had fewer specimens than Pleistocene samples (average of 10 versus 13 specimens), and fewer duplicate samples were analyzed. Since no effect of foraminiferal size fraction on B/Ca has been found [*Kerr et al.*, 2017], specimens of *C. wuellerstorfi* were picked from the >250 μm size fraction. Test frostiness and morphology were noted for every sample and the frostiest specimens were discarded when possible, though neither frostiness nor morphology were found to impart a consistent bias to the data (see section titled "Test of the effect of frostiness and morphology on benthic foraminiferal B/Ca" below). Plotted B/Ca values for the eleven youngest samples reflect the average of two to six

subsamples, separated on the basis of frostiness and morphology. Duplicate samples were analyzed for 58 out of 117 samples, and final B/Ca values reflect the average of the duplicates.

Samples were cleaned according to the protocol of [*Martin and Lea*, 2002], which includes reductive cleaning as well as multiple sonication steps, oxidative cleaning, and a weak acid leach. Samples were analyzed for trace metals by inductively coupled plasma-mass spectrometry on a Finnegan Element XR at the University of California, Santa Cruz following the methods of [*Brown et al.*, 2011]. Long-term instrumental precision of B/Ca measurements is ±3.6% (1σ), based on repeated analyses of in-house liquid consistency standards over many months. Estimated total uncertainty of B/Ca measurements is ±4.0% (1σ), based on the average standard deviation between duplicates (which were analyzed during different instrument runs). This value incorporates intra-sample Mg/Ca variability (i.e. inter-specimen variability), variability between instrument runs over many months, and instrumental uncertainty (as quantified above). Mn/Ca, which can be an indicator of contamination, averaged 0.18 mmol/mol and ranged from 0.008 μmol/mol to 0.423 mmol/mol, with higher values in the Pliocene samples. However, Mn/Ca shows no correlation with B/Ca ($R^2 = 0.043$), so the data and interpretations should be unaffected by contamination from Mn-bearing phases.

4.1.2 Mg/Ca analysis of planktic foraminifera

Forty to fifty *T. trilobus* specimens were picked from each sample and pooled to generate a downcore record of mixed layer temperature at site 806. Specimens

were picked from the 350-425 μm size fraction, and gently crushed prior to cleaning. Samples were cleaned according to the same protocol as described above for B/Ca analyses. Samples were analyzed for Ca, Mg, Mn, and Sr on a ThermoScientific iCap 7400 inductively-coupled plasma optical emission spectrometer (ICP-OES) at the University of California, Santa Cruz. The instrumental precision of our Mg/Ca data is ±1% (1σ), based on repeated measurements of an in-house liquid standard (FLCS2, Mg/Ca=3.31 mmol/mol) over many months. Estimated total uncertainty of Mg/Ca measurements is ±4% (1σ), based on repeated measurements of an in-house *T. trilobus* standard (KNR 110 2-58, Mg/Ca=3.75 mmol/mol). Similar to the estimate of B/Ca uncertainty, this value reflects intra-sample Mg/Ca variability (i.e. inter-specimen variability), variability between instrument runs over many months, and instrumental uncertainty (as quantified above). Mn/Ca averaged 0.112 mmol/mol and ranged from 0.015 mmol/mol to 0.230 mmol/mol, with higher values in the Pliocene samples, and is very weakly correlated with B/Ca ($R^2 = 0.26$). Wara et al. [*Wara et al.*, 2005] found similar levels of Mn/Ca in their samples from site 806. The likely source of manganese is manganese carbonate overgrowths, given that reductive cleaning was performed to remove manganese oxides. Because manganese carbonates have a Mg/Mn ratio of ~0.1 mol/mol [*Boyle*, 1983], they would contribute a maximum of ~0.02 mmol/mol Mg/Ca, which corresponds to a 0.06°C bias – too small to have any substantial effect on our interpretations.

## 5 Results

### *5.1 Test of the effect of frostiness and morphology on benthic foraminiferal B/Ca*

As with any species, there is some variability in morphology among individual specimens of *C. wuellerstorfi*, which for this species is mostly related to the convexity of the top and bottom sides, and the length/curvature of the chambers. [*Rae et al.*, 2011] described an effect of length/curvature of chambers on measured B/Ca, in which individuals with shorter chambers appeared to have significantly lower B/Ca than individuals with longer, more curved chambers. At site 806, Pliocene specimens of *C. wuellerstorfi* tend to be "frostier" (white, rather than translucent) and more convex than younger specimens. *C. wuellerstorfi* is also less abundant in the Pliocene than the late Pleistocene (as are all species for which a B/Ca to $\Delta[CO_3^{2-}]$ relationship has been quantified). Generating a downcore record of benthic foraminiferal B/Ca thus necessitates pooling individuals with variations in frostiness and morphology.

For this reason, we tested the potential effect of shell frostiness (degree of translucency or whiteness, a product of early diagenesis) and convexity, which is a significant source of variability among specimens at site 806, and not discussed in the [*Rae et al.*, 2011] study. Specimens were rated on frostiness from 1 to 7 and convexity from 1 to 6 (see Table S2 for complete description of rankings). Specimens in which the chambers were substantially shorter or less curved (like those of *C. mundulus*) were discarded, as were specimens with equally convex top and bottom sides. To test the effect of frostiness and morphology on benthic foraminiferal B/Ca,

we subsampled eleven sediment intervals in which *C. wuellerstorfi* was particularly abundant. Depending on abundance, two to six subsamples were created from each sediment interval. Each subsample consisted of several individuals of a given frostiness and morphology ranking.

We found that differences in frostiness and morphology do appear to yield B/Ca variability within a sediment interval (Figure 4). These differences are larger, on average, than differences between duplicate samples; the average standard deviation among subsamples is ±6%, compared to the average standard deviation between duplicates of ±4%. This discrepancy may indicate an effect of frostiness or morphology on B/Ca. It is also possible, however, that the reason for greater variability among subsamples than between duplicates is small sample size, rather than frostiness or morphology; i.e. high inter-specimen variability exists even within a single morphology or frostiness ranking. Subsamples consisted of 2 to 10 specimens (average 6), which was smaller than the duplicated samples (average 13 specimens). Importantly, apparent B/Ca differences on the basis of frostiness and morphology are inconsistent in direction and magnitude, such that they create measurement noise rather than a consistent bias. For this reason, we do not believe our downcore record is biased by changes in shell frostiness or morphology.

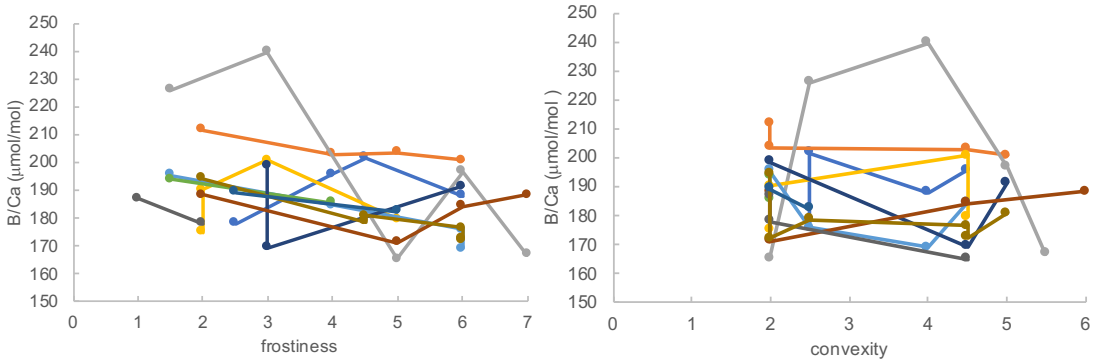


**Figure 4. Frostiness and convexity of *C. wuellerstorfi* specimens vs. B/Ca.** Higher numbers indicate greater frostiness or convexity. See Table S2 for description of rankings. Colors indicate subsamples from the same sediment interval. Though there is scatter among the subsamples, there is not a consistent trend of higher/lower B/Ca with greater frostiness or convexity.

*5.2 Coretop B/Ca and Mg/Ca data*

The coretop value for benthic foraminiferal B/Ca is 190.8 µmol/mol, the average of four sample splits with differing frostiness and morphology with B/Ca values ranging from 177.9 µmol/mol to 201.6 µmol/mol. This average value differs from coretop measurements from nearby site MW91-9 38 (0°N, 159.5°E, 2456 m, B/Ca=174 µmol/mol) [*Yu and Elderfield*, 2007], but is similar to the youngest data point (9 ka) from the [*Kerr et al.*, 2017] dataset, which was collected from our site (806) and has a value of 190.1 µmol/mol. Using the [*Yu et al.*, 2013] calibration, our coretop B/Ca value corresponds to a $\Delta[CO_3^{2-}]$ value of 12.5 µmol/kg, which is similar to the modern value of 10.5 µmol/kg, calculated for site 806 using WOCE data [*Dekens et al.*, 2002].

Our coretop value for Mg/Ca of *T. trilobus* is 3.832 mmol/mol. This value is very similar to other coretop measurements from site 806 (3.768 mmol/mol, 4.001 mmol/mol, 4.055 mmol/mol; [*Ford and Ravelo*, 2019; *Wara et al.*, 2005]), despite

each measurement being made on different instruments and/or using different calibration standards. The average of these measurements, weighted by sample size, is 3.85 mmol/mol. This corresponds to 29.4 ±0.2°C, using the [*Dekens et al.*, 2002] $\Delta[CO_3^{2-}]$-based calibration with $\Delta[CO_3^{2-}]$ estimated from our coretop B/Ca value. As such, the Mg/Ca temperature is very close to the modern measured SST at the site of 29.2°C [*Dekens et al.*, 2002].

*5.3 Sensitivity of reconstructed temperatures to choice of dissolution correction cutoff*

The [*Dekens et al.*, 2002] Mg/Ca-temperature calibration with $\Delta[CO_3^{2-}]$-based dissolution correction does not include an explicit cutoff value above which no correction is applied. Our test of coretop data from the WPWP shows that Mg/Ca data associated with high $\Delta[CO_3^{2-}]$ does not need to be corrected for dissolution, in general agreement with many previous studies of foraminiferal dissolution. Here we explore the effect of our choice of cutoff value on calculated temperatures.

We chose a cutoff value of 15 μmol/kg, which yields an average mid-early Pliocene (3-5.5 Ma) temperature of 28.67°C (not including an adjustment for changes in Mg/Ca of seawater, "unadjusted"). Other potential cutoff values are 21.3 μmol/kg, as proposed by [*Regenberg et al.*, 2014], and 12.75 μmol/kg, halfway between the points at which a dissolution correction does and does not yield a more accurate SST estimate among WPWP coretops (Figure 3). These cutoffs yield average unadjusted Pliocene temperatures of 28.53°C and 28.70°C, respectively. In general, using a cutoff means that some data points do not receive a dissolution correction. With

variable $\Delta[CO_3^{2-}]$ downcore, the use of a cutoff results in a different average calculated temperature than if applying a fixed correction, even if there is no change in the average value of $\Delta[CO_3^{2-}]$. However, our choice of cutoff (among reasonable values) has only a small effect on the overall temperature record.

*5.4 Downcore B/Ca and Mg/Ca records*

There is no clear long-term trend in benthic foraminiferal B/Ca at site 806 (Figure 5), as can be seen by referencing downcore data to the modern value. The temporal resolution of our dataset (~50 kyr) precludes the interpretation of any glacial-interglacial variability or lack thereof. There may be greater B/Ca variability among Pliocene samples than Pleistocene samples, which may reflect either climate variability or smaller sample size and fewer duplicates. Shell weight of T. trilobus at site 806 [*Wara et al.*, 2005] also shows no trend over the Plio-Pleistocene (Figure 5), which supports the lack of trend in our benthic foraminiferal B/Ca data.

Our Plio-Pleistocene Mg/Ca data match the record of [*Wara et al.*, 2005], with similar mean values and variability (Figure 5). Using B/Ca-derived values of $\Delta[CO_3^{2-}]$, rather than the modern value of $\Delta[CO_3^{2-}]$, to correct the Mg/Ca data for dissolution yields little overall change in the temperature reconstruction. There are no substantial changes in mean value, trend, or variability.

*5.5 Downcore carbonate coarse fraction record*

For comparison with the downcore benthic B/Ca record, I also examined the ratio of coarse material to total carbonate in each sediment sample (% >63μm $CaCO_3$). This metric has been proposed as another indicator of dissolution [*Broecker*

*and Clark*, 1999]. In the tropics, coarse material is almost entirely carbonate, and the ratio of coarse to fine carbonate varies with $\Delta[CO_3^{2-}]$, as increasing dissolution breaks foraminiferal shells into smaller fragments [*Broecker and Clark*, 1999]. For our 806 samples, we generated a record of % >63μm $CaCO_3$ by dividing the weight of the >63μm size fraction by the total dry bulk weight (this data was collected during sediment washing and sieving) divided by $\%CaCO_3$. The $\%CaCO_3$ is from shipboard data and is not from the same samples as ours; we used data from the nearest sample.

The % >63μm $CaCO_3$ data has a long-term trend, with lowest values in the Pliocene increasing toward present (Figure 6). This trend contrasts with the lack of trend in benthic B/Ca and planktic foraminiferal shell weight.

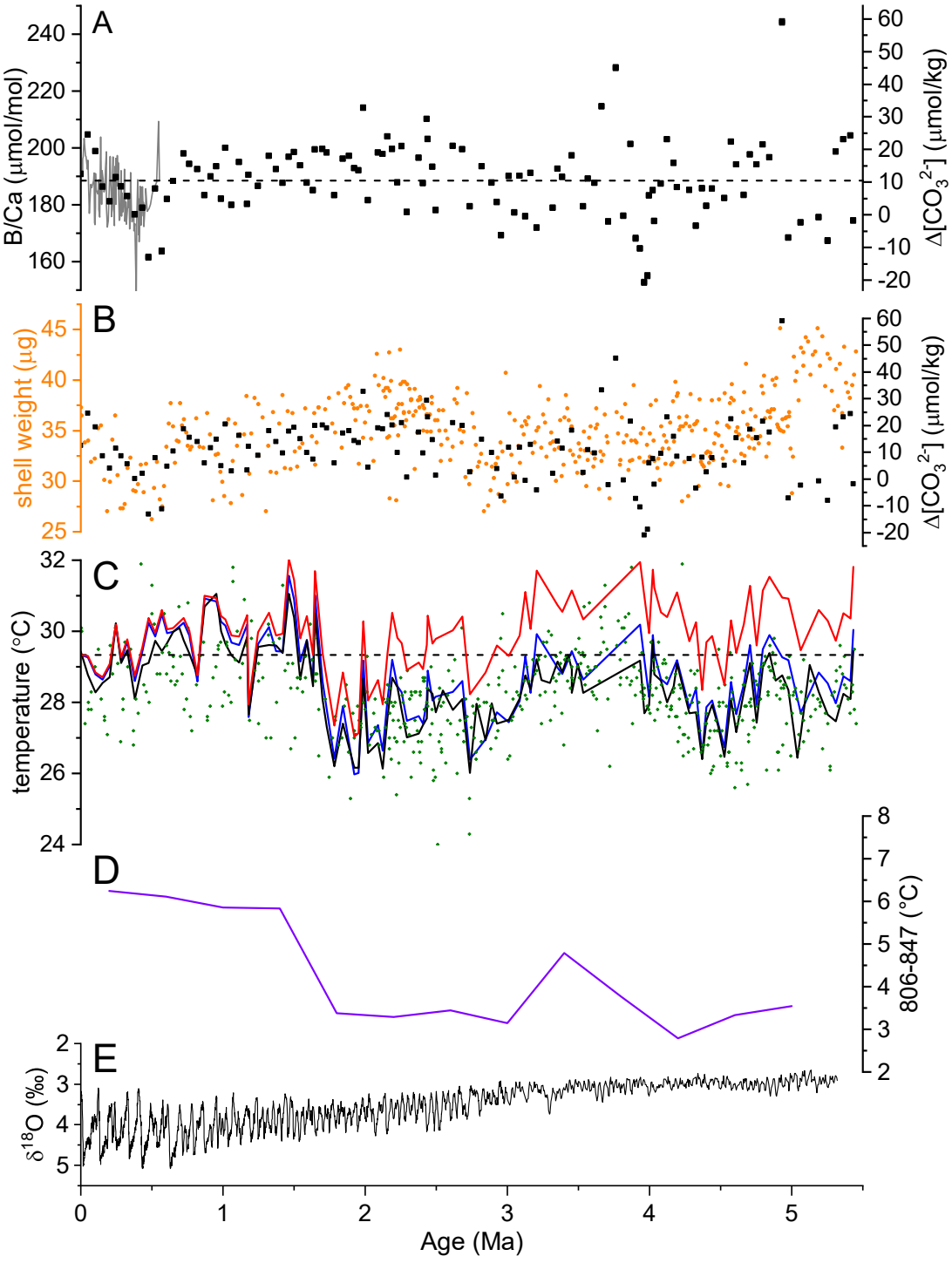


**Figure 5. New B/Ca data from site 806, and its application to the site 806 temperature record.**

A) New B/Ca data from *C. wuellerstorfi* and calculated $\Delta[CO_3^{2-}]$ (black squares), and [*Kerr et al.*, 2017] B/Ca data from site 806 (gray line). Dashed line shows modern

$\Delta[CO_3^{2-}]$ at site 806 [*Dekens et al.*, 2002]. B) Calculated $\Delta[CO_3^{2-}]$ (black squares) and *T. trilobus* shell weight data from site 806 [*Wara et al.*, 2005] (orange circles). C) New *T. trilobus* Mg/Ca data converted to temperature using modern $\Delta[CO_3^{2-}]$ for the dissolution correction (black line), using B/Ca-derived $\Delta[CO_3^{2-}]$ <15 μmol/kg for the dissolution correction (blue line), and adjusted for changes in Mg/Ca of seawater, calculated by taking the downcore anomaly of temperatures calculated with the Dekens-Evans formulation and adding it to the Dekens coretop temperature (red line) (see text for details). [*Wara et al.*, 2005] record is shown for context (green diamonds). Dashed line shows coretop temperature. D) Tropical Pacific zonal temperature gradient, calculated as the difference between the adjusted SST record at 806 (red curve, part C) minus the alkenone-based SST record at ODP site 847 (Figure 2). Data were binned at 0.4 Myr intervals. E) Benthic oxygen isotope stack [*Lisiecki and Raymo*, 2005].

## 6 Discussion

### *6.1 Comparison to other B/Ca records from the western tropical Pacific*

Our data has similar mean values and variability compared to a previously published benthic foraminiferal B/Ca dataset from site 806 which spans the last 500 kyr [*Kerr et al.*, 2017] (Figure 5); differences in temporal resolution preclude any detailed comparison of the two records. Other records from the region [*Yu et al.*, 2013] extend only through the past glacial cycle, or date to the mid-Miocene [*Ma et al.*, 2018]. Our data represent a significant extension of $\Delta[CO_3^{2-}]$ reconstructions regionally and globally, and are the first data from the Pliocene.

### *6.2 Implications of B/Ca data for Pliocene SSTs in the West Pacific Warm Pool*

Correcting planktic Mg/Ca data with contemporaneous (i.e. B/Ca-derived) values of $\Delta[CO_3^{2-}]$, rather than the modern value, does not amplify or reduce variability in reconstructed SSTs. As such, it appears that sample-to-sample variations in $\Delta[CO_3^{2-}]$ stemming from glacial-interglacial changes or other variability do not add

noise to the temperature record. Importantly, the lack of a long-term trend in benthic foraminiferal B/Ca, and thus $\Delta[CO_3^{2-}]$, at site 806 implies little bias from dissolution in the [*Wara et al.*, 2005] Pliocene SSTs.

*6.3 The effect of changes in $Mg/Ca_{sw}$*

There are several lines of evidence indicating that Mg/Ca of seawater may have changed over the past 5 Ma. Estimates of past seawater composition come from fluid inclusions in marine halite [*Horita et al.*, 2002; *Lowenstein et al.*, 2001], calcium carbonate veins [*Coggon et al.*, 2010; *Rausch et al.*, 2013], bottom water temperature and ice volume constraints [*Dekens et al.*, 2016], and temperature proxy offsets [*Evans et al.*, 2016; *O'Brien et al.*, 2014]. Estimates for the Pliocene range from 3.6 [*Horita et al.*, 2002] to 5.26 [*Rausch et al.*, 2013]. Here we use the reconstruction of [*Evans et al.*, 2016] because its values are intermediate between the published extremes, and it is continuous through the Plio-Pleistocene. We note, however, that the premise of this reconstruction is imperfect because temperature proxy offsets may have causes other than $Mg/Ca_{sw}$ changes, such as seasonality or depth habitat of proxy production, and dissolution. Improving reconstructions of $Mg/Ca_{sw}$ is thus an important and ongoing area of research.

To account for the effect of changes in $Mg/Ca_{sw}$ on our reconstructed WPWP temperatures, we use the calibration of [*Evans et al.*, 2016]. Culturing of planktic foraminifera has shown that changes in $Mg/Ca_{sw}$ likely affected the Mg/Ca paleothermometer through changes in the temperature sensitivity and partition coefficient, i.e. A and B in the equation $Mg/Ca = B \exp(AT)$. The calibration of

[*Evans et al.*, 2016] is the only one that accounts for these changes, by making A and B functions of Mg/Casw. To include a $\Delta[CO_3^{2-}]$-based dissolution correction, we combine the [*Dekens et al.*, 2002] and [*Evans et al.*, 2016] calibrations, by substituting the Mg/Casw-dependent values of A and B from [*Evans et al.*, 2016] into the [*Dekens et al.*, 2002] $\Delta[CO_3^{2-}]$-based equation, after adding a 10.3% adjustment to T. trilobus Mg/Ca values as described by [*Evans et al.*, 2016]. We also explored the effect of using a different dissolution correction. Applying the [*Regenberg et al.*, 2014] $\Delta[CO_3^{2-}]$-based dissolution correction then using the [*Evans et al.*, 2016] calibration, rather than using the Dekens-Evans formulation, results in average reconstructed Pliocene temperatures 0.3°C warmer than the Dekens-Evans formulation. We use the Dekens-Evans formulation rather than a [*Regenberg et al.*, 2014] plus [*Evans et al.*, 2016] approach because the [*Dekens et al.*, 2002] calibration produces the most accurate SSTs from coretops in the WPWP, as described in section 3.2. Overall, the choice of dissolution correction introduces a small uncertainty to our temperature reconstructions.

The Dekens-Evans formulation does not produce realistic coretop temperatures in the WPWP, with or without inclusion of the [*Dekens et al.*, 2002] dissolution correction. Our coretop Mg/Ca temperature using the Dekens-Evans formulation is 23.9°C (or 24.5°C using the [*Evans et al.*, 2016] calibration alone) compared to the modern measured SST of 29.2°C [*Dekens et al.*, 2002]. Using the [*Dekens et al.*, 2002] calibration with $\Delta[CO_3^{2-}]$-based dissolution correction alone, our coretop Mg/Ca temperature is 29.3°C – a much better match to modern SST.

Thus, to produce a temperature record with realistic values for the WPWP that also accounts for changes in $Mg/Ca_{sw}$, we take the coretop-downcore temperature anomaly using the Dekens-Evans formulation, and add that value to our coretop temperature using the [*Dekens et al.*, 2002] calibration alone. This is repeated for every downcore sample, and forms the red line on Figure 5. The difficulty the Evans calibration has in reproducing modern SST at the site raises doubt as to its ability to accurately quantify the effect of past changes in $Mg/Ca_{sw}$ on our temperature record. However, it is the only published calibration that incorporates a dependence on $Mg/Ca_{sw}$. Future improvement of Pliocene WPWP temperature estimates thus await refinements in Mg/Ca paleothermometry.

The [*Evans et al.*, 2016] reconstruction estimates $Mg/Ca_{sw}$ at 5 Ma to be 4.29, compared to 5.28 today, with most of the shift toward modern values occurring between 2.5 and 1 Ma. Thus, including an adjustment for changes in $Mg/Ca_{sw}$ raises reconstructed temperatures older than ~1 Ma (Figure 5). For the mid-early Pliocene, the average adjustment is +1.8°C.

### *6.4 Was the West Pacific Warm Pool warmer in the Pliocene than the late Holocene?*

#### 6.4.1 Estimated Pliocene-Holocene temperature difference

If dissolution is fixed at the modern value and $Mg/Ca_{sw}$ changes are not considered (black line on Figure 5c), the average temperature of the WPWP during the mid-early Pliocene (3.0-5.4 Ma) was 1.2°C cooler than the coretop. When using contemporaneous (i.e. B/Ca-derived) values of $\Delta[CO_3^{2-}]$ to correct the Mg/Ca data for dissolution (blue line on Figure 5c), the Pliocene-Holocene temperature difference

becomes -0.7°C. The difference between the variable-dissolution and the fixed-dissolution estimate is not due to a trend in dissolution; the Pliocene-Holocene difference in average $\Delta[CO_3^{2-}]$ is only 3.4 μmol/kg. It is largely due to variations in $\Delta[CO_3^{2-}]$ and the use of a cutoff for applying a dissolution correction. Adding an adjustment for changes in $Mg/Ca_{sw}$ (red line on Figure 5c) results in a Pliocene temperature of 30.4°C, and a Pliocene-Holocene temperature difference of +1.1°C.

### 6.4.2 Uncertainty of the estimated temperature difference

Sources of uncertainty in this estimate are 1) calibration uncertainty, 2) analytical uncertainty and standard error of the mean, 3) the effect of Pliocene salinity changes, 4) our choice of dissolution correction, and 5) the Pliocene value of $Mg/Ca_{sw}$. Uncertainty in the [*Evans et al.*, 2016] calibration comes from uncertainty in the Pliocene value of $Mg/Ca_{sw}$ (discussed below), since the seawater values determines the preexponential constant and temperature sensitivity. Uncertainty in the [*Yu et al.*, 2013] B/Ca- $\Delta[CO_3^{2-}]$ equation yields uncertainty in the Pliocene-Holocene temperature difference of +0.02°C and -0.05°C (from uncertainty in the slope) and +0.05°C and -0.06°C (from uncertainty in the y intercept). The plus and minus uncertainties are different because we use a cutoff value in $\Delta[CO_3^{2-}]$ when applying the dissolution correction.

Our knowledge of the average temperature during the Pliocene and the late Holocene depends on the number of samples and the variability among them. There are four measurements of late Holocene Mg/Ca at site 806, with a standard error of the mean equal to ±0.21°C. The mid-early Pliocene average temperature is comprised

of 40 measurements, with a standard deviation of 0.85°C and a standard error of the mean equal to ±0.13°C. In both cases, the standard error of the mean inherently includes the analytical uncertainty of each measurement and uncertainty in the B/Ca-derived value of $\Delta[CO_3^{2-}]$, which contributes uncertainty to the dissolution correction.

The WPWP is simulated to have been 0.1 to 0.2 psu fresher [*Haywood et al.*, 2007; *Rosenbloom et al.*, 2013] or 0.5 psu saltier [*Burls et al.*, 2017] during the Pliocene than today, which corresponds to a temperature bias of -0.1°C or +0.3°C. Our choice of dissolution correction also affects estimated temperatures; using a different cutoff value for applying the correction yields an average Pliocene temperature of 0.03°C higher or 0.14°C lower than our reported average value. Using the [*Regenberg et al.*, 2014] dissolution correction instead of the [*Dekens et al.*, 2002] correction raises the calculated Pliocene average temperature by 0.31°C.

The largest uncertainty is the Pliocene value of $Mg/Ca_{sw}$. The [*Evans et al.*, 2016] reconstruction gives an average value for $Mg/Ca_{sw}$ at 3-5 Ma of 4.29, with inner error bars of 4.01 to 4.5. This range of $Mg/Ca_{sw}$ values changes the calculated Pliocene average temperature by +0.67°C or -0.44°C. Overall, adding the all the aforementioned errors in quadrature yields an estimated uncertainty of +0.78°C and -0.62°C, for a final Pliocene-Holocene temperature difference of +1.1°C with a range of +0.5°C to +1.9°C.

### 6.4.3 Comparison to other estimates of Pliocene-Holocene temperature difference

Our estimate of the temperature of the WPWP during the mid- and early Pliocene is lower than that based on the $TEX_{86}$ temperature proxy, which was interpreted as showing the WPWP to be 2-2.5°C warmer in the Pliocene [*Zhang et al.*, 2014a]. However, the Zhang et al. [*Zhang et al.*, 2014a] estimate is based on the long-term smoothed trend, such that the Pliocene estimate is relative to a Pleistocene baseline rather than a Holocene baseline [*Ravelo et al.*, 2014]. Pliocene $TEX_{86}$ values are in fact very similar to coretop values [*Ravelo et al.*, 2014]. Also, numerous studies have shown that $TEX_{86}$ is biased toward subsurface temperatures in the tropics and subtropics [*Dong et al.*, 2015; *Hertzberg et al.*, 2016; *Jia et al.*, 2012; *Liddy et al.*, 2016; *Richey and Tierney*, 2016; *Seki et al.*, 2012]. The WPWP subsurface was indeed warmer during the Pliocene than today [*Ford et al.*, 2015b], so the trend in $TEX_{86}$ likely reflects subsurface rather than surface cooling [*Ravelo et al.*, 2014].

Our estimate is lower than the PlioMIP multi-model mean estimate of +1.5-2.0°C relative to preindustrial temperatures [*Haywood et al.*, 2013], though the uncertainty in our estimate overlaps the PlioMIP values. It is possible that the Pliocene WPWP was cooled through mechanisms that are not well represented in general circulation models, such as heat dissipation by storms or changes in cloud albedo [*Barreiro and Philander*, 2008; *Burls and Fedorov*, 2014; *Fedorov et al.*, 2010]. Our results validate those of [*Ford and Ravelo*, 2019], who reconstructed temperature variability during Pliocene glacials and interglacials in the WPWP and found an average temperature of +0.9°C relative to the Holocene. As described by

[*Ford and Ravelo*, 2019], their reconstructed temperatures yield a climate sensitivity in line with previous model-based estimates.

### *6.5 The Pliocene "El Padre" state and the long-term evolution of the tropical Pacific*

Does the idea of an El Padre state, a tropical Pacific mean state with a low east-west SST gradient similar to a modern El Niño event [*Ravelo et al.*, 2014], still hold for the Pliocene given the updated SSTs for the WPWP? In a word, yes. Figure 5d shows the difference between the updated WPWP SST record and the alkenone-based SST record from ODP 847 in the EEP ([*Dekens et al.*, 2008], shown in Figure 2), after each record has been binned and averaged at 0.4 Myr intervals. The results show that during the Pliocene, the east-west SST gradient was about half of the late Pleistocene/Holocene value of ~6.5°C. We note that these results are computed using the originally published alkenone temperatures [*Dekens et al.*, 2008]. Using the recently published BAYSPLINE calibration [*Tierney and Tingley*, 2018] raises the calculated temperature of the highest $U^{K'}_{37}$ values, resulting in a ~1°C lower zonal SST gradient in the Pliocene. Our results are qualitatively the same when comparing the WPWP record to any of the other EEP records shown in Figure 2. Overall, the updated SST records still support a Pliocene El Padre state.

An interesting feature of the WPWP data is the sudden warming at ~1.7 Ma. This feature persists in the SST reconstruction even after correcting for contemporaneous changes in $\Delta[CO_3^{2-}]$ (red line, Figure 5c). The rise in SST of the WPWP occurred at the same time as a drop in SST at high northern and southern latitudes, as recorded at ODP sites 882 and 1090 in the North Pacific and South

Atlantic [*Martinez-Garcia et al.*, 2010]. These changes at 1.7 Ma increased meridional and zonal temperature gradients to their modern values, and are hypothesized to reflect a shrinking of the subtropical gyres [*Martinez-Garcia et al.*, 2010].

### *6.6 Implications of the $\Delta[CO_3^{2-}]$ record for productivity and deep ocean circulation*

Carbonate mass accumulation rate ($CaCO_3$ MAR) was high at ODP site 806 in the Pliocene, and decreased toward present (Figure 6). All other sites in the region, except the deepest (ODP 804, at 3862 m), have the same trend. When examined in isolation, it is not possible to disentangle higher Pliocene productivity from decreased dissolution; both would cause the same trend. The $\Delta[CO_3^{2-}]$ record sheds light on this issue: the lack of trend implies no change in dissolution, at least at the depth of ODP site 806 (2520 m). Thus, higher $CaCO_3$ MAR in the Pliocene must reflect higher productivity. At deeper depths, as shown in the $CaCO_3$ MAR record from ODP 804, dissolution may have been higher in the Pliocene, in agreement with the CCD reconstruction of Farrell and Prell [*Farrell and Prell*, 1991] from the central Pacific. However, it appears that any change in seafloor corrosivity was not felt at the depth of ODP 806.

A lack of long-term trend in dissolution, as shown in the $\Delta[CO_3^{2-}]$ record, is supported by planktic foraminiferal shell weight data from ODP 806 [*Wara et al.*], which also has no trend (Figure 6). In contrast, the % >63μm $CaCO_3$ data from 806 does have a long-term trend, with lower values in the Pliocene increasing toward

present. (Figure 6). This implies greater dissolution in the Pliocene, in contrast to the B/Ca and shell weight data. However, it may also reflect increased winnowing of fine sediment in the later Pliocene and Pleistocene [*Berger et al.*, 1993]. Alternatively, the % >63μm $CaCO_3$ record may reflect an ecosystem shift. The $CaCO_3$ MAR data and benthic B/Ca data together imply higher productivity in the Pliocene, which may have taken the form of coccolith blooms that dominated the $CaCO_3$ sediment flux and overwhelmed foraminiferal deposition. Overall, the data demonstrate the utility of considering multiple lines of evidence when reconstructing changes in carbonate chemistry and sedimentation.

The $\Delta[CO_3^{2-}]$ record at 806 also provides a test of predicted changes in deep ocean circulation over the Plio-Pleistocene. For example, it was recently postulated that there was deep water production in the northwestern North Pacific (NPDW) during the Pliocene [*Burls et al.*, 2017]. This hypothesis was based on a general circulation model whose physics were altered to reproduce the reduced zonal and meridional SST gradients seen in Pliocene proxy data [e.g. *Fedorov et al.*, 2013]; this model spontaneously generated NPDW [*Burls et al.*, 2017]. The authors point to higher $CaCO_3$ MAR at ODP site 882 as evidence of increased ventilation. This hypothesis also predicts higher $\Delta[CO_3^{2-}]$ at site 806 in the Pliocene, if the North Pacific was more ventilated than today. However, the $\Delta[CO_3^{2-}]$ record has no long-term trend. If NPDW was active in the Pliocene, it does not seem to have flowed over site 806.

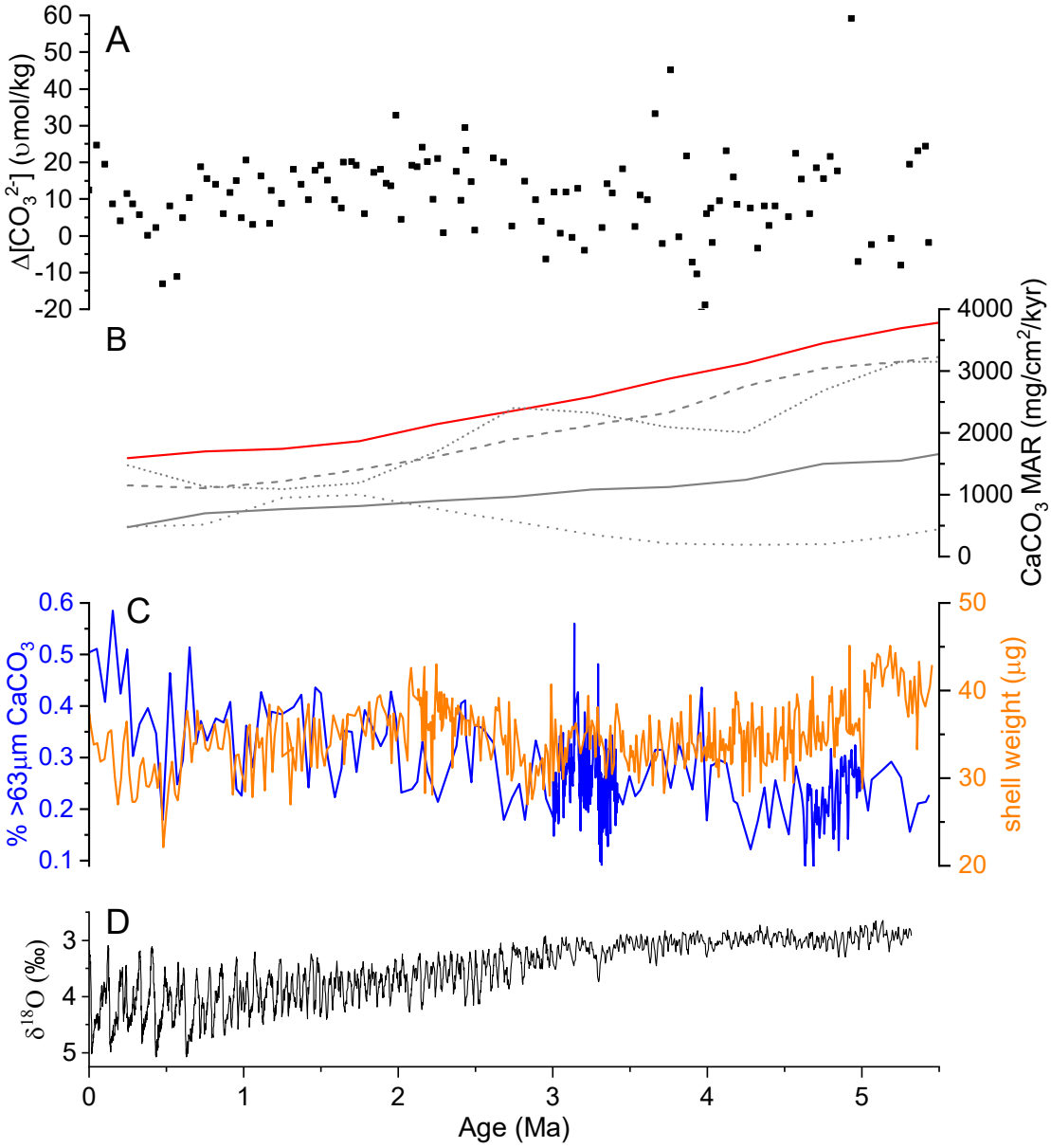


**Figure 6. Dissolution- and deep ocean circulation-relevant proxy data, from 806 and other sites.**

A) $\Delta[CO_3^{2-}]$ derived from benthic B/Ca at site 806 (this study). B) $CaCO_3$ MAR at site 806 (red) and nearby sites (gray), listed in order of core depth: 807 (2804 m, short dashed), 805 (3188 m, dashed), 803 (3410 m, solid), and 804 (3862 m, dotted). 806 is the shallowest site, at 2521 m. Data from [*Lyle*, 2003]. C) % >63μm $CaCO_3$ of marine sediments (blue) and average weight of *G. sacculifer* shells (orange) [*Wara et al.*, 2005], both at site 806. (D) Benthic $\delta^{18}O$ stack [*Lisiecki and Raymo*, 2005].

## 7 Conclusions

We generated a new record of benthic B/Ca at ODP site 806 spanning the past 5.5 Ma, to reconstruct the history of $\Delta[CO_3^{2-}]$ and thus calcite dissolution at the site. The record has no long-term trend, implying that the Mg/Ca-based SST record at the site is not biased by changes in dissolution. Also, short-term fluctuations in $\Delta[CO_3^{2-}]$ do not appear to create artificial variability in the temperature reconstruction. Changes in $Mg/Ca_{sw}$ created a ~1.8°C cold bias in the foraminiferal Mg/Ca, as estimated using the approach of [*Evans et al.*, 2016]. Adjusting the data for this effect results in a Pliocene WPWP temperature ~1.1°C warmer than the late Holocene. There are a number of uncertainties in this estimate, most importantly the value of $Mg/Ca_{sw}$ during the Pliocene. When including all relevant uncertainties, the WPWP is estimated to have been +0.5°C to +1.9°C warmer in the Pliocene than the late Holocene. Our estimate of Pliocene WPWP temperature is somewhat lower (though within uncertainty) of the PlioMIP estimate of +1.5°C to +2.0°C [*Haywood et al.*, 2013], and do not support the 2-2.5°C Plio-Pleistocene warming trend shown in $TEX_{86}$ data [*Zhang et al.*, 2014a]. Overall, the data still support a Pliocene El Padre state, with a much lower zonal SST gradient but not much warmer maximum temperatures.

**Supplemental materials for The Temperature of the West Pacific Warm Pool during the Pliocene**

**Table S1.** Biostratigraphic datums used to construct age model >4 Ma
**Table S2.** Description of frostiness and morphology rankings

| Event | Species | Depth in hole (mbsf) | Sample | Age (Ma) | Reference |
|---|---|---|---|---|---|
| LO | *Ceratolithus acutus* | 148.00 | 806B 16H-7 40 cm | 5.04 | Mayer et al. 1993 |
| LO | *Triquetrorhabdulus rugosus* | | 806B 17H-4 26 cm | 5.279 | Takayama 1993 |
| LO | *Discoaster quinqueramus* | 162.50 | 806B 18H-3 100 cm | 5.59 | Mayer et al. 1993 |

Ages of all events were taken from Raffi et al. 2006, instead of from the original sources.

**Table S1.**
Biostratigraphic datums used to construct age model at site 806 for samples older than 4 million years.

| Frostiness Ranking | Description |
|---|---|
| 1 | Maximally translucent with no sign of whiteness |
| 2 | Slight whiteness |
| 3 | Slightly more whiteness |
| 4 | Sutures are white, but chamber interiors are somewhat translucent |
| 5 | Shell is mostly white, with a few translucent spots |
| 6 | Shell is entirely white, but chamber sutures are very clearly defined |
| 7 | Shell is entirely white and chamber sutures are blurred |

| Morphology Ranking | Description |
|---|---|
| 1 | Shell is completely flat on top and bottom |
| 2 | Shell is very slightly convex on top, completely flat on bottom |
| 3 | Shell is more convex on top, completely flat on bottom |
| 4 | Shell is very convex on top, verging toward a central peak, completely flat on bottom |
| 5 | Top is convex (though no central peak), bottom slopes slightly inward from outside edge but has a flat central area |
| 6 | Shell is equally convex on top and bottom (discarded from analysis) |

**Table S2.**

Description of rankings used to describe *C. wuellerstorfi* specimens for frostiness and morphology tests.

## Chapter 5: Conclusions

This dissertation is composed of three projects that seek to elucidate connections between climatic forcing, tropical Pacific mean state, and El Niño strength, using case studies from warm periods of the past five million years. Each project uses trace metal analysis of foraminifera from marine sediments to reconstruct seawater temperature and chemistry. The findings highlight the importance of the thermocline in determining El Niño strength, and constrain the West Pacific Warm Pool's response to modern levels of atmospheric $CO_2$.

In Chapter 2 of this dissertation, "Dampened El Niño in the early and mid-Holocene due to insolation-forced deepening of the thermocline," I collected temperature proxy data from individual foraminifera from the central equatorial Pacific to reconstruct mixed-layer temperature distributions through the Holocene. I found that El Niño was dampened during both the mid- and the early Holocene, relative to the late Holocene, in agreement with model studies forced with Holocene boundary conditions [*White et al.*, 2018]. Out of several proposed mechanisms for insolation-forced dampening of ENSO, the one best supported by proxy data is a weakening of the upwelling feedback due to a warmer/deeper thermocline [*White et al.*, 2018]. This implies that extratropical conditions are more important than tropical conditions in dictating ENSO strength, in contrast to the arguments put forth by [*Clement et al.*, 1999; *Clement et al.*, 1996].

The conclusions in Chapter 2 rest on the early Holocene data, and on previously published records of subsurface temperature in the tropical Pacific.

Additional data on subsurface conditions in the eastern equatorial Pacific would strengthen my findings, since only a single record exists from this region and it is likely more important for ENSO than data from the western Pacific. Also, additional data from the early Holocene would be beneficial, since early Holocene data are critical for differentiating among mechanisms and there are fewer other records (compared to the mid-Holocene) to back up my findings. Single foraminiferal data from ODP site 849 would be a good candidate, since that site is on the equator and far enough west that temperature variability is dominated by interannual (including ENSO) variability, not seasonality [*Thirumalai et al.*, 2013].

In Chapter 3, "Dampened El Niño in the early Pliocene warm period," I collected the same type of data and took the same data analysis approach as in Chapter 2, using samples from ODP site 849 in the eastern equatorial Pacific. I collected data from eleven time intervals during the mid- and early Pliocene, to examine changes in El Niño strength as the tropical Pacific mean state evolved toward modern conditions. I found that El Niño was dampened throughout the early Pliocene, when the thermocline was deep and the vertical temperature gradient in the eastern equatorial Pacific was low [*Ford et al.*, 2015b]. By the mid-Pliocene, El Niño strength was sometimes dampened and sometimes similar to the late Holocene, appearing to vary on orbital and/or centennial timescales. This shift in ENSO behavior coincides with a shoaling of the thermocline, implying that stronger ocean-atmosphere coupling enabled periods of relatively stronger ENSO.

As with Chapter 2, the findings from Chapter 3 would be strengthened with more temperature data from the eastern equatorial Pacific. Generating a long-term SST record at my site to pair with the Ford et al. [*Ford et al.*, 2012] subsurface temperature record would yield valuable information on vertical stratification, which is likely more important for ENSO feedbacks than thermocline depth/temperature alone. Also, increasing the time resolution of existing subsurface temperature records would enable investigation of the causes of orbital-scale variations in El Niño strength during the mid-Pliocene, which can only be speculated at with current data.

In Chapter 4, "The temperature of the West Pacific Warm Pool in the Pliocene," I sought to constrain the response of the WPWP to modern levels of $pCO_2$. A previously published Mg/Ca-based SST record appears to show that the WPWP was about the same temperature today as it was in the Pliocene, despite higher-than-preindustrial $pCO_2$ [*Wara et al.*, 2005]. This finding was called into question upon publication of a new temperature record using the $TEX_{86}$ temperature proxy, which indicates a WPWP cooling trend since the Pliocene and differs markedly from the Mg/Ca temperature record. Because $TEX_{86}$ is biased by subsurface temperatures, the Mg/Ca proxy is the best approach available for reconstructing SST at this site, but achieving confidence in the Mg/Ca record requires tightening constraints on its own biases. I chose to focus on calcite dissolution, which can cause a large cold bias and is of unknown magnitude in the past. To constrain the effect of changes in dissolution on the Mg/Ca record, I collected benthic B/Ca data to reconstruct $\Delta[CO_3^{2-}]$, the parameter that controls dissolution. I found no long-term trend in benthic B/Ca at

ODP site 806 over the past 5.5 Myr, implying no bias from dissolution in the Mg/Ca record. I then estimated the effects of other non-temperature controls on foraminiferal Mg/Ca, including changes in Mg/Ca of seawater, and concluded that the West Pacific Warm Pool was ~1°C warmer in the Pliocene than today.

As discussed briefly in Chapter 4, one application of the $\Delta[CO_3^{2-}]$ data is to test whether there was deep water production in the North Pacific during the Pliocene [*Burls et al.*, 2017]. My data does not show higher $\Delta[CO_3^{2-}]$ in the Pliocene than today, and so does not support the hypothesis of NPDW. Interestingly, the benthic C isotope data does support NPDW formation. The benthic $\delta^{13}C$ record at 806 has a slight trend, with more positive values in the Pliocene and more negative values in the Pleistocene [*Karas et al.*, 2009]. In contrast, the benthic $\delta^{13}C$ record at ODP 849 (eastern equatorial Pacific, 3800 m depth), which is thought to reflect Circumpolar Deep Water and thus approximate global mean values under the modern ocean circulation regime [*Kwiek and Ravelo*, 1999], has no trend over the Plio-Pleistocene [*Mix et al.*, 1995]. Other sites in the North Pacific, including 1208 in the northwest Pacific and 1012 and 1018 in the northeast Pacific, have higher values in the Pliocene, similar to 806 [*Burls et al.*, 2017]. As such, benthic $\delta^{13}C$ data does support NPDW formation, since recently ventilated deep water should have more positive $\delta^{13}C$ than older deep water, and ODP 806 and other North Pacific sites would be upstream of ODP 849 with respect to NPDW flow [*Burls et al.*, 2017].

The discrepancy between benthic B/Ca and benthic $\delta^{13}C$ could be due to changes in air-sea exchange; greater air-sea exchange would raise $\delta^{13}C$ of surface

waters, which then sink to become deep waters [*Charles et al.*, 1993], without changing [$CO_3^{2-}$]. Thus, the benthic B/Ca data together with the benthic $\delta^{13}C$ data may indicate that a different and more proximal water mass, with a different air-sea exchange signature than Circumpolar Deep Water, was bathing 806 during the Pliocene. However, it is somewhat surprising that changes in deep ocean circulation and air-sea exchange should have exactly conspired to negate any change in $\Delta[CO_3^{2-}]$. More benthic B/Ca data are needed, from sites 849 (which records Circumpolar Deep Water) and 1208 (upstream of 806 with respect to NPDW), to separate out whole-ocean versus regional change in $\Delta[CO_3^{2-}]$ and distinguish between hypotheses.

Overall, my dissertation emphasizes the significance of the thermocline, which should help guide modeling efforts to predict ENSO's response to anthropogenic change. My findings agree with recent work showing that the future evolution of ENSO strength through 2100 will depend on changes in the strength of the thermocline feedback, though observations show the opposite trend to that predicted in CMIP5 [*Kim et al.*, 2014b], highlighting the need for further model refinements.

This dissertation also verifies a moderate sensitivity of the WPWP to $pCO_2$, verifying the work of [*Ford and Ravelo*, 2019] and implying a moderate Earth system sensitivity. A moderate Earth system sensitivity contrasts somewhat with recent findings of high climate sensitivity (5.5°C per doubling of $pCO_2$; [*Frey and Kay*, 2017]). However, the Pliocene likely had only 1.4 times higher $pCO_2$ than preindustrial, and the WPWP is expected to respond to $pCO_2$ change less than mid-

and high latitudes and upwelling regions, since its SST is not affected by ice-albedo feedbacks or changes in thermocline depth. Indeed, these regions were much warmer than today in the Pliocene [*Fedorov et al.*, 2013]. Future work by the community at large should focus on incorporating the results of this dissertation and other paleoclimate studies into simulations, in order to validate the models, better understand the past, and better predict the future under anthropogenic climate change.

## References


Burls, N. J., A. V. Fedorov, D. M. Sigman, S. L. Jaccard, R. Tiedemann, and G. H. Haug (2017), Active Pacific meridional overturning circulation (PMOC) during the warm Pliocene, Science Advances, 3.

Charles, C. D., J. D. Wright, and R. G. Fairbanks (1993), Thermodynamic influences on the marine carbon isotope record, Paleoceanography, 8(6), 691-697.

Clement, A. C., R. Seager, and M. A. Cane (1999), Orbital controls on the El Niño/Southern Oscillation and the tropical climate, Paleoceanography, 14(4), 441-456, doi: 10.1029/1999pa900013.

Clement, A. C., R. Seager, M. A. Cane, and S. E. Zebiak (1996), An Ocean Dynamical Thermostat, Journal of Climate, 9, 2190-2196.

Fedorov, A. V., C. M. Brierley, K. T. Lawrence, Z. Liu, P. S. Dekens, and A. C. Ravelo (2013), Patterns and mechanisms of early Pliocene warmth, Nature, 496(7443), 43-49, doi: 10.1038/nature12003.

Ford, H. L., and A. C. Ravelo (2019), Estimates of Pliocene Tropical Pacific Temperature Sensitivity to Radiative Greenhouse Gas Forcing, Paleoceanography and Paleoclimatology, doi: 10.1029/2018pa003461.

Ford, H. L., A. C. Ravelo, and S. Hovan (2012), A deep Eastern Equatorial Pacific thermocline during the early Pliocene warm period, Earth and Planetary Science Letters, 355-356, 152-161, doi: 10.1016/j.epsl.2012.08.027.

Ford, H. L., A. C. Ravelo, P. S. Dekens, J. P. LaRiviere, and M. W. Wara (2015b), The evolution of the equatorial thermocline and the early Pliocene El Padre mean state, Geophys Res Lett, 42, 4878-4887, doi: 10.1002/.

Frey, W. R., and J. E. Kay (2017), The influence of extratropical cloud phase and amount feedbacks on climate sensitivity, Climate Dynamics, 50(7-8), 3097-3116, doi: 10.1007/s00382-017-3796-5.

Karas, C., D. Nürnberg, A. K. Gupta, R. Tiedemann, K. Mohan, and T. Bickert (2009), Mid-Pliocene climate change amplified by a switch in Indonesian subsurface throughflow, Nature Geoscience, 2(6), 434-438, doi: 10.1038/ngeo520.

Kim, S. T., W. Cai, F.-F. Jin, A. Santoso, L. Wu, E. Guilyardi, and S.-I. An (2014b), Response of El Niño sea surface temperature variability to greenhouse warming, Nature Climate Change, 4(9), 786-790, doi: 10.1038/nclimate2326.

Kwiek, P. B., and A. C. Ravelo (1999), Pacific Ocean intermediate and deep water circulation during the Pliocene, Palaeogeography, Palaeoclimatology, Palaeoecology, 154, 191-217.

Mix, A. C., N. G. Pisias, W. Rugh, J. Wilson, A. Morey, and T. K. Hagelberg (1995), Benthic foraminifer stable isotope record from site 849 (0-5 Ma): Local and global climate changes, in Proceedings of the Ocean Drilling Program, Scientific Results, edited by N. G. Pisias, L. A. Mayer, T. R. Janecek, A. Palmer-Julson and T. H. van Andel, Ocean Drilling Program, College Station TX.

Thirumalai, K., J. W. Partin, C. S. Jackson, and T. M. Quinn (2013), Statistical constraints on El Niño Southern Oscillation reconstructions using individual foraminifera: A sensitivity analysis, Paleoceanography, 28(3), 401-412, doi: 10.1002/palo.20037.

Wara, M. W., A. C. Ravelo, and M. L. Delaney (2005), Permanent El Niño-like conditions during the Pliocene Warm Period, Science, 309, 758-761.

White, S. M., A. C. Ravelo, and P. J. Polissar (2018), Dampened El Niño in the early and mid-Holocene due to insolation-forced warming/deepening of the thermocline, Geophysical Research Letters, 45, doi: 10.1002/2017GL075433.

## References


An, S.-I., and J. Choi (2014), Mid-Holocene tropical Pacific climate state, annual cycle, and ENSO in PMIP2 and PMIP3, Climate Dynamics, 43(3-4), 957-970, doi: 10.1007/s00382-013-1880-z.

Anand, P., H. Elderfield, and M. H. Conte (2003), Calibration of Mg/Ca thermometry in planktonic foraminifera from a sediment trap time series, Paleoceanography, 18(2), doi: 10.1029/2002pa000846.

Bard, E., B. Hamelin, M. Arnold, L. Montaggioni, G. Cabioch, G. Faure, and F. Rougerie (1996), Deglacial sea-level record from Tahiti corals and the timing of global meltwater discharge, Nature, 382, 241-244.

Barreiro, M., and S. G. Philander (2008), Response of the tropical Pacific to changes in extratropical clouds, Climate Dynamics, 31(6), 713-729, doi: 10.1007/s00382-007-0363-5.

Barreiro, M., G. Philander, R. Pacanowski, and A. V. Fedorov (2005), Simulations of warm tropical conditions with application to middle Pliocene atmospheres, Climate Dynamics, 26(4), 349-365, doi: 10.1007/s00382-005-0086-4.

Bartoli, G., B. Hönisch, and R. E. Zeebe (2011), Atmospheric CO2decline during the Pliocene intensification of Northern Hemisphere glaciations, Paleoceanography, 26(4), n/a-n/a, doi: 10.1029/2010pa002055.

Benway, H. M., A. C. Mix, B. A. Haley, and G. P. Klinkhammer (2006), Eastern Pacific Warm Pool paleosalinity and climate variability: 0-30 kyr, Paleoceanography, 21(3), PA3008, doi: 10.1029/2005pa001208.

Berelson, W. M., et al. (1997), Biogenic budgets of particle rain, benthic remineralization and sediment accumulation in the equatorial Pacific, Deep Sea Research Part II: Topical Studies in Oceanography, 44(9-10), 2251-2282.

Berger, A. L. (1978), Long-term variations of caloric insolation resulting from the Earth's orbital elements, Quaternary Research, 9, 139-167.

Berger, W. H., M.-C. Bonneau, and F. L. Parker (1982), Foraminifera on the deep-sea floor: lysocline and dissolution rate, Oceanologica Acta 5(2), 249-258.

Berger, W. H., R. M. Leckie, T. R. Janecek, R. Stax, and T. Takayama (1993), Carbonate sedimentation on Ontong Java Plateau: highlights and open questions, in Proceedings of the Ocean Drilling Program, Scientific Results, edited by W. H. Berger, L. W. Kroenke and L. A. Mayer, pp. 711-744, Ocean Drilling Program, College Station, TX.

Bijma, J., B. Hönisch, and R. E. Zeebe (2002), Impact of the ocean carbonate chemistry on living foraminiferal shell weight: Comment on "Carbonate ion concentration in glacial-age deep waters of the Caribbean Sea" by W. S. Broecker and E. Clark, Geochemistry, Geophysics, Geosystems, 3(11), 1-7, doi: 10.1029/2002gc000388.

Bova, S. C., T. Herbert, Y. Rosenthal, J. Kalansky, M. Altabet, C. Chazen, A. Mojarro, and J. Zech (2015), Links between eastern equatorial Pacific stratification and atmospheric CO2 rise during the last deglaciation, Paleoceanography, 30(11), 1407-1424, doi: 10.1002/2015pa002816.

Boyle, E. A. (1983), Manganese carbonate overgrowths on foraminifera tests, Geochimica et Cosmochimica Acta, 47, 1815-1819.

Braconnot, P., Y. Luan, S. Brewer, and W. Zheng (2012), Impact of Earth's orbit and freshwater fluxes on Holocene climate mean seasonal cycle and ENSO characteristics, Climate Dynamics, 38(5-6), 1081-1092, doi: 10.1007/s00382-011-1029-x.

Brierley, C. M. (2015), Interannual climate variability seen in the Pliocene Model Intercomparison Project, Climate of the Past, 11(3), 605-618, doi: 10.5194/cp-11-605-2015.

Brierley, C. M., and A. V. Fedorov (2016), Comparing the impacts of Miocene–Pliocene changes in inter-ocean gateways on climate: Central American Seaway, Bering Strait, and Indonesia, Earth and Planetary Science Letters, 444, 116-130, doi: 10.1016/j.epsl.2016.03.010.

Broecker, W. S., and T.-H. Peng (1982), Tracers in the Sea, Lamont-Doherty Geological Observatory, Columbia University, Palisades, New York.

Broecker, W. S., and E. Clark (1999), CaCO3size distribution: A paleocarbonate ion proxy?, Paleoceanography, 14(5), 596-604, doi: 10.1029/1999pa900016.

Brown, R. E., L. D. Anderson, E. Thomas, and J. C. Zachos (2011), A core-top calibration of B/Ca in the benthic foraminifers Nuttallides umbonifera and Oridorsalis umbonatus: A proxy for Cenozoic bottom water carbonate saturation, Earth and Planetary Science Letters, 310(3-4), 360-368, doi: 10.1016/j.epsl.2011.08.023.

Brown, S. J., and H. Elderfield (1996), Variations in Mg/Ca and Sr/Ca ratios of planktonic foraminifera caused by postdepositional dissolution: Evidence of shallow Mg-dependent dissolution, Paleoceanography, 11(5), 543-551, doi: 10.1029/96pa01491.

Burls, N. J., and A. V. Fedorov (2014), Simulating Pliocene warmth and a permanent El Niño-like state: The role of cloud albedo, Paleoceanography, 29(10), 893-910, doi: 10.1002/2014pa002644.

Burls, N. J., A. V. Fedorov, D. M. Sigman, S. L. Jaccard, R. Tiedemann, and G. H. Haug (2017), Active Pacific meridional overturning circulation (PMOC) during the warm Pliocene, Science Advances, 3.

Bush, A. B. G. (2007), Extratropical Influences on the El Niño–Southern Oscillation through the Late Quaternary, Journal of Climate, 20(5), 788-800, doi: 10.1175/jcli4048.1.

Carre, M., J. P. Sachs, S. Purca, A. J. Schauer, P. Braconnot, R. A. Falcon, M. Julien, and D. Lavallee (2014), Holocene history of ENSO variance and asymmetry in the eastern tropical Pacific, Science, 345(6200), 1045-1048, doi: 10.1126/science.1228246.

Carton, J. A., and B. S. Giese (2008), A Reanalysis of Ocean Climate Using Simple Ocean Data Assimilation (SODA), Monthly Weather Review, 136(8), 2999-3017, doi: 10.1175/2007mwr1978.1.

Charles, C. D., J. D. Wright, and R. G. Fairbanks (1993), Thermodynamic influences on the marine carbon isotope record, Paleoceanography, 8(6), 691-697.

Chen, L., T. Li, Y. Yu, and S. K. Behera (2017), A possible explanation for the divergent projection of ENSO amplitude change under global warming, Climate Dynamics, 49, 3799-3811, doi: 10.1007/s00382-017-3544-x.

Chen, S., S. S. Hoffmann, D. C. Lund, K. M. Cobb, J. Emile-Geay, and J. F. Adkins (2016), A high-resolution speleothem record of western equatorial Pacific rainfall: Implications for Holocene ENSO evolution, Earth and Planetary Science Letters, 442, 61-71, doi: 10.1016/j.epsl.2016.02.050.

Chiang, J. C. H., Y. Fang, and P. Chang (2009), Pacific Climate Change and ENSO Activity in the Mid-Holocene, Journal of Climate, 22(4), 923-939, doi: 10.1175/2008jcli2644.1.

Christensen, J. H., et al. (2013), Climate Phenomena and their Relevance for Future Regional Climate Change, in Climate Change 2013: The Physical Science Basis. Contribution of Working Group I to the Fifth Assessment Report of the Intergovernmental Panel on Climate Change, edited by T. F. Stocker, D. Qin, G.-K. Plattner, M. Tignor, S. K. Allen, J. Boschung, A. Nauels, Y. Xia, V. Bex and P. M. Midgley, Cambridge University Press, Cambridge, United Kingdom and New York, NY, USA.

Clement, A. C., R. Seager, and M. A. Cane (1999), Orbital controls on the El Niño/Southern Oscillation and the tropical climate, Paleoceanography, 14(4), 441-456, doi: 10.1029/1999pa900013.

Clement, A. C., R. Seager, and M. A. Cane (2000), Suppression of El Niño during the Mid-Holocene by changes in the Earth's orbit, Paleoceanography, 15(6), 731-737, doi: 10.1029/1999pa000466.

Clement, A. C., R. Seager, M. A. Cane, and S. E. Zebiak (1996), An Ocean Dynamical Thermostat, Journal of Climate, 9, 2190-2196.

Cobb, K. M., C. D. Charles, H. Cheng, and R. L. Edwards (2003), El Niño-Southern Oscillation and tropical Pacific climate during the last millennium, Nature, 424, 271-276.

Cobb, K. M., N. Westphal, H. R. Sayani, J. T. Watson, E. Di Lorenzo, H. Cheng, R. L. Edwards, and C. D. Charles (2013), Highly variable El Niño-Southern Oscillation throughout the Holocene, Science, 339(6115), 67-70, doi: 10.1126/science.1228246.

Coggon, R. M., D. A. H. Teagle, C. E. Smith-Duque, J. C. Alt, and M. J. Cooper (2010), Reconstructing past seawater Mg/Ca and Sr/Ca from mid-ocean ridge flank calcium carbonate veins, Science, 327, 1114-1117.

Conroy, J. L., J. T. Overpeck, and J. E. Cole (2010), El Niño/Southern Oscillation and changes in the zonal gradient of tropical Pacific sea surfacetemperature over the last 1.2 ka, PAGES news, 18(1), 32-34.

Conroy, J. L., J. T. Overpeck, J. E. Cole, T. M. Shanahan, and M. Steinitz-Kannan (2008), Holocene changes in eastern tropical Pacific climate inferred from a Galápagos lake sediment record, Quaternary Science Reviews, 27(11-12), 1166-1180, doi: 10.1016/j.quascirev.2008.02.015.

Conte, M. H., M.-A. Sicre, C. Rühlemann, J. C. Weber, S. Schulte, D. Schulz-Bull, and T. Blanz (2006), Global temperature calibration of the alkenone unsaturation index (Uk′37) in surface waters and comparison with surface sediments, Geochemistry, Geophysics, Geosystems, 7(2), Q02005, doi: 10.1029/2005gc001054.

Dang, H., Z. Jian, F. Bassinot, P. Qiao, and X. Cheng (2012), Decoupled Holocene variability in surface and thermocline water temperatures of the Indo-Pacific Warm Pool, Geophysical Research Letters, 39(1), L01701, doi: 10.1029/2011gl050154.

de Villiers, S. (2005), Foraminiferal shell-weight evidence for sedimentary calcite dissolution above the lysocline, Deep Sea Research Part I: Oceanographic Research Papers, 52(5), 671-680, doi: 10.1016/j.dsr.2004.11.014.

Dekens, P. S., A. C. Ravelo, and M. D. McCarthy (2007), Warm upwelling regions in the Pliocene warm period, Paleoceanography, 22(3), n/a-n/a, doi: 10.1029/2006pa001394.

Dekens, P. S., A. C. Ravelo, and E. M. Griffith (2016), Moderate changes in Mg/Ca of seawater through the last 5 Ma, paper presented at International Conference on Paleoceanography, Utrecht, Netherlands.

Dekens, P. S., D. W. Lea, D. K. Pak, and H. J. Spero (2002), Core top calibration of Mg/Ca in tropical foraminifera: refining paleotemperature estimation, Geochemistry, Geophysics, Geosystems, 3(4).

Dekens, P. S., A. C. Ravelo, M. D. McCarthy, and C. A. Edwards (2008), A 5 million year comparison of Mg/Ca and alkenone paleothermometers, Geochemistry, Geophysics, Geosystems, 9(10), n/a-n/a, doi: 10.1029/2007gc001931.

DiNezio, P. N., B. P. Kirtman, A. C. Clement, S.-K. Lee, G. A. Vecchi, and A. Wittenberg (2012), Mean Climate Controls on the Simulated Response of ENSO to Increasing Greenhouse Gases, Journal of Climate, 25(21), 7399-7420, doi: 10.1175/jcli-d-11-00494.1.

DiNezio, P. N., A. Clement, G. A. Vecchi, B. Soden, A. J. Broccoli, B. L. Otto-Bliesner, and P. Braconnot (2011), The response of the Walker circulation to Last Glacial Maximum forcing: Implications for detection in proxies, Paleoceanography, 26(3), PA3217, doi: 10.1029/2010pa002083.

Dong, L., L. Li, Q. Li, H. Wang, and C. L. Zhang (2015), Hydroclimate implications of thermocline variability in the southern South China Sea over the past 180,000yr, Quaternary Research, 83(2), 370-377, doi: 10.1016/j.yqres.2014.12.003.

Dowsett, H. J., and M. M. Robinson (2009), Mid-Pliocene equatorial Pacific sea surface temperature reconstruction: a multi-proxy perspective, Philos Trans A Math Phys Eng Sci, 367(1886), 109-125, doi: 10.1098/rsta.2008.0206.

Dowsett, H. J., M. Robinson, A. M. Haywood, U. Salzmann, D. Hill, L. E. Sohl, M. Chandler, M. Williams, K. Foley, and D. K. Stoll (2010), The PRISM3D paleoenvironmental reconstruction, Stratigraphy, 7(2-3), 123-139.

Driscoll, R., M. Eliot, T. Russon, K. Welsh, Y. Yokoyama, and A. Tudhope (2014), ENSO reconstructions over the past 60 ka using giant clams (Tridacna sp.)

from Papua New Guinea, Geophysical Research Letters, 41, 6819-6825, doi: 10.1002/.

Druffel, E. R. M., and S. Griffin (1993), Large variations of surface ocean radiocarbon: Evidence of circulation changes in the southwestern Pacific, Journal of Geophysical Research, 98(C11), 20249, doi: 10.1029/93jc02113.

Duprey, N., C. E. Lazareth, T. Corrège, F. Le Cornec, C. Maes, N. Pujol, M. Madeng-Yogo, S. Caquineau, C. Soares Derome, and G. Cabioch (2012), Early mid-Holocene SST variability and surface-ocean water balance in the southwest Pacific, Paleoceanography, 27(4), PA4207, doi: 10.1029/2012pa002350.

Dyez, K. A., and A. C. Ravelo (2012), Late Pleistocene tropical Pacific temperature sensitivity to radiative greenhouse gas forcing, Geology, 41(1), 23-26, doi: 10.1130/g33425.1.

Eggins, S., P. De Deckker, and J. Marshall (2003), Mg/Ca variation in planktonic foraminifera tests: implications for reconstructing palaeo-seawater temperature and habitat migration, Earth and Planetary Science Letters, 212(3-4), 291-306, doi: 10.1016/s0012-821x(03)00283-8.

Elderfield, H., M. Vautravers, and M. Cooper (2002), The relationship between shell size and Mg/Ca,Sr/Ca, d18O, and d13C of species of planktonic foraminifera, Geochemistry, Geophysics, Geosystems, 3(8).

Emile-Geay, J., M. Cane, R. Seager, A. Kaplan, and P. Almasi (2007), El Niño as a mediator of the solar influence on climate, Paleoceanography, 22(3), PA3210, doi: 10.1029/2006pa001304.

Emile-Geay, J., et al. (2016), Links between tropical Pacific seasonal, interannual and orbital variability during the Holocene, Nature Geoscience, doi: 10.1038/ngeo2608.

Evans, D., C. Brierley, M. E. Raymo, J. Erez, and W. Müller (2016), Planktic foraminifera shell chemistry response to seawater chemistry: Pliocene–Pleistocene seawater Mg/Ca, temperature and sea level change, Earth and Planetary Science Letters, 438, 139-148, doi: 10.1016/j.epsl.2016.01.013.

Evans, M. N., R. G. Fairbanks, and J. L. Rubenstone (1998), The thermal oceanographic signal of El Nino reconstructed from a Kiritimati Island coral, Journal of Geophysical Research, 104, 13409-13421.

Farrell, J. W., and W. L. Prell (1991), Pacific CaCO3 preservation and d18O since 4 Ma: paleoceanographic and paleoclimatic implications, Paleoceanography, 6(4), 485-498.

Faul, K. L., A. C. Ravelo, and M. L. Delaney (2000), Reconstructions of upwelling, productivity, and photic zone depth in the eastern equatorial Pacific Ocean using planktonic foraminiferal stable isotopes and abundances, Journal of Foraminiferal Research, 30(2), 110-125.

Fedorov, A. V., C. M. Brierley, and K. Emanuel (2010), Tropical cyclones and permanent El Niño in the early Pliocene epoch, Nature, 463(7284), 1066-1070, doi: 10.1038/nature08831.

Fedorov, A. V., N. J. Burls, K. T. Lawrence, and L. C. Peterson (2015), Tightly linked zonal and meridional sea surface temperature gradients over the past five million years, Nature Geoscience, 8(12), 975-980, doi: 10.1038/ngeo2577.

Fedorov, A. V., C. M. Brierley, K. T. Lawrence, Z. Liu, P. S. Dekens, and A. C. Ravelo (2013), Patterns and mechanisms of early Pliocene warmth, Nature, 496(7443), 43-49, doi: 10.1038/nature12003.

Feely, R. A., et al. (2008), CLIVAR CO2 Sections P16S_2005 (6 January - 19 February 2005) and P16N_2006 (13 February - 30 March, 2006). Ed. A. Kozyr, in *Carbon Dioxide, Hydrographic, and Chemical Data Obtained During the R/Vs Roger Revelle and Thomas G. Thompson Repeat Hydrography Cruises in the Pacific Ocean*, edited by O. R. N. L. Carbon Dioxide Information Analysis Center, U.S. Department of Energy, Oak Ridge, Tennessee.

Fehrenbacher, J., P. A. Martin, and G. Eshel (2006), Glacial deep water carbonate chemistry inferred from foraminiferal Mg/Ca: A case study from the western tropical Atlantic, Geochemistry, Geophysics, Geosystems, 7(9), n/a-n/a, doi: 10.1029/2005gc001156.

Feng, R., and C. J. Poulsen (2014), Andean elevation control on tropical Pacific climate and ENSO, Paleoceanography, 29(8), 795-809, doi: 10.1002/2014pa002640.

Ford, H. L., and A. C. Ravelo (2019), Estimates of Pliocene Tropical Pacific Temperature Sensitivity to Radiative Greenhouse Gas Forcing, Paleoceanography and Paleoclimatology, doi: 10.1029/2018pa003461.

Ford, H. L., A. C. Ravelo, and S. Hovan (2012), A deep Eastern Equatorial Pacific thermocline during the early Pliocene warm period, Earth and Planetary Science Letters, 355-356, 152-161, doi: 10.1016/j.epsl.2012.08.027.

Ford, H. L., A. C. Ravelo, and P. J. Polissar (2015a), Reduced El Niño-Southern Oscillation during the Last Glacial Maximum, Science, 347(6219), 255-258.

Ford, H. L., A. C. Ravelo, P. S. Dekens, J. P. LaRiviere, and M. W. Wara (2015b), The evolution of the equatorial thermocline and the early Pliocene El Padre mean state, Geophys Res Lett, 42, 4878-4887, doi: 10.1002/.

Fraser, N., W. Kuhnt, A. Holbourn, T. Bolliet, N. Andersen, T. Blanz, and L. Beaufort (2014), Precipitation variability within the West Pacific Warm Pool over the past 120ka: Evidence from the Davao Gulf, southern Philippines, Paleoceanography, 29, 1094-1110, doi: doi:10.1002/ 2013PA002599.

Frey, W. R., and J. E. Kay (2017), The influence of extratropical cloud phase and amount feedbacks on climate sensitivity, Climate Dynamics, 50(7-8), 3097-3116, doi: 10.1007/s00382-017-3796-5.

Gill, E. C., B. Rajagopalan, P. Molnar, and T. M. Marchitto (2016), Reduced-dimension reconstruction of the equatorial Pacific SST and zonal wind fields over the past 10,000 years using Mg/Ca and alkenone records, Paleoceanography, doi: 10.1002/2016pa002948.

Gray, W. R., and D. Evans (2019), Nonthermal Influences on Mg/Ca in Planktonic Foraminifera: A Review of Culture Studies and Application to the Last Glacial Maximum, Paleoceanography and Paleoclimatology, 34(3), 306-315, doi: 10.1029/2018pa003517.

Ham, Y.-G., and J.-S. Kug (2016), ENSO amplitude changes due to greenhouse warming in CMIP5: Role of mean tropical precipitation in the twentieth century, Geophysical Research Letters, 43, 433-430, doi: 10.1002/2015GL066864.

Hanawa, K., and L. D. Talley (2001), Mode Waters, International Geophysics Series, 77, 373-386.

Haynes, L., B. Honisch, K. A. Dyez, K. Holland, Y. Rosenthal, C. R. Fish, A. V. Subhas, and J. W. B. Rae (2017), Calibration of the B/Ca proxy in the planktic foraminifer Orbulina universa to Paleocene seawater conditions, Paleoceanography, 32, doi: 10.1002/.

Haywood, A. M., P. J. Valdes, and V. L. Peck (2007), A permanent El Niño-like state during the Pliocene?, Paleoceanography, 22(1), n/a-n/a, doi: 10.1029/2006pa001323.

Haywood, A. M., et al. (2013), Large-scale features of Pliocene climate: results from the Pliocene Model Intercomparison Project, Climate of the Past, 9(1), 191-209, doi: 10.5194/cp-9-191-2013.

Hemming, N. G., and G. N. Hanson (1992), Boron isotopic composition and concentration in modern marine carbonates, Geochimica et Cosmochimica Acta, 56, 537-543.

Hertzberg, J. E., M. W. Schmidt, T. S. Bianchi, R. W. Smith, M. R. Shields, and F. Marcantonio (2016), Comparison of eastern tropical Pacific TEX86 and Globigerinoides ruber Mg/Ca derived sea surface temperatures: Insights from the Holocene and Last Glacial Maximum, Earth and Planetary Science Letters, 434, 320-332, doi: 10.1016/j.epsl.2015.11.050.

Hill, D. J., et al. (2014), Evaluating the dominant components of warming in Pliocene climate simulations, Climate of the Past, 10(1), 79-90, doi: 10.5194/cp-10-79-2014.

Hönisch, B., K. A. Allen, D. W. Lea, H. J. Spero, S. M. Eggins, J. Arbuszewski, P. deMenocal, Y. Rosenthal, A. D. Russell, and H. Elderfield (2013), The influence of salinity on Mg/Ca in planktic foraminifers – Evidence from

cultures, core-top sediments and complementary δ18O, Geochimica et Cosmochimica Acta, 121, 196-213, doi: 10.1016/j.gca.2013.07.028.

Horita, J., H. Zimmermann, and H. D. Holland (2002), Chemical evolution of seawater during the Phanerozoic: implications from the record of marine evaporites, Geochimica et Cosmochimica Acta, 66(21), 3733-3756.

Jahnke, R., D. Heggie, S. Emerson, and V. Grundmanis (1982), Pore waters of the central Pacific Ocean: nutrient results, Earth and Planetary Science Letters, 61, 233-256.

Jia, G., J. Zhang, J. Chen, P. a. Peng, and C. L. Zhang (2012), Archaeal tetraether lipids record subsurface water temperature in the South China Sea, Organic Geochemistry, 50, 68-77, doi: 10.1016/j.orggeochem.2012.07.002.

Jochum, M., B. Fox-Kemper, P. H. Molnar, and C. Shields (2009), Differences in the Indonesian seaway in a coupled climate model and their relevance to Pliocene climate and El Niño, Paleoceanography, 24(1), n/a-n/a, doi: 10.1029/2008pa001678.

Johnson, G. C., and M. J. McPhaden (1999), Interior pycnocline flow from the subtropical to the equatorial Pacific Ocean, Journal of Physical Oceanography, 29, 3073-3089.

Johnstone, H. J. H., J. Yu, H. Elderfield, and M. Schulz (2011), Improving temperature estimates derived from Mg/Ca of planktonic foraminifera using X-ray computed tomography–based dissolution index, XDX, Paleoceanography, 26(1), doi: 10.1029/2009pa001902.

Kaiser, J., E. Schefuss, F. Lamy, M. Mohtadi, and D. Hebbeln (2008), Glacial to Holocene changes in sea surface temperature and coastal vegetation in north central Chile: high versus low latitude forcing, Quaternary Science Reviews, 27, 2064-2075.

Kalansky, J., Y. Rosenthal, T. Herbert, S. Bova, and M. Altabet (2015), Southern Ocean contributions to the Eastern Equatorial Pacific heat content during the Holocene, Earth and Planetary Science Letters, 424, 158-167, doi: 10.1016/j.epsl.2015.05.013.

Karamperidou, C., P. N. Di Nezio, A. Timmermann, F.-F. Jin, and K. M. Cobb (2015), The response of ENSO flavors to mid-Holocene climate: Implications for proxy interpretation, Paleoceanography, 30(5), 527-547, doi: 10.1002/2014pa002742.

Karas, C., D. Nürnberg, A. K. Gupta, R. Tiedemann, K. Mohan, and T. Bickert (2009), Mid-Pliocene climate change amplified by a switch in Indonesian subsurface throughflow, Nature Geoscience, 2(6), 434-438, doi: 10.1038/ngeo520.

Kerr, J., R. Rickaby, J. Yu, H. Elderfield, and A. Y. Sadekov (2017), The effect of ocean alkalinity and carbon transfer on deep-sea carbonate ion concentration during the past five glacial cycles, Earth and Planetary Science Letters, 471, 42-53, doi: 10.1016/j.epsl.2017.04.042.

Khider, D., G. Huerta, C. Jackson, L. D. Stott, and J. Emile-Geay (2015), A Bayesian, multivariate calibration forGlobigerinoides ruberMg/Ca, Geochemistry, Geophysics, Geosystems, 16(9), 2916-2932, doi: 10.1002/2015gc005844.

Kim, S. T., W. Cai, F.-F. Jin, and J.-Y. Yu (2014a), ENSO stability in coupled climate models and its association with mean state, Climate Dynamics, 42(11-12), 3313-3321, doi: 10.1007/s00382-013-1833-6.

Kim, S. T., W. Cai, F.-F. Jin, A. Santoso, L. Wu, E. Guilyardi, and S.-I. An (2014b), Response of El Niño sea surface temperature variability to greenhouse warming, Nature Climate Change, 4(9), 786-790, doi: 10.1038/nclimate2326.

Koutavas, A., and S. Joanides (2012), El Niño-Southern Oscillation extrema in the Holocene and Last Glacial Maximum, Paleoceanography, 27(4), PA4208, doi: 10.1029/2012pa002378.

Kwiek, P. B., and A. C. Ravelo (1999), Pacific Ocean intermediate and deep water circulation during the Pliocene, Palaeogeography, Palaeoclimatology, Palaeoecology, 154, 191-217.

Lawrence, K. T., Z. Liu, and T. D. Herbert (2006), Evolution of the eastern tropical Pacific through Plio-Pleistocene glaciation, Science, 312(5770), 79-83, doi: 10.1126/science.1120395.

Lea, D. W., T. A. Mashiotta, and H. J. Spero (1999), Controls on magnesium and strontium uptake in planktonic foraminifera determined by live culturing, Geochimica et Cosmochimica Acta, 63(16), 2369-2379.

Lea, D. W., D. K. Pak, and H. J. Spero (2000), Climate impact of late Quaternary equatorial Pacific sea surface temperature variations, Science, 289, 1719-1724.

Leduc, G., L. Vidal, O. Cartapanis, and E. Bard (2009), Modes of eastern equatorial Pacific thermocline variability: Implications for ENSO dynamics over the last glacial period, Paleoceanography, 24(3), PA3202, doi: 10.1029/2008pa001701.

Leduc, G., R. Schneider, J. H. Kim, and G. Lohmann (2010), Holocene and Eemian sea surface temperature trends as revealed by alkenone and Mg/Ca paleothermometry, Quaternary Science Reviews, 29(7-8), 989-1004, doi: 10.1016/j.quascirev.2010.01.004.

Lemarchand, D., J. Gaillardet, E. Lewin, and C. J. Allegre (2002), Boron isotope systematics in large rivers: implications for the marine boron budget and paleo-pH reconstruction over the Cenozoic, Chemical Geology, 190, 123-140.

Liddy, H. M., S. J. Feakins, and J. E. Tierney (2016), Cooling and drying in northeast Africa across the Pliocene, Earth and Planetary Science Letters, 449, 430-438, doi: 10.1016/j.epsl.2016.05.005.

Lisiecki, L. E., and M. E. Raymo (2005), A Pliocene-Pleistocene stack of 57 globally distributed benthic δ18O records, Paleoceanography, 20(1), n/a-n/a, doi: 10.1029/2004pa001071.

Liu, Z., J. Kutzbach, and L. Wu (2000), Modeling climate shift of El Niño variability in the Holocene, Geophysical Research Letters, 27(15), 2265-2268.

Liu, Z., Z. Lu, X. Wen, B. L. Otto-Bliesner, A. Timmermann, and K. M. Cobb (2014), Evolution and forcing mechanisms of El Niño over the past 21,000 years, Nature, 515(7528), 550-553, doi: 10.1038/nature13963.

Locarnini, R. A., et al. (2013), World Ocean Atlas 2013, Volume 1: Temperature, edited by S. Levitus, p. 40, NOAA Atlas NESDIS 73, U.S. Government Printing Office, Washington, D.C.

Lowenstein, T. K., M. N. Timofeeff, S. T. Brennan, L. A. Hardie, and R. V. Demicco (2001), Oscillations in Phanerozoic Seawater Chemistry: Evidence from Fluid Inclusions, Science, 294, 1086-1088.

Lu, P., and J. P. McCreary (1995), Influence of the ITCZ on the flow of thermocline water from the subtropical to the equatorial Pacific Ocean, Journal of Physical Oceanography, 25, 3076-3088.

Lyle, M. (2003), Neogene carbonate burial in the Pacific Ocean, Paleoceanography, 18(3), doi: 10.1029/2002pa000777.

Lynch-Stieglitz, J., et al. (2015), Glacial-interglacial changes in central tropical Pacific surface seawater property gradients, Paleoceanography, 30(5), 423-438, doi: 10.1002/2014pa002746.

Ma, X., J. Tian, W. Ma, K. Li, and J. Yu (2018), Changes of deep Pacific overturning circulation and carbonate chemistry during middle Miocene East Antarctic ice sheet expansion, Earth and Planetary Science Letters, 484, 253-263, doi: 10.1016/j.epsl.2017.12.002.

Manucharyan, G. E., and A. V. Fedorov (2014), Robust ENSO across a Wide Range of Climates, Journal of Climate, 27(15), 5836-5850, doi: 10.1175/jcli-d-13-00759.1.

Marchitto, T. M., R. Muscheler, J. D. Ortiz, J. D. Carriquiry, and A. van Geen (2010), Dynamical response of the tropical Pacific Ocean to solar forcing during the early Holocene, Science, 330(6009), 1378-1381, doi: 10.1126/science.1194887.

Martin, P. A., and D. W. Lea (2002), A simple evaluation of cleaning procedures on fossil benthic foraminiferal Mg/Ca, Geochemistry, Geophysics, Geosystems, 3(10), 1-8, doi: 10.1029/2001gc000280.

Martinez-Garcia, A., A. Rosell-Mele, E. L. McClymont, R. Gersonde, and G. H. Haug (2010), Subpolar link to the emergence of the modern equatorial Pacific cold tongue, Science, 328, 1550-1553.

Mayer, L. A., N. Pisias, and T. Janecek (1992), ODP Leg 138 introduction, in Proceedings of the Ocean DRilling Program, Initial Reports, edited, Ocean Drilling Program, College Station, TX.

McGregor, H. V., and M. K. Gagan (2004), Western Pacific coral δ18O records of anomalous Holocene variability in the El Niño–Southern Oscillation, Geophysical Research Letters, 31(11), doi: 10.1029/2004gl019972.

McGregor, H. V., M. J. Fischer, M. K. Gagan, D. Fink, S. J. Phipps, H. Wong, and C. D. Woodroffe (2013), A weak El Niño/Southern Oscillation with delayed seasonal growth around 4,300 years ago, Nature Geoscience, 6(11), 949-953, doi: 10.1038/ngeo1936.

Medina-Elizalde, M., D. W. Lea, and M. S. Fantle (2008), Implications of seawater Mg/Ca variability for Plio-Pleistocene tropical climate reconstruction, Earth and Planetary Science Letters, 269(3-4), 585-595, doi: 10.1016/j.epsl.2008.03.014.

Mix, A. C., N. G. Pisias, W. Rugh, J. Wilson, A. Morey, and T. K. Hagelberg (1995), Benthic foraminifer stable isotope record from site 849 (0-5 Ma): Local and global climate changes, in Proceedings of the Ocean Drilling Program, Scientific Results, edited by N. G. Pisias, L. A. Mayer, T. R. Janecek, A. Palmer-Julson and T. H. van Andel, Ocean Drilling Program, College Station TX.

Molnar, P., and M. A. Cane (2002), El Niño's tropical climate and teleconnections as a blueprint for pre-Ice Age climates, Paleoceanography, 17(2).

Moy, C. M., G. O. Seltzer, D. T. Rodbell, and D. M. Anderson (2002), Variability of El Nino-Southern Oscillation activity at millennial timescales during the Holocene epoch, Nature, 420(6912), 162-165, doi: 10.1038/nature01163.

O'Brien, C. L., G. L. Foster, M. A. Martínez-Botí, R. Abell, J. W. B. Rae, and R. D. Pancost (2014), High sea surface temperatures in tropical warm pools during the Pliocene, Nature Geoscience, 7(8), 606-611, doi: 10.1038/ngeo2194.

O'Connor, B. M., R. A. Fine, K. A. Maillet, and D. B. Olson (2002), Formation rates of subtropical underwater in the Pacific Ocean, Deep Sea Research Part I: Oceanographic Research Papers, 49, 1571-1590.

Otto-Bliesner, B. L., E. C. Brady, S.-I. Shin, Z. Liu, and C. Shields (2003), Modeling El Niño and its tropical teleconnections during the last glacial-interglacial cycle, Geophysical Research Letters, 30(23), doi: 10.1029/2003gl018553.

Pagani, M., Z. Liu, J. LaRiviere, and A. C. Ravelo (2009), High Earth-system climate sensitivity determined from Pliocene carbon dioxide concentrations, Nature Geoscience, 3(1), 27-30, doi: 10.1038/ngeo724.

Pausata, F. S. R., Q. Zhang, F. Muschitiello, Z. Lu, L. Chafik, E. M. Niedermeyer, J. C. Stager, K. M. Cobb, and Z. Liu (2017), Greening of the Sahara suppressed ENSO activity during the mid-Holocene, Nat Commun, 8, 16020, doi: 10.1038/ncomms16020.

Rae, J. W. B., G. L. Foster, D. N. Schmidt, and T. Elliott (2011), Boron isotopes and B/Ca in benthic foraminifera: Proxies for the deep ocean carbonate system, Earth and Planetary Science Letters, 302(3-4), 403-413, doi: 10.1016/j.epsl.2010.12.034.

Raitzsch, M., E. C. Hathorne, H. Kuhnert, J. Groeneveld, and T. Bickert (2011), Modern and late Pleistocene B/Ca ratios of the benthic foraminifer Planulina wuellerstorfi determined with laser ablation ICP-MS, Geology, 39(11), 1039-1042, doi: 10.1130/g32009.1.

Rashid, H. A., A. C. Hirst, and S. J. Marsland (2016), An atmospheric mechanism for ENSO amplitude changes under an abrupt quadrupling of CO2 concentration in CMIP5 models, Geophysical Research Letters, 43, 1687-1694, doi: 10.1002/2015GL066768.

Rausch, S., F. Böhm, W. Bach, A. Klügel, and A. Eisenhauer (2013), Calcium carbonate veins in ocean crust record a threefold increase of seawater Mg/Ca

in the past 30 million years, Earth and Planetary Science Letters, 362, 215-224, doi: 10.1016/j.epsl.2012.12.005.

Ravelo, A. C., P. S. Dekens, and M. McCarthy (2006), Evidence for El Niño–like conditions during the Pliocene, GSA Today, 16(3), 4, doi: 10.1130/1052-5173(2006)016<4:efenlc>2.0.co;2.

Ravelo, A. C., K. T. Lawrence, A. V. Fedorov, and H. L. Ford (2014), Comment on "A 12-million-year temperature history of the tropical Pacific Ocean", Science, 346(6216).

Rayner, N. A. (2003), Global analyses of sea surface temperature, sea ice, and night marine air temperature since the late nineteenth century, Journal of Geophysical Research, 108(D14), doi: 10.1029/2002jd002670.

Regenberg, M., A. Regenberg, D. Garbe-Schönberg, and D. W. Lea (2014), Global dissolution effects on planktonic foraminiferal Mg/Ca ratios controlled by the calcite-saturation state of bottom waters, Paleoceanography, 29(3), 127-142, doi: 10.1002/2013pa002492.

Regenberg, M., D. Nürnberg, S. Steph, J. Groeneveld, D. Garbe-Schönberg, R. Tiedemann, and W.-C. Dullo (2006), Assessing the effect of dissolution on planktonic foraminiferal Mg/Ca ratios: Evidence from Caribbean core tops, Geochemistry, Geophysics, Geosystems, 7(7), n/a-n/a, doi: 10.1029/2005gc001019.

Reimer, P. J., et al. (2013), IntCal13 and Marine13 radiocarbon age calibration curves 0–50,000 years cal BP, Radiocarbon, 55(4), 1869-1887.

Richey, J. N., and J. E. Tierney (2016), GDGT and alkenone flux in the northern Gulf of Mexico: Implications for the TEX86and UK'37paleothermometers, Paleoceanography, 31(12), 1547-1561, doi: 10.1002/2016pa003032.

Robbins, L. L., M. E. Hansen, J. A. Kleypas, and S. C. Meylan (2010), CO2calc—A user-friendly seawater carbon calculator for Windows, Max OS X, and iOS (iPhone), in *U.S. Geological Survey Open-File Report 2010–1280, 17 p.*, edited.

Roberts, W. H. G., D. S. Battisti, and A. W. Tudhope (2014), ENSO in the Mid-Holocene according to CSM and HadCM3, Journal of Climate, 27(3), 1223-1242, doi: 10.1175/jcli-d-13-00251.1.

Rodbell, D. T., G. O. Seltzer, D. M. Anderson, M. B. Abbott, D. B. Enfield, and J. H. Newman (1999), An ~15,000 year record of El Nino-driven alluviation in southwestern Ecuador, Science, 283, 516-520.

Rohling, E. J., M. Medina-Elizalde, J. G. Shepherd, M. Siddall, and J. D. Stanford (2012), Sea Surface and High-Latitude Temperature Sensitivity to Radiative Forcing of Climate over Several Glacial Cycles, Journal of Climate, 25(5), 1635-1656, doi: 10.1175/2011jcli4078.1.

Rongstad, B. L., T. M. Marchitto, and J. C. Herguera (2017), Understanding the Effects of Dissolution on the Mg/Ca Paleothermometer in Planktic Foraminifera: Evidence From a Novel Individual Foraminifera Method, Paleoceanography, 32(12), 1386-1402, doi: 10.1002/2017pa003179.

Rosenbloom, N. A., B. L. Otto-Bliesner, E. C. Brady, and P. J. Lawrence (2013), Simulating the mid-Pliocene Warm Period with the CCSM4 model, Geoscientific Model Development, 6(2), 549-561, doi: 10.5194/gmd-6-549-2013.

Rosenthal, Y., and G. P. Lohmann (2002), Accurate estimation of sea surface temperatures using dissolution-corrected calibrations for Mg/Ca paleothermometry, Paleoceanography, 17(3), 16-11-16-16, doi: 10.1029/2001pa000749.

Rosenthal, Y., G. P. Lohmann, K. C. Lohmann, and R. M. Sherrell (2000), Incorporation and preservation of Mg inGlobigerinoides sacculifer:implications for reconstructing the temperature and18O/16O of seawater, Paleoceanography, 15(1), 135-145, doi: 10.1029/1999pa000415.

Rousselle, G., C. Beltran, M.-A. Sicre, I. Raffi, and M. De Rafélis (2013), Changes in sea-surface conditions in the Equatorial Pacific during the middle Miocene–Pliocene as inferred from coccolith geochemistry, Earth and Planetary Science Letters, 361, 412-421, doi: 10.1016/j.epsl.2012.11.003.

Rustic, G. T., A. Koutavas, T. M. Marchitto, and B. K. Linsley (2015), Dynamical excitation of the tropical Pacific Ocean and ENSO variability by Little Ice Age cooling, Science, 350(6267), 1537-1541, doi: 10.1126/science.aac9937.

Sadekov, A. Y., S. M. Eggins, and P. De Deckker (2005), Characterization of Mg/Ca distributions in planktonic foraminifera species by electron microprobe mapping, Geochemistry, Geophysics, Geosystems, 6(12), n/a-n/a, doi: 10.1029/2005gc000973.

Sadekov, A. Y., S. M. Eggins, P. De Deckker, U. Ninnemann, W. Kuhnt, and F. Bassinot (2009), Surface and subsurface seawater temperature reconstruction using Mg/Ca microanalysis of planktonic foraminifera Globigerinoides ruber, Globigerinoides sacculifer, and Pulleniatina obliquiloculata, Paleoceanography, 24(3), doi: 10.1029/2008pa001664.

Sadekov, A. Y., R. Ganeshram, L. Pichevin, R. Berdin, E. McClymont, H. Elderfield, and A. W. Tudhope (2013), Palaeoclimate reconstructions reveal a strong link between El Niño-Southern Oscillation and Tropical Pacific mean state, Nat Commun, 4, 2692, doi: 10.1038/ncomms3692.

Scroxton, N., S. G. Bonham, R. E. M. Rickaby, S. H. F. Lawrence, M. Hermoso, and A. M. Haywood (2011), Persistent El Niño-Southern Oscillation variation during the Pliocene Epoch, Paleoceanography, 26(2), n/a-n/a, doi: 10.1029/2010pa002097.

Seki, O., G. L. Foster, D. N. Schmidt, A. Mackensen, K. Kawamura, and R. D. Pancost (2010), Alkenone and boron-based Pliocene pCO2 records, Earth and Planetary Science Letters, 292(1-2), 201-211, doi: 10.1016/j.epsl.2010.01.037.

Seki, O., D. N. Schmidt, S. Schouten, E. C. Hopmans, J. S. Sinninghe Damsté, and R. D. Pancost (2012), Paleoceanographic changes in the Eastern Equatorial Pacific over the last 10 Myr, Paleoceanography, 27(3), doi: 10.1029/2011pa002158.

Shukla, S. P., M. A. Chandler, J. Jonas, L. E. Sohl, K. Mankoff, and H. Dowsett (2009), Impact of a permanent El Niño (El Padre) and Indian Ocean Dipole in warm Pliocene climates, Paleoceanography, 24(2), n/a-n/a, doi: 10.1029/2008pa001682.

Song, Z., M. Latif, W. Park, U. Krebs-Kanzow, and B. Schneider (2017), Influence of seaway changes during the Pliocene on tropical Pacific climate in the Kiel climate model: mean state, annual cycle, ENSO, and their interactions, Climate Dynamics, 48(11-12), 3725-3740, doi: 10.1007/s00382-016-3298-x.

Spezzaferri, S., M. Kucera, P. N. Pearson, B. S. Wade, S. Rappo, C. R. Poole, R. Morard, and C. Stalder (2015), Fossil and genetic evidence for the polyphyletic nature of the planktonic foraminifera "Globigerinoides", and description of the new genus Trilobatus, PLoS One, 10(5), e0128108, doi: 10.1371/journal.pone.0128108.

Steph, S., R. Tiedemann, M. Prange, J. Groeneveld, M. Schulz, A. Timmermann, D. Nürnberg, C. Rühlemann, C. Saukel, and G. H. Haug (2010), Early Pliocene increase in thermohaline overturning: A precondition for the development of the modern equatorial Pacific cold tongue, Paleoceanography, 25(2), doi: 10.1029/2008pa001645.

Stott, L., A. Timmermann, and R. Thunell (2007), Southern hemisphere and deep-sea warming led deglacial atmospheric CO2 rise and tropical warming, Science, 318(5849), 435-438.

Stuiver, M., and P. J. Reimer (1993), Extended 14C data base and revised Calib3.0 14C age calibration program, Radiocarbon, 35(1), 215-230.

Thirumalai, K., J. W. Partin, C. S. Jackson, and T. M. Quinn (2013), Statistical constraints on El Niño Southern Oscillation reconstructions using individual foraminifera: A sensitivity analysis, Paleoceanography, 28(3), 401-412, doi: 10.1002/palo.20037.

Thompson, D. M., et al. (2017), Tropical Pacific climate variability over the last 6000 years as recorded in Bainbridge Crater Lake, Galápagos, Paleoceanography, doi: 10.1002/2017pa003089.

Thunell, R. C., W. B. Curry, and S. Honjo (1983), Seasonal variation in the flux of planktonic foraminifera: time series sediment trap results from the Panama Basin, Earth and Planetary Science Letters, 64, 44-55.

Tian, B., G. J. Zhang, and V. Ramanathan (2001), Het balance in the Pacific warm pool atmosphere during TOGA COARE and CEPEX, Journal of Climate, 14, 1881-1893.

Tierney, J. E., and M. P. Tingley (2018), BAYSPLINE: A New Calibration for the Alkenone Paleothermometer, Paleoceanography and Paleoclimatology, 33(3), 281-301, doi: 10.1002/2017pa003201.

Timmermann, A., J. Sachs, and O. E. Timm (2014), Assessing divergent SST behavior during the last 21 ka derived from alkenones andG. ruber-Mg/Ca in the equatorial Pacific, Paleoceanography, 29(6), 680-696, doi: 10.1002/2013pa002598.

Timmermann, A., et al. (2007), The Influence of a Weakening of the Atlantic Meridional Overturning Circulation on ENSO, Journal of Climate, 20(19), 4899-4919, doi: 10.1175/jcli4283.1.

Tindall, J. C., A. M. Haywood, and F. W. Howell (2016), Accounting for centennial-scale variability when detecting changes in ENSO: A study of the Pliocene, Paleoceanography, doi: 10.1002/2016pa002951.

Toggweiler, J. R., K. Dixon, and W. S. Broecker (1991), The Peru upwelling and the ventilation of the South Pacific thermocline, Journal of Geophysical Research, 96(C11), 20,467-420,497, doi: 0.1029/91JC02063.

Trauth, M. H., M. Sarnthein, and M. Arnold (1997), Bioturbational mixing depth and carbon flux at the seafloor, Paleoceanography, 12(3), 517-526.

Trenberth, K. E. (1997), The definition of El Nino, Bulletin of the American Meteorological Society, 78(12), 2771-2777.

Tudhope, A. W., C. P. Chilcott, M. T. McCulloch, E. R. Cook, J. Chappell, R. M. Ellam, D. W. Lea, J. M. Lough, and G. B. Shimmield (2001), Variability in the El Nino-Southern Oscillation through a glacial-interglacial cycle, Science, 291(5508), 1511-1517, doi: 10.1126/science.1057969.

Vetter, L., H. J. Spero, A. D. Russell, and J. S. Fehrenbacher (2013), LA-ICP-MS depth profiling perspective on cleaning protocols for elemental analyses in planktic foraminifers, Geochemistry, Geophysics, Geosystems, 14(8), 2916-2931, doi: 10.1002/ggge.20163.

von der Heydt, A. S., A. Nnafie, and H. A. Dijkstra (2011), Cold tongue/Warm pool and ENSO dynamics in the Pliocene, Climate of the Past, 7(3), 903-915, doi: 10.5194/cp-7-903-2011.

Wara, M. W., A. C. Ravelo, and M. L. Delaney (2005), Permanent El Niño-like conditions during the Pliocene Warm Period, Science, 309, 758-761.

Watanabe, T., et al. (2011), Permanent El Niño during the Pliocene warm period not supported by coral evidence, Nature, 471(7337), 209-211, doi: 10.1038/nature09777.

Watkins, J. M., A. C. Mix, and J. Wilson (1996), Living planktic foraminifera: tracers of circulation and productivity regimes in the central equatorial Pacific, Deep Sea Research Part II: Topical Studies in Oceanography, 43(4-6), 1257-1282.

White, S. M., A. C. Ravelo, and P. J. Polissar (2018), Dampened El Niño in the early and mid-Holocene due to insolation-forced warming/deepening of the thermocline, Geophysical Research Letters, 45, doi: 10.1002/2017GL075433.

Wittenberg, A. T. (2009), Are historical records sufficient to constrain ENSO simulations?, Geophysical Research Letters, 36(12), doi: 10.1029/2009gl038710.

Wittenberg, A. T., A. Rosati, T. L. Delworth, G. A. Vecchi, and F. Zeng (2014), ENSO Modulation: Is It Decadally Predictable?, Journal of Climate, 27(7), 2667-2681, doi: 10.1175/jcli-d-13-00577.1.

Wong, A. P. S., and G. C. Johnson (2003), South Pacific Eastern Subtropical Mode Water, Journal of Physical Oceanography, 33, 1493-1509.

Woodroffe, C. D. (2003), Mid-late Holocene El Niño variability in the equatorial Pacific from coral microatolls, Geophysical Research Letters, 30(7), doi: 10.1029/2002gl015868.

Xu, J., A. Holbourn, W. Kuhnt, Z. Jian, and H. Kawamura (2008), Changes in the thermocline structure of the Indonesian outflow during Terminations I and II, Earth and Planetary Science Letters, 273(1-2), 152-162, doi: 10.1016/j.epsl.2008.06.029.

Yu, J., and H. Elderfield (2007), Benthic foraminiferal B/Ca ratios reflect deep water carbonate saturation state, Earth and Planetary Science Letters, 258(1-2), 73-86, doi: 10.1016/j.epsl.2007.03.025.

Yu, J., G. L. Foster, H. Elderfield, W. S. Broecker, and E. Clark (2010a), An evaluation of benthic foraminiferal B/Ca and δ11B for deep ocean carbonate ion and pH reconstructions, Earth and Planetary Science Letters, 293(1-2), 114-120, doi: 10.1016/j.epsl.2010.02.029.

Yu, J., W. S. Broecker, H. Elderfield, Z. Jin, J. McManus, and F. Zhang (2010b), Loss of Carbon from the deep sea since the last glacial maximum, Science, 330, 1084-1087.

Yu, J., R. F. Anderson, Z. Jin, J. W. B. Rae, B. N. Opdyke, and S. M. Eggins (2013), Responses of the deep ocean carbonate system to carbon reorganization during the Last Glacial–interglacial cycle, Quaternary Science Reviews, 76, 39-52, doi: 10.1016/j.quascirev.2013.06.020.

Zaunbrecher, L. K., K. M. Cobb, J. W. Beck, C. D. Charles, E. R. M. Druffel, R. G. Fairbanks, S. Griffin, and H. R. Sayani (2010), Coral records of central tropical Pacific radiocarbon variability during the last millennium, Paleoceanography, 25(4), doi: 10.1029/2009pa001788.

Zhang, X., et al. (2012), Changes in equatorial Pacific thermocline depth in response to Panamanian seaway closure: Insights from a multi-model study, Earth and Planetary Science Letters, 317-318, 76-84, doi: 10.1016/j.epsl.2011.11.028.

Zhang, Y. G., M. Pagani, and Z. Liu (2014a), A 12-million-year temperature history of the tropical Pacific Ocean, Science, 344(6179), 84-87, doi: 10.1126/science.1246172.

Zhang, Z., G. Leduc, and J. P. Sachs (2014b), El Niño evolution during the Holocene revealed by a biomarker rain gauge in the Galápagos Islands, Earth and Planetary Science Letters, 404, 420-434, doi: 10.1016/j.epsl.2014.07.013.

Zheng, X.-T., S.-P. Xie, L.-H. Lv, and Z.-Q. Zhou (2016), Intermodel uncertainty in ENSO amplitude change tied to Pacific Ocean warming pattern, Journal of Climate, 29, 7265-7279, doi: 10.1175/JCLI-D-16-0039.1.